SYNTHESIS AND PHYSICO-CHEMICAL CHARACTERISATION OF Zr, Ru AND In INTRODUCED MFI ZEOLITE

A THESIS SUBMITTED TO GAUHATI UNIVERSITY FOR AWARD OF DEGREE OF DOCTOR OF PHILOSOPHY IN CHEMISTRY IN THE FACULTY OF SCIENCE

BY

KISHOR KR SHAH
DEPARTMENT OF CHEMISTRY
GAUHATI UNIVERSITY, GUWAHATI, ASSAM (INDIA)

OCTOBER- 2012

SYNTHESIS AND PHYSICO-CHEMICAL CHARACTERISATION OF Zr, Ru AND In INTRODUCED MFI ZEOLITE

A THESIS SUBMITTED TO GAUHATI UNIVERSITY FOR AWARD OF DEGREE OF DOCTOR OF PHILOSOPHY IN CHEMISTRY IN THE FACULTY OF SCIENCE

BY

KISHOR KR SHAH
DEPARTMENT OF CHEMISTRY
GAUHATI UNIVERSITY, GUWAHATI, ASSAM (INDIA)

OCTOBER- 2012

From:
Prof. Anup Kumar Talukdar
M.Sc., Ph. D. (G.U.) DCCE (Tokyo)
Professor in Chemistry
Mobile: +9198640-73504

Department of Chemistry
Gauhati University, Guwahati-781014
http://www.gauhati.ac.in/chemistry/index.htm

To,

The Academic registrar

Gauhati University

This is to certify that Kishor Kr. Shah, Assistant Professor, Department of Chemistry, ADP College Nagaon, has carried out his research work entitled ***"Synthesis and Physico-Chemical Characterisation of Zr, Ru and In Introduced MFI Zeolite"*** for the degree of Doctor of Philosophy (Ph.D.) in the Department of Chemistry, Gauhati University under my guidance and supervision.

The thesis is the outcome of his investigation, examination, analysis and understanding. He has fulfilled all the requirements laid down in regulation of the Ph.D. examination of this university. No part of this thesis has been submitted to this university or any other university for any degree or diploma.

Date: 23.4.2013
Place: Gauhati University

(Dr. A. K. Talukdar)
Professor,
Department Of Chemistry
Gauhati University
Research Guide

DECLARATION

I would like to declare that this work was solely completed by me under the guidance of Prof. Anup Kumar Talukdar, Department of Chemistry, Gauhati University and this thesis or any part thereof has not been submitted by me for any research degree to this university or any other university or institution.

Kishor Kr Shah

Kishor Kr Shah

ACKNOWLEDGEMENT

It is with pleasure, I express my deep sense of gratitude to **Prof. A.K.TALUKDAR** *for his enlightening discussions and unfailing guidance at every stage of the research programme. He is really a sense of my guide, philosopher and more than a friend. Also I profusely thank him for the opportunity that he gave me to work with him.*

I also express my thanks to **Prof. P.J. Das** *(former Head, Department of Chemistry, Gauhati University) and* **Prof. D.C.Deka** *, Head, Department of Chemistry, Gauhati University for providing all necessary infrastructural facilities during my research tenure.*

I am thankful to **Prof. Arun Chattopadhyay,** *Head, Department of Chemistry, IIT Guwahati, for helping me during the characterization of the synthesized samples.*

I am also grateful to the Centre for Nano Technology, IIT Guwahati, Department of Physics, Tezpur University, USIC, Gauhati University, CIF, IIT Bombay, CIF, NEHU, Shillong , IASST, Guwahati and also the Department of Chemistry, Gauhati University for helping me during characterization of the synthesized samples.

My heartfelt thanks go to **Dr. S. U. Ahmed,** *Principal, ADP College, Nagaon for his permission to carry out the research and for his advice, suggestions and constant encouragement during the period of the research.*

I am also thankful to my lab mates **Dr. M.N. Thakuria, Dr. R. Patgiri, Dr. B. Kalita, Mrs. D.M. Pathak, Mr. J.Saikia, Mr. D. Saikia, Mr. N. Barman** *and all others for constant help and support during the period of research without which it would have been quite difficult for me to complete the research work.*

I sincerely thank **Dr. N. Pattanayak, Mr. B. K. Borah, Mr. A. N. Sarma, Dr. M. K. Hazarika, Dr. A. Bharali, Mr. S. Saikia** *and* **Mr. H. Bhuyan** *for their suggestions and help at various stages of my research.*

Finally I am extremely grateful to my Parents whose unfailing courage and counsel nurtured and motivated me to pursue this research. I am more than indebted to my brothers, whose sacrificial love and affection made me to stand at this juncture. I am also thankful to my wife for her constant support during the period of the research.

Last but not the least, I bow my head in front of the **Almighty** *for providing such an opportunity to work in science.*

Finally, I apologize for the omissions I made in my attempt to enumerate those who have contributed.

Kishor Kr Shah

Kishor Kr Shah

Contents.....

Chapter 1: Introduction

Chapter 3: Synthesis and Characterization of In and Ru incorporated MFI Zeolite

Chapter 4: Catalytic Activity of the Synthesized Samples

List of Figures

List of Tables

List of Schemes

List of Relations

Abbreviations

IUPAC :	International Union for Pure and Applied chemistry
ZSM:	Zeolite Socony Mobil
MCM:	Mobil Crystalline Material
SAPO:	Silicoaluminophosphate
MeAPO:	Metal Alumino Phosphate
BDDT:	Brunauer Deming Deming and Teller
MFI:	Mobil Five
SBU :	Secondary Building Units
CEC :	Cation Exchange Capacity
TMA :	Tetramethylammonium
TPA:	Tetrapropylammonium
XRD:	X-ray Diffraction
FTIR:	Fourier Transform Infrared spectroscopy
UV:	Ultra Violet
DRS:	Diffused Reflectance Spectroscopy
SEM:	Scanning Electron Microscopy
TGA:	Thermogravimetric analysis
BET :	Brunauer, Emmett and Teller
EDX:	Energy dispersive X-ray
CL:	Catechol
HQ:	Hydroquinone
GC-MS:	Gas Chromatography and Mass Spectroscopy
TOS:	Time on Stream

Notations

Å :	Angstrom
θ:	Bragg angle
λ :	Wave length
g :	Gram
h :	Hour
K :	Kelvin
T :	Temperature
p_o :	Saturated vapour pressure
nm:	Nano meter
m:	Meter
cm:	Centimeter

CHAPTER 1

INTRODUCTION

Chapter Summary

This chapter contains a brief introduction on porous materials, hysteresis loop, types of isotherm etc. based on current literature review. This chapter initiates with an extensive discussion of zeolites, mainly their general synthesis, nomenclature, structure, properties, modifications, characterization and applications. This chapter also contains the advantages of using fluoride gel as mineralizer.

1. Porous Materials

Based on their pore size, porous materials can be classified into three classes:

Microporous (pore size < 2 nm), mesoporous (pore size 2-50 nm) and macroporous (pore size >50 nm) materials, according to International Union for Pure and Applied Chemistry (IUPAC) [1]. Again, porous solids with pores of the size of molecular dimensions 0.2-0.3 nm in diameter, which can separate components of a mixture on the basis of molecular size and shape like sieves are called molecular sieves. Thus microporous materials are a sub-category of molecular sieves. Mesoporous materials can be considered as mesoporous molecular sieves although its pore diameter falls outside the molecular sieve range since molecular sieves concern initially materials with microporosity and a crystalline structure, while mesoporous framework is often an amorphous solid. A schematic representation of classification of porous materials is given in **Scheme 1.1.**

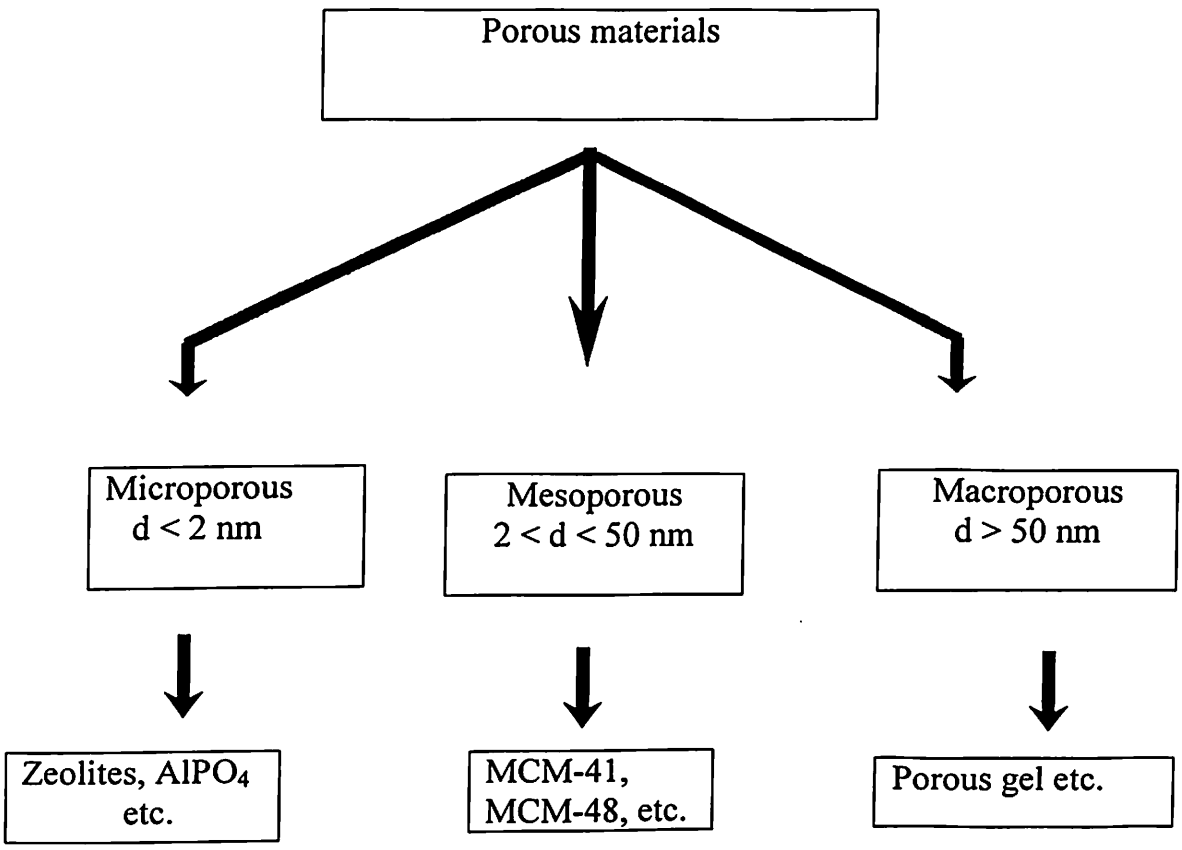

Scheme 1.1 Classification of the porous materials

1.1 History of molecular sieve materials

The porous materials have received utmost importance because of their molecular sieve properties among other properties. The theme of research on molecular sieve materials over the past nearly 60 years has been a quest for new structures and compositions. The major discoveries and advances in molecular sieve materials during that period are summarized in **Table 1.1.**

Table 1.1 Evolution of molecular sieve materials.

Time of initial discovery	Composition
Late 1940s to early 1950s	Low Si/Al ratio zeolites
Mid - 1950s to late 1960s	High Si/Al ratio zeolites
Early 1970s	SiO_2 molecular sieves
Late 1970s	$AlPO_4$ molecular sieves
Late 1970s to early 1980s	SAPO and MeAPO molecular sieves
Late 1970s	Metallo - silicates, aluminosilicates
Early to mid - 1980s	$AlPO_4$ - based molecular sieves
Early to mid - 1990s	Metallo-phosphates, Mesoporous molecular sieves, Octahedral – tetrahedral frameworks
Late 1990s	Metal organic frameworks
2000s	UZM aluminosilicate zeolites, Si/Al = 2 – 30 Germanosilicate zeolites SiO_2 molecular sieves in fluoride media

1.2 Types of isotherms of porous materials

There are six generic types of adsorption isotherms that have been observed in gas adsorption in porous materials, despite the multitude of different adsorbent/adsorbate combinations that have been employed. The

IUPAC classification scheme [2], based on the system devised by Brunauer, Deming, Deming, and Teller (the "BDDT" scheme), [3] is shown in **Figure 1.1.** These isotherm types are characteristic of (I) microporous materials or materials with strong adsorption in the first layer but negligible adsorption after that; (II) non-porous materials with relatively strong adsorbate-adsorbent interactions; (III) non-porous materials with weak adsorbate-adsorbent interactions; (IV) mesoporous materials with strong adsorbate-adsorbent interactions; (V) mesoporous materials with weak adsorbate-adsorbent interactions.

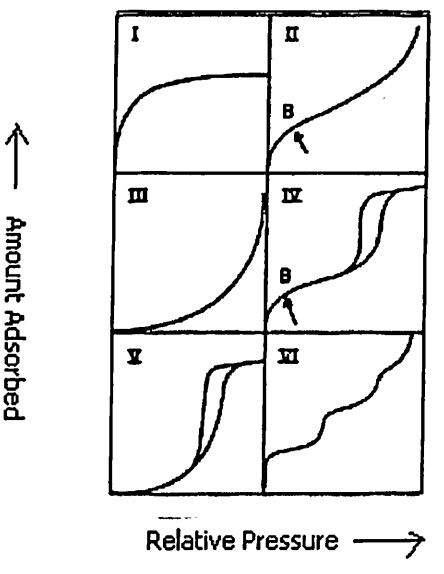

Fig.1.1 Different types of isotherms of porous materials

Types III and V are extremely rare, except in the case of water adsorbed on charcoal, graphite, or other hydrophobic surfaces. In these cases, however, it is nearly all that is ever seen. The Type VI isotherm was not part of the original BDDT scheme [3] and is very rare. It represents stepwise multilayer adsorption on a uniform, non-porous surface. Examples are argon or krypton on graphitized carbon at 77 K [2].

1.3 Hysteresis loop

A great deal of information can be learned about the magnetic properties of a material by studying its hysteresis loop. A hysteresis loop shows the relationship between the induced magnetic flux density **(B)** and the magnetizing force **(H).** It is often referred to as the B-H loop. The IUPAC classifies four different types of hysteresis loops, which are shown in **Figure 1.2.** Type H1 hysteresis are characteristic of well-defined mesopores with a narrow range of diameters somewhere between 4 nm and 50 nm. In such cases, it is typically assumed that the desorption branch of the isotherm yields a better reflection of the true pore size, since desorption is not hindered by nucleation. Types H3 and H4 hysteresis indicate broad distributions of pores, and are typically difficult isotherms from which to extract size distributions. Type H2 hysteresis, with asymmetric loops, indicate large pore volumes and typically a wide distribution of pores. Isotherms with Type H2, H3, or H4 hysteresis typically have their lower closure points dictated by the tensile strength effect.

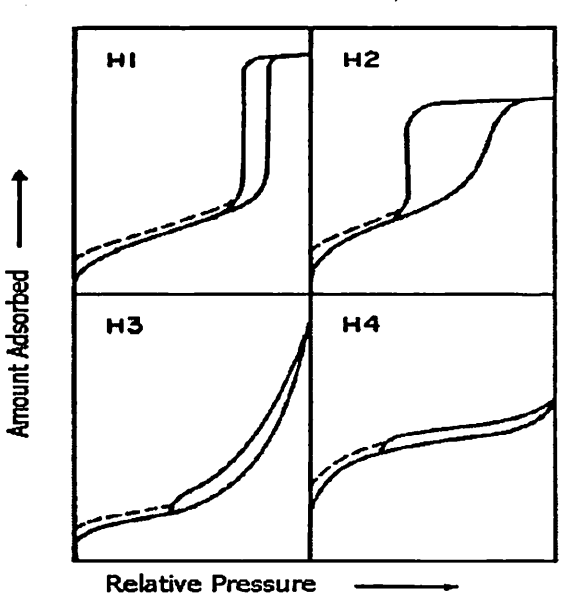

Fig. 1.2 Different types of hysteresis loops

1.4 Zeolite: A brief idea

Zeolites are natural or synthetic crystalline microporous aluminosilicates consisting of tetrahedral units producing open framework structures. They can be represented by the general formula:

$$M_{2n}O.Al_2O_3.xSiO_2.y\,H_2O$$

where M is an exchangeable metal cation of valency n for balancing the framework charge, x can assume a value equal to or greater than 2 following Lowenstein's rule(Al-O-Al linkages in zeolite frameworks are forbidden), and y represents the number of water molecules present in the voids of the three dimensional network[4]. Zeolites have an open framework structure of three dimensional SiO_4 and AlO_4 tetrahedral units which generates a network of pores and cavities having molecular dimensions. The presence of one Al^{3+} ion in the tetrahedral position brings one unit negative charge in the framework. Loosely held inorganic cations (alkali or alkaline earth metal) or organic cations are trapped inside the tetrahedral network cavities preserving the electroneutrality of the zeolite. Some of these extra framework cations are amenable to cation exchange. The aluminosilicate framework of the zeolite is rigid enough to avoid collapsing and the micropore volume previously occupied by water is made available to reversibly adsorb other polar molecules [5-8].

1.5 History of zeolites

Swedish mineralogist Axel F. Cronstedt discovered natural zeolite, stilbite in 1756 [9], which was the beginning of the zeolite history. He named those hydrated aluminosilicate minerals as "zeolites" [originating from Greek words *zein* and *lithos* meaning to boil and rock respectively], because such minerals fused readily with intumescence (the phenomenon of melting and

boiling at the same time) when heated in a blowpipe flame [4]. Due to limited availability of the material, much improvement in the research field was not observed for the next 200 years [10]. Extensive research work on zeolites began in the 1930's, when Richard M. Barrer started systematic studies on zeolite synthesis under high pressure and temperature and on the characterization of zeolite structure and chemistry [10, 11]. Mobil (USA) developed the research activities on zeolites by introducing organic cations into zeolite synthesis in the 1960's and started to discover the catalytic importance of their MFI type zeolites in the 1970's[10,12]. Till now several zeolite materials have been successfully prepared through continued synthetic efforts with new framework topologies, compositions and properties which correspond to 174 structure types of zeolites.

1.6 Nomenclature of zeolite

"The Structure Commission of the International Zeolite Association" and IUPAC have assigned each zeolite structure with official three-letter codes [13, 14]. The codes are derived from the name of the zeolite or the type of material, e.g. FAU from **fau**jasite, LTA from **L**inde **T**ype **A**, MFI from ZSM-5 (Zeolite Socony **M**obil **F**ive)[14]. The IUPAC designation and year of innovation of some zeolites are given in **Table 1.2.**

Table 1.2 IUPAC designation of some zeolites and year of innovation

Zeolite	IUPAC Nomenclature	Year	Zeolite	IUPAC Nomenclature	Year
Analchime	ANA	1978	Linde Type A	LTA	1978
ALPO-11	AEL	1987	ZSM-5	MFI	1978
Beta	BEA	1992	Mordenite	MOR	1978
Erionite	ERI	1978	MCM-22	MWW	1997
Faujasite	FAU	1978	SSZ-23	STT-23	1998

1.7 Classification of zeolites

Compositional variation of zeolites (silicon to aluminium ratio) can be used to classify zeolites into low silica and high silica zeolites. Typical examples of low silica zeolites are A, X and Y. These zeolites cannot be synthesized over a wide range of silicon to aluminium ratio. On the contrary, high silica zeolites can be synthesized over a wide range of silica to alumina ratio, a classical example being ZSM-5, whose acidity can be tuned to desired level. Zeolites can also be classified on the basis of the SBU, as small pore zeolites with 8 membered rings like MTN, NU-l; medium pore zeolites, MFI, MEL; large pore zeolites FAU, MTW and extra large pore zeolites-UDT (Meir et al., 1992).

There are many naturally occurring zeolites but the mordenite and faujasite classes are of the greatest interest as catalysts. The name of some natural and synthetic zeolites is listed in **Table 1.3** [15].

Table 1.3 Some natural and synthetic zeolites

Name	Formula	Ring size
Faujasite^{n}	$Na_{58}Al_{58}Si_{134}O_{384}.24H_2O$	4,6,12
Natrolite^{n}	$Na_{16}Al_{16}Si_{24}O_{80}.16H_2O$	4,8
Stilbite^{n}	$Na_4Ca_8Al_{20}Si_{52}O_{144}.56H_2O$	4,5,6,8,10
Linde A^{s}	$Na_{12}Al_{12}Si_{12}O_{48}.27H_2O$	4,6,8
ZSM-5^{s}	$Na_3Al_3Si_{93}O_{192}.16H_2O$	4,5,6,7,8,10
Boggsite^{n}	$Na_{2.9}Ca_{7.8}Al_{18.3}Si_{77.5}O_{192.7}0H_2O$	4,5,6,10,12
Sodalite^{n}	$Na_6Al_6Si_6O_{24}.2H_2O$	4,6
Mordenite^{n}	$Na_8Al_8Si_{40}O_{96}.24H_2O$	4,5,6,8,12

n-natural s-synthetic

1.8 Structure of zeolites

Like most silicates - the zeolites are based on TO_4 tetrahedra (the primary building units), where T is an aluminium or silicon atom (phosphorus in aluminophosphates). The T atom of the TO_4 tetrahedron is located at each of the corners, and the oxygens are located towards the mid-points of the lines joining each T atom .The vast 3-dimensional networks are a result of all four corners for the tetrahedra being shared, producing low density microporous materials. The chemical composition of the framework, the nature of the extra framework species and the type of post-synthesis modification play a very important role in determining the specific properties of a particular zeolitic material. Consequently, structural analysis is a fundamental aspect of zeolite chemistry [16].

Zeolite structures can be thought to exist of finite or infinite (chains, layers etc.) component units. The three different structural variations of zeolite are:

(a) Chain-like structures which generally form needle-like prismatic crystals,e.g. natrolite.

(b) Sheet-like structures where the crystals are flattened platy or tubular with usually good basal cleavages, e.g. heulandites.

(c) Framework structures where the crystals are more equant in dimension, e.g. chabazite.

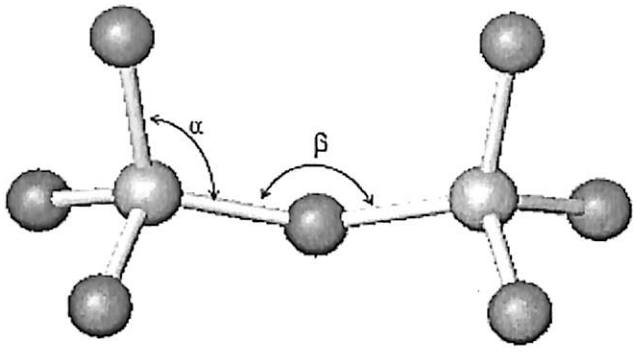

Fig.1.3 TO_4 tetrahedra where α is the O-T-O bond angle and β is the T-O-T bond angle

Zeolite framework can be classified on the basis of various schemes like by pore opening, structural subunit, channel system, framework density, loop configurations and/or by coordination sequences [17]. The zeolite framework consists of cross-linked TO_4 tetrahedra where T is Al or Si. Each T atoms occupy four connected vertices of a three dimensional network and the oxygen occupy two connected positions between the four connected vertices [17]. Having been derived from silicate type network structures, the O/T ratio in a zeolite structure is always equal to 2 [17]. The O-T-O bond angle (α in **Figure 1.3**) is close to the ideal tetrahedra bond angle of 109.5°. The T-O-T bond angle (β in **Figure 1.3**) is much more flexible than the O-T-O bond angle and is usually around 140° to 165°[17].

The TO_4 tetrahedra are often referred to as the primary building units of zeolite structures. Primary building units are linked together to form secondary building units. The notation n^im^i is often used to describe the number and type of rings that make up a cage within a structure. An example of the notation is shown in **Figure 1.4** with the cancrinite cage structure. The cancrinite cage structure is described with the notation 4^66^5 which means that it is composed of six 4-rings and five 6-rings.

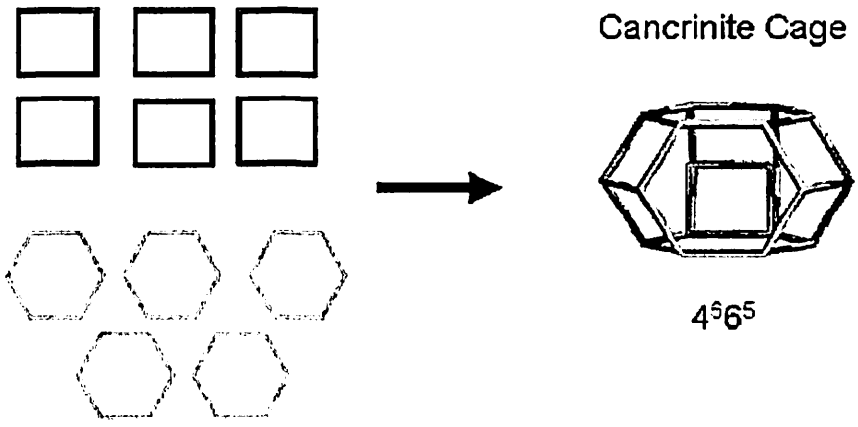

Fig.1.4 Cancrinite cage structure built from six 4-ring and five 6-ring secondary building units

At present, it is possible to visualize all possible existing structures of zeolites with nine such building units; these units are called secondary building units (**SBU**'s). These secondary building units can contain up to 16 T atoms. The SBU's are formed by condensation of the primary building units. Such building units basically consist of n-ring structures which contain as many as 20 tetrahedra and as little as 4 [18]. These are shown in the **Figure 1.5.**These 9 units can be linked with different combinations forming cages or channels within the structure to form all the known zeolite structures. Connecting different ring sizes leads to different cage structures. Each corner in the secondary building units represents the center of a tetrahedra.

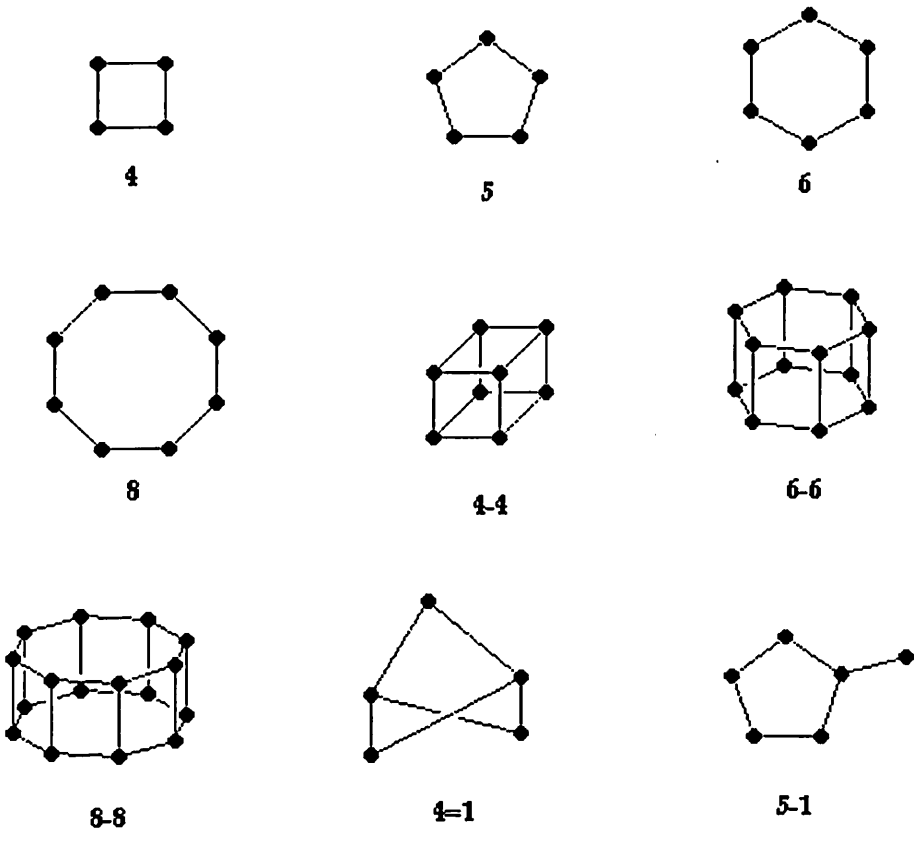

Fig.1.5 Secondary building units of zeolite structure

The framework topology of zeolites consists of primary (the basic building unit) and secondary (the composite building units) building units [19].

Structural Defects: Zeolite framework structures that are closely related often form under very similar conditions leads to the formation of stacking faults or intergrowth structures. The first zeolite intergrowths examined was that of the members of ABC-6 family of structures, zeolite offretite (OFF) and erionite (ERI) with AABAAB and AABAAC 6 ring stacking sequences respectively [20] in which case as the number of C layers increases, the end number of OFF becomes the end number of ERI.

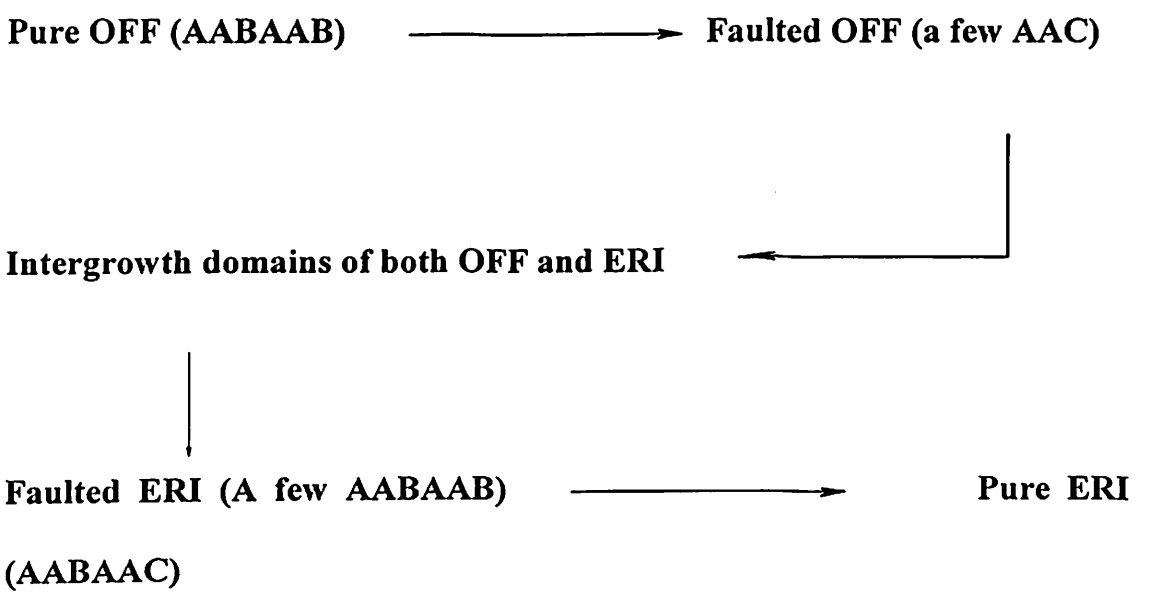

If a stacking fault occurs regularly, a new framework type with a new repeat period is formed. High-resolution electron micrographs of a faulted material will show the local stacking sequences and domain sizes quite clearly [21].

1.9 Properties of zeolites

Zeolites have found wide range of applications due to some of their important properties, which are discussed below:

1.9.1 Acidity of zeolites

The catalytic activity of zeolites is associated with the two types of acid sites:

Brönsted acid sites: When Al^{3+} substitutes Si^{4+} in the framework of zeolite one excess negative charge per aluminium atom is introduced. This negative charge can be compensated either by a proton or extra framework

cation, which is exchangeable that makes zeolites as ion exchangers. If the charge compensation occurs through proton, Bronsted acidity results that make zeolites suitable for acid catalyzed reactions.

This types of acid sites also arises from the bridging hydroxyl group in SiO(H)Al which is associated with tetrahedrally coordinated or framework Al atoms. Each tetrahedrally coordinated Al atom contributes to one potential Brönsted Acid Site [22].

Lewis acid sites: This types of acid sites are capable of accepting electron pairs from adsorbed species like tri-coordinated Al^{+3} [23]. The Lewis acidity is due to the presence of extra framework aluminum species.

There are different ways of generating acid sites in zeolite structure. Two most easy ways are

1. Treating zeolite with ammonium nitrate then calcining it at 480^0 C **(Scheme 1.2) (Figure 1.6).**

2. Directly treating with hydrochloric acid **(Scheme-3) (Figure 1.7).**

Scheme 1.2

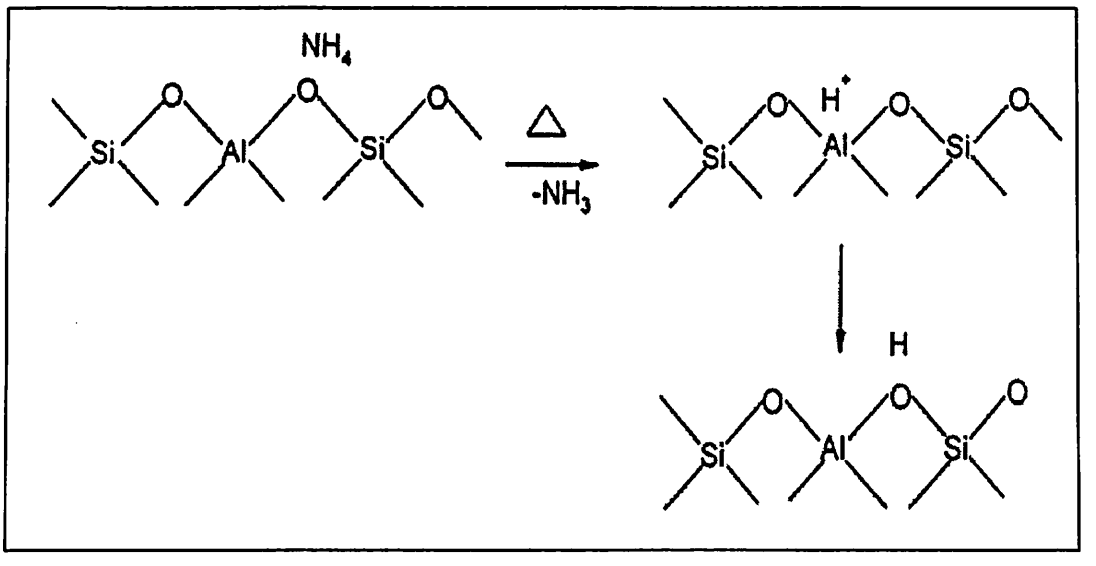

Fig.1.6 Generation of acid sites in MFI by treating with NH_4NO_3

Scheme 1.3

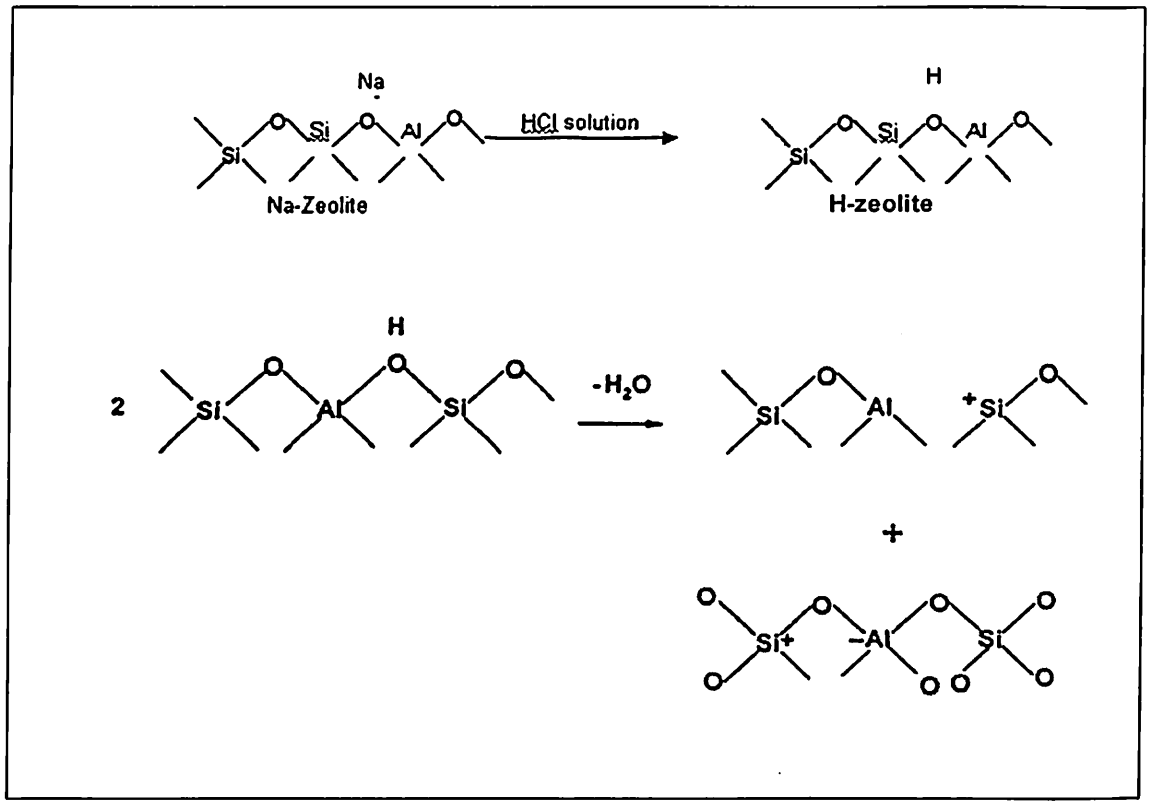

Fig.1.7 Generation of acid sites in MFI by direct treatment HCl.

1.9.2 Molecular sieving property

The three-dimensional framework of zeolites contains a series of channels and voids. These volumes contain cations and water molecules. When water is removed the voids created can take in other molecules. The geometry is the source of the ability of zeolites to separate mixtures of molecules (gases and liquids) on the basis of their effective sizes. Zeolites are therefore described as 'molecular sieves'. There are three types of shape selectivity found in zeolite:

Reactant shape selectivity

It takes place when zeolite catalyst acts as a molecular sieve and excludes certain molecular sizes and structures from the intracrystalline voids (**Figure 1.8**), while other less bulky molecules are able to enter; a whole

variety of zeolite types with different sizes (and shapes) of the pore orifices are available so that this critical exclusion limit can be varied over a wide range of molecular sizes.

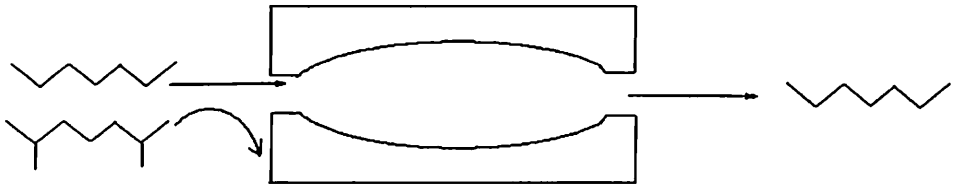

Fig.1.8 Reactant shape selectivity of MFI

Transition state shape selectivity

It occurs when the spatial configuration around a transition state or a reaction intermediate located in the intracrystalline volume is such that only certain configurations are possible (**Figure 1.9**). Transalkylation reactions of alkylaromatics are textbook examples of this kind of selectivity. In other cases, it is not always easy to distinguish between product and transition state shape selectivity. If the catalyst can be synthesized with crystal sizes which are significantly different, the distinction is easily made as only the former selectivity is dependent on crystal size. Transition state shape-selectivity is traditionally linked to the suppression of undesired side reactions such as coke formation.

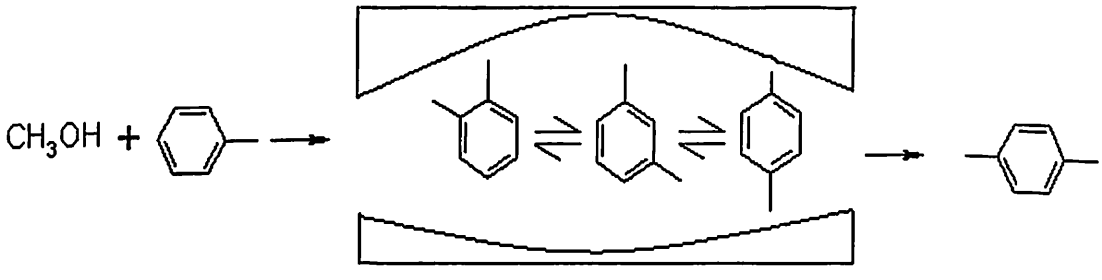

Fig.1.9 Transition state shape selectivity of MFI

Product shape selectivity

It is the result of discrete diffusivities of the different reaction products in the pores of the zeolite crystals (**Figure 1.10**); typical examples are the isomerization reactions of alkylaromatics. This selectivity is not only dependent on the pore size but also on the crystal size of the catalyst particles.

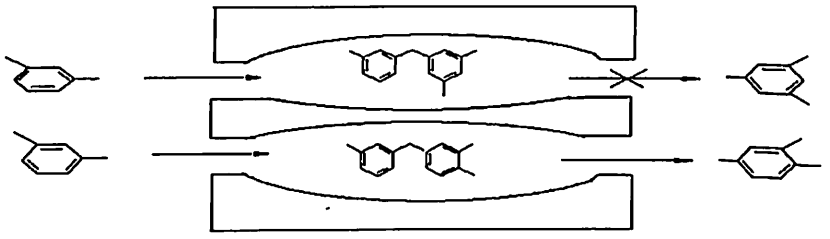

Fig.1.10 Product shape selectivity of MFI

1.9.3 Ion exchange property

Zeolite cages are occupied by ions such as sodium or potassium, these ions are readily exchanged in external solutions (**Figure 1.11**). These cations are primarily present in the structure of the zeolite to counter balance the negative charge generated during isomorphous substitution of silicon atoms by other trivalent metal atoms in the tetrahedral sites [24]. As a result the zeolites have high cation exchange capacity (CEC) and it increases with the increase in aluminium content [25]. The cation exchange process is fully reversible. There are two alternative and equally valid ways of expressing a binary exchange reaction (and consequently the thermodynamic equilibrium constant).

The first of these (most commonly employed) was used by Vanselow [26]:

$$Z_B\ A^{Z_A+}\ (\text{solution}) + Z_A\ BL_{Z_B} \rightleftharpoons Z_A\ B^{Z_B+}\ (\text{solution}) + Z_B A L_{Z_A}$$

Where Z_A and Z_B are respectively the valencies of the exchanging cations A and B. There are also co-anions Y present in the external solution, which maintain electroneutrality in that phase, and these co-anions may be regarded as providing the "exchange capacity" of the electrolyte solution external to the zeolite. L is defined as a portion of zeolite framework holding unit negative charge. Note that the above equation excludes consideration of salt inclusion [27, 28] within the exchanger, since this would involve a net transfer of some co-anions Y from one phase to the other, resulting in an increase in the exchange capacity of the zeolite at the expense of the solution. However, adequate allowance for the possibility of salt inclusion may be made if required [29].

A second way of expressing the reaction may be traced to Gapon [30]:

$$Z_B\ A^{Z_A+}\ (\text{solution}) + Z_A Z_B\ B_{(1/Z_B)}\ L \rightleftharpoons Z_A\ B^{Z_B+}\ (\text{solution}) + Z_A Z_B\ A_{(1/Z_A)}\ L$$

The stoichiometric quantities of A, B, L (and consequently Y) involved in the second eq^n are seen to be the same as in the first eq^n, making the second eq^n an alternative (if less familiar) way of expressing the exchange reaction.

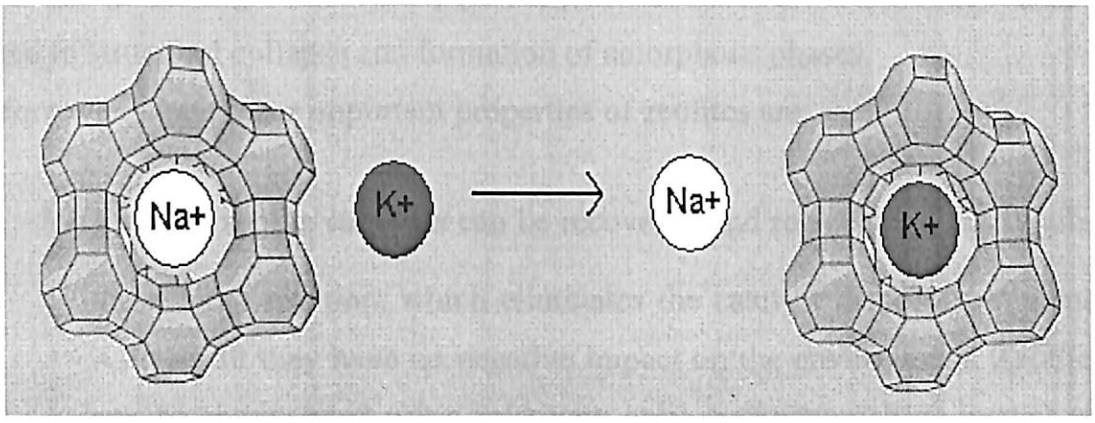

Fig. 1.11 Ion exchange properties of zeolite

1.9.4 Adsorption in zeolites

Due to high porosity zeolites provide a high capacity to absorb guest molecules into the voids of the zeolite structure. Adsorption properties of zeolites are used in different industrial processes, such as drying, separation of mixtures etc. CO_2 removal from nitrogen rejection plants using zeolite 4A is an important industrial process. Zeolites are also used in drying alcohols, benzene, natural gas, ethylene, methanol etc. Zeolites are also used for abatement of pollution due to this property.

1.9.5 Stability of zeolites

Zeolites have high thermal and hydrothermal stability. This property of zeolites makes them very important for catalysis with high reaction temperature. The enhanced stability of the zeolites depends on three main factors: aluminium content, crystal size and sodium level. Larger the crystal size and lower the aluminium and sodium content, more will be stability of the zeolite. There is a variation in thermal stability for different zeolites over a large temperature range. The amount of water loss from the zeolitic pores and

the fundamental solid state transformation are the main factors for structural changes governing their stability [31, 32]. The structural transformation might lead to structural collapse and formation of amorphous phases.
Moreover, some other important properties of zeolites are:

- The solid zeolite catalysts can be recovered and regenerated easily after the desired reaction, which eliminates the catalyst disposal problems. As a result they have no negative impact on the environment. Zeolites can be regenerated using relatively easy methods such as heating to remove adsorbed materials, ion exchanging with sodium to remove cations, or pressure swing to remove adsorbed gases.
- Separation of reactants and products from the catalysts is easy and inexpensive, thus simplifying their repeated use.
- The very large surface area of zeolites has also increased their application manifold.
- High concentration of active sites (acid sites), whose number and strength can be modified in a wide range.
- Possibility of modulating the electronic properties of the active sites.
- Possibility of doping other metals in zeolite framework for use in oxidation chemistry [33].

1.10 Synthesis of zeolite

In general, for synthesis of zeolite an alkaline solution or fluoride solution is taken to this solution desired amount of template is added slowly with constant stirring, by an electrical stirrer. To the resulting solution required amount of silicon source is added slowly with constant stirring. The mixture is thoroughly stirred for half an hour to make a homogeneous gel (A).

In another beaker desired amount of H_2O is taken and to this required amount of aluminium source and salt (for *insitu* modification of the zeolite) is

added slowly with constant stirring. The mixture is thoroughly stirred for half an hour to make a homogeneous gel (B).

Now the gel (A) is added to the gel (B) and the resulting mixture is stirred thoroughly for about 3 hours. The gel is then transferred to a teflon based stainless steel autoclave and is heated in an oven at around 473 K. It is then filtered, washed with de-ionized water and dried at room temperature overnight. It is then calcined in a furnace at about ~ 753 K for about 6 hours. The sample thus prepared is Na form of the zeolite.

For preparation of the acid catalyst the synthesized sample is refluxed with 15% NH_4NO_3 at around 353 K for three times. Finally, it is washed, dried at room temperature and calcined in a furnace at about ~ 753 K for about 6 hours to get the H- form of the catalyst. The raw materials required for the synthesis of zeolites, the source of raw materials and their functions are given in **Table 1.4.**

The flow diagramme of the synthesis system of MFI is

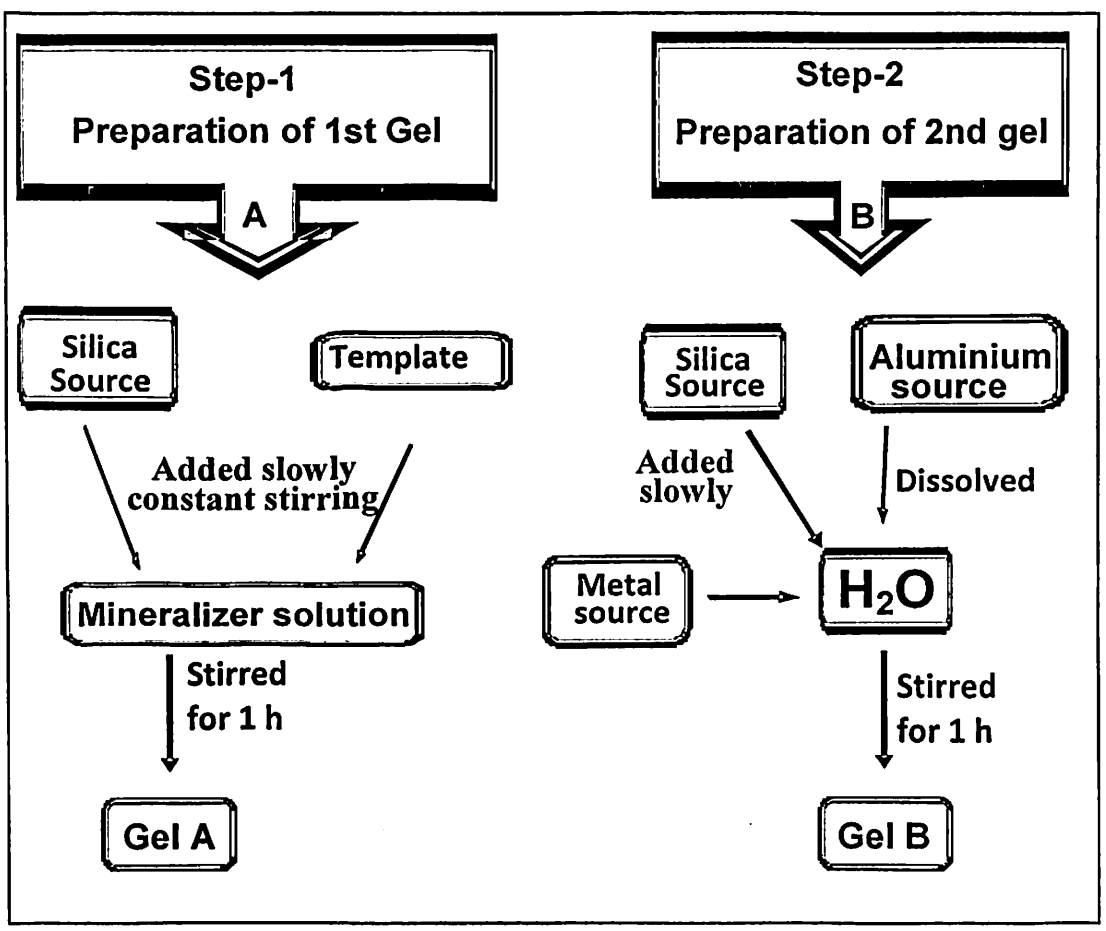

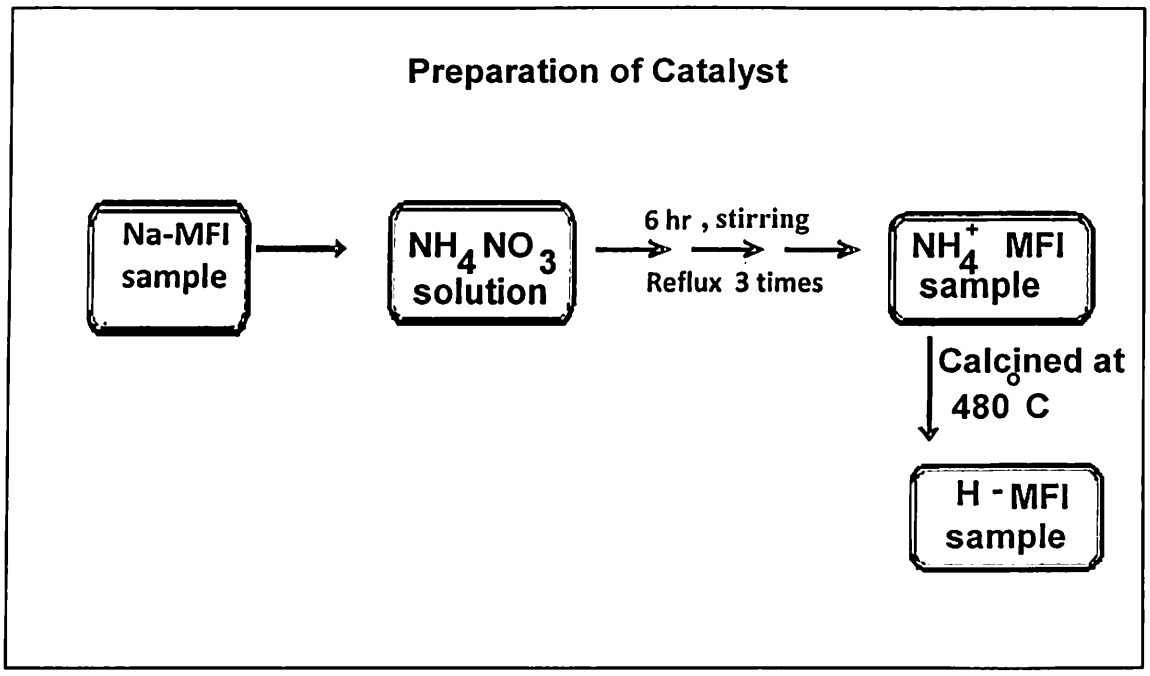
Preparation of Catalyst
Na-MFI sample
NH_4NO_3 solution
6 hr , stirring
Reflux 3 times
NH_4^+ MFI sample
Calcined at 480 °C
H - MFI sample

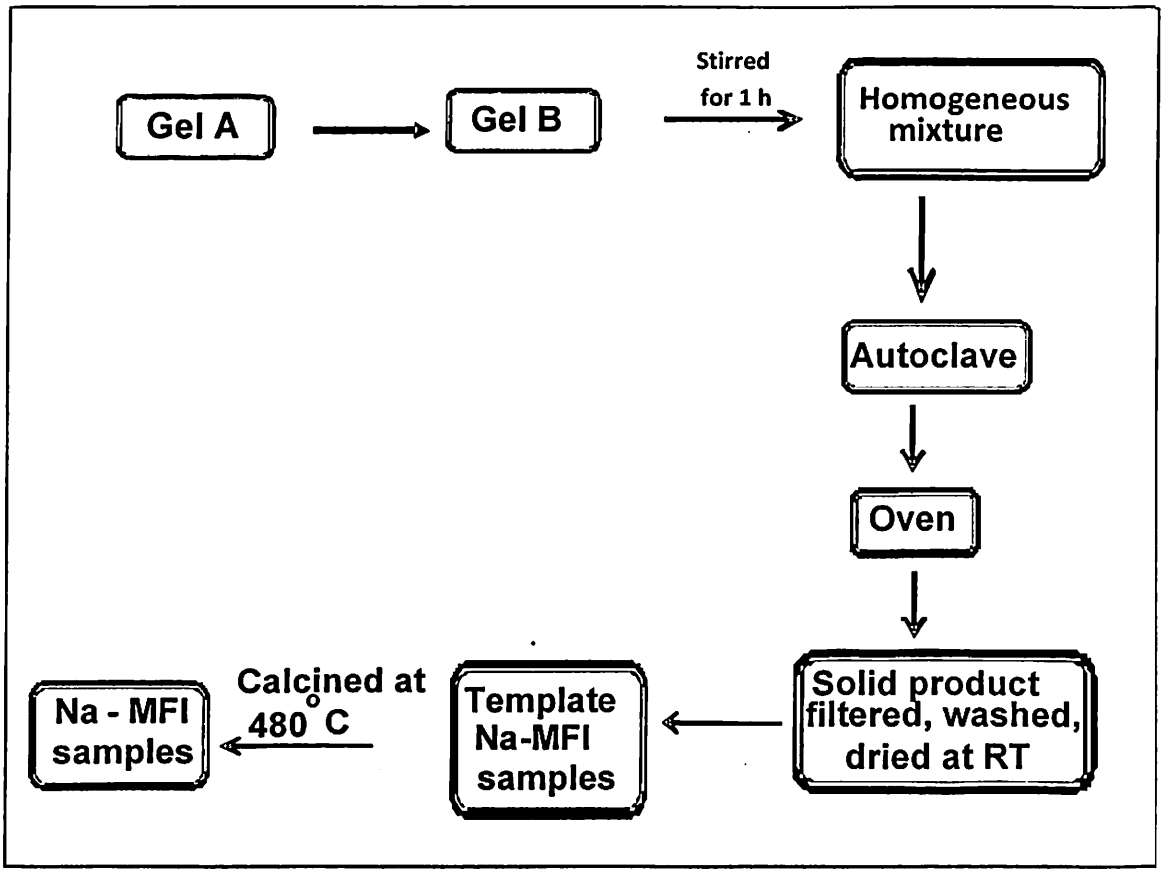
Gel A
Gel B
Stirred for 1 h
Homogeneous mixture
Autoclave
Oven
Solid product filtered, washed, dried at RT
Template Na-MFI samples
Calcined at 480 °C
Na - MFI samples

Table 1.4 The raw materials, the source of raw materials and their function in the zeolite synthesis

Raw Material	Source	Function
Silica	Soluble silicates and their hydrates, silica sols, fumed silica, silica gels, glasses, silicon esters, clays, volcanic tuffs, sand and quartz etc.	Primary building units of the framework.
Alumina	Metal aluminates like sodium aluminate, aluminium sulphates, aluminium alkoxides, freshly prepared aluminium hydroxides, alumina, aluminium phosphates, natural aluminium sources obtained from glasses, sediments, feldspars and aluminium rich industrial wastes etc.	Primary building units of the framework, origin of framework charge.
Metal hydroxides, metal fluorides	Alkali and alkaline earth metal hydroxides, alkali metal fluorides, ammonium fluorides etc.	Hydroxide and fluoride ions act as mineralizer and guest molecules, alkali metal cations act as counter ion of AlO_2.
Organic quaternary ammonium salt	Tetrapropyl ammonium ions, tetrabutylammonium ions tec.	Structure directing agent, guest molecule
Water	De-ionized water	Solvent, guest molecule

1.10.1 Role of template in zeolite synthesis

The frequent association of certain alkali cations with the presence of smaller cage structures led to the concept of a mechanistic role that was designated "templating." Templates are cationic species added to synthesis media to aid/guide in the polymerization/organization of the anionic building blocks that form the framework. In one of the first broad studies of zeolite crystallization in the presence of mixed alkali-organic bases, Aiello and Barrer [34] explained the observed structure specificity of the mixed cations by introducing the concept of templating of the different cage structures by the larger organic and smaller alkali cations. In particular, the quaternary organic tetramethylammonium (TMA) appeared to play an important role in the formation of the OFF and MAZ structures, since these structures were not observed in its absence. The authors suggested that the TMA helped form the aluminosiicate precursor of the gmelinite cage building unit that was common to both structures through a templating action. In a subsequent study of the role of multiple cations, H. Khatami [35] postulated that in the synthesis of zeolites from systems containing ternary, quarternary, or higher numbers of cations, "the zeolite framework structure is determined by one or at most two cations depending on their type and size. Additional cations, should they be included in the lattice, affect the zeolite properties but have minimal or no influence on the structure topology". In 1973 Flanigen reviewed the concepts governing zeolite crystallization and observed that cations play "a prominent structure-directing role in zeolite crystallization. The unique structural characteristics of zeolite frameworks containing polyhedral cages have led to the postulation that the cation stabilizes the formation of structural subunits which are the precursors or nucleating species in crystallization." [36- 38]. The many zeolite compositions and complex cation base systems were compelling examples of the structure-directing role of the cation and the cation "templating" concept. In this early context "templating" and "structure-directing" were synonymous. While talking to the role of template, we may conclude that the template helps in the formation of highly ordered uniform

channels (**Figure 1.12**). The Small individual quaternary alkyl chain length acts as an agent to generate the formation of micropores in the solids.

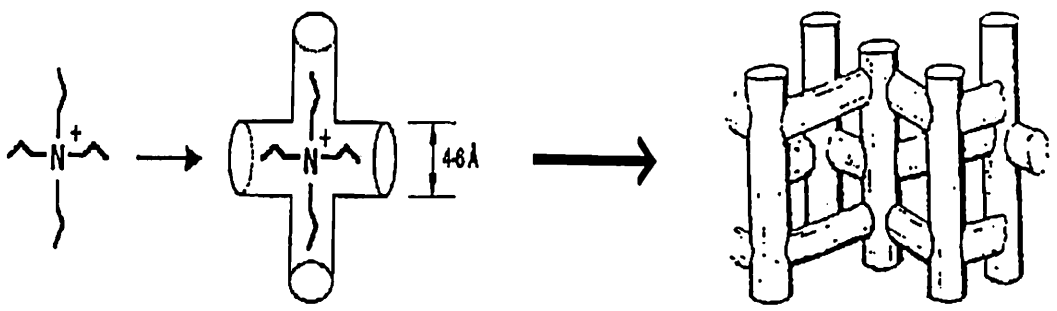

Fig.1.12. Role of TPA-Br in micropore formation in MFI

1.10.2 Factors effecting the formation of zeolite

Synthesis of the zeolites depends mainly on the following factors:

(i) **Temperature:** For many zeolites the raising synthesis temperatures within a certain zeolite synthesis field increases the crystal growth rate [39-41]. As shown in **Figures [1.13 a]** and **[1.13 b]** for zeolite A and zeolite ZSM-5 (MFI), increasing temperature influences the crystal growth rate. In the case of zeolite A the crystal size does not change significantly compared to substantial variation in the ZSM-5 product.

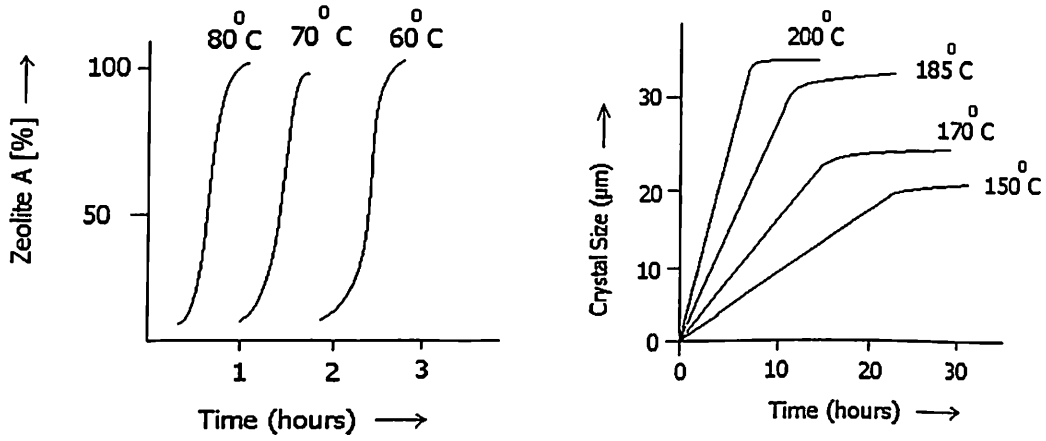

[a] [b]

Fig.1.13 Influence of temperature on the crystallization of [a] Zeolite A and [b] Zeolite ZSM-5.

(ii) **Initial mole ratio:** The framework structure and composition of the crystallized product is greatly influenced by the SiO_2/Al_2O_3 ratio in the reaction system. Low Si/Al ratio (Si/Al ≤ 5) and strong alkalinity is the suitable condition for the preparation of zeolites A (LTA), X (FAU) and hydroxysodalite (SOD), whereas high Si/Al ratio and weak alkalinity is suitable condition for the preparation of zeolites like zeolite beta (BEA), ZSM-11 (MEL) and ZSM-5 (MFI). In general an increase in the SiO_2/Al_2O_3 molar gel ratio increases the thermal stability, acid resistance and hydrophobicity and decreases the ion-exchange capacity [42].

(iii) **Crystallization time:** The crystallization time plays an important role in zeolite synthesis. Increase in crystalline time favours the formation of more crystalline product. However, it is reported that zeolites are thermodynamically metastable phases. In general, Ostwald's law of successive transformation is followed in zeolite synthesis, i.e. from amorphous to metastable to more stable phase. Hence monitoring the reaction time, any particular phase can be identified [43, 44]. However, thermodynamics alone

cannot rationalize the formation of zeolites, kinetics must also be considered [45].

(iv) **pH of the gel:** Raising pH of the synthesis mixtures using OH^- ,mainly influences the crystallization of a certain zeolite in a positive way within the synthesis field. For zeolite A and zeolite ZSM-5 respectively, increasing the pH shows an increase in the crystallization rate. The OH^- is a strong mineralizing agent for bringing reactants into solution. The higher the pH and thus the concentration of dissolved reactants the more the rate of crystal growth of zeolites is enhanced [39, 46].

(v) **Seeding:** In the seeding method, a small amount (2-5 wt %) of the pre-synthesized zeolite material is introduced in the synthetic gel system, in order to have faster crystallization towards a given zeolite and control the size of final crystals [47].

(vi) **Stirring time:** The crystallization kinetics is greatly influenced by the stirring time. The production of small crystals and selectivity for the formation of different zeolite phases can effectively be modified by stirring time. Smaller crystals are obtained by stirring since super saturation can be rapidly achieved due to the accelerated mass transfer [47].

(vii) **Aging period:** The period from homogeneous mixing of the reagents to the onset of heating to the crystallization temperature is referred to as aging. The aging process influences the nucleation crystallization of zeolites by increasing the nucleation rate, reducing the induction period and duration of crystallization period, reducing the crystal size and by increasing the crystal population [48].It also acts as a good factor for the uniformity of the pores.

1.11 Zeolites as catalysts

Depending on the applications, molecular sieves are suitably modified structurally or chemically or in both ways. Chemical treatment, hydrothermal treatment, chemical vapour deposition and selective coking are the well

known methods for the modification of the zeolites. Molecular sieves can also be modified by varying the composition. In zeolites the compositional variation can be achieved by varying the Si/Al ratio or the extent of exchange of cations. Another method, that is of enormous importance, is the variation by isomorphous substitution. The replacement of Si in a purely siliceous molecular sieve by statistically compatible element is termed as isomorphous substitution. Isomorphous substitution of various hetero elements like Al, B, Ga, Ti and Fe have been carried out on various molecular sieves and the resulting systems are promising catalysts for various selective reactions (Perego et al., 1986; Szostak, 1989; Corma, 1997; Arneds et al., 1997). Isomorphous substitution in general can be carried out either to generate acidic or redox properties within the catalytic system. Zeolites have been explored as industrial catalysts in petrochemical and fine chemical industries. In most of these cases, the catalytic activity is due to their acidic nature. This has been in general achieved by isomorphous substitution where tetrahedral silicon will be replaced by a heteroatom. In the case of zeolites this heteroatom will be in general aluminium (Holderich et al., 1991). With the substitution of one aluminium in silicon network, a unit negative charge will be generated. In general this negative charge will be compensated by sodium ions, which are present in the synthetic gel. However, the exchanging these sodium ions with ammonium ions followed by high temperature calcination, one can generate acidic properties in the catalyst. Zeolites are used in a host of acid catalyzed reactions such as alkylation and acylation. The active sites in zeolites are mainly Brönsted acid sites and to some extent the Lewis acid sites. Lewis acidity is formed as a result of trigonally co-ordinated aluminium ions in tetrahedral lattice. Among various zeolites, faujasite, mordenite and ZSM-5 type zeolites are widely used as catalysts. The faujasite type zeolite, namely zeolite-Y has been mainly used for the fluid catalytic cracking and hydrocracking reactions. Mordenite is used in isomerization of light alkenes for octane enhancement of gasoline. ZSM-5 is used widely for the production of fine chemicals. A large array of organic reactions such as isomerization,

rearrangement, alkylation, hydroxylation and acylation has been studied and in all these cases, ZSM-5 has been exploited as a potential catalyst.

1.12 Modification of zeolites

Due to enhanced structural diversity as well as possibility of insertion of the transition metals into the framework structures by isomorphous substitution of silicon or/and aluminium, Zeolite provides considerable research interest in the catalysis field. Some of the important properties of zeolites like their structural features, surface area, crystallinity, pore size etc as well as their inherent properties like acidity, shape selectivity, catalytic properties etc can be modified by appropriate design. It is found that the modified zeolites are finding more applications as heterogeneous catalysts as compared to that the zeolites obtained by direct hydrothermal process [48].

Zeolites can be modified mainly by the following two methods:

(i) By *insitu* modification

(ii) By post synthesis method

The different approaches for the modification of zeolite is shown in **Scheme 1.4.**

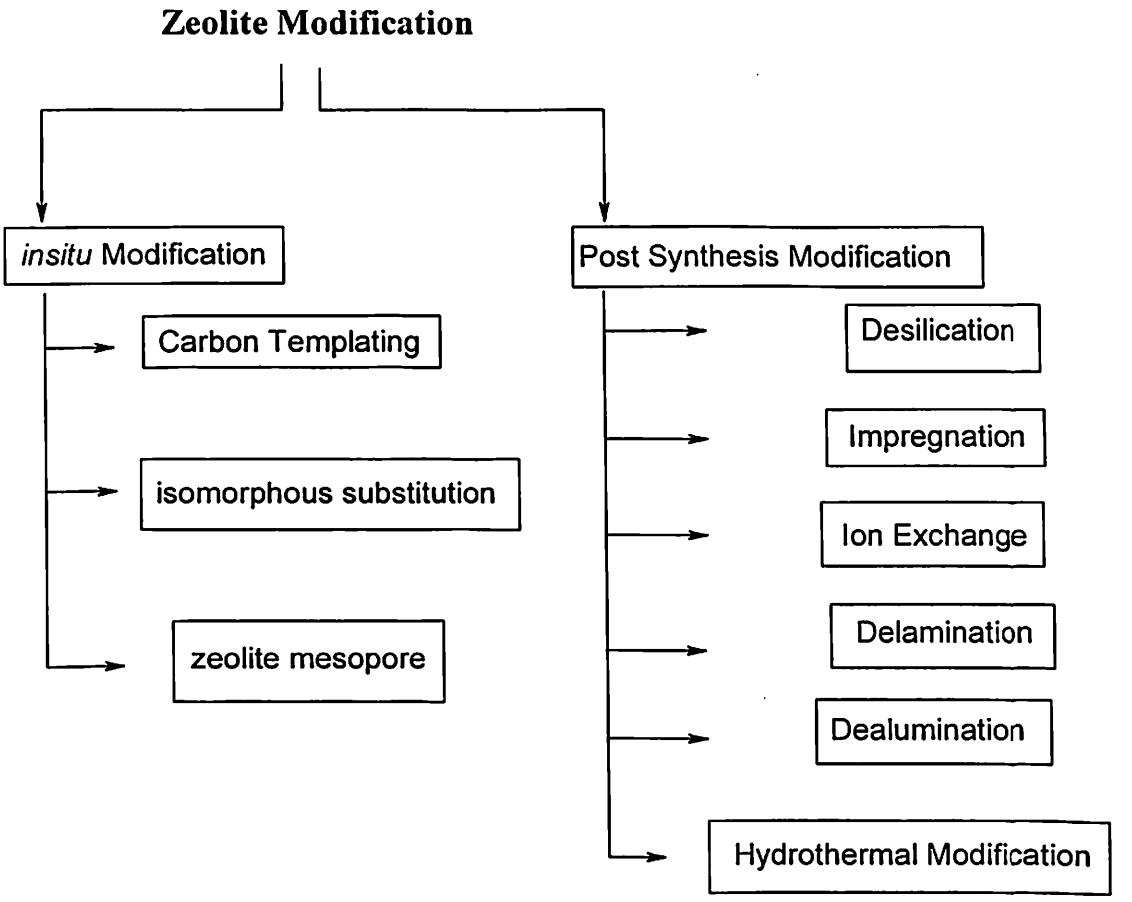

Scheme1.4 Different approaches to modify zeolites for improving their structural features and inherent properties.

(i) *Insitu* modification

(a) Carbon templating: This method is applied in order to obtain a crystalline, highly acidic material with appreciable amount of mesoporosity. This type of modification is carried out by hydrothermal synthesis of mesoporous zeolite in presence of a template with mesoscopic dimensions like carbon black, carbon rods, carbon spheres or carbon nanofibres [49-51]. Zeolite crystal consisting of extra voids in mesoporous range is obtained by removing the carbon template by calcination.

(b) Isomorphous substitution: The molecular sieves when synthesized are obtained in neutral form, so, some suitable method should be adopted to

generate catalytic properties within these materials. This, in general, has been achieved by isomorphous substitution. The isomorphous replacement of Al or Si in the zeolite framework by other heteroatoms to prepare metallosilicates having new physicochemical and catalytic properties is also an important research subject in the field of zeolite chemistry [52]. Isomorphous substitution in zeolite is achieved by incorporation of the desired metal during crystallization under hydrothermal conditions. This results into materials that do not occur naturally. Introduction of transition-metal ions into the zeolite lattice is very interesting because these ions are known to exhibit catalytic activity in homogeneous as well as heterogeneous catalysis. Incorporation of trivalent and tetravalent metal ions into zeolite framework can modify the physicochemical properties such as acidity strength [53], while incorporation of transition metal ions such as Zr, Ru etc. makes zeolites oxidation catalysts, which have been shown to be active in liquid-phase reactions with hydrogen peroxide as an oxidant [54,55]. Chu et al. [53] reported the substitution of Fe into the framework of MFI type silicalite (ferrisilicate), which has a weaker acid strength than its Al or Ga analogues and used it as an oxidation catalyst.

However, the following points have to be considered for an effective substitution (Szostak, 1989).

[i] Substitution of A by B is governed by their radius ratio. Closer the difference between their radius values, greater is the extent of isomorphous substitution.

[ii] The ability of the ion to form tetrahedral oxide ion coordination decides the possibility of isomorphous substitution in molecular sieves.

[iii] The ratios of electro negativities and ionization potentials of the ions A and B also limit isomorphous substitution.

However, it is important to note that ionic charge is not a deciding factor for the feasibility of isomorphous substitution. It only decides the overall framework charge of the molecular sieve. The ionic radii of some of the elements reported to have isomorphously substituted in the zeolite framework are given in **Table 1.5.**

Table 1.5. Metal ions exhibiting tetrahedral coordination and their ionic radii (Szostak, 1989).

Metal ion	Radius (Å)
B^{+3}	0.25
Fe^{+2}	0.77
Fe^{+3}	0.63
Ga^{+3}	0.61
P^{+5}	0.31
Ti^{+4}	0.56
V^{+5}	0.49
Cr^{+3}	0.63

(c) Zeolite-mesopore composite: Several approaches have been made to synthesize a new type of nano composite materials both micro- and mesopores to provide some interesting features. The stability and acidity of mesoporous materials can be improved by preparing composite materials consisting of microporous domains (zeolites) inside mesoporous supports. For example, preparation of composite materials like beta/MCM-48 [58], beta/TUD-1[57] and MOR/MCM-41[58].

(ii) Post synthesis modification

(a) Desilication: The desilicated forms of the zeolites X, Y and ZSM-5 are prepared by the selective removal of silicon atoms from the parent zeolites in an aqueous solution of base [59]. Desilication of conventional zeolites in

alkaline medium generates variable intracrystalline mesoporosity, but inevitably changes other properties such as the Si/Al ratio and aluminium distribution. Assessing the individual effects of porosity and composition on the catalytic performance of desilicated zeolites is relevant for their optimal design. This treatment, which decreases the Si/Al ratio while keeping the zeolite framework almost unmodified, enhances the ion exchange capacities of all the zeolites, a property which can be exploited industrially for the X and Y zeolites since the desilicated forms had higher total ion removal rates of calcium and magnesium ions from hard water. Similarly, desilication results in a higher density of acid sites. In catalytic testing studies, the desilicated ZSM-5 zeolite was found to display a higher total conversion in the dehydration of absolute ethanol into ethylene, however the selectivity for ethylene was higher for the parent zeolite at lower reaction temperatures.

(b) Impregnation: Impregnation of zeolites does not change the basic structure of zeolites but is employed for modifying the surface behavior, acidity, basicity, reforming capability etc. This modification process is quite simple and can be tried in different concentration of the impregnating species to attain the desired property. A few examples of impregnations are – modification of FAU zeolite by CsOH to induce basic properties [59], modification of β zeolite by Pt impregnation shows high reforming capability to naphthenic feeds [60], E. David [61] prepared Mg clusters in zeolite 4A for use in catalytic processes. Zeolites play an excellent role as supporting material for metals [62]. Chemical nature and high surface area makes zeolites highly versatile for impregnation of metals.

(c) Ion exchange: Zeolites have a network of pores and cavities having molecular dimensions. The network of pores can accommodate a wide variety of cations, such as Na^+, K^+, Ca^{2+}, Mg^{2+} and others. These positive ions are rather loosely held and can readily be exchanged for others in a contact solution. Barrer [52], first reported that by ion exchange modification of zeolites, their molecular sieving properties can be intensely changed. In order

to meet the best requirements of some applications like water softening and purification, for octane enhancement and good gasoline selectivity, in pollution abatement and toxic waste management etc. zeolites had been modified both by cation exchange method as well as by rare earth exchange method for tailoring the molecular sieves. In order to enhance the sorption capacities of zeolites, the exchangeable K^+ and Na^+ cations in zeolite framework can be stoichiometrically exchanged by other mono-, di- or trivalent cations. Ion exchange process can simply be carried out by stirring a zeolite with the salt solution containing the cation to be exchanged with the cation of the zeolite at a particular temperature. Ion exchange can also be carried out via solid-solid reaction between the zeolite and the salt or oxide in hydrothermal conditions [63, 64].

(d) Delamination: The delamination of the layered precursor of the zeolite results in the formation of individual layers of variable thickness. The resultant material presents the strong acidity and stability, characteristic of the zeolite, but at the same time, offers the high accessibility to large molecules characteristic of the amorphous aluminosilicates. Much improvement in diffusion of initial products in catalytic applications, reducing consecutive reactions [65] is found in delaminated materials.

(e) Dealumination: Dealumination process is employed for the selective extraction of Al from the zeolite framework leading to the formation of more stable high silica zeolites with large pores/mesopores [66, 67]. The created mesopores are isolated and donot constitute an interconnected network of pores. The dealumination of zeolite can be carried by steaming, treatment with ammonium hexafluorosilicate, and with silicon tetrachloride. The zeolite framework can be dealuminated most effectively through ion exchange into the sodium form followed by treatment with silicon tetrachloride. The crystalline structure remains essentially intact.

(f) Hydrothermal modification: This modification is carried out for expulsion of tetrahedral Al from the framework into non-framework position. This modification is performed heating ammonium exchanged zeolites in presence of steam. On modification the framework Si/Al ratio increases while unit cell size decreases [1]. Thus ultrastable zeolites having fewer ion exchange as well as Brönsted acid sites are obtained.

1.13 Removal of template

Removal of the template plays an important role in the preparation of final microporous solid. In order to preserve the final micro-structure, in general, removal of the template can be achieved by calcination process, where the as synthesized material will be subjected to a controlled heat treatment. Calcination has to be done in a flow of inert gases at the initial stages followed by the flow of air. This is to maintain the crystallinity of the material.

1.14 Choice of fluoride medium

A significant breakthrough in the field of zeolite synthesis occurred when hydroxyl anions were replaced by fluorides, making the synthesis possible in neutral and even in acidic media (pH =5) [68]. Synthesis using a fluoride containing medium obtained by replacing the hydroxyl ion (OH^-) with fluoride ion (F^-) as a mineralizing agent, produces zeolites at lower pH values, but with the same morphology as the alkaline route [69].

Later on, Guth and Kessler developed the synthesis of several microporous materials: aluminosilicates, aluminophosphates and gallophosphates via this alternative non-alkaline route [70-74]. The use of the fluoride ion as mineralizer (by using NH_4F source) instead of the conventionally used hydroxide ion presents several advantages:

- Fewer metastable phases are formed which implies a certain ease of preparation of any desired zeolite [73,75 ,76]
- Synthesis of materials not obtainable in alkaline media like the 20-T-ring gallophosphate cloverite [77]
- Formation of large crystals with few defects which are of interest as model host materials (for adsorption or diffusion studies) [78]
- Neutral (or acidic) medium enables the incorporation of elements sparingly soluble in alkaline media: Co^{2+},Fe^{3+},Ti^{4+} [72,73]
- Direct formation of the quarternary ammonium form ZSM-5, instead of Na-ZSM-5 avoiding repeated ion-exchange; so only a calcination step is needed to burn off the template and to obtain the acidic H-ZSM-5.

Recent studies have shown that even after calcination fluorine remains occluded inside the small cages found in the MFI structure [75,78,79]. Inspite of the numerous advantages of the synthesis in fluoride media, the presence of such highly electronegative element modifies the electron density around the neighbouring Si by the formation of $[Si_{4/2}F]^-$ entities [78-80]. Thus, this may also influence the catalytic properties of the zeolite.

The introduction of transition metal cations inside zeolite micropores and/or framework, led to the development of many redox catalysts or even bifunctional catalysts [81,82].Along with the design of novel ''tailor-made catalysts'' came the necessity to develop new characterization methods giving informations about the metal introduced in the framework (quantity, location, geometry), which are of primary importance to understand the catalytic activity.

1.15 Characterization of microporous materials

Characterization is one of the most important aspects in any type of synthesis. Without proper characterization we cannot definitely say that the

desired material is formed. For catalytic characterization of Zeolites, the important methods used are X-ray Diffraction (XRD), Fourier Transform Infrared spectroscopy (FTIR), UV-Visible diffused reflectance spectroscopy (DRS), Scanning Electron Microscopy (SEM), Thermogravimetric analysis (TGA), N_2 Adsorption-desorption isotherm etc. These techniques have been employed in order to understand the physico-chemical properties like formation of the microphase, incorporation of the heteroatom in the framework, thermal stability, pore size, morphology and active surface area.

1.15.1 X-ray diffraction (XRD)

XRD is one of the most important techniques in catalytic characterization. The principle of XRD, suggested by Bragg [83] is that reflection of X-ray can take place only at certain angles which are determined by the wavelength of the X-ray and the distance between the planes in the crystal. The fundamental equation which gives a simple relation between the wave length of the X-ray (λ) the interplaner distance (d) in the crystal and the angle of reflection (Θ) is known as Bragg equation which is

$$n\lambda = 2d\sin\Theta$$

XRD study helps mainly in identification of the phase, crystallization and dimension of crystals. Microporous molecular sieves show characteristic peaks in the 2θ range of $5\text{-}50^0$, whereas the mesoporous materials exhibit characteristic peaks in the low angle region between $1.5\text{-}10^0$ (2θ). Crystallinity of the MFI samples is calculated using the following relation:

$$\%C = 100 \text{ X } I_{hkl}/ (I_b + I_{hkl})$$

For a particular crystallographic plane (*hkl*) where, I_{hkl} is the corrected integral XRD peak intensity and I_b is the integral background intensity for the same plane. Scherrer formula $D_{hkl} = K\lambda/ (\beta \text{ X } \cos\theta)$ was used to determine the crystallite dimension (D_{hkl}) of the identified crystalline phase [84]. Here, β is the full width at half maximum; K is the shape factor; θ_{hkl} is the Bragg angle

and λ is the wavelength of Cu $K\alpha_1$ radiation. The information obtained from XRD patterns are given in **Table 1.6.**

Table 1.6 Information obtained from XRD patterns [85].

Feature	Information
Peak positions (2θ values)	Unit cell dimensions
Non-indexable lines	Presence of a crystalline impurity (or incorrect indexing)
Systematically absent reflections	Symmetry
Background	Presence (or absence) of amorphous material
Width of peaks	Crystallite (domain) size Stress / strain
Peak intensities	Stacking faults Crystal structure

1.15.2 Fourier transform infrared spectroscopy (FT-IR)

When infra red light is passed through a sample, some of the frequencies are absorbed while other frequencies are transmitted through the sample without being adsorbed. If we plot absorbance or transmittance against frequency the result is an IR spectrum. A particular molecule only absorb IR light of particular frequency if there is an energy transition within the molecule such that $\Delta E = h\nu$. The transition involved in IR absorption is associated with vibrational change within the molecule. From the characteristic band appeared, we can identify the sample [86]. The KBr pellet technique is frequently used for investigations of vibrations of the framework [87-89]. IR spectrums are shown by molecules when vibrational motion is accompanied by a change in the dipole moment of the molecule [90].

Vibrations of the frameworks of zeolites give rise to typical bands in the mid and far infrared. A distinction is made between external and internal vibrations of the TO_4 tetrahedra (with, for example, T = Si or Al). The positions of bands due to vibrations of external linkages are often very sensitive to structure. The assignments of main IR bands are given in **Table 1.7**.

Table 1.7 The assignments of the main IR bands [87].

Structure	Vibrational Mode	Absorbance Band
Internal tetrahedra	Asymmetric stretching	920-1250 cm^{-1}
	Symmetric stretching	650-720 cm^{-1}
	T-O bending	420-500 cm^{-1}
External linkages	Double ring vibrations	500 - 650 cm^{-1}
	Pore opening vibrations	300 - 420 cm^{-1}
	Symmetrical stretch	750 - 820 cm^{-1}
	Asymmetrical stretch	1050 - 1150 cm^{-1}

1.15.3 Thermal gravimetric analysis (TGA)

This method is used to determine the thermal stability, acidity as well as the isomorphous substitution in the zeolite. In the pure silica sample the differential gravimetry (DTG) shows an asymmetric, well defined single reaction interval commencing at 388^0C and ending at 626^0C. There is very little water loss and no drift in the DTG base line is observed, indicating the presence of hydrophobic material. Mass losses upto ~ 475^0 C can be attributed to the degradation of three types of TPA^+ cations occluded in the framework as identified by El Hage-Al Asswad [91] and co-workers. Losses above

~ 475^0 C, causing the asymmetrical reaction interval is due to those TPA^+ cations which are ion-paired to occluded mineralizer anions. In case of the DTG traces of the metal substituted gel compositions the reaction intervals increase with the increasing mole fractions and there are extended intermediate plateaus, which are due to the overlap of occluded and ion-paired losses, producing a DTG trace displaying two stages of weight loss. There is also broadening of the second mass loss interval with increasing levels of substitution. These changes are due to the increasing negative charges introduced into the previously uncharged pure silica framework being counter balanced by the cationic species. TGA can be used to accurately detect the desorption of basic molecules from a zeolite as a function of temperature and the resulting data can be used to calculate the acid site strength and distribution of various zeolites. The acidity of a zeolite is calculated by the following formula and reported in units of millimoles of acid sites per gram of zeolite.

Acidity = (% Mass Loss/100) (1/MW of Base) (1000 mg/1g)

Where MW stands for molecular weight of the base.

1.15.4 Diffuse reflectance UV-Vis spectroscopy

This is an important technique in characterizing sample where the absorption of UV-VIS radiation by a molecule leads to transition among the electronic energy level of the molecule [92]. The UV–Vis diffuse reflectance spectroscopy is a suitable technique to study solids, particularly dispersed oxides [93] and metal ions in constrained environment such as MCM, zeolites and clay materials [94–96] to obtain information on the coordination environment, oxidation state of the embedded transition and rare earth metal ions. The absorption in the UV-Vis range arises because of "ligand to metal charge transfer" (L→M). The position of the L→M band depends on the ligand field symmetry surrounding the metal centre. Hexa-coordinted L→M electronic transitions require less energy than for a tetra-coordinated metal ion.

Transitions in the UV region 200-400 nm are of great interest for most of the isomorphously substituted microporous and mesoporous metallo-silicate materials.

1.15.5 N_2 adsorption-desorption isotherm

Most methods used to measure surface area of solid catalysts are based on the isothermal adsorption of nitrogen. Either a single point or multipoint method is used to calculate the surface area. At Engelhard, the multipoint Brunauer, Emmett and Teller (BET) method is used to measure total surface area of fresh and equilibrium moving bed and fluid catalytic cracking (FCC) catalysts. It is also used as a quality control tool during catalyst manufacture. The textural properties of the metal substituted calcined zeolites are also evaluated from the nitrogen adsorption-desorption isotherm. As per IUPAC classification of adsorption in microporous material [97], N_2 adsorption-desorption isotherms of the calcined zeolites exhibit high nitrogen uptakes at low relative pressures. The closure of the hysteresis loop around 0.4 P/P_0 relative pressures is due to the well-known tensile strength effect of the adsorptive, and does not represent any physical porosity at this particular relative pressure [98]. The sub step observed between 0.1 and 0.3 relative pressures in the isotherm is a characteristic of MFI-type zeolites [98] and is associated with a fluid-to- solid-like phase transition of the adsorbed nitrogen in the microporous network. These isotherms also reflect nitrogen uptake in the MFI type micropores at low P/P_0 followed by capillary condensation in the void spaces created by the packing of nanoparticles. Micropore volume, micro pore area and external surface area were calculated using t-plot method. N_2 adsorption is also observed at high relative pressures, which is explained to originate from the N_2 adsorption in the interparticle voids. At intermediate relative pressure, a significant adsorption takes place due to the N_2 adsorption on the external zeolite surface.

1.15.6 Scanning electron microscopy (SEM)

SEM is used to observe the surface topography that is terraces, steps, kinks and dislocations on a surface of solid samples. In this technique a focused beam of electrons with a well defined de-Broglie wave length replaces the lamp found in traditional light microscope. Instead of glass or quartz lenses, magnetic fields are used to focus the beam. Electrons scattered from the small irradiated area are detected and the electrical signal is sent to a video screen. An image of the surface is then obtained by scanning the electron beam and the detector across the sample. SEM imaging is often preferred in place of optical imaging because of the enhanced depth of field. The information that can be drawn from SEM pictures of zeolites is given in **Table 1.8.**

Table 1.8 Informations drawn from SEM pictures of zeolites [99].

Subjects	Details
Crystal form	Type of zeolite Aspect ratio Influence on crystal growth, eg. inhibition of crystal faces that indicate the presence of an unknown factor Crystal size distribution phenomena, eg. Aggregation / twinning / intergrowth Indication of single crystals
External surface	Relative roughness Secondary nucleation effects
Purity of the phase	Other zeolite types Amorphous material
Unknown species	New material?

1.16 Description of MFI zeolite used in the present investigation

ZSM-5 (MFI) catalyst was first synthesized by Argauer and Landolt in 1972 [100]. MFI is a synthetic zeolite, closely related to ZSM-11(MEL). There are many ways to synthesize MFI, a common method is as follows [101]:

$$SiO_2 + NaAlO_2 + NaOH + N(CH_2CH_2CH_3)_4Br + H_2O \rightarrow MFI$$

MFI is typically prepared at high temperature and high pressure in a Teflon-coated autoclave and can be prepared using varying ratios of $SiO_2$and Al containing compounds. MFI Zeolite is composed of several pentasil units linked together by oxygen bridges to form pentasil chains. A pentasil unit consists of eight five-membered rings. In these rings, the vertices are Al or Si and an O is assumed to be bonded between the vertices. The pentasil chains are interconnected by oxygen bridges to form corrugated sheets with 10-ring holes. Like the pentasil units, each 10-ring hole has Al or Si as vertices with an O assumed to be bonded between each vertex. Each corrugated sheet is connected by oxygen bridges to form a structure with "straight 10-ring channels running parallel to the corrugations and sinusoidal 10-ring channels perpendicular to the sheets" [102]. Adjacent layers of the sheets are related by an inversion point. The estimated pore size of the channel running parallel with the corrugations is 5.4–5.6 Å [103]. The crystallographic unit cell of MFI has 96 T sites (Si or Al), 192 O sites, and a number of compensating cations depending on the Si/Al ratio, which ranges from 12 to infinity. The structure is orthorhombic at high temperatures, but a phase transition to the monoclinic occurs on cooling below a transition temperature, located between 300 and 350 K [104,105].

1.17 Objectives of the present research work

The advent of supra-molecular chemistry has given a new thrust to this field of porous solids. Even though various oxide materials have been prepared in mesoporous and microporous form, lack of proper crystallinity of the resulting solids made them not suitable for industrial applications. However, constructing solids with expected porous texture and architecture is one of the dreams of scientists. There are a number of possibilities and combinations for building up supra-molecular structures over which the porous solids can be constructed. It is therefore necessary to examine and probe scientifically the suitability of these materials especially with respect to their surface properties for the possible technical applications envisaged. The motivation of the present study is therefore to synthesize microporous solids at lower pH range and to examine their catalytic activity for some typical organic transformations.

The catalytic activity of molecular sieves can be improved by the incorporation of heteroatoms into the framework structure. The introduction of metals like Zr, Ru and In inside zeolite micropores and/or framework leads to the development of many redox catalysts or even bifunctional catalysts [106,107].

Zirconia-based materials have wide applications in the field of catalysis in dehydration, hydrogenation, hydroxylation, oxidation and epoxidation reactions owing to the moderate acidity and oxidizing capabilities.

In-MFI samples have found wide range of applications for selective catalytic reduction [108].

The Ru^{3+} ion has a larger ionic radius (0.69 Å) than Al^{3+} (0.57 Å) and like iron (preceding member of Group 8), it has a tendency to form insoluble hydroxides in a basic environment and an ability to change oxidation state that is why it can be used as redox catalyst in many organic reactions.

The Zr-HMFI catalyst was prepared by ion-exchange using a commercial H-MFI zeolite as the starting material. However, the catalysts prepared in this method have low surface areas which restrict their industrial applications. There are early claims of synthesis of crystalline zirconium

silicas with zeolitic properties, details of which are not available in the literature. Dongare et al. reported the synthesis and characterization Zr-MFI [109]. However synthesis was carried out in presence of solvent and crystallization was completed in 48 h.

Methods that have been tried so far for the preparation of In-MFI are the ion-exchange, precipitation, mechanical mixing and dry techniques based on the use of $InCl_3$: solid-state ion exchange, sublimation, and transport reaction processes mainly, but the *insitu* modification of the MFI zeolites with indium have not yet been reported.

The incorporation of ruthenium into zeolites has been recently reviewed [110]. This has been achieved using potassium ruthenate (VI), K_2RuO_4, and tetra-n-propylammonium perruthenate (VII), $(Pr_4N)RuO_4$. The method is somewhat cumbersome and quite a lengthy process. In the present study ruthenium salts are used as a source of Ru and the process takes comparatively shorter time for completion.

The specific aims of the present study are

- Synthesis of MFI zeolite in a broad range of silicon to aluminium ratios using fluoride gel as mineralizer.
- *in-situ* modification of the MFI samples (SAR= 200 and 100) by introduction of Zr, Ru & In metal.
- Characterization of the synthesized and modified samples by XRD, FT-IR, TGA, UV-Vis (DRS), N_2 adsorption and SEM techniques.
- Study of the catalytic activity of the synthesized and modified MFI zeolite with respect to organic reactions like hydroxylation of phenol.

1.18 Reference

[1] K.S.W.Sing, D.H. Everett, R.A.W. Haul, L. Moscou, R.A. Pierotti, J. Rouquerol, T. Siemieniewska, *pure Appl.Chem.* 57 (1985) 603.

[2] K. S. W.Sing, D. H. Everett, R. A. W. Haul, L. Moscou, R. A. Pierotti, J. Rouquerol and T. Siemeieniewska, *"Reporting Physisorption Data for Gas/Solid Systems with Special Reference to the Determination of Surface Area and Porosity." Pure Appl. Chem.* 57 (4): (1985) 603.

[3] S. Brunauer, L. S. Deming, W. E. Deming and E.Teller, *"On a Theory of the van der Waals Adsorption of Gases." J. Am. Chem. Soc.* 62 (7): (1940) 1723.

[4] A.F. Cronstedt, *Observation and Descriptions: On an unknown Mineral Species called Zeolites*, R.V. Ballmoos, J.B. Higgins, M.M.J. Treacy(Eds.),Proc. Int. Zeolite Conf. 9th Butterworthh-Heinemann, Boston(1993) 3.

[5] L. Moscou, *Introduction to Zeolite Science and Practice*, H.V. Bekkum, E.M. Flanigen, P.A. Jacobs, J.C. Jansen (Eds), Elsevier, Amsterdam, *Stud. Surf. Sci. Catal.* 58 (1991)1.

[6] T. Maesen, B. Marcus, *Introduction to Zeolite Science and Practice,*2nd Edn., H.V. Bekkum, E.M. Flanigen, P.A. Jacobs, J.C. Jansen (Eds), Elsevier, Amsterdam, *Stud. Surf. Sci. Catal.* 137 (2001) 1.

[7] D.H. Lauriente, Y. Inoguchi, *The Chemical Economics Handbook-SRI Consulting*, (2005)599.1000 A-599.02 K.

[8] F.D. Renzo, F. Fajula, *Introduction to molecular sieves: trends of evolution of the Zeolite Community*, J. Cejka, H.V. Bekkum (Eds.), Elsevier, Amsterdam, *Stud. Surf. Sci. Catal.* 157 (2005) 2.

[9] A.F. Cronstedt, *Akad.Handl. Stockholm* 18 (1756) 120.

[10] E.M. Flanigen, *Introduction to Zeolite Science and Practice,*2nd Edn., H. V. Bekkum, E.M. Flanigen, P.A. Jacobs, J.C. Jansen (Eds.), Elsevier, Amsterdam, *Stud. Surf. Sci. Catal.* 137 (2001) 11.

[11] R.M. Barrer, *Proc. Roy. Soc.* 167 A (1938) 392.

[12] N.Y.Chen, *Ind.Eng.Chem.Res.*40(2001) 4157.

[13] C.Baerlocher, L.B.McCusker, http:// www.iza-structure.org/databases.

[14] C.Baerlocher, W.M.Meier, D.H.Olson, *Atlas of Zeolite Framework Types* (formerly Atlas of Zeolite Structure Types), Elsevier, Amsterdam (2001).

[15] J.V. Smith, *Chem. Rev.* 1988, 88, 149, W.M. Meier,; D.H. Olson, *Atlas of Zeolite Structure Types*, 2nd Ed.,; Butterworths: London, 1987

[16] L.B.McCusker, C. Baerlocher, *Introduction to Zeolite Science and Practice,* 2nd Edn., H.V. Bekkum, E.M. Flanigen, P.A. Jacobs, J.C. Jansen (Eds.), Elsevier, Amsterdam, *Stud. Surf. Sci. Catal.* 137 (2001) 37.

[17] R. F. Lobo, "*Handbook of Zeolite Science and Technology*" Marcel Dekker Inc. 2003.

[18] C.D. Williams, *Zeolites*, University of Wolverhampton.

[19] R. Szostak, *Molecular Sieves: Principles of Synthesis and Identification,* Van Nostrand Reinhold, New York (1989).

[20] J. M. Bennett, J.A. Gard, *Nature* (London) 214 (1967) 1005.

[21] L.B. McCusker, C. Baerlocher, *Introduction to Zeolite Science and Practice*, 2nd Edn., H.V. Bekkum, E.M. Flanigen, P.A. Jacobs, J.C. Jansen (Eds.), Elsevier,Amsterdam, *Stud. Surf. Sci. Catal.*, 137 (2001) 56.

[22] J. Scherzer, *Octane Enhancing Zeolites FCC catalysis*, Marcel Dekkar Inc. (1990) 44.

[23] A. Ramsaran, *Desilicated ZSM-5 Zeolite as Catalyst for the dehydration of ethanol*, Ph.D. thesis, Concordia University (1996) 26.

[24] A. Dyer, *Introduction to Zeolite Science and Practice*, 3rd Rev. Edn., J. Cejka, H.V. Bekkum, A.Corma, F. Schiith (Eds.), Elsevier, Amsterdam, *Stud. Surf. Sci. Catal.*168 (2007) 525.

[25] J.D. Pless, R.S. Maxwell, M.L.F. Philips, K.B. Helean, M.Y. Axness, T.A. Nenoff, *Chem. Mater.* 17 (2005) 5101.

[26] A.P. Vanselow, *Soil Sci.* 33 (1932) 95.

[27] S.G. Fegan and B.M. Lowe, *Proc. 6th Int. Zeolite Conf.*, 288, Butterworths, U.K.(1984).

[28] R.M. Barrer and A.J. Walker, *Trans. Faraday Soc.* 60 (1964) 171.

[29] G.L. Gaines and H.C. Thomas, *J.Chem. Phys.* 21 (1953) 714.

[30] Y.N. Gapon, *J.Gen. Chem.*, USSR 3 (1933) 144.

[31] J.W. Carey, D.L. Bish, *American Mineralogist* 81 (1996) 952.

[32] R.T. Wilkin and H.L. Barnes, *American Mineralogist* 85 (2000) 1329.

[33] Z. Gabelica and S.Valange, *Micropor. Mesopor.Mater.*, 30 (1999) 57.

[34] R Aiello, R M. Barrer, *J. Chem.Cos.* (1970) 1470.

[35] H. Khatami, *Proceedings of Third International Conf. on Molecular Sieves*, J. B. Uytterhoeven (ed.) Leuven Univ. Press, (1973) 167.

[36] E M. Flanigen, *Adv. Chem. Ser.* 121, R. F. Gould (ed.), (1973) 119.

[37] R M. Barrer, *Molecular Sieves, Soc, Chem. Ind.*, London, (1968) 39.

[38] W. M. Meier, *Molecular Sieves, Soc. Chem. Ind.*, London, (1968) 10.

[39] M.H. Zahedi-Niaki, P.N.Joshi, S. Kaliaguine, *Chem. Commun.* (Cambridge) 11 (1996) 1373.

[40] M.M. Harding, B.M. Kariuki, *Acta Crystallogr, Sect.C, Cryst. Struct.Commun*, C50 (6) (1994) 852.

[41] J.L.Paillaud, B.Marler, H.Kessler, *Chem. Commun.* 11 (1996) 1293.

[42] R. Kumar, *Catalysis: Principles and Applications*, B. Viswanathan, S. Sivasankar, A.V. Ramaswamy (Eds.), (2002) 75.

[43] R. Kumar, *Catalysis: Principles and Applications*, B. Viswanathan, S. Sivasankar, A.V. Ramaswamy (Eds.), (2002) 79.

[44] J. Yu, *Introduction to Zeolite Science and Practice*, 3rd Rev. Edn., J. Cejka, H.V.Bekkum, A. Corma, F. Schiith (Eds.), (2007) 57.

[45] M.E. Davis, R.F.Lobo, *Chem. Mater.* 4 (1992) 756.

[46] L.Schreyeck, J. Stumbe, P. Caullet, J.C.Mougenel,B. Marler, *Micropor. Mesopor. Mater,* 22 (1998) 87.

[47] J. Yu, *Introduction to Zeolite Science and Practice*, 3rd Rev. Edn., J. Cejka, H.V.Bekkum, A. Corma, F. Schiith (Eds.), (2007) 60.

[48] H.V. Bekkum, H.W. Kouwenhoven, Recl Trav. Chim. Pays-Bas 108 (1989) 283.

[49] C.H. Christensen, K. Johannsen, I.Schmidt, C.H. Christensen, *J.Am. Chem.Soc.* 125 (2003) 13370.

[50] Y. Tao, K. Kanoh, K. Kaneko, *J. Am. Chem. Soc.* 125 (2003) 6044.

[51] A.H. Janssen, I. Schmidt, C.J.H. Jacobsen, A.J. Koster, K.P. de Jong, *Micropor. Mesopor. Mater.* 65 (2003) 59.

[52] R.M. Barrer, *Hydrothermal Chemistry of Zeolite* (Academic Press, London, (1982) 251.

[53] C.T.-W. Chu, C.D. Chang, *J. Phys. Chem.* 89 (1985) 1569.

[54] M. Tramasso, G. Perego and B. Notari, *U.S. Patent* 4410501 (1983).

[55] J. Kornatowski, M. Sychev, V. Goncharuk, W.H. Baur, *Stud. Surf. Sci. Catal.* 65 (1991) 581.

[56] P.Prokesova, S.Mintova, J.Cejka, T.Bein, *Micropor.Mesopor.Mater.* 64 (2003) 165.

[57] P.Waller,Z. Shan,L. Marchese,G.Tartaglione,W.Zhou,J.C.Jansen,T. Maschmeyer,*Chem.Eur.J.* 10 (2004) 4970.

[58] S.Wang,T. Dou,Y.Zhang,X.Li, Z.Yan, *Catal. Commun.*6 (2005) 91.

[59] M.D.Romero, G. Ovejero, Rodriguez and J.M. Gomez, *Micropor. Mesopor. Mater.* 81 (2005) 313.

[60] P.G. Smirniotis and E. Ruckenstein, *Catal. Letters* 17 (1992) 341.

[61] E. David, *J Achievements in Materials and Manufacturing Engineering* 19 (2006) 26.

[62] H.D. van Heijnsbergen, G. von Helden, M.A. Duncan and G. Meijer, *J. Chem. Phys.* 116 (2002) 2400.

[63] A.V. Kucherov, A.A. Slinkin, *Zeolites* 6 (1986) 175; 7 (1987) 43.

[64] A.V. Kucherov, A.A. Slinkin, G.K. Beyer, G.Bordley, *J.Chem.Soc., Faraday Trans. I* 85 (1989) 3087.

[65] A. Corma, V. Fornes, S.B. Pergher, T.L.M. Maesen, J.G. Buglass, *Nature* 396 (1998) 353.

[66] H.K.Beyer, *Molecular Sieves Science and Technology-Post-Synthesis Modification*, H.G.Karge, J. Weitkamp (Eds.), *Springer*, Berlin,3 (2002) 203.

[67] J. Scherzer, *ACS Symp. Ser.* 248 (1984) 157.

[68] E.M. Flanigen, R.L. Patton, US 4,073,865, United States, 1978.

[69] H. Kessler, J. Patarin and C.Schott Darie, *Advanced Zeolite Science and Applications.* Vol.85, *Stud. Surf. Sci. Catal.*, Eds: J.C. et.al., (1995) 75.

[70] H. Kessler, J. Patarin, C. Schott-Darie, *Stud. Surf. Sci. Catal.* 85 (1994) 75.

[71] J.L. Guth, H. Kessler, M. Bourgogne, Fr 2564451, France, 1984.

[72] J.L. Guth, P Caullet, *J. Chem. Phys.*83(1986) 155.

[73] J.L. Guth, H. Kessler, J.M. Higel, J.M. Lamblin, J. Patarin, A Seive, J.M. Chezeau, R. Wey, *zeolite synthesis*, in : ACS Symp.Ser. 398, Washington DC, (1989) 176.

[74] J.L.Guth, L. Delmotte, M. Soulard, N. Brunard, J.F. Joly, D. Espinat, *Zeolites* 12 (1992) 929.

[75] M.A.Camblor, L.A. Villaescusa, M.J. Diaz-Cabanas, *Topic Catal.* 9 (1999) 59.

[76] S.A.Axon, J. Klinowski, *J.Chem. Soc. Faraday Trans.* 86 (1990) 3679.

[77] M. Estermann, L.B. McCusker, C. Baerlocher, A. Merrouche, H. Kessler, *Nature*, 352 (1991) 320.

[78] F. Schuth, W. Schmidt, *Adv. Mater.*14 (2002) 629.

[79] C.A.Fyfe, D.H. Brouwer, A.R.Lewis, J.M. Chezeau, *J.Am. Chem. Soc.* 123 (2001) 6882.

[80] H.Koller, A. Wolker, H. Eckert, C. Panz, P. Behrens, Angew, *Chem.Int.* Ed. Eng. 36 (1997) 2823.

[81] D. Ma, Y. Shu, X. Han, X. Liu, Y. Xu, X. Bao, *J. Phys. Chem.* B 105 (2001)1786.

[82] A. Corma, L.T. Nemeth, M. Renz, S. Valencia, *Nature* 412 (2001) 423.

[83] Puri, Sarma, Kalia, *Principle of physical chemistry*, (2005) 462.

[84] C.I. Round, C.D. Williams, K. Latham, C.V.A. Duke, *Chem. Mater.* 13 (2001) 468.

[85] L.B. McCusker, *Verified Synthesis of Zeolitic Materials*, H.Robson (Ed.) 2nd revised edition (2001) 47.

[86] William kemp, *Organic spectroscopy*, (2004) 20.

[87] E. M. Flanigen, H. Khatami, H. A. Seymenski, *Adv. Chemistry Series* 101, E. M. Flanigen, L B. Sand (eds.), *Am. Chem. Soc.*, Washington, D. C. (1971) 201.

[88] E. Geidel, H. Böhlig, Ch. Peuker, W. Pilz, in *Stud. Surf. Sci. Catalysis* 65, G. Ohlmann, H. Pfeifer, R. Fricke (eds), *Elsevier*, Amsterdam, (1991) 511.

[89] F. Bauer, E. Geidel, Ch. Peuker, W. Pilz, *Zeolites* 17 (1996) 278.

[90] Puri, Sarma, Kalia, *Principle of physical chemistry*, (2005) 253.

[91] J. El-Hage-Al Asswad, N. Dewaele, J.B. Nagy, R.A. Hubert, Z. Gabelica, F.G. Demuanne, F. Crea, R. Aiello, and A. Nastro, *Zeolites*,8 (1988) 221.

[92] William Kemp, *Organic spectroscopy*, (2004) 244.

[93] B.M. Weckhuysen, R.A. Schoonheydt, *Catal. Today* 49 (1999) 441.

[94] R.K. Rana, B. Viswanathan, *Catal. Lett.* 52 (1998) 25.

[95] K.A. Carrado, S.L. Suib, N.D. Skoularikis, R.W. Coughlin, *Inorg. Chem.* 25 (1986) 4217.

[96] S.W. Karickhoff, G.W. Bailey, *Clays Clay Miner.* 21 (1973) 59.

[97] S.J. Gregg, K.S.W. Sing, Adsorption, *Surface Area and Porosity*, 2nd Edn. (Academic Press, London, (1982).

[98] J. Perez-Ramirez, J.C. Groen, A. Bruckner, M.S. Kumar, U. Bentrup, M.N. Debbagh, L.A. Villaescusa, *J. Catal.* 232 (2005) 318.

[99] K.Jansen, *Verified Synthesis of Zeolitic Materials*, H.Robson (editor) 2nd revised edition (2001) 55.

[100] U.S. Patent 3,702,886.

[101] H.Lermer,; M. Draeger,; J. Steffen,; K.K.Unger, (1985). "Synthesis and structure refinement of ZSM—5 single crystals". *Zeolites* **5** (3): 131.

[102] J. Cejka, H. van Bekkum, *Zeolites and Ordered Mesoporous Materials: Progress and Prospects*. Ed (2005) 157.

[103] C.R.A. Catlow, *Modeling of Structure and Reactivity in Zeolites*, Ed (1992). Academic Press, Ltd.: London.

[104] D.G. Hay, G.W. West (1985). "Examination of the monoclinic/ orthorhombic transition in silicalite using XRD and silicon NMR". *J. Phy. Chem.* ,89 (7): 1070.

[105] R.Grau-Crespo,E.Acuay,A.R.Ruiz alvador (2002), *Chem. Comm.* (21):2544.

[106] D. Ma, Y. Shu, X. Han, X. Liu, Y. Xu, X. Bao, *J. Phys. Chem.* B 105 (2001) 1786.

[107] A. Corma, L.T. Nemeth, M. Renz, S. Valencia, *Nature,*412 (2001) 423.

[108] T. Sowade et al., *J. Catal.*, 214 (2003) 100.

[109] M K Dongare, P Singh, P P Moghe and P Ratnasamy, *Zeolites*, 11 (1991) 690.

[110] M. Breysse, M. Cattenot, V. Kougionas, J. C. Lavalley, F. Mauge, J. L. Portefaix and J. L. Zotin, *J. Catal.*, 1997, 168(2), 143; S. K. Das and P. K. Dutta, *Micropor. Mesopor. Mater.*, 1998, 22(1-3), 475; P. K. Dutta, *J. Incl. Phenom. Mol. Recogit. Chem.*, 21 (1995) 215.

CHAPTER-2

Synthesis and Characterization of Parent and Zr incorporated MFI Zeolite

Chapter Summary

This chapter contains the synthesis of parent MFI and their characterization by XRD, FT-IR, N_2 adsorption desorption isotherm and SEM. This chapter also contains description on *insitu* modification of MFI zeolite by isomorphous substitution of Zr in zeolite framework and characterization of the synthesized samples by XRD, FT-IR, TGA, UV-Vis (DRS), N_2 adsorption desorption isotherm, SEM and EDX.

2. Introduction

2.1 Synthesis of MFI zeolite

MFI zeolites were synthesized using different routes. In the seventies and also in later stages MFI zeolite was synthesized in the temperature range of 393-453 K under autogeneous pressure in an autoclavation period of about 7 days [1]. A reduction in the autoclavation time to 48 h, in the synthesis of MFI zeolite was reported by Robson et al. [2] and Barrer et al. [3] by application of nucleated gel method. The autoclavation time was further reduced to 4-12 h in the presence of promoters, by modified synthesis technique [4, 5]. However, promoter induced number of drawbacks in the synthesis of MFI zeolite. These include difficulty in the incorporation of metal ions in the tetrahedral positions, decrease in the percentage of crystallinity, difficulty in controlling the Si/Al ratio, low yield of product etc. Synthesis of highly crystalline MFI zeolite was reported by Kulkarni et al.[6] without using any promoter in the temperature range of 503-523 K in an autoclavation period of 4-10 h. Various organic solvents were used at high pressure in all

those processes mentioned above and the overall synthesis was 20-26 h. A significant breakthrough in the field of zeolite synthesis occurred when hydroxyl anions were replaced by fluorides, making the synthesis possible in neutral and even in acidic media [7].

2.1.1 *Insitu* modification of MFI zeolite

The catalytic activity of molecular sieves can be improved by the incorporation of heteroatoms into the framework structure. The introduction of transition metal cations inside zeolite micropores and/or framework leads to the development of many redox catalysts or even bifunctional catalysts [8, 9]. Zirconia-based materials have wide applications in the field of catalysis in dehydration, hydrogenation, hydroxylation, oxidation and epoxidation reactions owing to the moderate acidity and oxidizing capabilities. Zirconium based zeolite catalysts were investigated for the first time in selective catalytic reduction of NO by hydrocarbon (HC-SCR) [10]. The Zr-HMFI catalyst was prepared by ion-exchange using a commercial H-MFI zeolite as the starting material. However, the catalysts prepared in this method have low surface areas which restrict their industrial applications. Ion exchanged materials also have sensitivity towards solvents used attracting leaching problem.

There are early claims of synthesis of crystalline zirconium silicas with zeolitic properties, details of which are not available in the literature. Dongare et al. reported the synthesis and characterization Zr-MFI [11]. However synthesis was carried out in presence of solvent and crystallization was completed in 48 h.

In the present work Zr-MFI, In-MFI and Ru-MFI samples were synthesized.

2.2. Designation of the Samples

2.2.1 Designation of the Parent MFI Sample

Parent MFI samples are simply designated as S followed by the silicon to aluminium molar ratio. For example an MFI sample synthesized with Si to Al ratio 100 is designated as shown below:

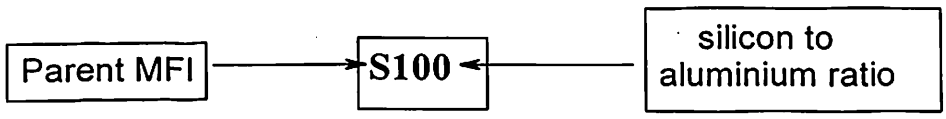

2.2.2 Designation of the Zr incorporated MFI sample

Zirconium incorporated into the framework of MFI samples are designated as S followed by silicon to (Al + Zr) molar ratio. Zr is written after this which is followed by aluminium to zirconium molar ratio. For example, a framework substituted Zr-MFI with silicon to (Al + Zr) molar ratio of 100 and aluminium to zirconium ratio of 3 is designated as shown below:

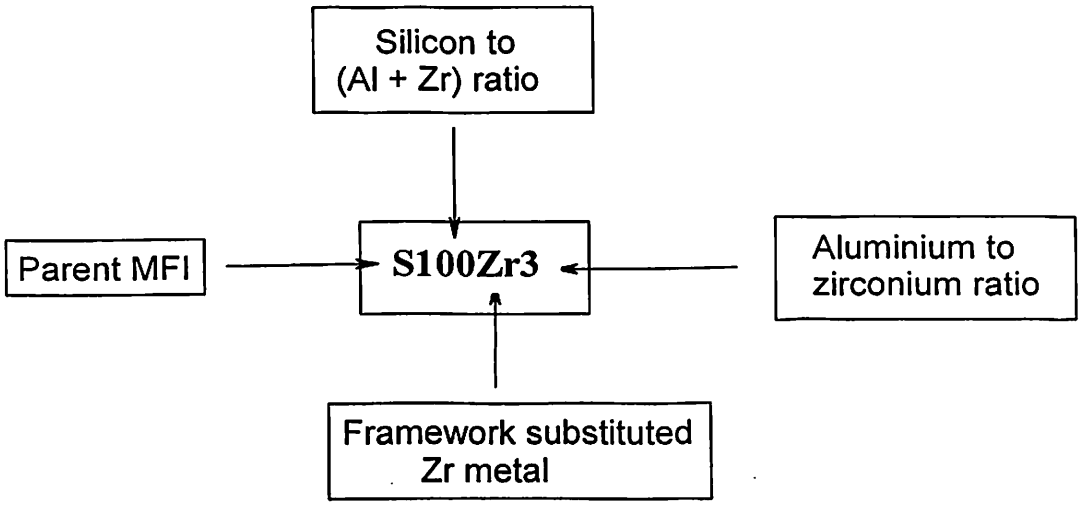

2.2.3 Designation of the In incorporated MFI sample

The designation scheme is exactly same as that of Zr incorporated MFI except that In is used in place of Zr for obvious reason. For example, In-MFI with silicon to (Al + In) molar ratio of 100 and aluminium to indium molar ratio of 3 is designated as shown below:

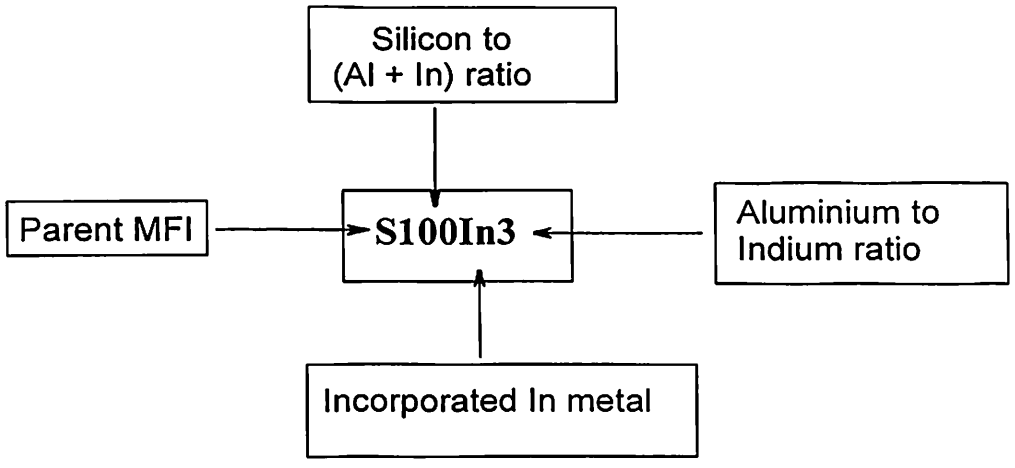

2.2.4 Designation of the Ru incorporated MFI sample

Ruthenium incorporated MFI samples are also designated as S followed by silicon to (Al + Ru) molar ratio after which Ru is written followed by aluminium to ruthenium molar ratio. For example, Ru-MFI with silicon to (Al + Ru) molar ratio of 100 and aluminium to ruthenium molar ratio of 3 is designated as shown below:

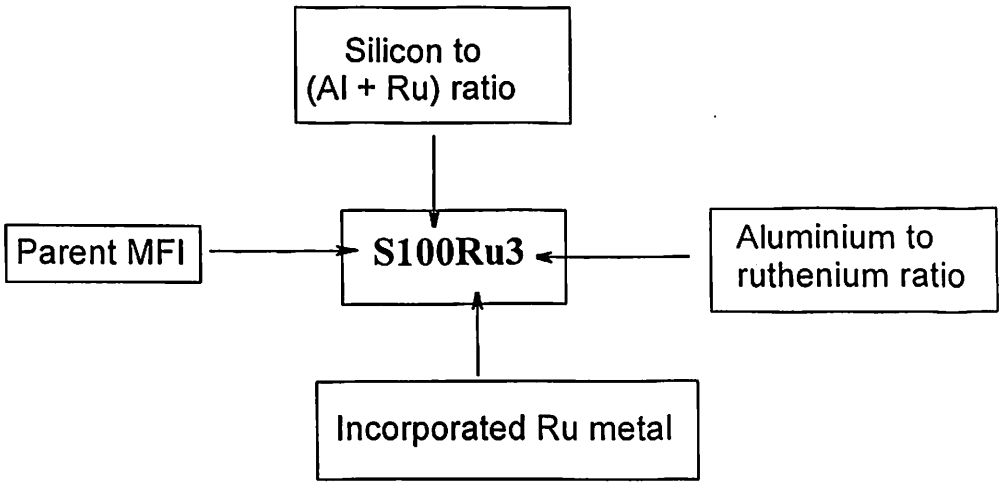

2.3 Experimental

2.3.1 Source of chemicals

Chemicals used for the synthesis of MFI Zeolites and modified MFI Zeolites are sodium aluminate (Kemphasol), tetrapropylammonium bromide (Lancaster), sodium fluoride (Fluka Chemika 99%), zirconium oxynitrate hydrate (Aldrich 99%)), fumed silica (BDH) and de-ionized water.

2.3.2 Synthesis of MFI zeolite

Two samples of MFI Zeolites were synthesized in the silicon to aluminium ratio of 100 and 200 by hydrothermal process using fluoride gel as mineralizer. A typical procedure for the synthesis of MFI zeolite with silicon to aluminium ratio of 100 is given below:

Si/Al = 100, NaF/SiO_2 = 1, SiO_2/Al_2O = 200, TPA-Br/SiO_2 = 0.07, H_2O/SiO_2 = 80

Calculated amount of NaF was dissolved slowly to 23 mL of de-ionized H_2O. To this solution required amount of TPA-Br was added slowly with continuous stirring. The solution was stirred for 15 min and a part of the required SiO_2 was added slowly to this mixture. The resulting mixture (A) was stirred for another half an hour. Calculated amount of $NaAlO_2$ was dissolved in 97 mL of de-ionized water slowly. To the solution the remaining part of required SiO_2 was added slowly with continuous stirring. The resulting mixture (B) is stirred for another half an hour. The mixture A was added to mixture B slowly and stirred continuously for 3 hrs at pH 6-7 to get homogeneous gel. The whole mass was then autoclaved in a teflon-lined stainless steel vessel maintained at 473 K inside an oven for 25 h. It was then cooled, filtered (Whatman No 42) and washed with de-ionized water several times. The sample was dried in the filter paper at room temperature for about

12 h and at 383 K for 6 h. This was then calcined at 753 K to remove the template.

The same procedure was applied for the synthesis of other MFI zeolite (S 200). **Table 2.1** shows the molar ratios of the components in the initial gel and other conditions maintained during the synthesis of the zeolite samples.

Table2.1 Molar ratios of the components in the gel and other conditions maintained during the synthesis of the MFI zeolite samples.

Sample designation	Si: Al	TPA-Br: SiO_2	NaF: SiO_2	H_2O: SiO_2	Autoclavation time (h)	pH of the gel
S100	100	0.07	1	80	25	7.0
S200	200	0.07	1	80	24	6.9

2.3.3 Modification of MFI zeolite

Insitu modification of MFI zeolite

Synthesis of Zr incorporated MFI zeolite

Four samples of Zr-MFI Zeolite were synthesized with different Si to (Al + Zr) and different Al to Zr molar ratios. A typical procedure for the synthesis of MFI zeolite with silicon to aluminium and zirconium ratio of 100 and Al: Zr ratio of 3:1 is stated below with the following initial gel molar composition:

Si/Al=100/0.75, NaF/SiO_2=1, SiO_2/Al_2O_3=200, TPA-Br/SiO_2=0.07, H_2O/SiO_2=80, Si/Zr=100/0.25

A calculated amount of NaF was dissolved slowly to 23 mL of de-ionized H_2O. To this solution 1.551 g of TPA-Br was added slowly with continuous

stirring. The solution was stirred for 15 min and 1.2947g of SiO_2 was added slowly to this mixture. The resulting mixture (A) was stirred for another half an hour. The required amount of $NaAlO_2$ was dissolved in 97 mL of de-ionized water slowly in another beaker. To this solution calculated amount of zirconium oxynitrate hydrate was added and the mixture was stirred for 10 min. 3.705g of SiO_2 was also added to the solution slowly with continuous stirring. The resulting mixture (B) was stirred for another half an hour. The mixture A was added to mixture B slowly and stirred continuously for 3 hrs at pH 6-7 to get a homogeneous gel. The whole sample was then autoclaved in a teflon-lined stainless steel vessel maintained at 473 K inside an oven for 25 h. It was then cooled, filtered (Whatman No 42) and washed with de-ionized water several times. The sample was dried on the filter paper at room temperature for about 12 h and at 383 K for 6 h. It was then calcined at 753 K to remove the template.

The same procedure was applied to synthesize other samples of Zr incorporated MFI zeolite with different Si/(Al+Zr) and Al:Zr ratios. **Table 2.2** shows the molar ratios of the components in the gel and other conditions maintained during the synthesis of the zeolite samples.

Table 2.2 Molar ratios of the components in the gel and other conditions maintained during the synthesis of the MFI zeolite samples.

Sample	Si: (Al +Zr)	Al:Zr	TPA-Br: SiO_2	NaF: SiO_2	H_2O: SiO_2	Autoclavation time (h)	pH of the gel
S100Zr3	100	3	0.07	1	80	25	7.0
S100Zr6	100	6	0.07	1	80	24	6.9
S100Zr9	100	9	0.07	1	80	24	6.8
S200Zr6	200	6	0.07	1	80	24	6.9

2.4 Characterization of the synthesized samples

2.4.1 X-ray diffraction

X-ray powder diffraction analysis was undertaken using a Bruker D-8 Advance X-ray Diffractometer with CuK_α radiation of wavelength 1.5418Å operated at voltage = 40 kV and current = 40 mA and a Miniflex Advance X-ray Diffractometer with CuK_α radiation of wavelength 1.5418 Å operated at voltage = 30 kV and current = 15 mA. The XRD data were collected in 2θ range 5-50^0 (step size 0.05^0, step time 0.5 s).

2.4.2 Fourier transform infrared (FTIR) spectroscopy

A PerkinElmer RX 1 FT-IR Spectrophotometer was used for recording the FT-IR spectra of the samples in the form of KBr pellets in mid-IR region of 1500-450 cm^{-1} (resolution 8 cm^{-1}).

2.4.3 Diffuse reflectance UV-Vis spectroscopy

UV-Vis spectra of the samples were obtained from a U-4100 spectrophotometer equipped with a diffuse reflectance attachment using solid sample holder, in the wavelength region of 200-600 nm at a scan speed of 600 nm min^{-1} (sampling interval: 2.00 nm). The base line correction was made using barium sulphate as the reference standard.

2.4.4 Thermo gravimetric analysis (TGA)

A METTLER TOLEDO TG analyzer (model = TGA/DSC-1) was used for recording the TGA data. TGA was carried out from 313 to 1023 K with a heating rate of 10 K/min under a N_2 flow.

2.4.5 N_2 adsorption desorption

The N_2 adsorption-desorption isotherms of the samples were obtained using nitrogen as adsorbate at 77.15 K on a Micromeritics (model: Tristar 3000) surface area and porosity analyzer for determining the specific surface

area, pore volume and pore size of the synthesized samples. The analysis bath temperature was 77.15 K. The calcined samples were degassed for 6 h at 673 K and then gradual heating to 623 K in continous flow of N_2 and maintained at that temperature for 12 h. The samples were then slowly cooled down to 383 K under N_2 atmosphere and the anhydrous weight of the sample was taken prior to N_2 adsorption-desorption measurement. Finally, the sample was chilled to ~77 K using liquid nitrogen and the adsorption of nitrogen was carried out at different equilibrium pressures.

2.4.6 Scanning electron microscopy (SEM)

Scanning electron micrographs of the MFI samples were taken for investigation of the particle morphology using a JEOL JSM-6390 LV scanning electron microscope operating at accelerating voltage of 15-20 kV. The samples for SEM were prepared by spreading the powdered zeolite on a double sided carbon tape stuck to the SEM stage. The excess sample was dusted off by a small air sprayer. Further, the samples were coated with gold thin film in a sputter coater to prevent surface charging and to protect from thermal damage and also to make the sample conducting.

2.4.7 Energy dispersive X-ray analysis (EDX)

The elemental composition of the calcined samples was determined by energy dispersive X-ray analysis (EDX) at 20 kV scanning several areas and normalizing to get average values using a JSM-7600F energy dispersive X-ray analyzer.

2.5 Results and discussion

2.5.1 Synthesis of MFI zeolite

A systematic study was conducted to synthesize MFI zeolite using different silicon to aluminium ratio in the absence of any promoter, organic solvent or

sulphuric acid and also avoiding any seeding gel. The synthesized MFI samples were identified by comparison of both the d-spacing and relative intensities in their XRD patterns with those reported in the literature[12] and were found to be in excellent agreement. **Figures 2.1** and **2.2** show the XRD patterns of MFI samples synthesized using different silicon to aluminium ratios. From these figures it is found that prominent peaks are obtained in the 2θ ranges 6.5 and 22.5 which are the characteristic peaks of MFI zeolites.

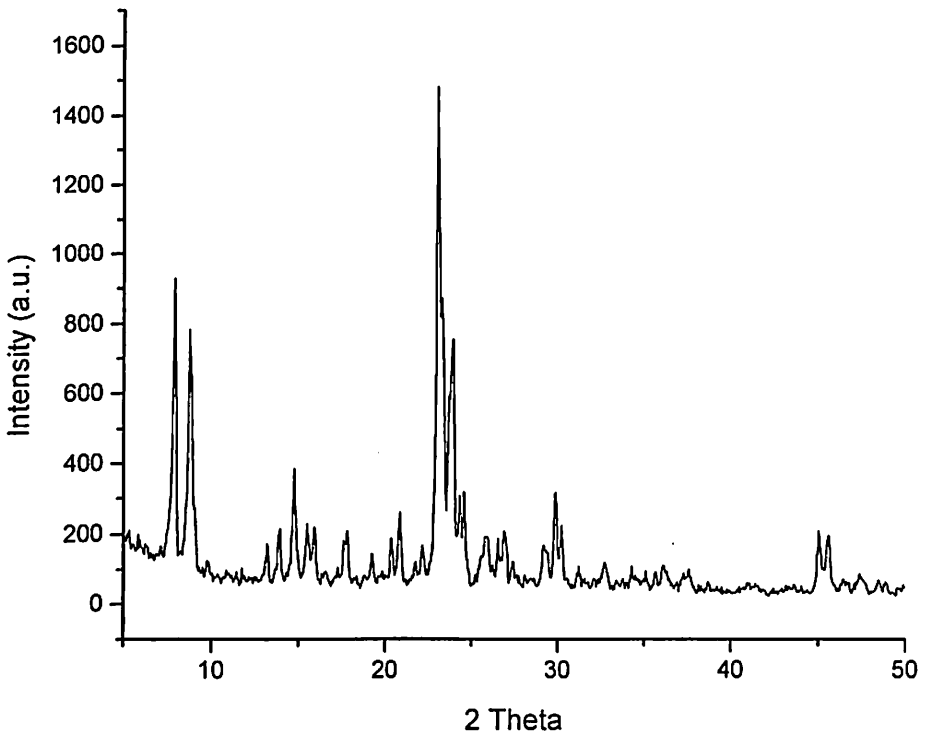

Fig. 2.1 XRD patterns of S100

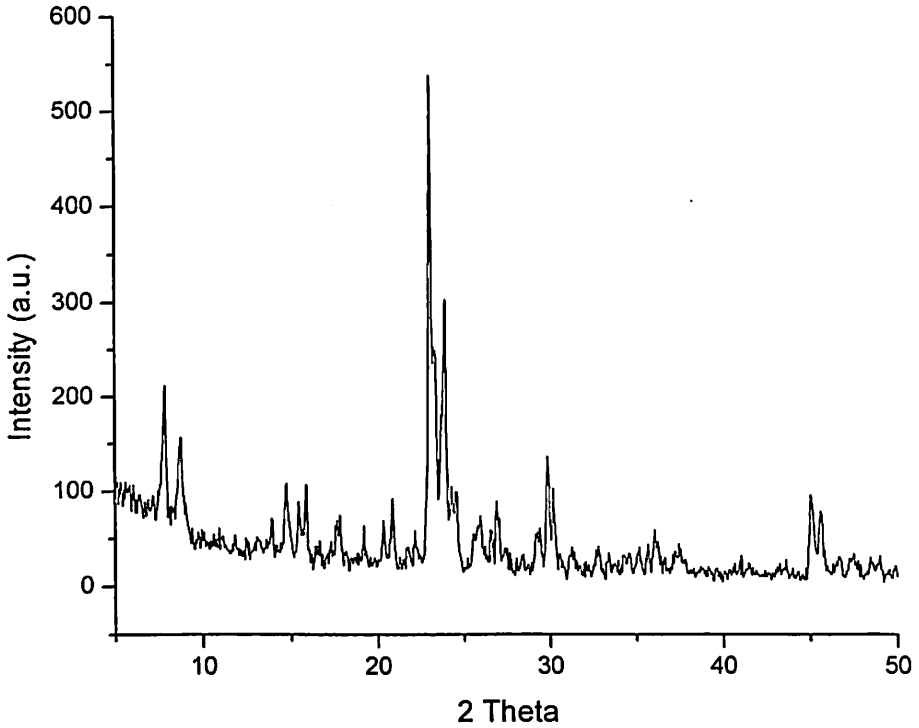

Fig.2.2 XRD patterns of S200

Crystallinity of the MFI samples is calculated using the following relation:

$$\%C = 100 \text{ X } I_{hkl} / (I_b + I_{hkl}) \qquad \textbf{Relation 1}$$

for a particular crystallographic plane (*hkl*) where, I_{hkl} is the corrected integral XRD peak intensity and I_b is the integral background intensity for the same plane. The percentage of crystallinity with reference to one of the most significant peaks (*501*) is presented in **Table 2.3.** All the samples under the present investigation were found to exhibit high crystallinity up to (~ 95%).

The Scherrer formula

$$D_{hkl} = K\lambda / (\beta \text{ X } \cos\theta) \qquad \textbf{Relation 2}$$

was used to determine the crystallite dimension (D_{hkl}) of the identified crystalline phase [13]. Here, β is the full width at half maximum; K is the shape factor (taken to be 0.9); θ_{hkl} is the Bragg angle and λ is the wavelength

of Cu $K\alpha_1$(1.5418Å). The factor 5.73 is used to convert the value of β from degree to radian to obtain D_{hkl} in nanometer unit. The crystallite size of the samples is presented in **Table 2.3**. The average crystallite sizes of the synthesized samples were found to be almost equal to 47 nm.

Table 2.3 Crystallite size and percentage of crystallinity (% C)$_{hkl}$ of the synthesized MFI sample

Sample	Si: Al	Crystallite size (nm) (*501*)	%C from XRD	% C from IR
S100	100	47	95.87	92.3
S200	200	46	95.56	91.4

Figures 2.3 and **2.4** show the FT-IR spectra of MFI samples synthesized using different Si to Al ratio. FT-IR results confirm the formation of a zeolite phase in all cases showing distinct absorbance bands near 1080 (internal asymmetric stretch), 790 (external symmetric stretch), 540 (double ring vibration) and 450 cm^{-1} (T–O bending). The absorption bands near 550 cm^{-1} have been assigned to the presence of double 5-member rings indicating formation of MFI structure [14]. The external asymmetric stretching vibration around 1225 cm^{-1} present in the spectra of MFI structures is assigned to four chains of 5-member rings arranged around a two-fold screw axis. The IR method of finding relative crystallinity of the samples is achieved by calculating the optical density (OD) ratio of the peaks near 540 and 450 cm^{-1} [15, 16]. The results are given in **Table 2.3** and are found to be in good agreement with those calculated from XRD studies.

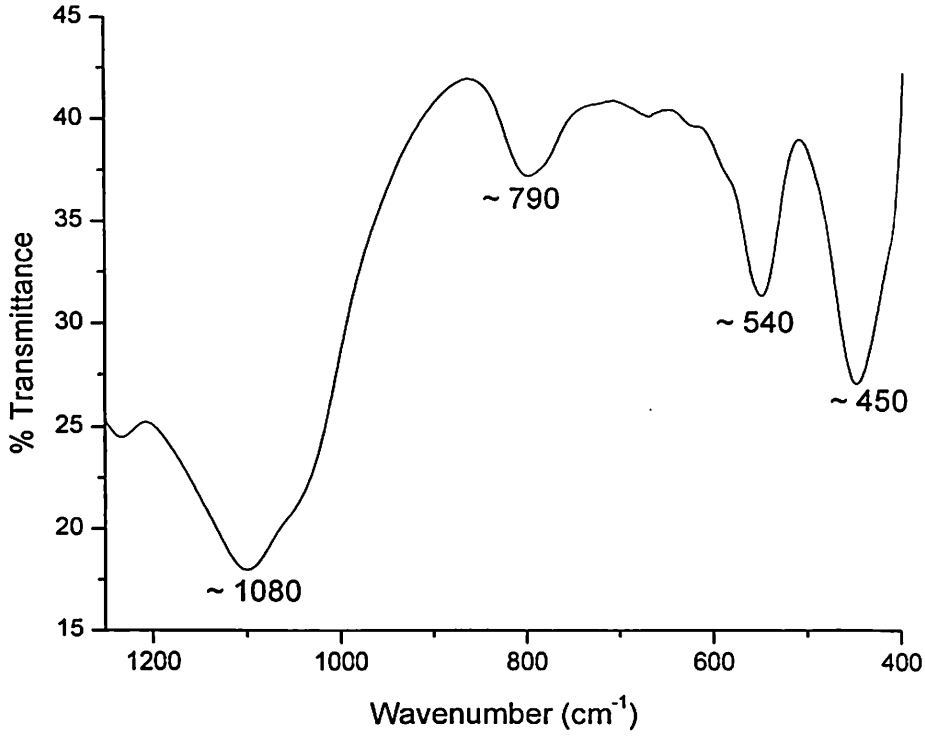

Fig.2.3 FT-IR spectra of S100

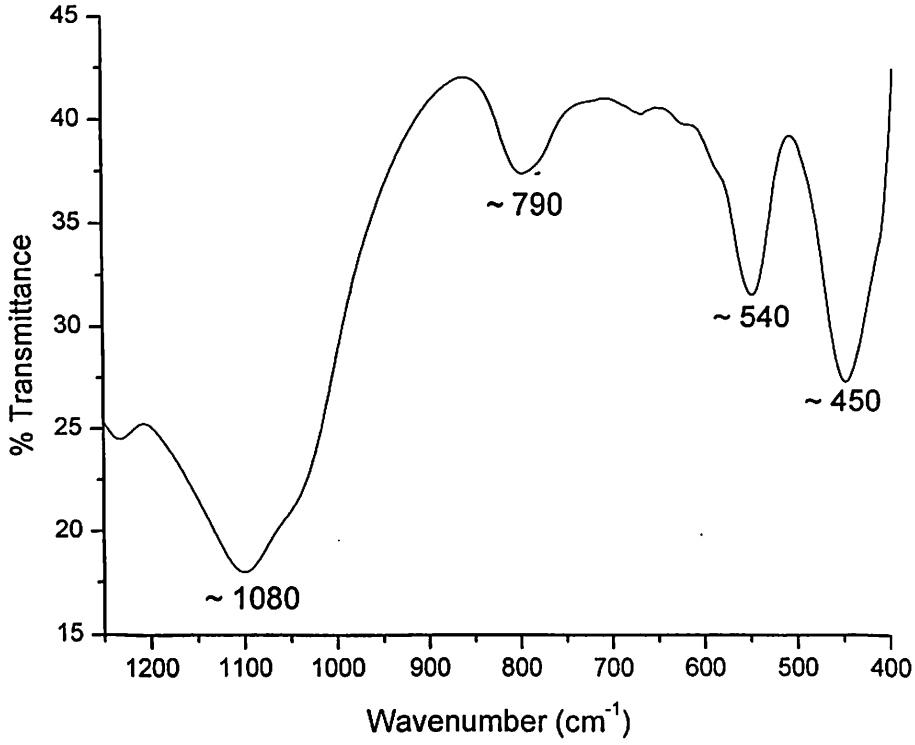

Fig. 2.4 FT-IR spectra of S200

Nitrogen adsorption isotherms of calcined MFI samples S 100 and S 200 are depicted in **Figures 2.5** and **2.6** respectively. The N_2 adsorption isotherms of the MFI samples basically belong to the IUPAC type 1 classification which is indicative of microporosity. On the basis of the fact that an increase in the volume of adsorption of nitrogen at 77 K occured at a relative pressure of ~0.18 for a zeolite, Bonardet et al.[17] studied the nature of nitrogen below and above this relative pressure by *in situ* ^{15}N NMR and reported the existence of two states of nitrogen. The first adsorbed phase occurs within the smaller dimension of the void network pore followed by formation of the second phase within the larger void spaces. This means that adsorption in the channels of MFI zeolite samples, as usual, proceeds in two steps. Firstly, localized adsorption occurs at preferential high energy sites and secondly, clustering occurs around the adsorbed molecule. Specific surface area, pore size and pore volume of the synthesized samples are depicted in **Table 2.4**. The analysis showed that the specific surface area of the synthesised samples was ~355 m^2g^{-1} , pore volume ~ 0.174 cm^3g^{-1} and that of pore size ~ 0.51(micropore) to ~ 2.1 (mesopore) nm.

Table.2.4 Specific surface area, pore size and pore volume of the synthesized samples

Sample	Surface area (BET)(m^2g^{-1})	Pore volume (cm^3/g)	Mesopore size (nm)	Micropore size (nm)
S100	355.34	0.175	2.1	0.51
S200	355.38	0.174	2.1	0.51

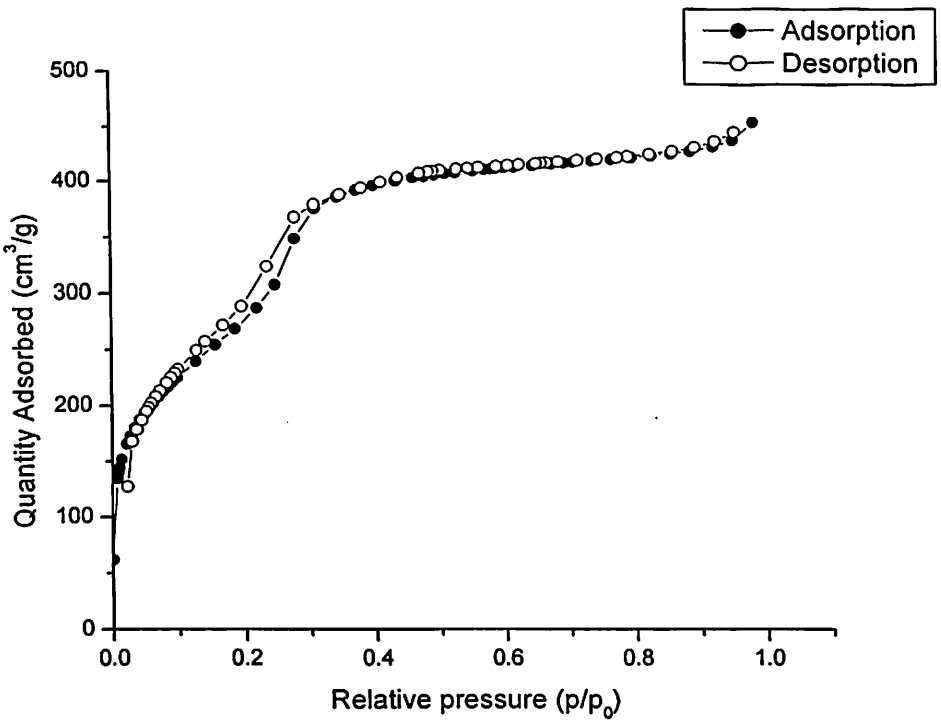

Fig. 2.5 Nitrogen adsorption isotherm of calcined S100 sample

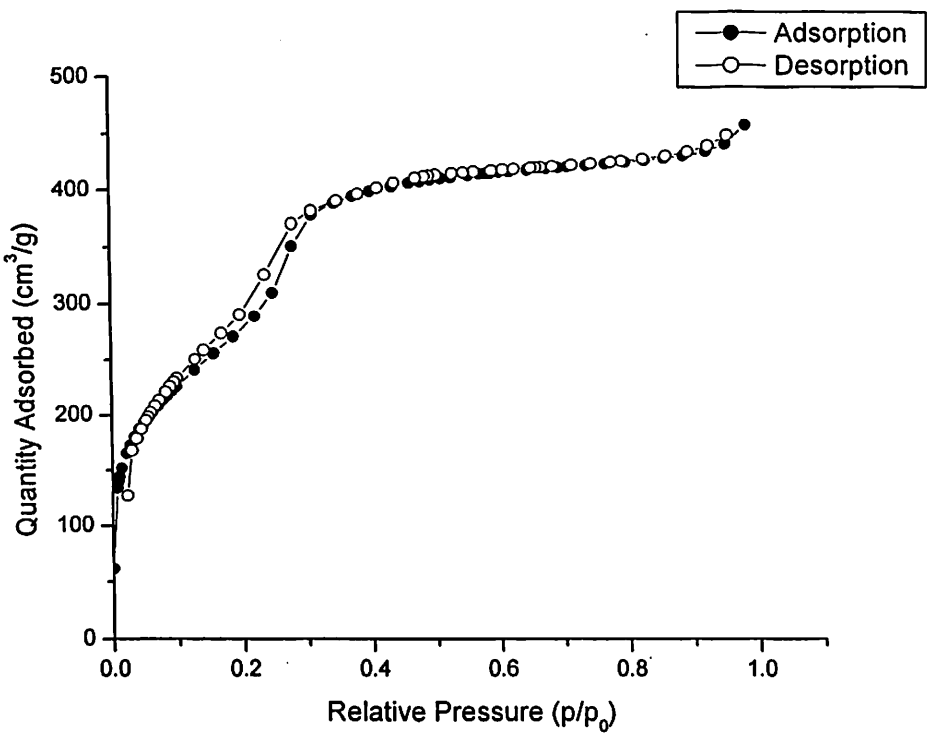

Fig. 2.6 Nitrogen adsorption isotherm of calcined S200 sample

The size and shape of the crystalline MFI particles were investigated by SEM analysis. SEM micrographs of the synthesized samples S100 and S200 are shown in **Figures 2.7** and **2.8** respectively. From the micrographs it can be seen that quite uniform rectangular and twinned rectangular shaped MFI particles were formed and the size of the particles was found to be nearly 28 μm.

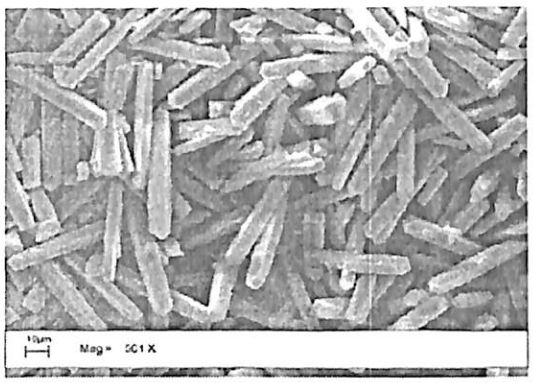

Fig.2.7 SEM picture of S100

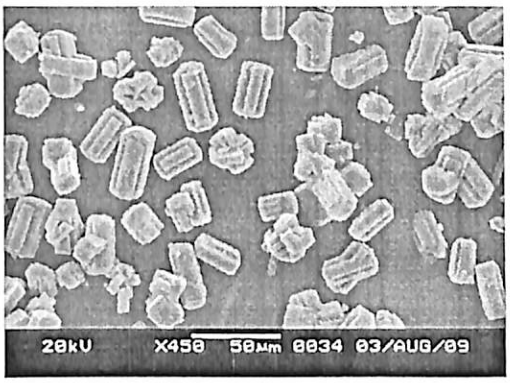

Fig.2.8 SEM picture of S200

2.5.2 *Insitu* modification of MFI zeolite

After successfully synthesizing MFI samples in fluoride medium a systematic study was conducted to synthesize zirconium incorporated MFI zeolite in the Si to Al and Zr ratios of 100 and 200 and Al to Zr ratio 3-9 using fumed silica as silicon source and fluoride as mineralizing agent in the absence of any organic solvent or sulphuric acid and also avoiding any seeding gel. The synthesized MFI samples were identified by comparison of both the d-spacing and relative intensities in their XRD patterns with those reported in the literature[12] and were found to be in excellent agreement. **Figures 2.9** to **2.12** shows the XRD patterns of synthesized Zr-MFI samples. Prominent peaks are observed in 2θ values around 6.5 and 22.5 with a few additional shoulder peaks in all the Zr incorporated MFI samples suggesting formation of pure phase of the zeolite. Expansion of unit cell parameter shown in **Table 2.5** indicates the successful incorporation of zirconium in the framework. The

shift in 2θ values is presented in **Table 2.6** while **Figure 2.13** shows the shift of the prominent peaks towards lower 2θ values with increasing level of Zr substitution with respect to the parent MFI. It may be noticed that with increasing level of substitution the peaks shift towards lower 2θ values indicating successful incorporation of Zr into the framework of MFI [18].

Crystallinity of the MFI samples is calculated using **Relation 1.** The percentage of crystallinity with reference to one of the most significant peaks (*501*) is presented in **Table 2.7**. All the samples under the present investigation were found to exhibit high crystallinity from 94% to ~97%.

The crystallite size of the synthesized samples were calculated using **Relation 2**. The crystallite size of the samples ranges from about 49 to 59 nm. The change in unit cell volume of the samples with increasing level of Zr substitution is presented in **Table 2.5**. The unit cell volumes are found to increase with the increasing level of metal substitution.

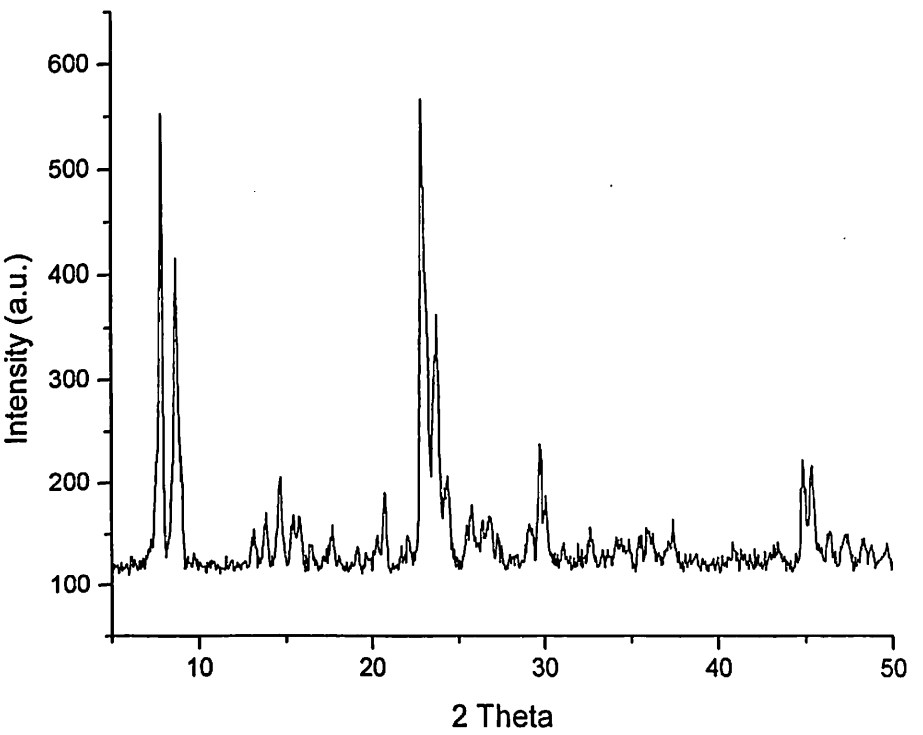

Fig.2.9 XRD patterns of S100Zr3

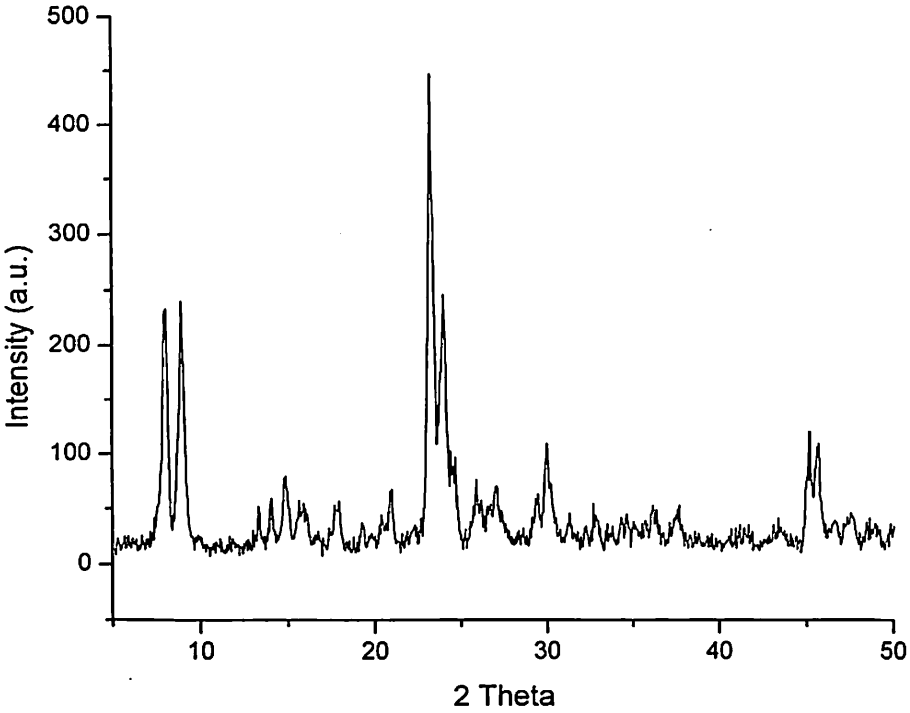

Fig.2.10 XRD patterns of S100Zr6

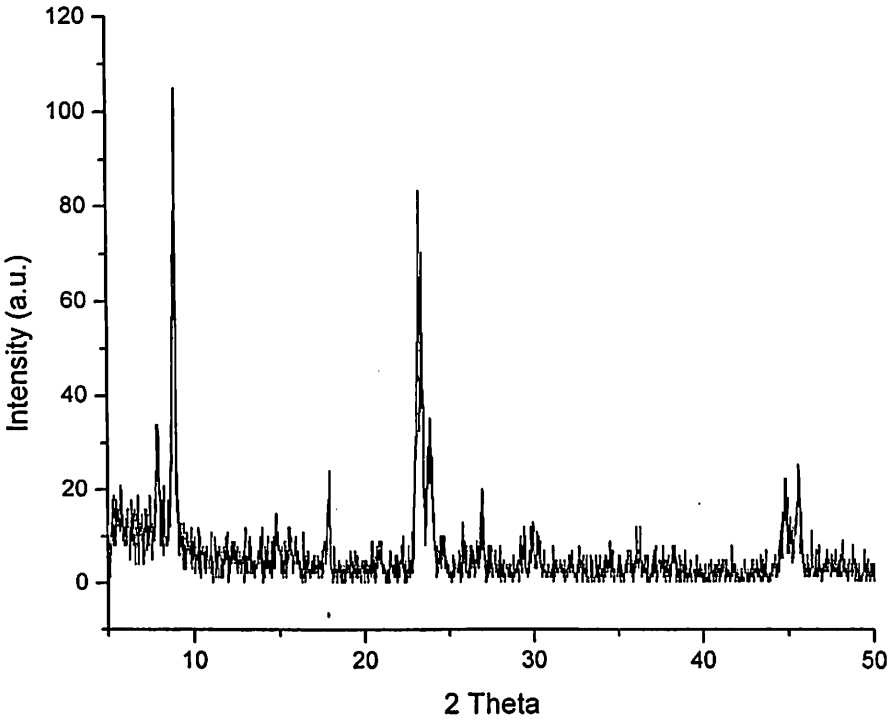

Fig. 2.11 XRD patterns of S100Zr9

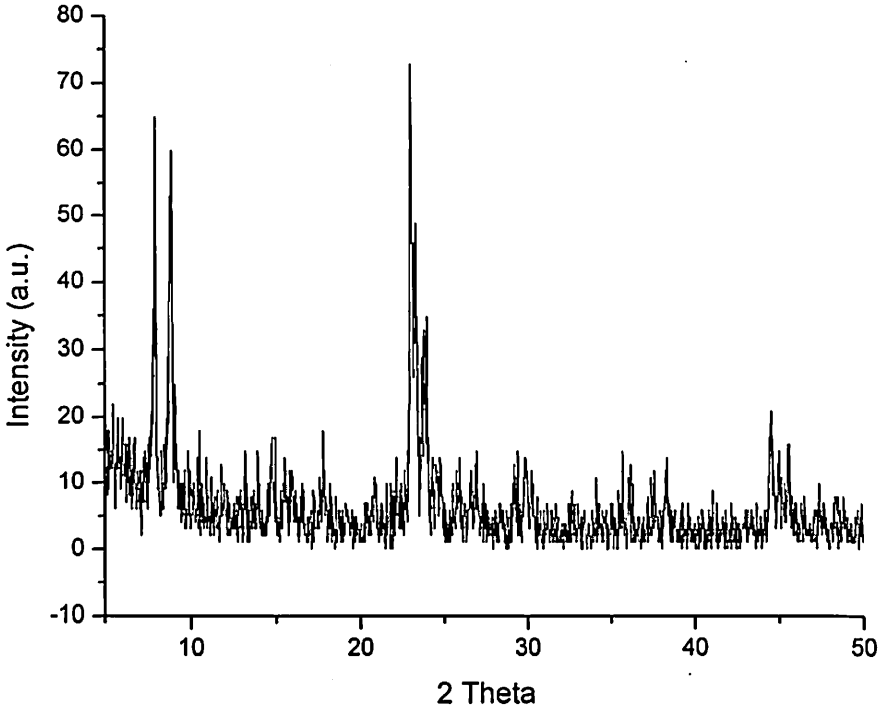

Fig.2.12 XRD patterns of S200Zr6

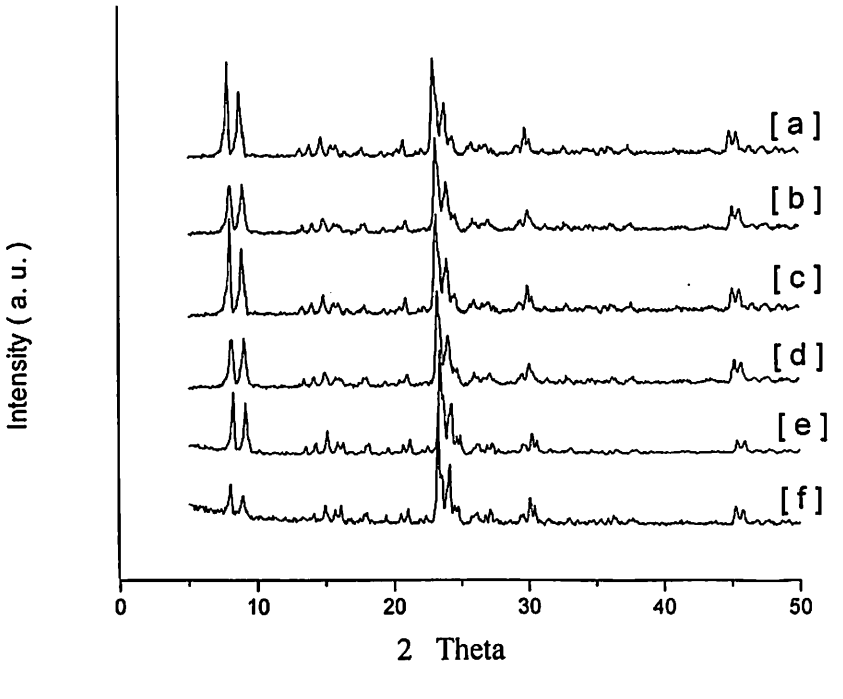

Fig.2.13 Shifting of 2 theta values of prominent peaks with increasing level of Zr substitution w.r.t. parent MFI(a) S100Zr3 (b) S100Zr6 (c) S100Zr9 (d) S200Zr6 (e) S100 (f) S200

Table 2.5 Unit cell parameters of Zr-MFI samples

Sample	Si : (Al+Zr)	Al : Zr	Unit cell edges (Å)			Unit cell volume ($Å^3$)
			a	b	c	
S100Zr3	100	3	14.02	19.92	15.21	4247.8
S100Zr6	100	6	13.94	19.85	15.10	4178.3
S100Zr9	100	9	13.87	19.78	14.95	4101.5
S200Zr6	200	6	13.76	19.69	14.83	4017.9
S100	100	-	13.59	19.71	14.64	3921.4
S200	200	-	13.53	19.64	14.60	3879.6

Table 2.6. Shift in 2θ value of *501* peaks of the Zr-MFI samples with respect to parent MFI.

Sample	Zr^{+4} mol in the gel	Position of the prominent peak (*501*)	Shift in the 2θ value w r t parent MFI
S200	-	23.39	-
S100	-	23.41	-
S100Zr3	0.25	22.95	0.46
S100Zr6	0.125	23.11	0.30
S100Zr9	0.1	23.15	0.26
S200Zr6	0.0625	23.22	0.19

Table 2.7 Crystallite size and percentage of crystallinity (% C)$_{hkl}$ of the synthesized Zr-MFI sample

Sample	Si: (Al+Zr)	Al:Zr	Crystallite size (nm) (*501*)	(%C)$_{501}$ from XRD	% C from IR
S100Zr3	100	3	52	94.21	90.3
S100Zr6	100	6	56	97.07	92.4
S100Zr9	100	9	59	97.26	93.2
S200Zr6	200	6	49	96.86	92.5

Figures 2.14 to **2.17** show the FT-IR spectra of synthesized Zr incorporated MFI samples. IR results confirm the formation of MFI zeolite in all cases showing distinct absorbance bands near 1080 (internal asymmetric stretch), 790 (external symmetric stretch), 540 (double ring vibration) and 450 cm^{-1} (T–O bending). The zirconium substituted series shows a distortion of the spectra between 1250 – 900 cm^{-1} (**Figure 2.18**). This region of the spectrum can be assigned to asymmetrical T-O-T stretching and is indicative of heteroatom substitution [14]. The absorption bands near 550 cm^{-1} have been assigned to the presence of double 5-member rings in the structure [14]. The external asymmetric stretching vibration around 1225 cm^{-1} is present in the spectra of structures assigned to four chains of 5-member rings arranged around a two-fold screw axis. The distortion of the spectra was not consistent with increasing levels of substitution as reported previously [13]. All the IR spectra of synthesized Zr incorporated MFI samples show a characteristic absorption peak at 960 cm^{-1}, which confirmed the incorporation of zirconium into the lattice framework [19]. The IR method of finding relative crystallinity of the samples is achieved by calculating the optical density (OD) ratio of the peaks near 540 and 450 cm^{-1}. The results are given in **Table 2.7** and are found to be in good agreement with those calculated from XRD studies.

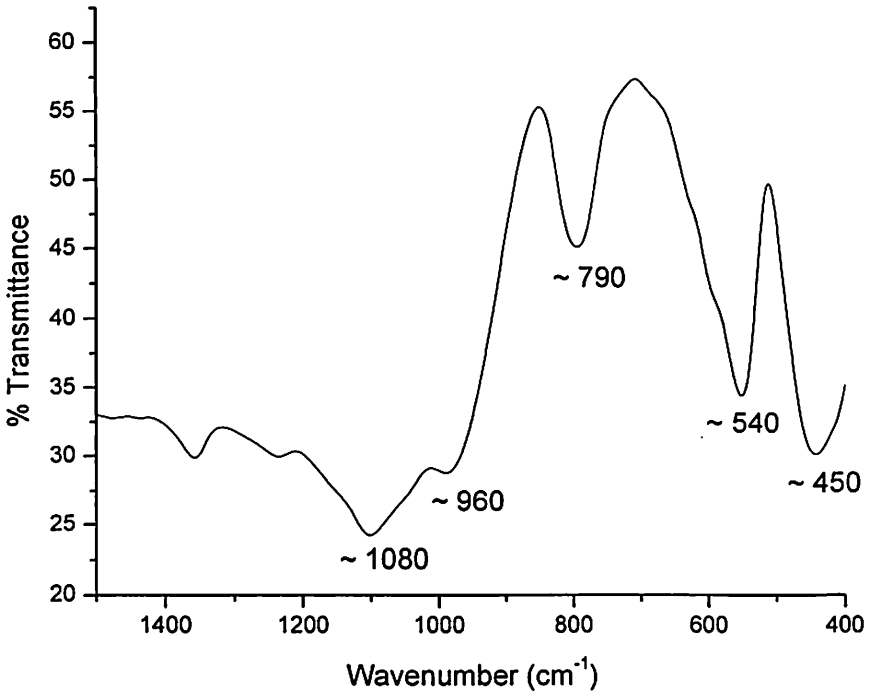

Fig. 2.14 FT-IR spectra of S100Zr3

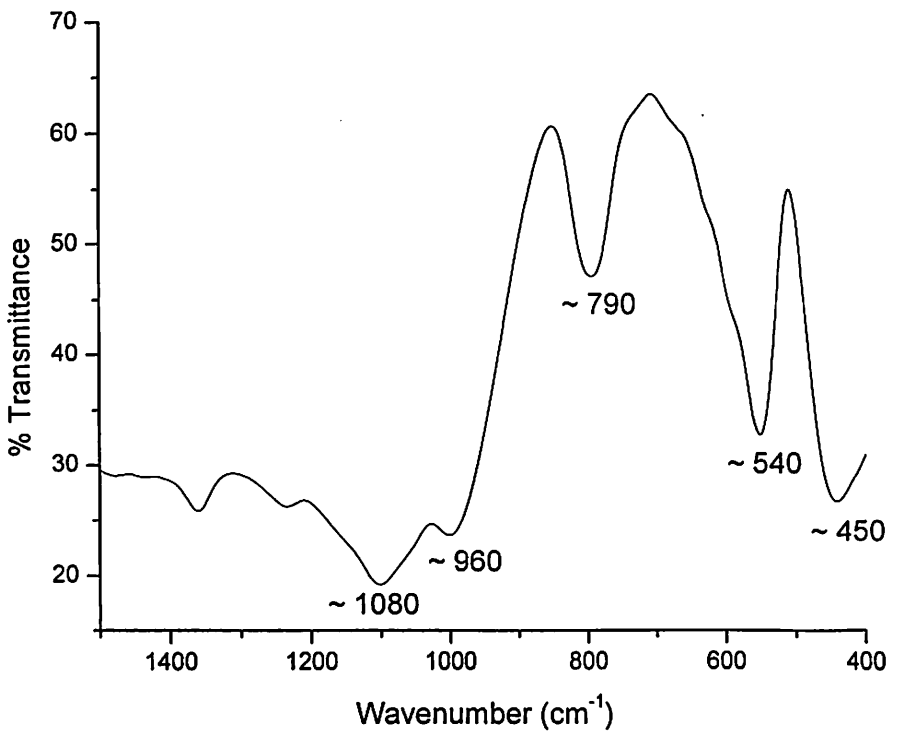

Fig.2.15 FT-IR spectra of S100Zr6

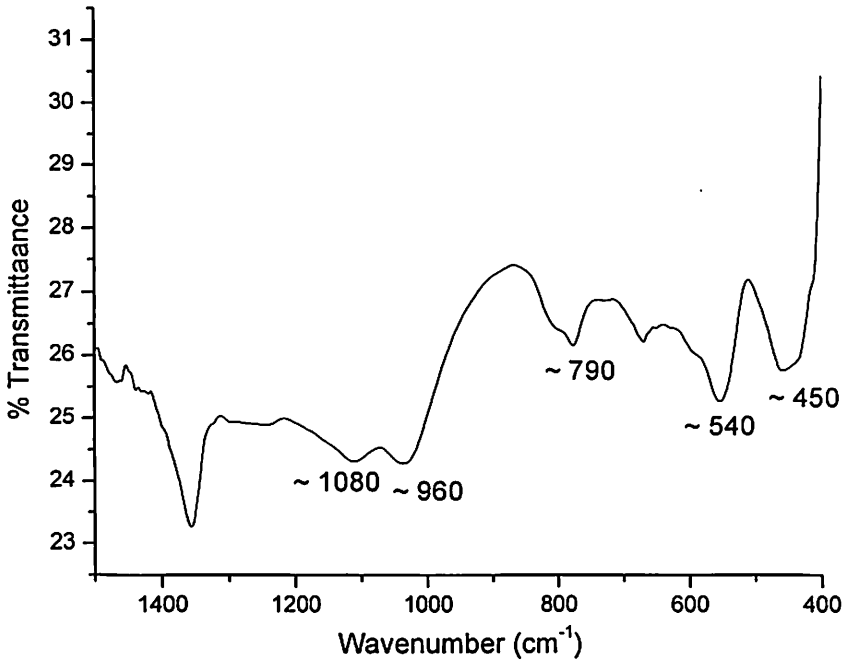

Fig. 2.16 FT-IR spectra of S100Zr9

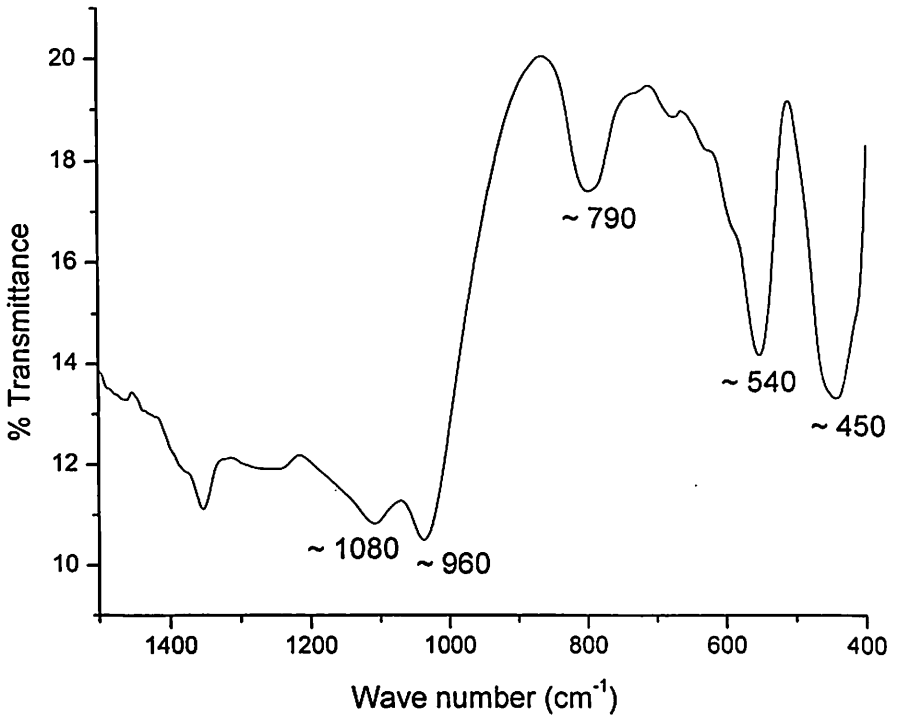

Fig.2.17 FT-IR spectra of S200Zr6

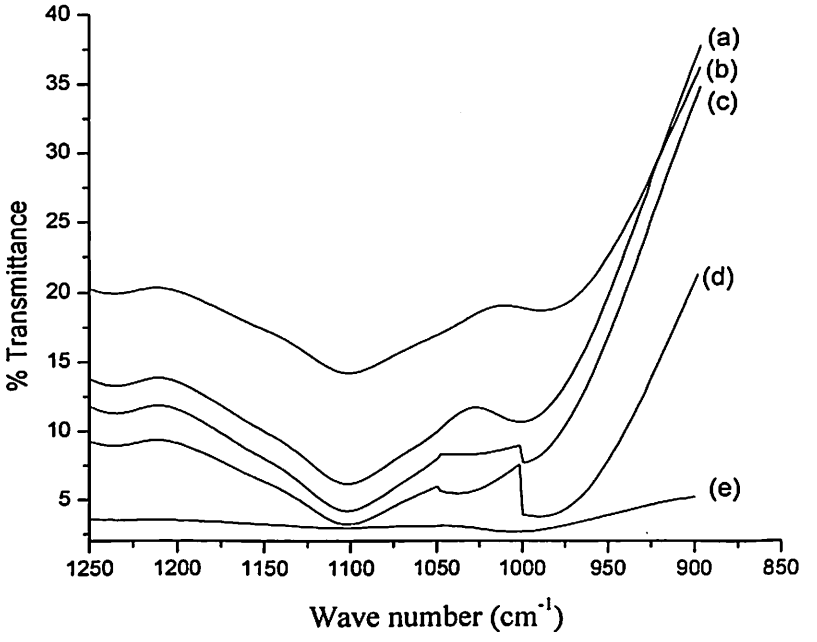

Fig.2.18 FT-IR spectra of Zr-MFI samples synthesized (a) S100Zr3 (b) S100Zr6 (c) S100Zr9 (d) S200Zr6 (e) S100 showing distortion in the range 900-1250 cm^{-1} wrt parent MFI

The TGA curves of Zr-MFI zeolites samples are shown in **Figures 2.19** to **2.22**. The initial mass loss up to 423 K is attributed to physically adsorbed water in the porous materials [20]. Beyond 423 K mass loss increased in the temperature range 423-893 K while it decreased in the temperatures beyond 893 K. The mass loss during second and third phase can be attributed to the degradation of four types of TPA^+ cation inside the zeolite structure [21]. The first two types are TPA^+ cations ion-paired to crystal surface defects and TPA^+ cations occluded in the zeolite channels respectively. These two types are least strongly bound and therefore, more easily lost at a comparatively lower temperature range (423-773 K). The cation species that neutralize internal framework defects and TPA^+ cations that neutralize the framework negative metal centers (MO_4^-) coordinated into the silica framework are the third and fourth types of TPA^+ cations which are more strongly bound counter ion species and thus lost at high temperature above 893 K. In the present work it

is observed that as the level of Zr content increases (simultaneously as the Al content decreases) in the MFI structure, the mass loss increases in the temperature range above 423-893 K and decreases in the temperature range 893-1023 K. This is because as the Zr^{4+} content increases (and hence the Al^{3+} content decreases) in the framework structure, the concentration of framework negative metal centers (MO_4^-) decreases and thus the number of the fourth type of TPA^+ cation that neutralizes the framework negative metal centers also decreases. Consequently the major parts of TPA^+ cations are present as first two types (i. e. associated with the crystal surface defects and also as occluded in the zeolite channels). This explains the increase in mass loss in the temperature range 423-893 K as compared to that beyond 893 K. The percentage weight losses for various temperature ranges for different samples are presented in **Table 2.8.**

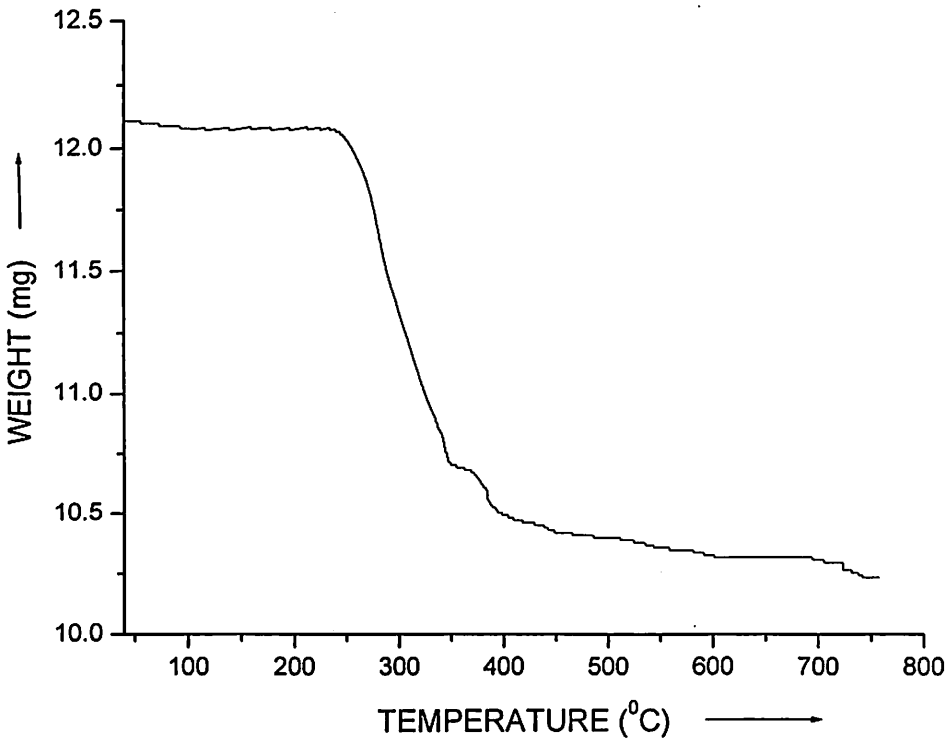

Fig.2.19 TGA Curve of S100Zr3

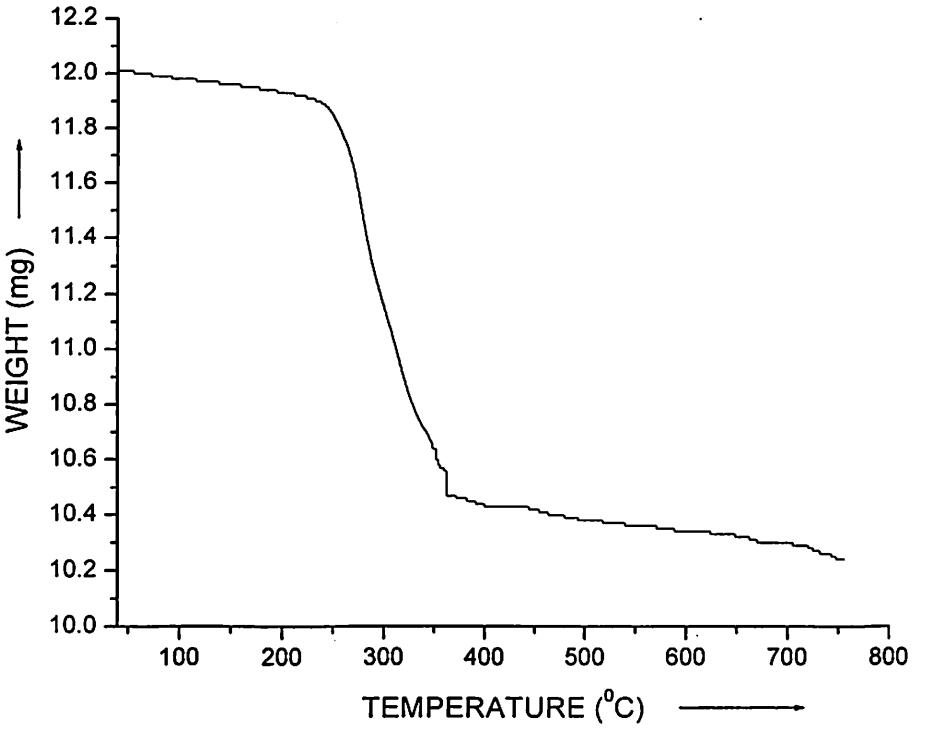

Fig.2.20 TGA curve of S100Zr6

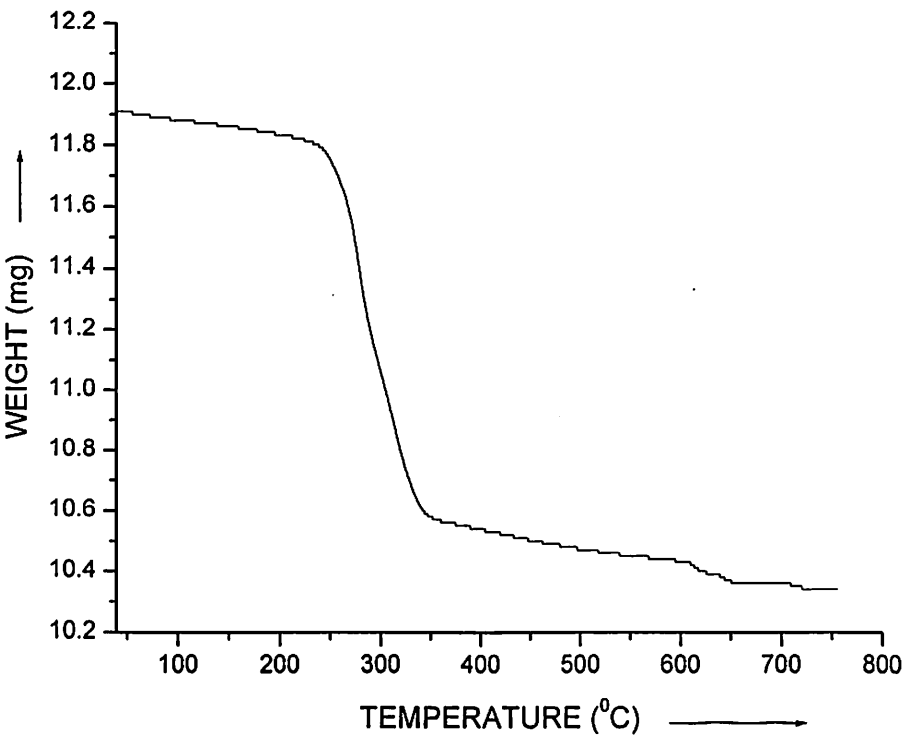

Fig.2.21 TGA curve of S100Zr9

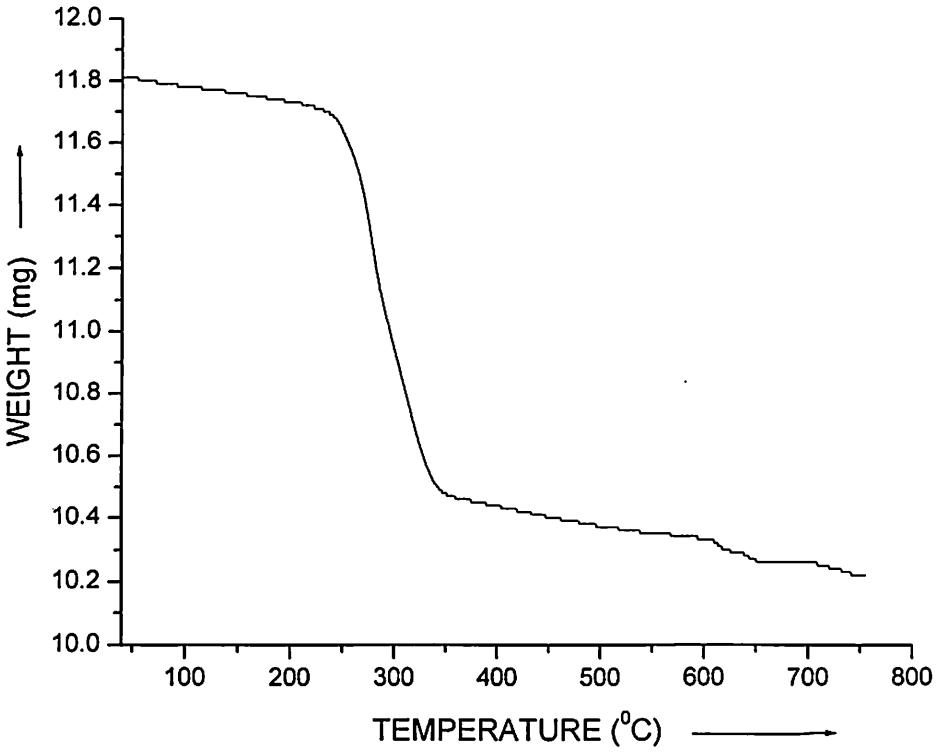

Fig.2.22 TGA curve of S200Zr6

Table 2.8 Percentage of weight loss of the Zr-MFI samples observed during TG analysis

Sample	Zr^{4+} mol in gel	Temperature range (K)	% Weight loss	Total % weight loss as synthesized samples
S100Zr3	0.25	273-473	2.68	16.26
		473-893	12.11	
		893-1023	1.47	
S100Zr6	0.125	273-473	2.57	15.60
		473-893	11.54	
		893-1023	1.49	
S100Zr9	0.1	273-473	2.93	15.04
		473-893	10.59	
		893-1023	1.52	
S200Zr6	0.0625	273-473	2.49	14.20
		473-893	10.10	
		893-1023	1.61	

The UV-Vis-DR spectra of the Zr-MFI samples are shown in **Figures 2.23** to **2.26**. The UV-Vis-DR spectra of the Zr-MFI samples indicate the existence of a band at around 210 nm. The band at around 210 nm is assigned for zirconium with tetrahedral coordination [22]. This means that zirconium metal has been incorporated into the framework of MFI structure although some species may be present as extra framework.

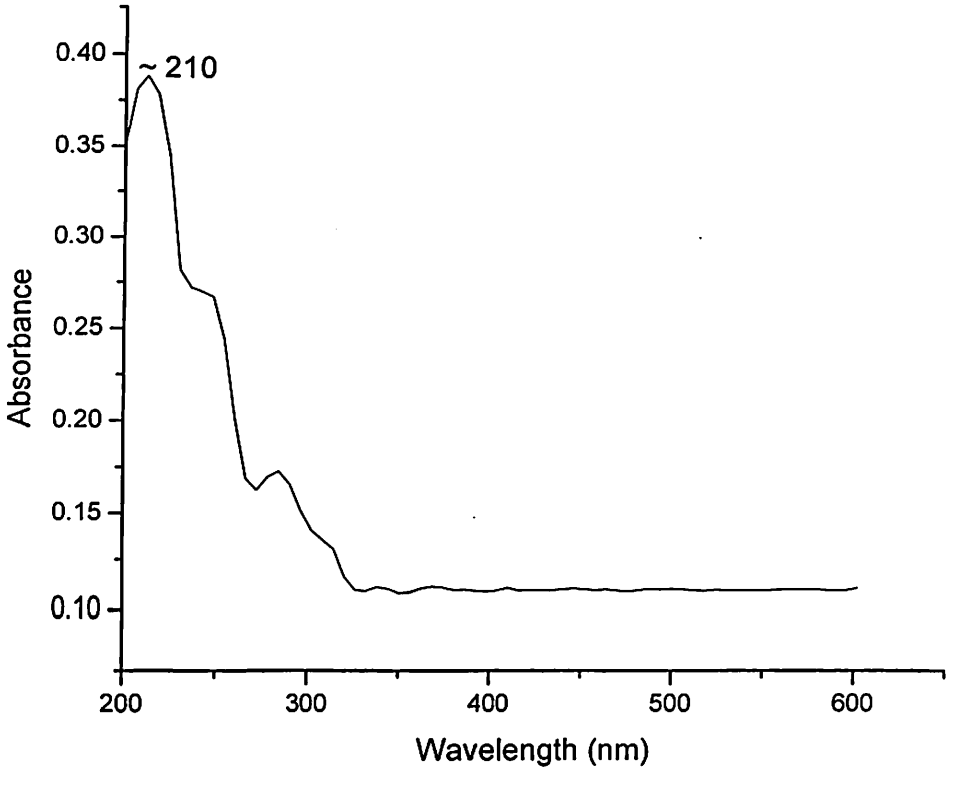

Fig.2.23 UV-Vis DR spectra of S100Zr3

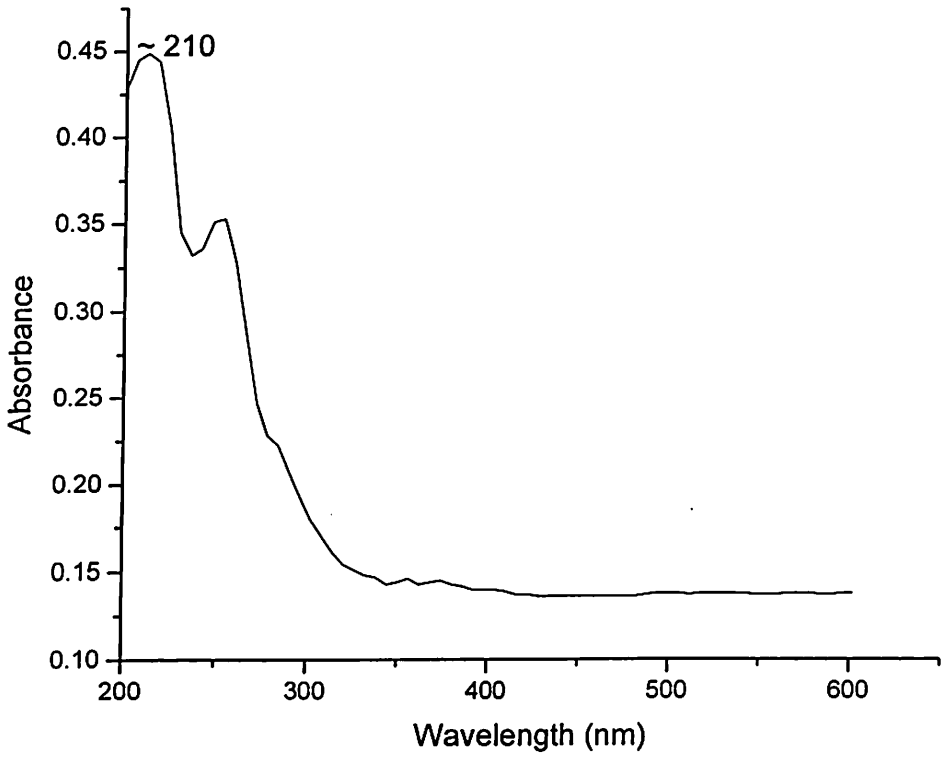

Fig.2.24 UV-Vis DR spectra of S100Zr6

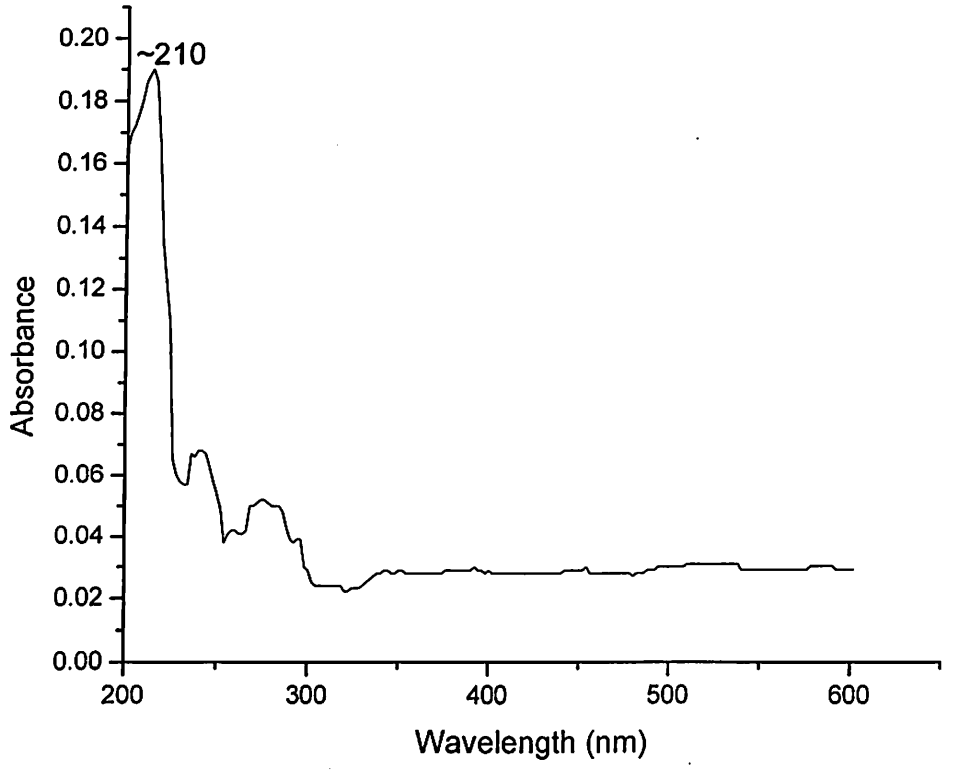

Fig.2.25 UV-Vis DR spectra of S100Zr9

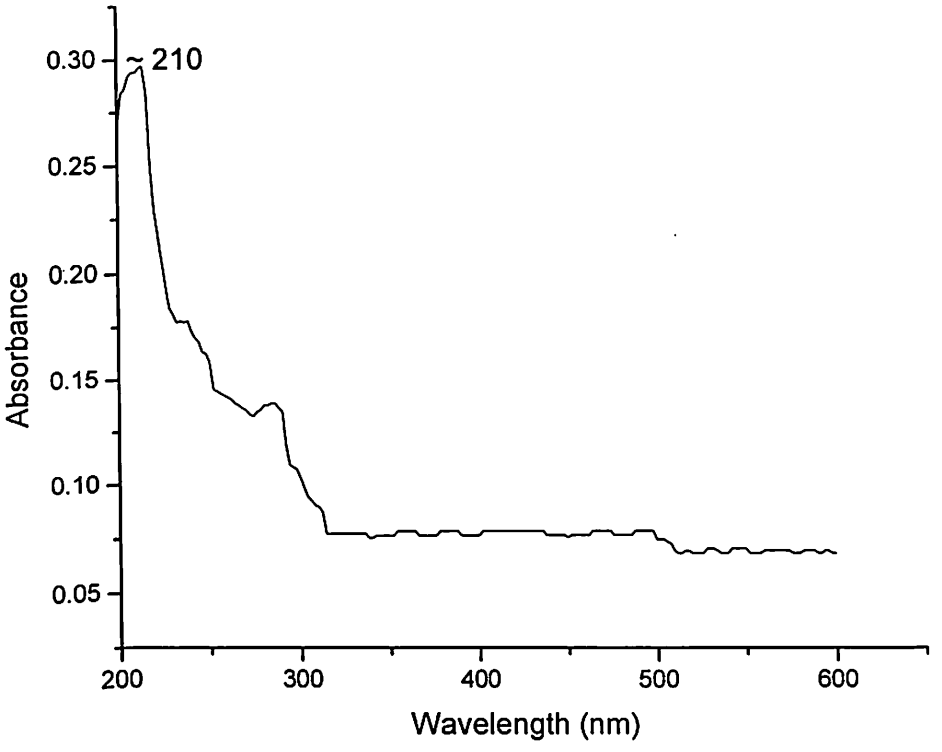

Fig. 2.26 UV-Vis DR Spectra of S200Zr6

Nitrogen adsorption isotherms of calcined Zr-MFI samples are depicted in **Figures 2.27** to **2.30**. The N_2 adsorption isotherms of the zirconium incorporated zeolite samples have type H-1 hysteresis loops with almost vertical adsorption desorption branches at P/P_0 = 0.12 to 0.21, which come from agglomerates of uniform particles. These types of hysteresis loop at these relative pressures are unusual and may be associated with the presence of micropores arising from textural microporosity or to the 'inkwell' uniform micropore geometry connecting to some mesopores. The analysis also showed that the specific surface area ranged from ~356 to ~365 m^2g^{-1} and pore volume ranged from 0.178 to 0.189 cm^3g^{-1} as the content of the Zr in the gel increased from 0.0625 to 0.25 M in the MFI samples. This means that with the increase in the level of substitution of zirconium, the surface area as well as the pore volume increased. The specific surface area, pore volume and pore size of the synthesized samples are shown in **Table 2.9**. The pore size of the

synthesized samples were found to be both in mesoporous (~2.1 nm) and microporous range (~0.50 nm).

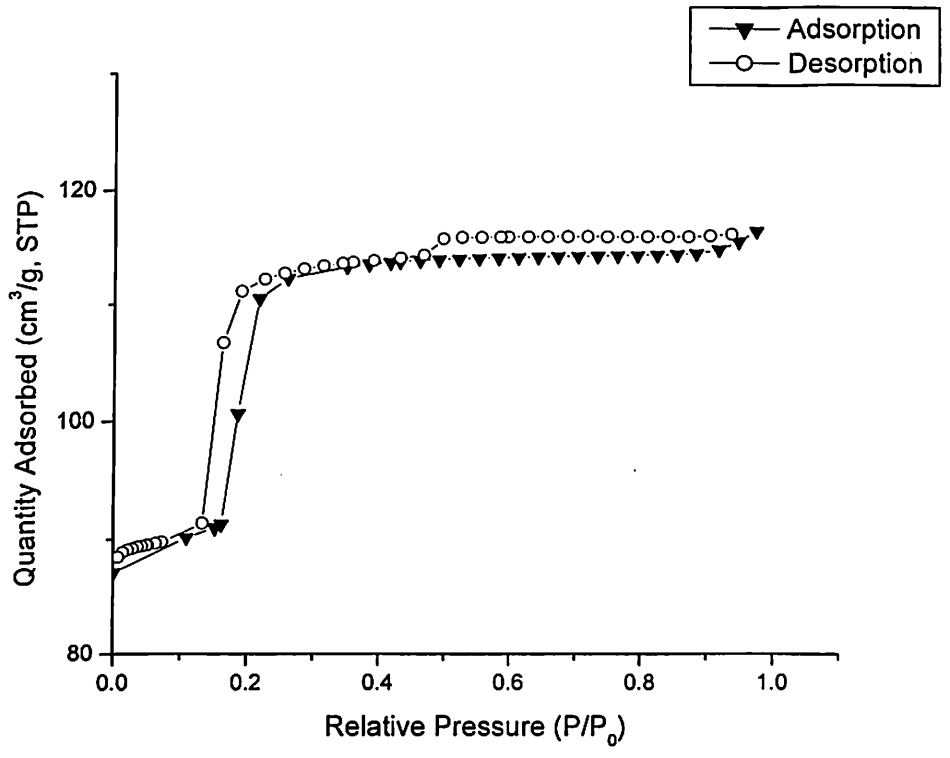

Fig. 2.27 Nitrogen adsorption isotherm of calcined S100Zr3

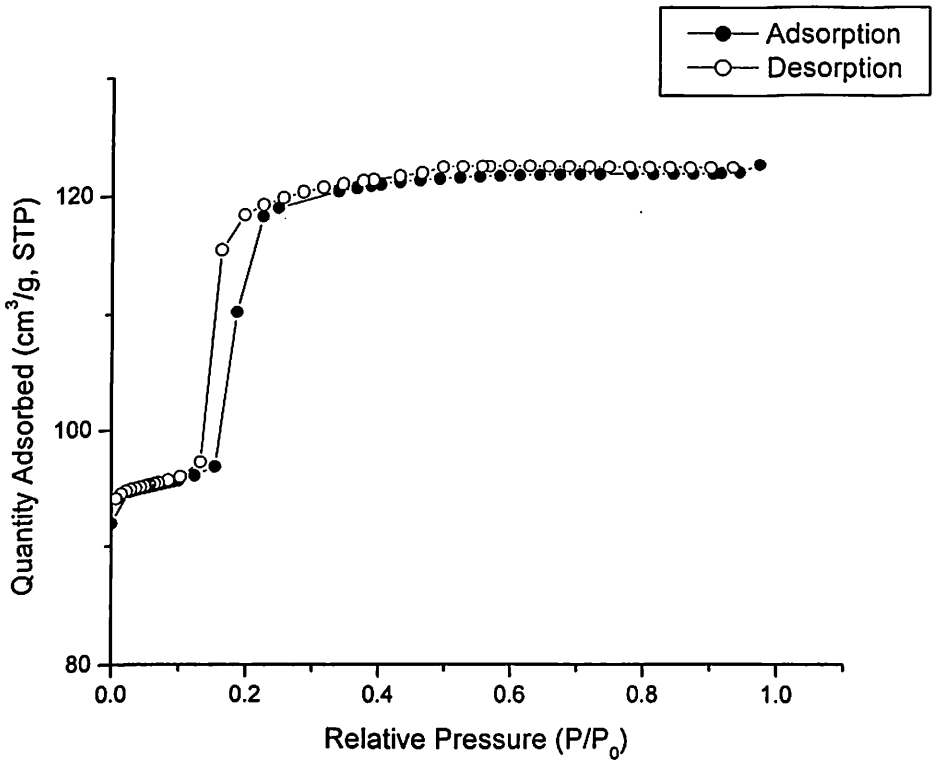

Fig.2.28 Nitrogen adsorption isotherm of calcined S100Zr6

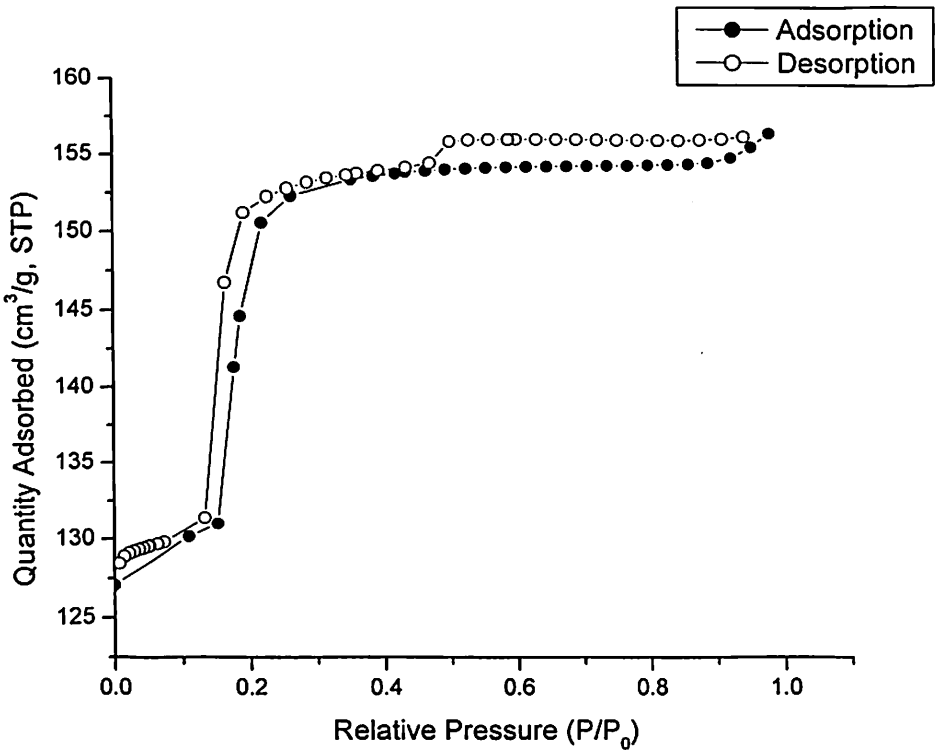

Fig.2.29 Nitrogen adsorption isotherm of calcined S100Zr9

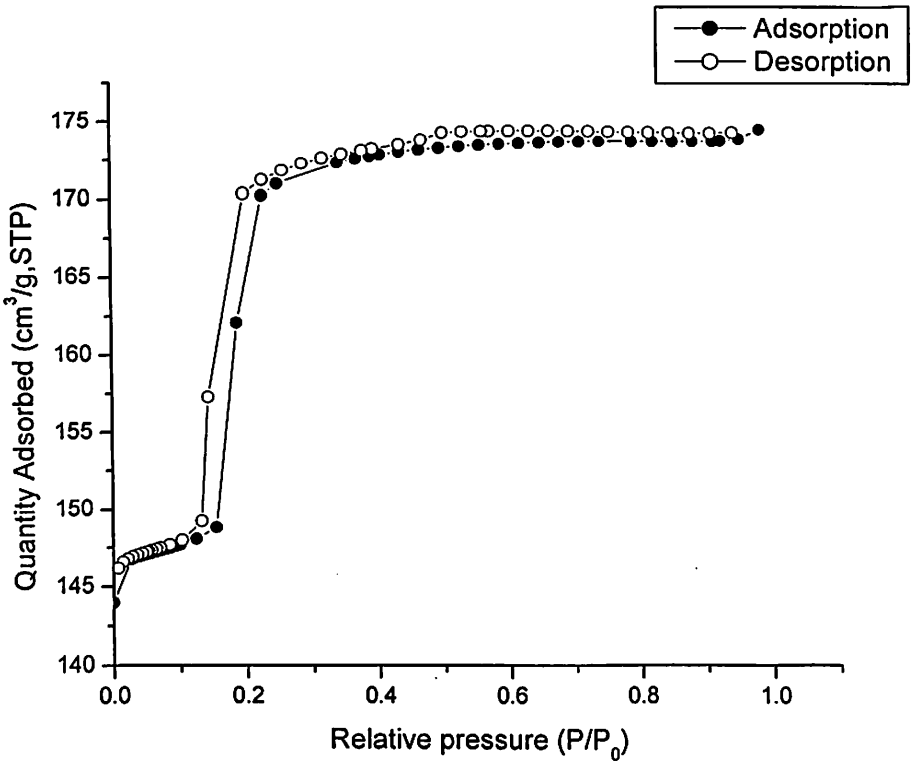

Fig.2.30 Nitrogen adsorption isotherm of calcined S200Zr6

Table 2.9 Specific surface area, pore size and pore volume of synthesized Zr-MFI samples

Sample	Zr^{4+} mol in gel	Surface area (BET,m^2g^{-1})	Pore volume (cm^3g^{-1})	Mesopore size (nm)	Micropore size (nm)
S100Zr3	0.25	365.67	0.189	2.1	0.51
S100Zr6	0.125	361.21	0.180	2.2	0.54
S100Zr9	0.1	360.22	0.179	2.4	0.52
S200Zr6	0.0625	356.78	0.178	2.2	0.51

The amount of Zr incorporated in the samples were analyzed by EDX and the results are shown in **Table 2.10.**

Table 2.10 Theoretical and determined amount of Zr incorporated in the synthesized samples

Sample	In the gel		pH of the gel	In the sample (calculated from EDX)	
	Si:(Al+ Zr)	Al:Zr		Si:(Al+ Zr)	Al:Zr
S100Zr3	100	3	7.0	142	1.8
S100Zr6	100	6	6.9	145	4.5
S100Zr9	100	9	6.8	147	6.8
S200Zr6	200	6	6.9	234	3.5

The size and shape of the crystalline MFI particles were investigated by SEM analysis. SEM micrographs of synthesized Zr-MFI samples are shown in **Figures 2.31** to **2.34**. From the micrographs of zirconium incorporated samples it can be seen that quite uniform rectangular and twinned rectangular shaped MFI particles were formed and the size of the particles was found to be nearly 28 μm. Isomorphously zirconium substituted zeolite samples synthesized using different metal concentration in the gel did not show any distinct difference in morphological features among themselves. However, their shape and size are markedly different from undoped MFI [**Figure 2.7**]. Again, lower Zr containing samples showed greater agglomeration of the particles which may be due to residual silica remaining during crystallization process. Crystal growth (crystallinity and crystallite size) increases with increasing metal concentration in the gel. Otherwise, no major change in MFI phases due to variation in Zr concentration was observed.

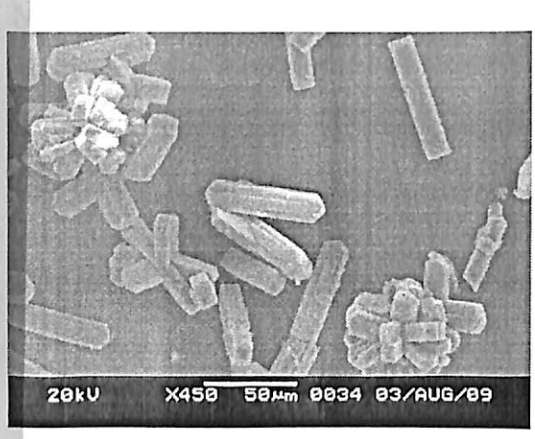

Fig.2.31 SEM picture of S100Zr3

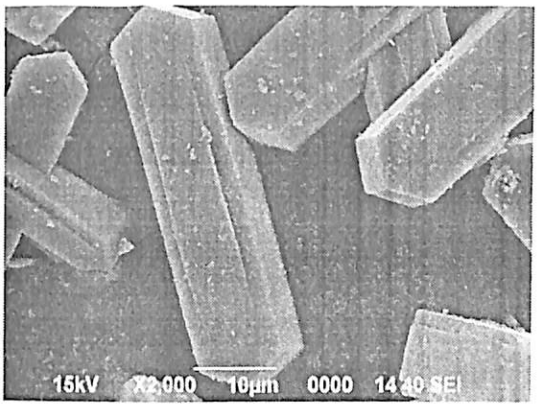

Fig.2.32 SEM picture of S100Zr6

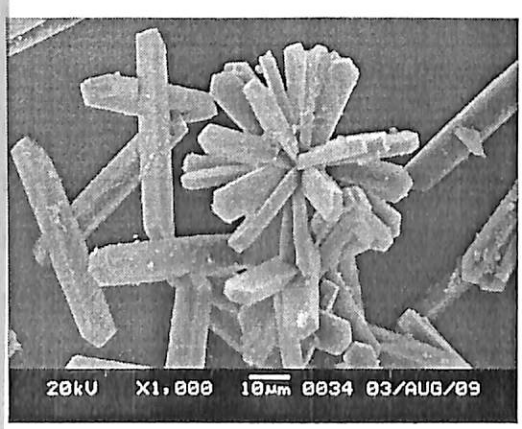

Fig.2.33 SEM picture of S100Zr9

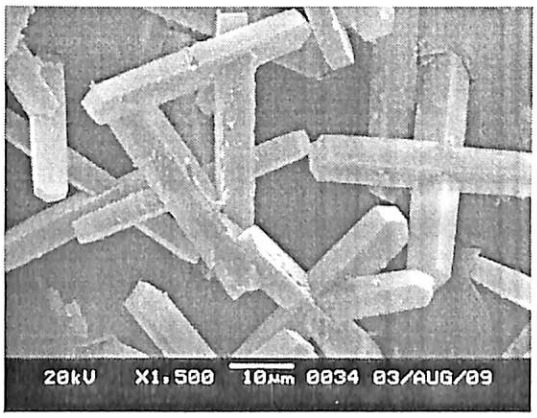

Fig.2.34 SEM picture of S200Zr6

2.6 Conclusion

A green approach has been successfully utilized to synthesize nanocrystalline MFI zeolite with a very broad range of silicon to aluminium ratios. Pure phases of MFI zeolite were obtained in absence of any promoter, organic solvent or sulphuric acid. XRD patterns of the samples confirm the formation of MFI zeolite phase and the results are well supported by FT-IR data. The analysis has shown that the specific surface area of the synthesized samples was ~355 m^2g^{-1}, pore volume ~ 0.174 cm^3g^{-1} and that of pore size ~ 0.51(micropore) to ~ 2.1 (mesopore) nm.

Zr incorporated MFI has been successfully synthesized using fluoride gel as mineralizer in slightly acidic or neutral media. The quality of synthesized samples are characterized by XRD, FT-IR, TGA, UV-Vis (DRS), N_2 adsorption-desorption isotherm and SEM and are found to be highly satisfactory. XRD and FTIR spectra of the samples confirm the formation of MFI zeolite phase, while thermogravimetric analysis as well as the DR spectra supported the successful incorporation of Zr in the tetrahedral position. All the samples under the present investigation were found to exhibit high crystallinity upto (~ 97%). The crystallite sizes of the samples are found in the range from about 49 to 59 nm. The unit cell volumes are found to increase with the increasing level of metal substitution. From thermogravimetric analysis it is observed that as the level of Zr content increased (simultaneously as the Al content decreased) in the MFI structure, the mass loss increased in the temperature range above 423-893 K and decreased in the temperature range 893-1023 K. The nitrogen adsorption isotherm analysis has shown that the specific surface area of the synthesized samples increases from ~356 to ~365 m^2g^{-1} and pore volume increases from 0.178 to 0.189 cm^3g^{-1} as the content of the Zr in the structure (gel) increases from 0.0625 to 0.25 M for the MFI samples. Isomorphously substituted zirconium zeolite samples synthesized using different metal concentration in the gel do not show any distinct difference in morphological features among themselves. However, their shape and size are markedly different from undoped MFI. Again, lower Zr containing samples show greater agglomeration of the particles which may be due to residual silica remaining during crystallization process.

2.7 References

[1] R.J. Argauer, G.R. Landolt, US Patent,(1972) 3702886.

[2] H.Robson, *Micropor. Mater.* 22 (1998) 626.

[3] R.M. Barrer, *Hydrothermal Chemistry of Zeolites*, Academic Press, New York (1982).

[4] A.Thangaraj, M. J. Eapen, S. Sivasanker, P. Ratnaswamy, *Zeolites* 12 (1992) 943.

[5] P. Kumar, A. Bhaumik, R.K. Ahedi, S. Ganapathy, *Nature* 381 (1996) 298.

[6] S.J.Kulkarni, P. Srinivasu, N. Narender, K.V. Raghavan, *Catal. Commun.* 3 (2002) 113.

[7] E.M. Flanigen, R.L. Patton, US 4,073,865, United States, (1978).

[8] D. Ma, Y. Shu, X. Han, X. Liu, Y. Xu, X. Bao, *J. Phys. Chem.* B 105 (2001) 1786.

[9] A. Corma, L.T. Nemeth, M. Renz, S. Valencia, *Nature,* 412 (2001) 423.

[10] C. Wang et al. *Appl. Catal. A: General,* 334 (2008) 137.

[11] M K Dongare, P Singh, P P Moghe and P Ratnasamy, *Zeolites*, 11 (1991) 690.

[12] M.M.J. Treacy, J.B. Higgins (Eds.) *Collection of Simulated XRD Powder Patterns for Zeolites*, Elsevier, (2001) 234.

[13] C.I. Round, C.D. Williams, K. Latham, C.V.A. Duke, Chem. Mater. 13 (2001) 468.

[14] R. Szostak, *Molecular Sieve*, 2nd Edn. (Blackie-Academic & Professional, London, (1998) 306.

[15] K.F.M.G.J. Scholle, W.S. Veeman, P. Frenken, G.P.M. Velden, *Appl. Catal.*,17 (1985) 233.

[16] J.C. Jansen, F.J.Gaag, H. Bekkum, *Zeolites,* 4 (1984) 369.

[17] J. Bonardet, J. Fraissard, K. Onger, D. Kumar, M. Ferrero, J. Ragle, W. C. Conner, *Stud. Surf. Sci. Catal,* 87 (1994) 319.

[18] W. Zhan, G. Lu, G.Yanglong, G. Yun, W.Yanqin, W. Yunsong, Z. Zhigang, Liu Xiaohui, *J. Rare Earths,* 26, 4 (2008) 515.

[19] B. Rakshe, V. Ramaswamy, S.G Hegde, R. Vetrivel, A.V. Ramaswamy, *Catal. Lett.* ,45 (1997) 41.

[20] J.L. Guth, H. Kessler, J.M. Higel, J.M. Lamblin, J. Patarin, A Seive, J.M. Chezeau, R. Wey, *zeolite synthesis*, in : ACS Symp. Ser. 398, Washington DC, (1989) 176.

[21] J.L.Guth, L. Delmotte, M. Soulard, N. Brunard, J.F. Joly, D. Espinat, *Zeolites,* 12 (1992) 929.

[22] L. B. Newalkar, O. Johnson, S.R. Komarneni, *J. Phys. Chem.* B 105 (2001) 8356.

CHAPTER-3

Synthesis and Characterization of In and Ru incorporated MFI Zeolite

Chapter Summary

The first part of this chapter contains the *insitu* modification of MFI zeolite by incorporation of In and their characterization by XRD, FT-IR, TGA, UV-Vis (DRS), N_2 adsorption desorption isotherm and SEM. The latter part of this chapter contains the *insitu* modification of MFI zeolite by incorporation of Ru and their characterization by XRD, FT-IR, TGA, UV-Vis (DRS), N_2 adsorption desorption isotherm and SEM.

3. Introduction

The isomorphous replacement of Al or Si in the zeolite framework by heteroatoms produces new materials with significantly modified physico/chemical and catalytic properties [1]. These materials have the potential to carry out petrochemical and/or organic reactions [2]. Three different methods have usually been applied for preparation of metal-containing catalyst of MFI structure: (i) synthesis of Isomorphously substituted metal silicates with an appropriate metal content in the framework [3]; (ii) conventional (aqueous phase) ion-exchange [4]; (iii) solid state ion-exchange procedure: an intimate mixture of the respective metal precursor (oxide or chloride) and H-form of zeolite followed by a controlled heat treatment in oxidative or reductive atmosphere [5,6].

The In-containing MFI zeolite catalysts have been reported to prepare using five different methods [7]:

(i) ion-exchange in $In(NO_3)_3$ solution with Na-MFI (Si/Al= 40) sample, (ii) solid state ion-exchange started from H-MFI and In_2O_3 in oxidative atmosphere, (iii) solid state ion-exchange started from H-MFI and In_2O_3 in reductive atmosphere, (iv) solid state ion-exchange started from H-MFI and

$InCl_3$ in oxidative atmosphere, (v) solid state ion-exchange started from H-MFI and $InCl_3$ in reductive atmosphere.

Methods that have been reported to prepare In-MFI so far for the are ion-exchange, precipitation, mechanical mixing, and dry techniques based on the use of $InCl_3$: solid-state ion exchange, sublimation, and transport reaction processes mainly, but the attempt for *insitu* modification of the MFI zeolites with indium have not yet been reported.

The incorporation of ruthenium into zeolites has been recently reviewed [8]. The ionic radius (0.69 Å) of Ru^{3+} ion is larger than Al^{3+} (0.57 Å) and, like iron (preceding member of Group 8), it has an ability to change oxidation state and a tendency to form insoluble hydroxides in a basic environment. This has been reported to achieve using potassium ruthenate (VI), K_2RuO_4, and tetra-n-propylammonium perruthenate (VII), $(Pr_4N)RuO_4$. The method is somewhat unwieldy and quite a lengthy process also. In the present study ruthenium salts are used as a source of Ru and the process takes comparatively shorter time for completion.

3.1 Experimental

3.1.1 Source of chemicals

Chemicals used for the synthesis of In and Ru incorporated MFI zeolites are sodium aluminate (Kemphasol), tetrapropylammonium bromide (Lancaster), sodium fluoride (Fluka Chemika 99%), indium nitrate hydrate (Aldrich 99%), ruthenium chloride (Merck), fumed silica (BDH) and de-ionized water.

3.1.2 Synthesis of In incorporated MFI zeolite

Three samples of MFI Zeolite containing In were synthesized in the Si to Al and In ratios of 100 and different Al to In ratios. A typical procedure for the synthesis of MFI zeolite with silicon to aluminium and indium ratio of 100

and Al: In ratio of 1:1 is stated below with the following gel molar composition:

Si/Al=100/0.5, NaF/SiO_2=1, SiO_2/Al_2O_3=200, TPA-Br/SiO_2=0.07, H_2O/SiO_2=80, Si/In=100/0.5

Calculated amount of NaF was dissolved slowly to 23 mL of de-ionized H_2O. To this solution 1.551 g of TPA-Br was added slowly with continuous stirring. The solution was stirred for 15 min and 1.2947g of SiO_2 was added slowly to this mixture. The resulting mixture (A) was stirred for another half an hour. Required amount of $NaAlO_2$ was dissolved in 97 mL of de-ionized water slowly. To the solution desired amount of indium nitrate hydrate was added and stirred for 10 min. 3.705g of SiO_2 was also added slowly to this with continuous stirring. The resulting mixture (B) is stirred for another half an hour. The mixture A was added to mixture B slowly and stirred continuously for 3 h at pH 6-7 to get homogeneous gel. The whole mass was then autoclaved in a teflon-lined stainless steel vessel maintained at 473 K inside an oven for 25 h. It was then cooled, filtered (Whatman No 42) and washed with de-ionized water several times. The sample was dried at room temperature for about 12 h and at 383 K for 6 h. This was then calcined at 753 K to remove the template. The same procedure was applied to synthesize other samples of In incorporated MFI zeolite with different Al:In ratios. **Table 3.1** shows the molar ratios of the components in the gel and other conditions maintained during the synthesis of In-MFI zeolite samples.

Table 3.1 Molar ratios of the components in the gel and other conditions maintained during the synthesis of In-MFI zeolite samples

Sample	Si: (Al+In)	Al:In	TPA-Br: SiO_2	NaF: SiO_2	H_2O: SiO_2	Autoclavation Time (h)	pH of the gel
S100In1	100	1	0.07	1	80	25	6.9
S100In2	100	2	0.07	1	80	24	6.8
S100In3	100	3	0.07	1	80	24	6.7

3.1.3 Synthesis of Ru incorporated MFI zeolite

Three samples of MFI Zeolite containing Ru were synthesized in the Si to Al and Ru ratios of 100 and different Al to Ru ratio. A typical procedure for the synthesis of MFI zeolite with silicon to aluminium and ruthenium ratio of 100 and Al: Ru ratio of 1:1 is stated below with the following gel molar composition:

$Si/Al=100/0.5$, $NaF/SiO_2=1$, $SiO_2/Al_2O_3=200$, $TPA\text{-}Br/SiO_2=0.07$, $H_2O/SiO_2=80$, $Si/Ru=100/0.5$

Calculated amount of NaF was dissolved slowly to 23 mL of de-ionized H_2O. To this solution 1.551 g of TPA-Br was added slowly with continuous stirring. The solution was stirred for 15 min and 1.2947g of SiO_2 was added slowly to this mixture. The resulting mixture (A) was stirred for another half an hour. Required amount of $NaAlO_2$ was dissolved in 97 mL of de-ionized water slowly. To the solution desired amount of ruthenium chloride was added and stirred for 10 min. 3.705g of SiO_2 was also added slowly to this with continuous stirring. The resulting mixture (B) is stirred for another half an hour. The mixture A was added to mixture B slowly and stirred continuously

for 3 h at pH 6-7 to get homogeneous gel. The whole mass was then autoclaved in a teflon-lined stainless steel vessel maintained at 473 K inside an oven for 25 h. It was then cooled, filtered (Whatman No 42) and washed with de-ionized water several times. The sample was dried at room temperature for about 12 h and at 383 K for 6 h. This was then calcined at 753 K to remove the template. The same procedure was applied to synthesize other samples of Ru incorporated MFI zeolite with different Al:Ru ratios. **Table 3.2** shows the molar ratios of the components in the gel and other conditions maintained during the synthesis of Ru-MFI zeolite samples.

Table 3.2 Molar ratios of the components in the gel and other conditions maintained during the synthesis of Ru-MFI zeolite samples

Sample	Si: (Al+Ru)	Al:Ru	TPA-Br: SiO_2	NaF: SiO_2	H_2O: SiO_2	Autoclavation Time (h)	pH of the gel
S100Ru1	100	1	0.07	1	80	24	7.1
S100Ru2	100	2	0.07	1	80	25	6.9
S100Ru3	100	3	0.07	1	80	23	6.8

3.2 Characterization of the synthesized samples

3.2.1 X-ray diffraction

X-ray powder diffraction analysis was undertaken using a Bruker D-8 Advance X-ray Diffractometer with CuK_α radiation of wavelength 1.5418Å operated at voltage = 40 kV and current = 40 mA and a Miniflex Advance X-ray Diffractometer with CuK_α radiation of wavelength 1.5418 Å operated at voltage = 30 kV and current = 15 mA. The XRD data were collected in 2θ range $5\text{-}50^0$ (step size 0.05^0, step time 0.5 s).

3.2.2 Fourier transform infrared (FTIR) spectroscopy

A PerkinElmer RX 1 FT-IR Spectrophotometer was used for recording the FT-IR spectra of the samples in the form of KBr pellets in mid-IR region of 1500-450 cm^{-1} (resolution 8 cm^{-1}).

3.2.3 Diffuse reflectance UV-Vis spectroscopy

UV-Vis spectra of the samples were obtained from a U-4100 Spectrophotometer equipped with a diffuse reflectance attachment using solid sample holder, in the wavelength region of 200-600 nm at a scan speed of 600 nm min^{-1} (sampling interval: 2.00 nm). The base line correction was made using barium sulphate as the reference standard.

3.2.4 Thermo gravimetric analysis (TGA)

A METTLER TOLEDO TG analyzer (model = TGA/DSC-1) was used for recording the TGA data. TGA was carried out from 313 to 1023 K with a heating rate of 10 K/min under a N_2 flow.

3.2.5 N_2 adsorption-desorption

The N_2 adsorption-desorption isotherms of the samples were obtained using nitrogen as adsorbate at 77.15 K on a Micromeritics (model: Tristar 3000) surface area and porosity analyzer for determining the specific surface area, pore volume and pore size of the synthesized samples. The analysis bath temp was 77.15 K. The calcined samples were degassed for 6 h at 673 K and then gradual heating to 623 K in continuous flow of N_2 and maintained at that temperature for 12 h. The samples were then slowly cooled down to 383 K under N_2 atmosphere and the anhydrous weight of the sample was taken

prior to N_2 adsorption-desorption measurement. Finally, the sample was chilled to 77.15 K using liquid nitrogen and the adsorption of nitrogen was carried out at different equilibrium pressures.

3.2.6 Scanning electron microscopy (SEM)

Scanning electron micrographs of the MFI samples were taken for investigation of the particle morphology using a JEOL JSM-6390 LV Scanning Electron Microscope operating at accelerating voltage of 15-20 kV. The samples for SEM were prepared by spreading the powdered zeolite on a double sided carbon tape stuck to the SEM stage. The excess sample was dusted off by a small air sprayer. Further, the samples were coated with gold thin film in a sputter coater to prevent surface charging and to protect from thermal damage and also to make the sample conducting.

3.3 Results and Discussion

3.3.1 Synthesis of In incorporated MFI zeolite

A systematic study was conducted to synthesize indium incorporated MFI zeolite using silicon to aluminium and indium ratio of 100 and different aluminium to indium ratio in the absence of any promoter, organic solvent or sulphuric acid and also avoiding any seeding gel. The synthesized In-MFI samples were identified by comparison of both the d-spacing and relative intensities in their XRD patterns with those reported in the literature [9] and were found to be in excellent agreement. **Figures 3.1** to **3.3** show the XRD patterns of In-MFI samples synthesized using different aluminium to indium ratios. In all the samples the prominent peaks were observed in 2θ values around 6.5 and 22.5 with a few additional shoulder peaks in all the In incorporated MFI samples suggesting formation of pure phase of the zeolite. Expansion of unit cell in its parameter shown in **Table 3.3**, indicates the successful incorporation of indium in the framework. The unit cell volumes

are found to increase with the increasing level of metal substitution. It may be noticed that with increasing level of substitution the peaks shift towards lower 2θ values indicating successful incorporation of In into the framework of MFI [10]. The shift in 2θ values is presented in **Table 3.4.** The shift of the prominent peaks towards lower 2θ values with increasing level of In substitution with respect to the parent MFI is shown **Figure 3.4.**

Crystallinity of the MFI samples is calculated using **Relation 1** (chapter-2).

The percentage of crystallinity with reference to three significant peaks (*101*), (*501*) and (*303*) as well as the average percentage crystallinity is presented in **Table 3.5.** All the samples under the present investigation were found to exhibit high crystallinity (~ 92%).

The crystallite sizes of the synthesized samples were calculated using **Relation 2** (chapter-2). The crystallite size of the samples ranges from about 49 to 55 nm.

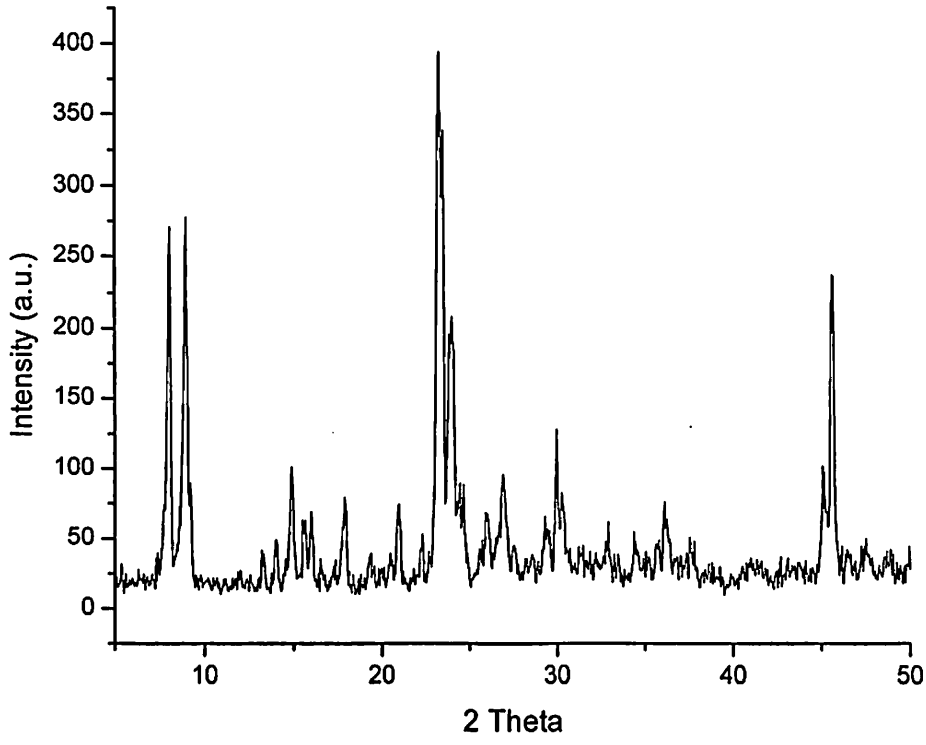

Fig.3.1 XRD patterns of S100In1

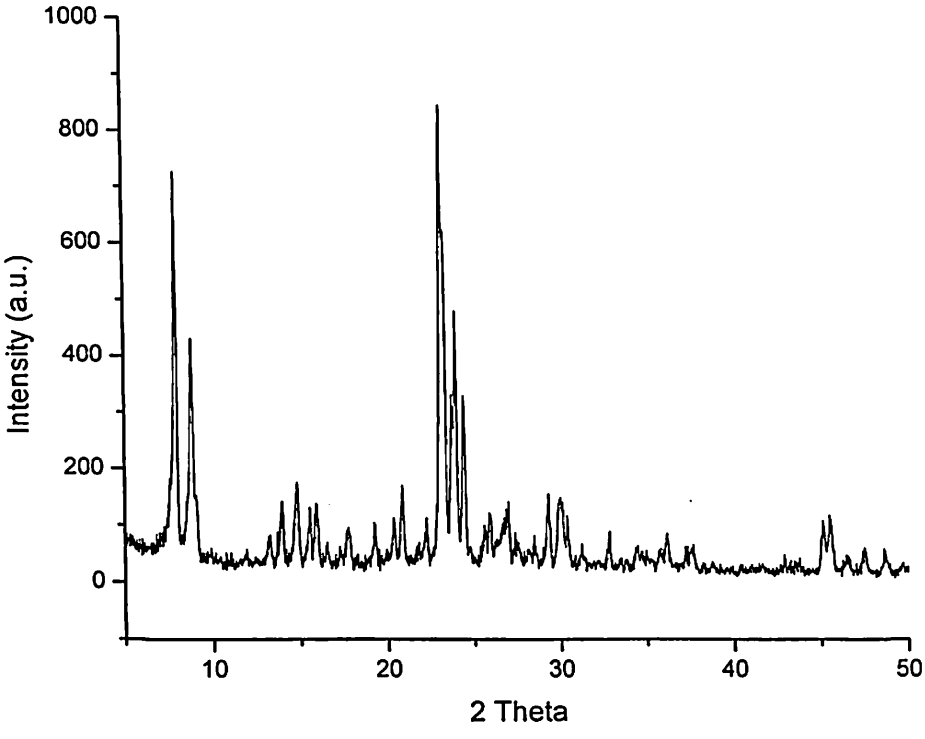

Fig.3.2 XRD patterns of S100In2

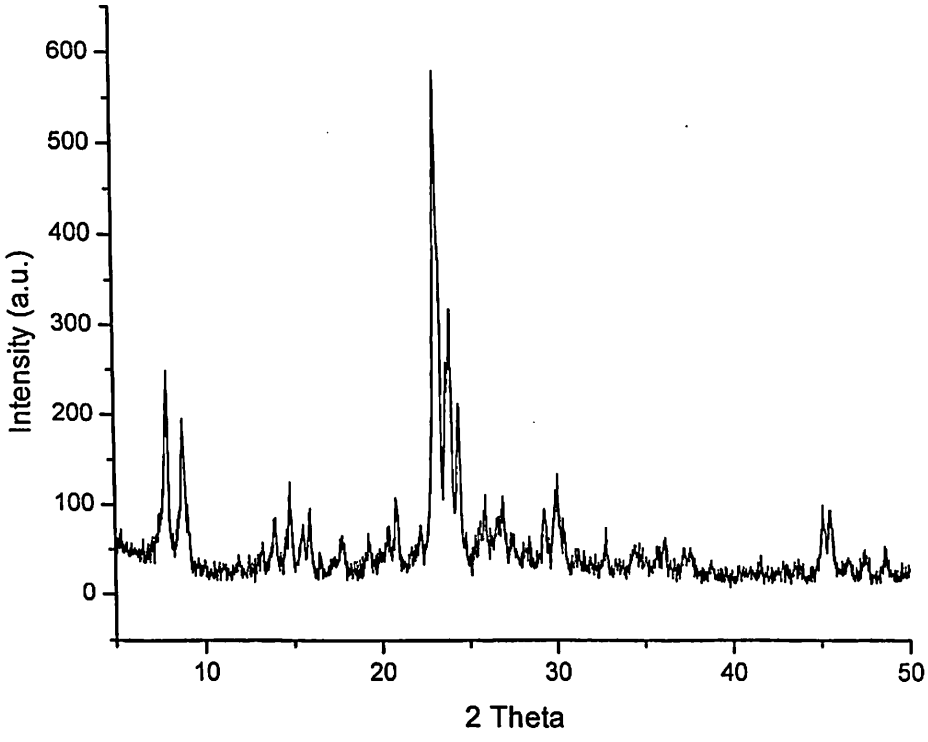

Fig.3.3 XRD patterns of S100In3

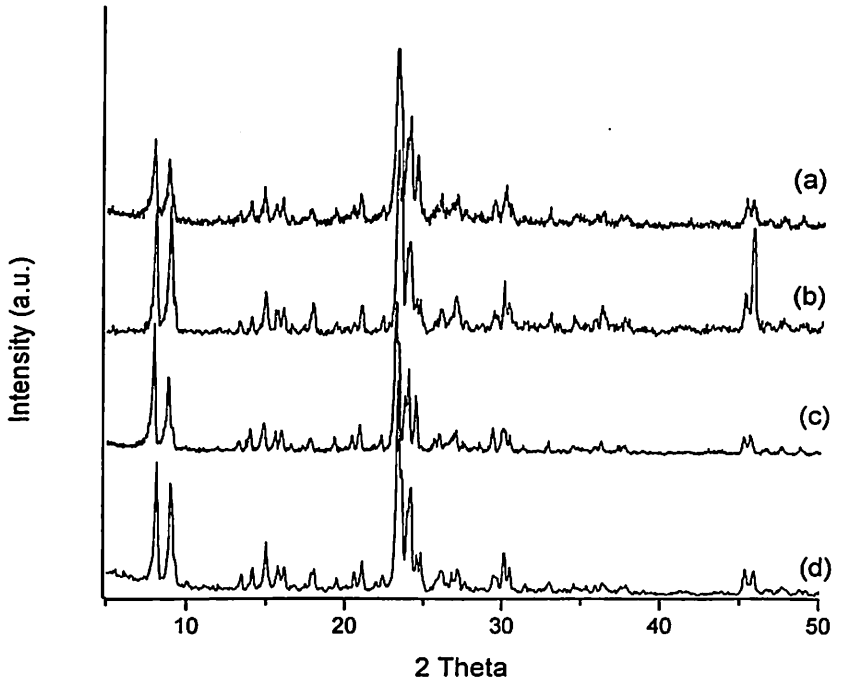

Fig.3.4 Shifting of 2 theta values of prominent peaks with increasing level of In substitution wrt parent MFI (a) S100In1 (b) S100In2 (c) S100In3 (d) S100

Table 3.3 Expansion of unit cell with increasing level of In in MFI samples

Sample	Si : Al	Al : In	Unit cell edges (Å)			Unit Cell Volume ($Å^3$)
			a	b	c	
S100In1	100	1	13.72	19.82	14.81	4027.29
S100In2	100	2	13.68	19.78	14.71	3980.38
S100In3	100	3	13.64	19.75	14.69	3957.34
S100	100	-	13.59	19.71	14.64	3921.45

Table 3.4 Shift in 2θ value of 501 peaks of the In-MFI samples with respect to parent MFI

Sample	In^{+3} mol in the gel	Position of the prominent peak (*501*)	Shift in the 2θ value wrt parent MFI
S100	-	23.36	-
S100In1	0.50	23.09	0.27
S100In2	0.33	23.22	0.14
S100In3	0.25	23.24	0.12

Table 3.5 Crystallite size and percentage of crystallinity $(\%C)_{hkl}$ of the synthesized In-MFI sample

Sample	Si: Al or Si:(Al+In)	Al: In	Crystallite size (nm) (*501*)	(%C)from XRD	% C from IR
S100In1	100	1	52	89.91	85.57
S100In2	100	2	54	93.49	89.25
S100In3	100	3	55	91.16	88.12
S100	100	0.0	49	91.62	89.77

Figures 3.5 to **3.7** show the FT-IR spectra of synthesized MFI samples. IR results confirm the formation of MFI zeolite in all cases showing distinct absorbance bands near 1080 (internal asymmetric stretch), 790 (external symmetric stretch), 540 (double ring vibration) and 450 cm^{-1} (T–O bending). The absorption bands near 550 cm^{-1} have been assigned to the presence of double 5-member rings in the structure [11]. The external asymmetric stretching vibration around 1225 cm^{-1} is present in the spectra of structures assigned to four chains of 5-member rings arranged around a twofold screw axis. The distortion of the spectra was not consistent with increasing levels of

substitution as reported previously [12]. All the IR spectra of synthesized In incorporated MFI samples show an additional absorption peak at 990 cm^{-1} and according to some authors [13] this is an indication of incorporation of heteroatom into the lattice framework. The IR method of finding relative crystallinity of the samples is achieved by calculating the optical density (OD) ratio of the peaks near 540 and 450 cm^{-1}. The results are given in **Table 3.5** and are found to be in good agreement with those calculated from XRD studies.

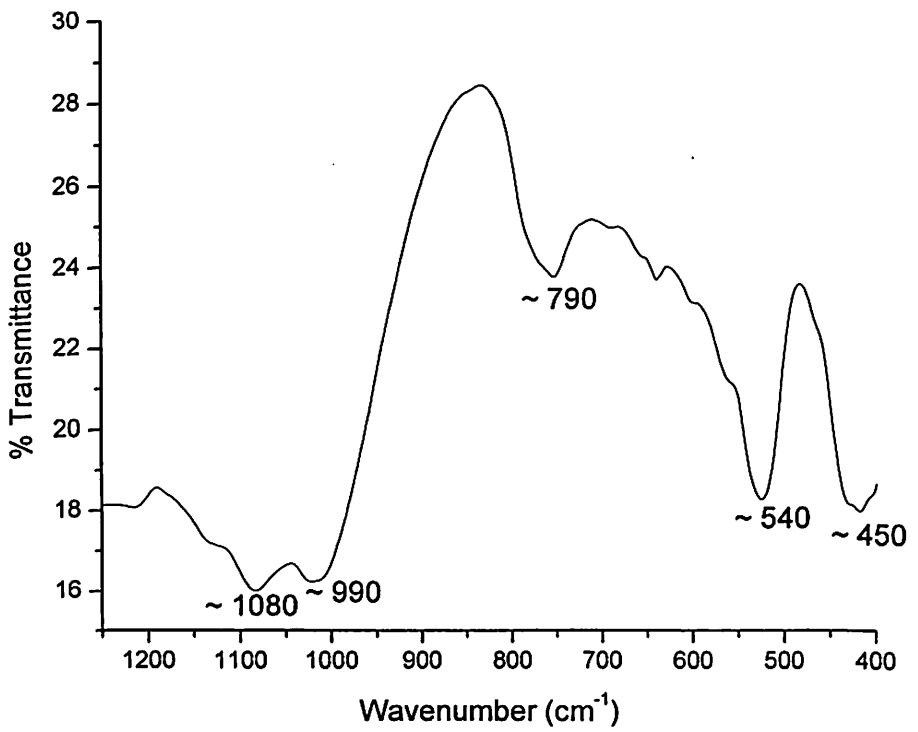

Fig.3.5 FT-IR spectra of S100In1

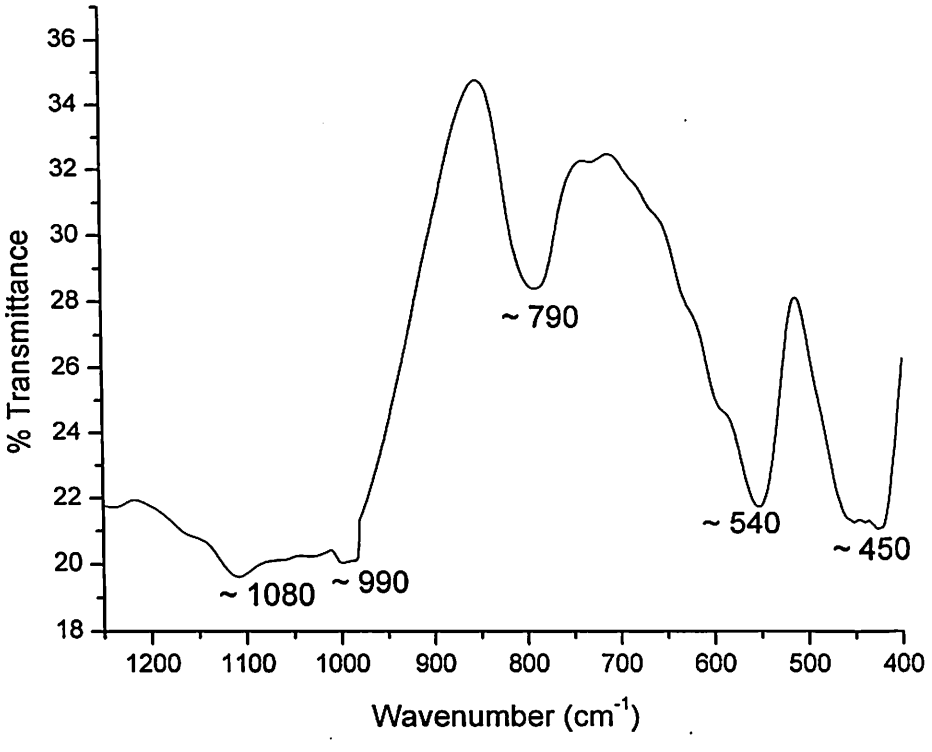

Fig.3.6 FT-IR spectra of S100In2

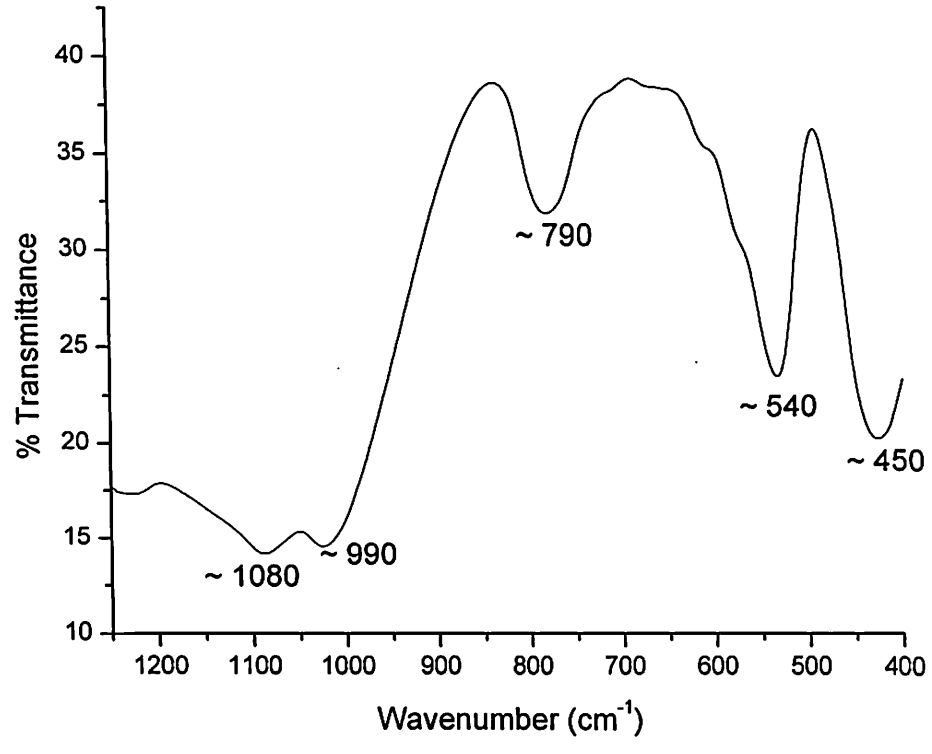

Fig.3.7 FT-IR spectra of S100In3

The TGA curves of In-MFI zeolites samples are shown in **Figures 3.8** to **3.10**. The initial mass loss up to 423 K is attributed to physically adsorbed water in the porous materials [14]. Beyond 423 K mass loss increased in the temperature range 423-893 K while it decreased in the temperatures beyond 893 K. The mass loss during second and third phase can be attributed to the degradation of four types of TPA^+ cations inside the zeolite structure [15]. The first two types are TPA^+ cations ion-paired to crystal surface defects and TPA^+ cations occluded in the zeolite channels. These two types are least strongly bound and therefore, more easily lost at a comparatively lower temperature range (423-773 K). The TPA^+ cations that neutralize the framework negative metal centers (MO_4^-) coordinated into the silica framework are the third types of TPA^+ cations which are more strongly bound counter ion species and thus lost at high temperature above 893 K. In the present work it is observed that the mass loss is more or less constant in the three temperature ranges even if the level of In content increases (simultaneously Al content decreases) in the MFI structure. This is because both indium and aluminium are present in +3 oxidation states in the framework of MFI structure and resultant charge on MO_4 remains same. The percentage weight losses for various temperature ranges for different samples are presented in **Table 3.6.**

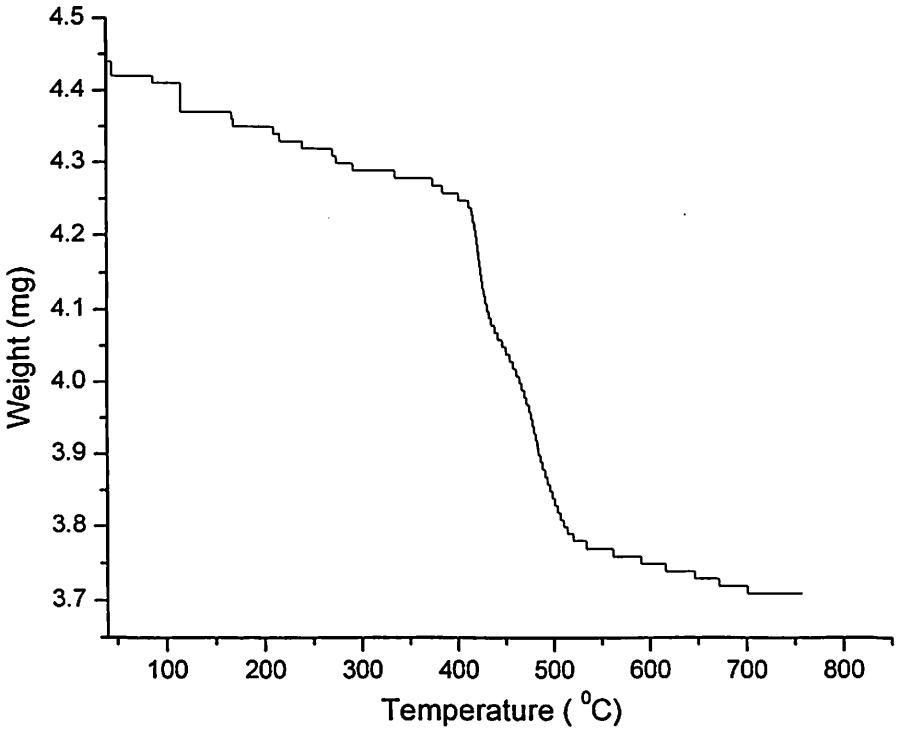

Fig.3.8 TGA curve of S100In1

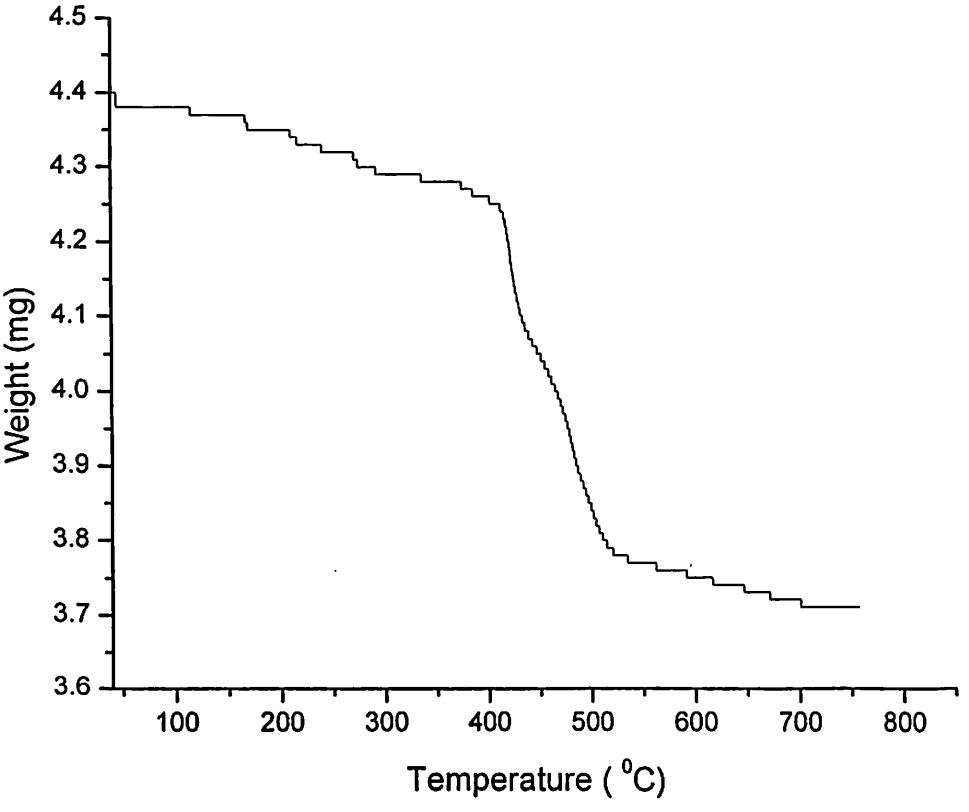

Fig.3.9 TGA curve of S100In2

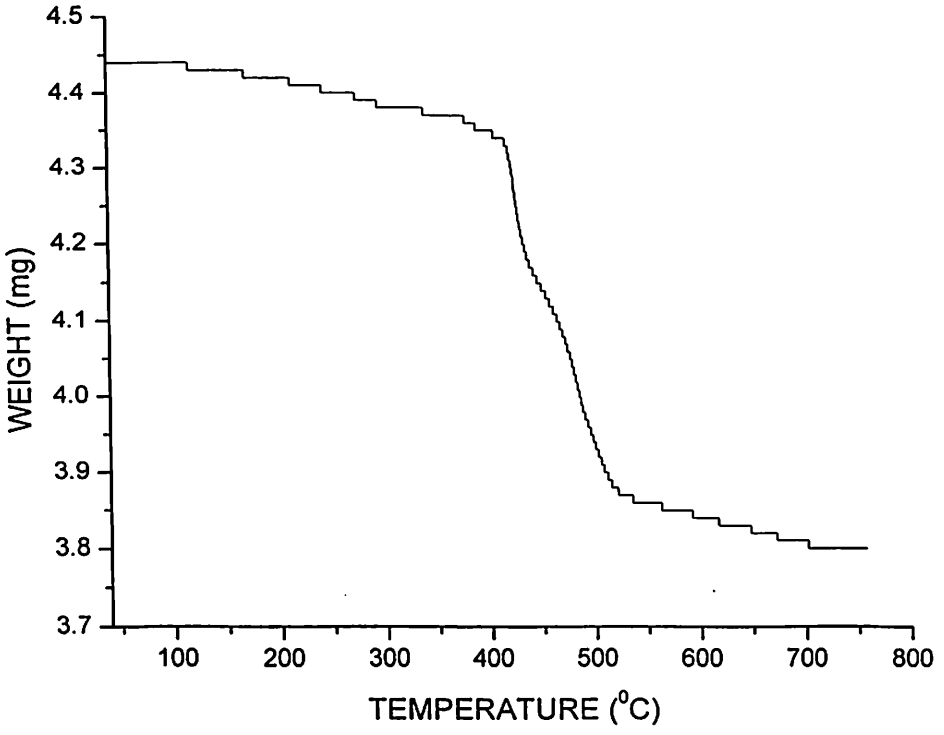

Fig.3.10 TGA curve of S100In3

Table 3.6 Percentage of weight loss of the In-MFI samples observed during TG Analysis

Sample	In^{3+} mol in the gel	Temperature range (K)	% Weight Loss	Total % Weight Loss as synthesised sample
S100In1	0.50	313-423	1.08	15.27
		423-893	12.70	
		893-1023	1.49	
S100In2	0.33	313-423	1.32	14.64
		423-893	11.74	
		893-1023	1.58	
S100In3	0.25	313-423	1.36	14.59
		423-893	11.64	
		893-1023	1.59	

The UV-Vis-DR spectra of the In-MFI samples are shown in **Figures 3.11** to **3.13**. The UV-Vis-DR spectra of the In-MFI samples indicate the existence of a band at around 212 nm. The band at around 212 nm is assigned for heteroatom with tetrahedral coordination [16]. This means that indium metal has been incorporated into the framework of MFI structure although some species may be present as extra framework.

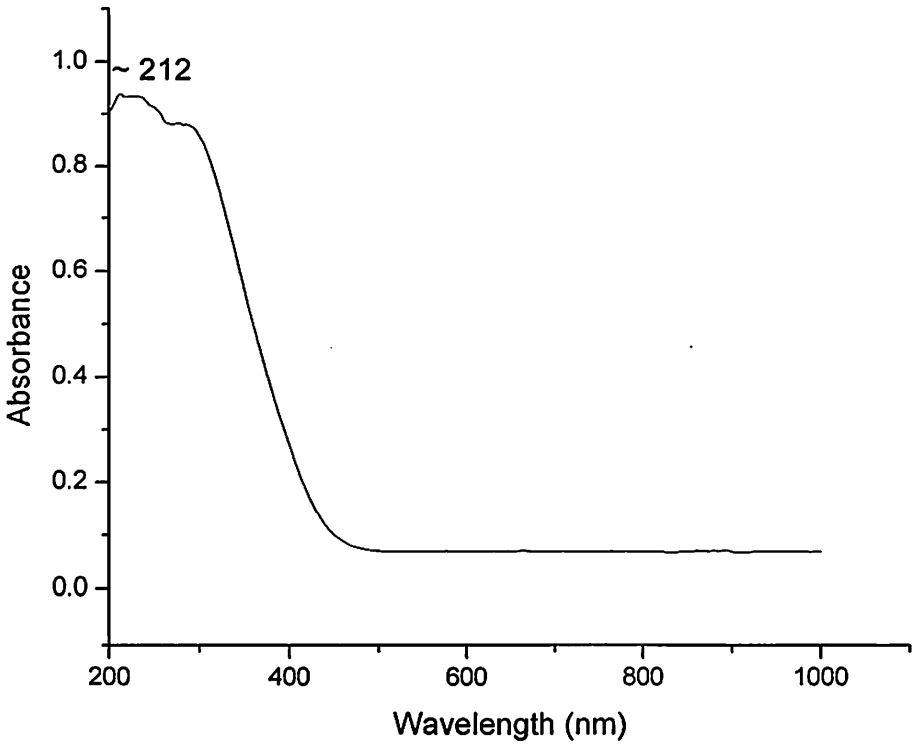

Fig.3.11 UV-Vis (DR) spectra of S100In1

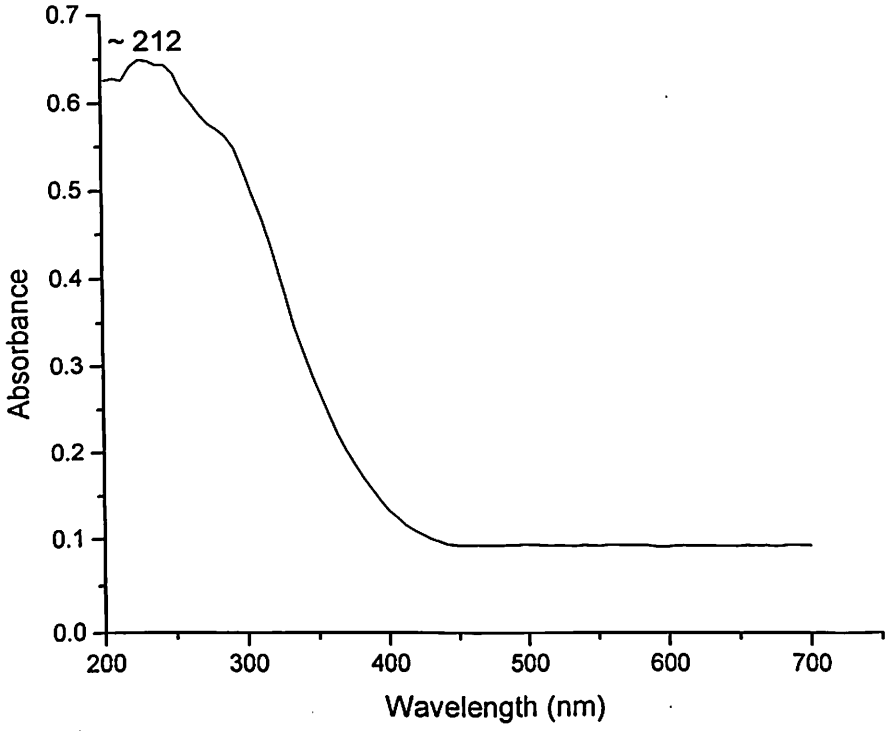

Fig.3.12 UV-Vis (DR) spectra of S100In2

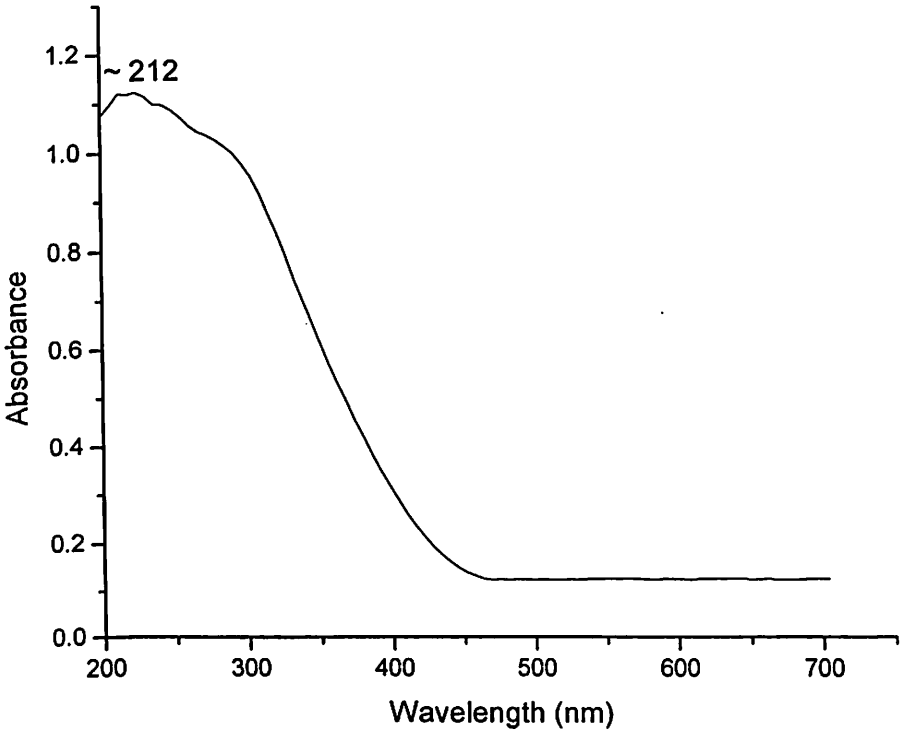

Fig.3.13 UV-Vis (DR) spectra of S100In3

Nitrogen adsorption isotherms of calcined In-MFI samples are depicted in **Figures 3.14** to **3.16**. The N_2 adsorption isotherms of the MFI samples basically belong to the IUPAC type 1 classification which is indicative of microporosity. Bonardet et al.[17] studied the nature of nitrogen below and above this relative pressure of 0.18 by *in situ* ^{15}N NMR and reported the existence of two states of nitrogen. As explained earlier (chapter 2, page number 64) the first adsorbed phase occurs within the smaller dimension of the void network pore followed by formation of the second phase within the larger void spaces. The N_2 adsorption isotherms of the indium incorporated zeolite samples have type H-1 hysteresis loops with less vertical adsorption desorption branches than those for Zr-MFI samples at p/p_0 = 0.12 to 0.21. In case of In-MFI samples also there is possibility of presence of some mesopore connecting to textural micropores. The analysis also showed that the specific surface area ranged from ~357 to ~361 m^2g^{-1} and the pore volume of the synthesized samples ranged from 0.177 to 0.182 cm^3g^{-1} as the content of the indium in the gel increased from 0.25 to 0.50 M for the MFI samples. The surface area as well as the pore volume increases with increase of indium content in the samples. Specific surface area, pore size and pore volume of synthesized In-MFI Samples are shown in **Table 3.7**. The pore size is found to be both in microporous and mesoporous range.

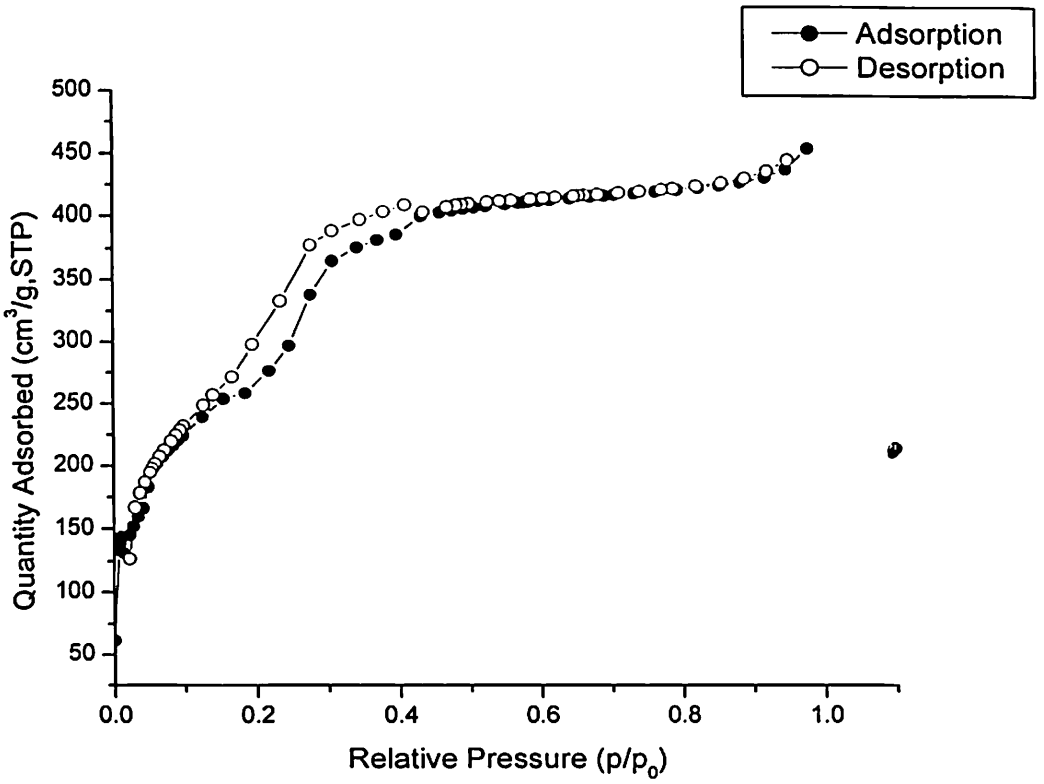

Fig.3.14 Nitrogen adsorption isotherm of calcined S100In1

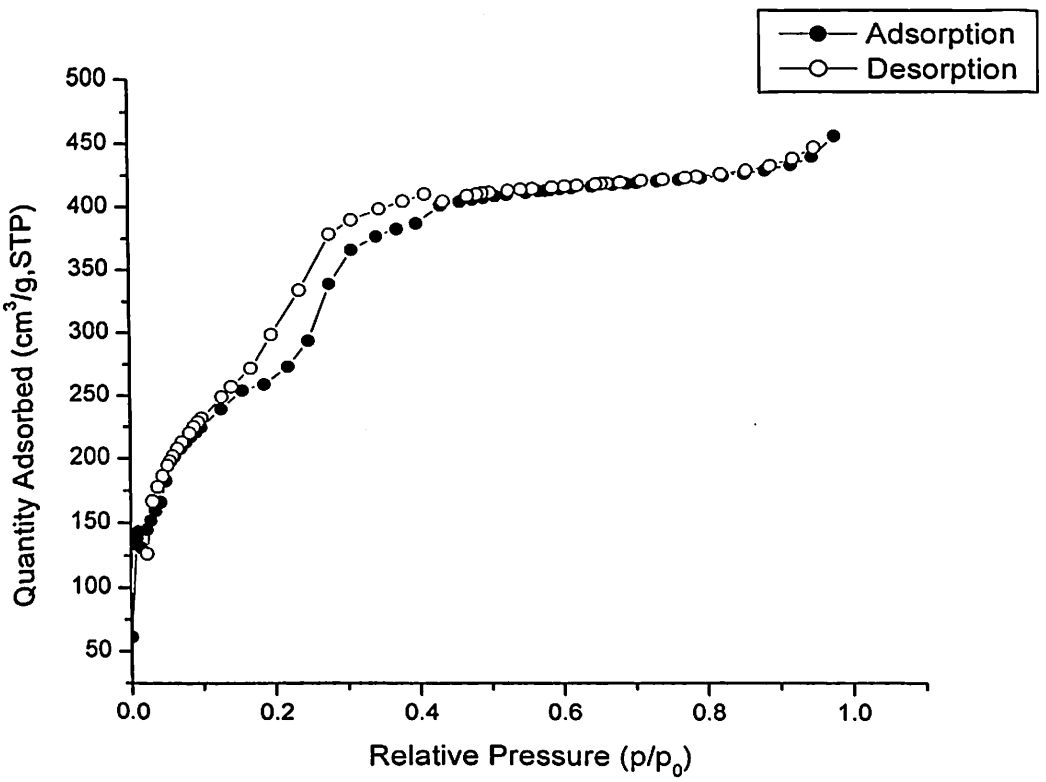

Fig.3.15 Nitrogen adsorption isotherm of calcined S100In2

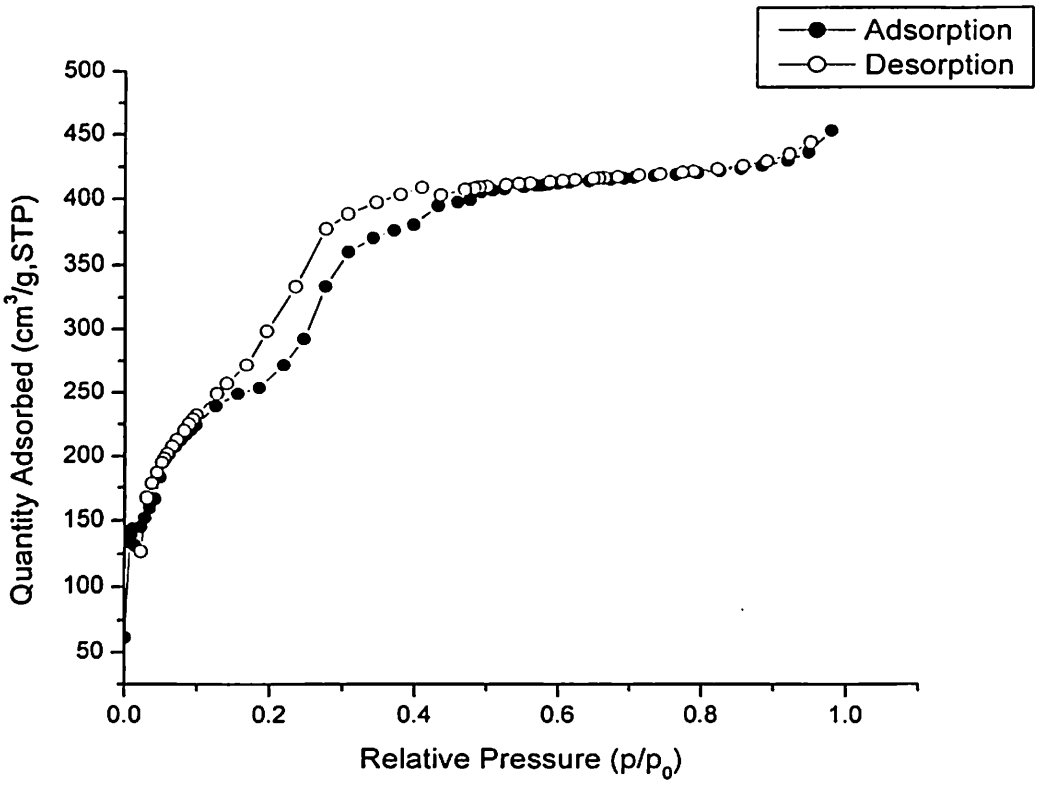

Fig.3.16 Nitrogen adsorption isotherm of calcined S100In3

Table 3.7 Specific surface area, pore size and pore volume of synthesized In-MFI Samples

Sample	In^{3+} mol in gel	Surface area (BET)(m^2g^{-1})	Pore volume (cm^3g^{-1})	Mesopore size (nm)	Micropore size (nm)
S100In1	0.50	361.27	0.182	2.2	0.52
S100In2	0.33	358.81	0.178	2.1	0.53
S100In3	0.25	357.22	0.177	2.3	0.54
S100	-	355.34	0.175	2.1	0.51

The size and shape of the crystalline MFI particles were investigated by SEM analysis. SEM micrographs of synthesized In-MFI samples are shown in **Figures 3.17** to **3.19**. From the micrographs of indium incorporated samples it can be seen that quite uniform rectangular and twinned rectangular shaped MFI particles were formed and the size of the particles was found to be nearly 26 μm. Indium substituted zeolite samples synthesized using different metal concentration in the gel did not show any distinct difference in morphological features among themselves. However, their shape and size are markedly different from undoped MFI [**Figure 2.7**]. Again, lower In containing samples showed greater agglomeration of the particles which may be due to residual silica remaining during crystallization process. Crystal growth (crystallinity and crystallite size) increases with increasing metal concentration in the gel. Otherwise, no major change in MFI phases due to variation in In concentration was observed.

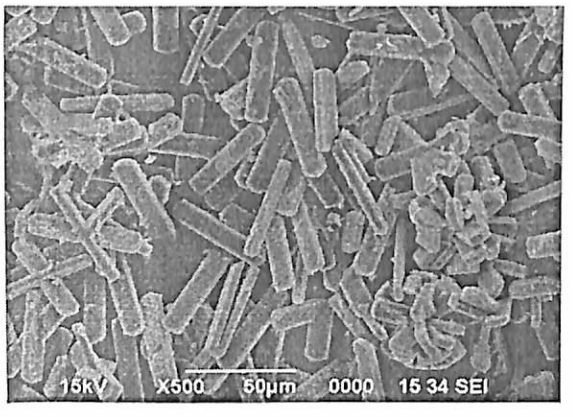

Fig.3.17 SEM picture of S100In1

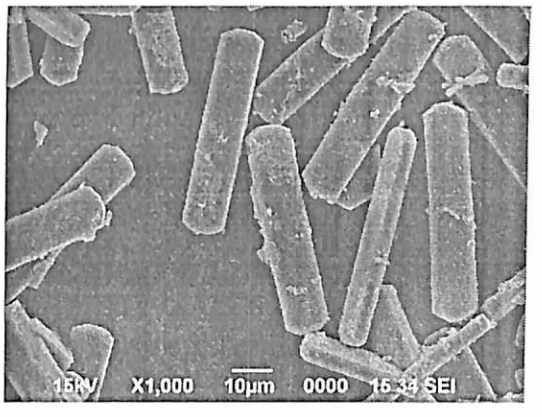

Fig.3.18 SEM picture of S100In2

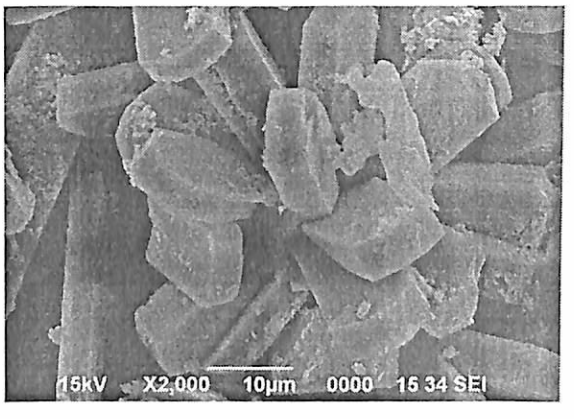

Fig.3.19 SEM picture of S100In3

3.3.2 Synthesis of Ru incorporated MFI zeolite

A systematic study was conducted to synthesize ruthenium incorporated MFI zeolite using silicon to aluminium and ruthenium ratio of 100 and different aluminium to ruthenium ratio in the absence of any promoter, organic solvent or sulphuric acid and also avoiding any seeding gel. The synthesized Ru-MFI samples were identified by comparison of both the d-spacing and relative intensities in their XRD patterns with those reported in the literature[9] and were found to be in excellent agreement. **Figure 3.20** to **3.22** show the XRD patterns of Ru-MFI samples synthesized using different aluminium to ruthenium ratios. In all the samples the Prominent peaks were observed in 2θ values around 6.5 and 22.5 with a few additional shoulder peaks in all the Ru incorporated MFI samples suggesting formation of pure phase of the zeolite. Expansion of unit cell in its parameter shown in **Table 3.8**, indicates the successful incorporation of ruthenium in the framework. The unit cell volumes are found to increase with the increasing level of metal substitution. It may be noticed that with increasing level of substitution the peaks shift towards lower 2θ values indicating successful incorporation of Ru into the framework of MFI [10]. The shift in 2θ values is presented in **Table 3.9**. The shift of the prominent peaks towards lower 2θ values with increasing level of Ru substitution with respect to the parent MFI is shown **Fig 3.23**.

Crystallinity of the MFI samples is calculated using **Relation 1** (chapter-2).

The percentage of crystallinity with reference to three significant peaks (*101*), (*501*) and (*303*) as well as the average percentage crystallinity is presented in **Table 3.10**. All the samples under the present investigation were found to exhibit high crystallinity (~ 91%).

The crystallite sizes of the synthesized samples were calculated using **Relation 2** (chapter-2). The crystallite size of the samples ranges from about 53 to 57 nm.

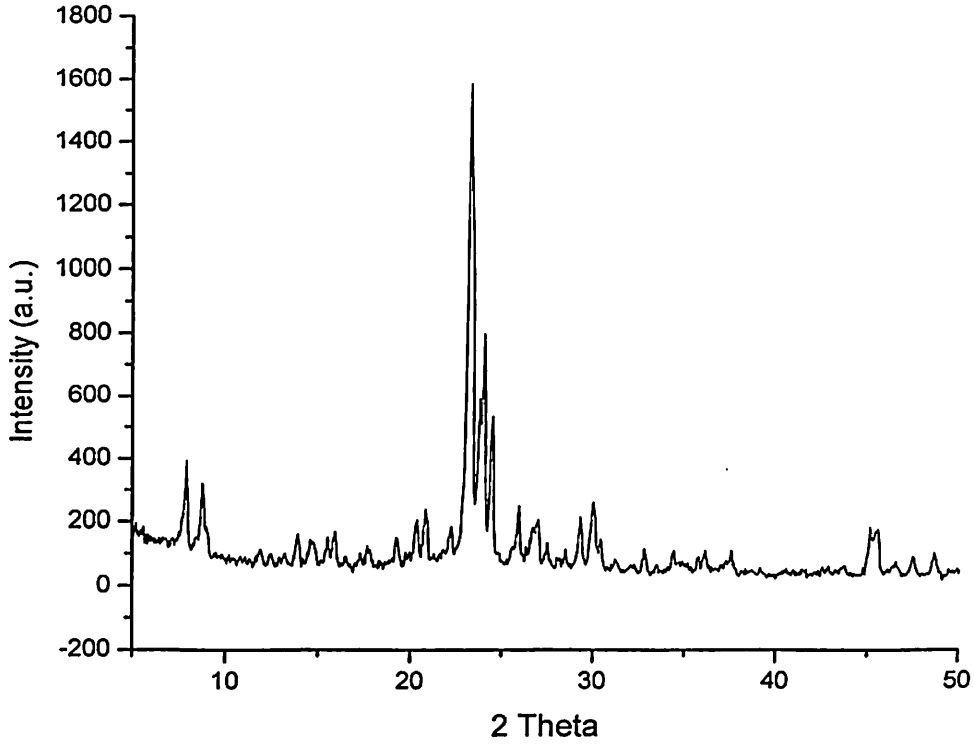

Fig.3.20 XRD patterns of S100Ru1

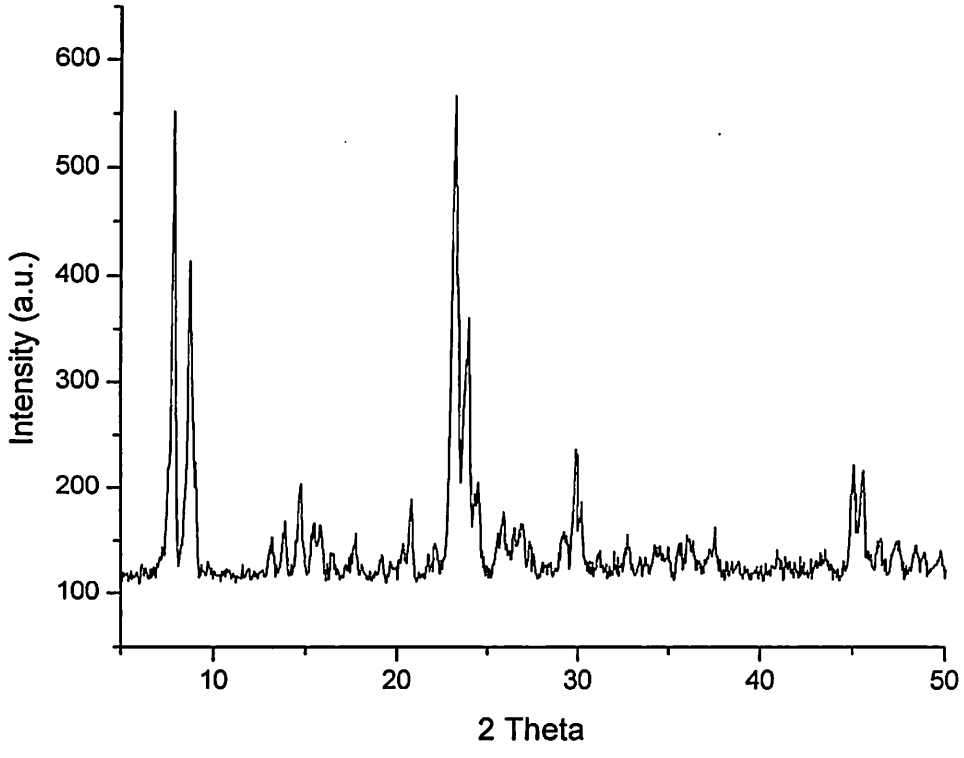

Fig.3.21 XRD patterns of S100Ru2

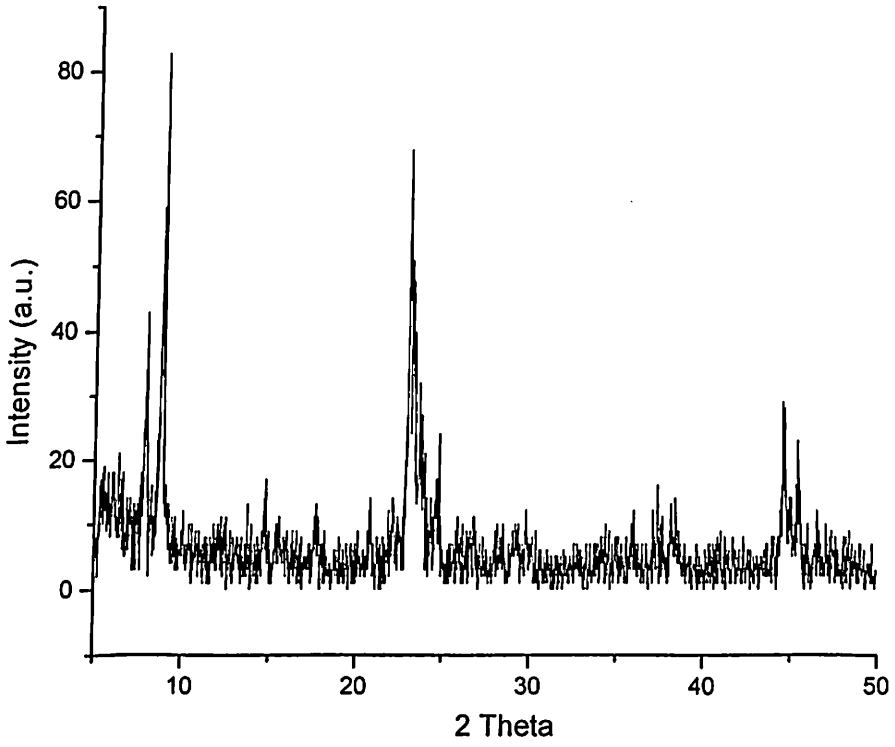

Fig.3.22 XRD patterns S100Ru3

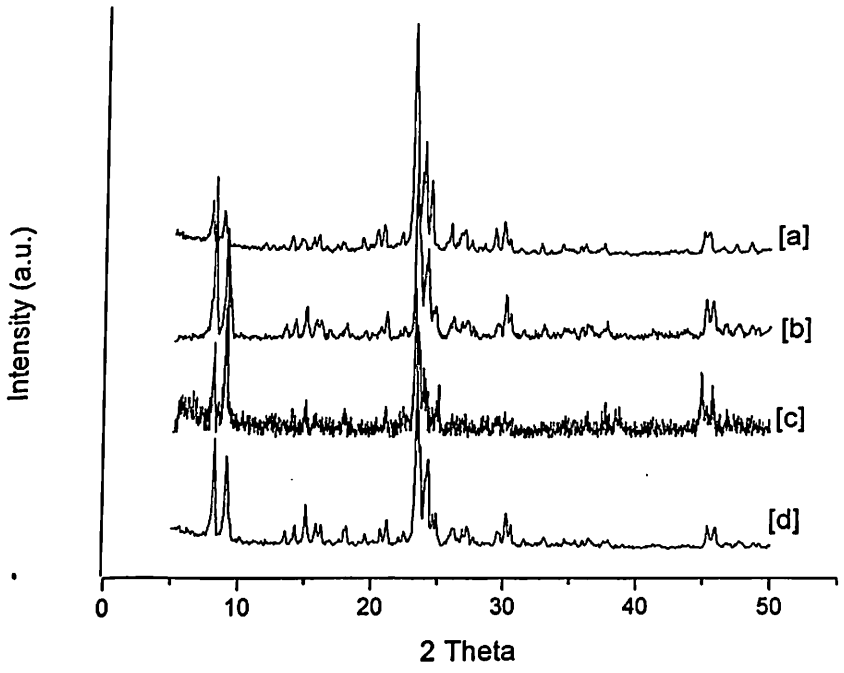

Fig.3.23 Shifting of 2 theta values of prominent peaks with increasing level of Ru substitution wrt parent MFI [a] S100Ru1 [b] S100Ru2 [c] S100Ru3 [d] S100

Table 3.8 Expansion of unit cell with increasing level of Ru in MFI samples

Sample	Si : Al	Al : Ru	Unit cell edges (Å)			Unit Cell volume ($Å^3$)
			a	b	c	
S100Ru1	100	1	13.98	19.85	14.96	4151.44
S100Ru2	100	2	13.91	19.79	14.91	4104.41
S100Ru3	100	3	13.74	19.76	14.79	4015.52
S100	100	-	13.59	19.71	14.64	3921.45

Table 3.9 Shift in 2θ value of 501 peaks of the Ru-MFI samples with respect to parent MFI

Sample	Ru^{+3} mol in the gel	Position of the prominent peak (*501*)	Shift in the 2θ value wrt parent MFI
S100	-	23.36	-
S100Ru1	0.50	23.07	0.29
S100Ru2	0.33	23.19	0.17
S100Ru3	0.25	23.22	0.14

Table 3.10 Crystallite size and percentage of crystallinity $(\%C)_{hkl}$ of the synthesized Ru-MFI sample

Sample	Si: Al or Si:(Al+Ru)	Al: Ru	Crystallite size (nm) (*501*)	%C from XRD	% C from IR
S100Ru1	100	1	53	89.97	86.47
S100Ru2	100	2	54	93.51	89.45
S100Ru3	100	3	57	91.20	87.32
S100	100	0.0	49	91.62	87.47

Figure 3.24 to **3.26** show the FT-IR spectra of synthesized MFI samples. IR results confirm the formation of MFI zeolite in all cases showing distinct absorbance bands near 1080 (internal asymmetric stretch), 790 (external

symmetric stretch), *540 (double ring vibration) and 450 cm^{-1} (T–O bending).* The absorption bands near 550 cm^{-1} have been assigned to the presence of double 5-member rings in the structure [11]. The external asymmetric stretching vibration around 1225 cm^{-1} is present in the spectra of structures assigned to four chains of 5-member rings arranged around a twofold screw axis. The distortion of the spectra was not consistent with increasing levels of substitution as reported previously [12]. As discussed in case of indium incorporated MFI, the absorption peak at 990 cm^{-1} may be considered as indication of incorporation of ruthenium into the lattice framework [13]. The IR method of finding relative crystallinity of the samples is achieved by calculating the optical density (OD) ratio of the peaks near 540 and 450 cm^{-1}. The results are given in **Table 3.10** and are found to be in good agreement with those calculated from XRD studies.

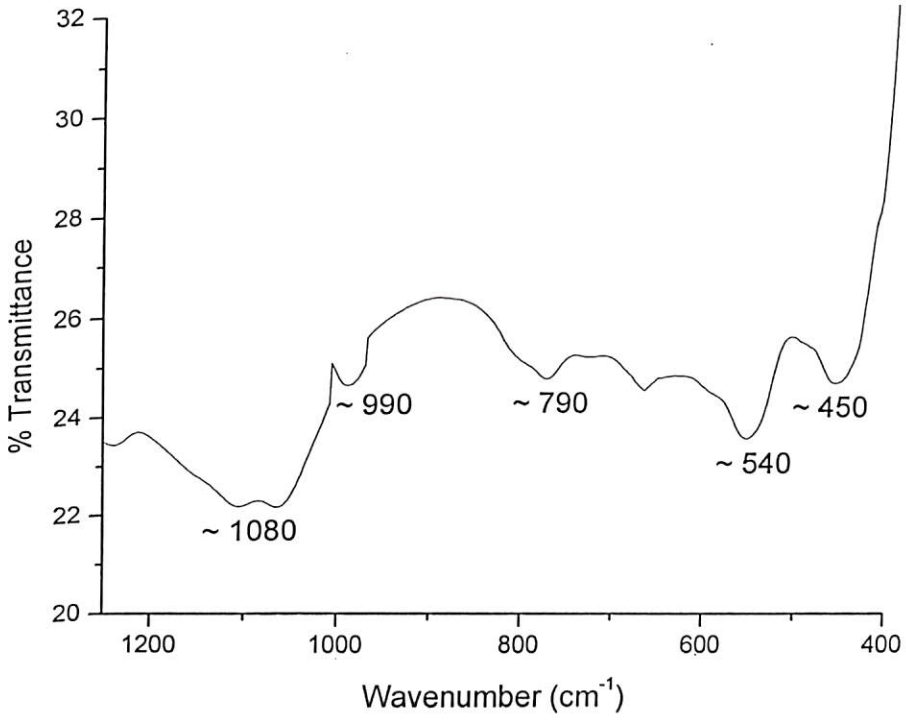

Fig.3.24 FT-IR spectra of S100Ru1

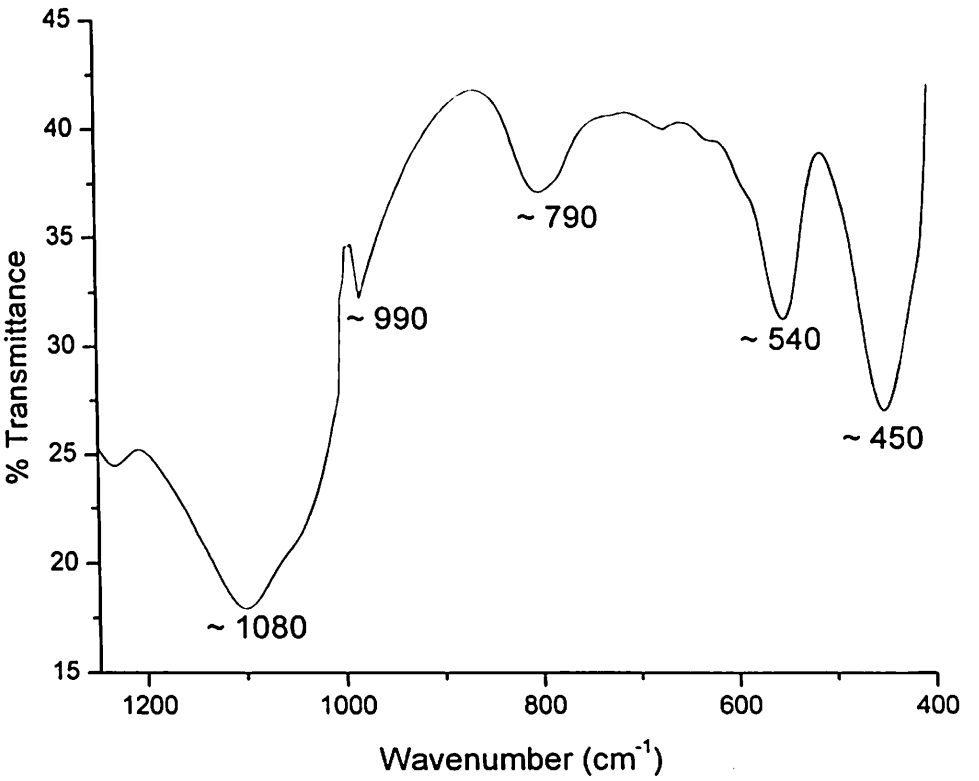

Fig.3.25 FT-IR spectra of S100Ru2

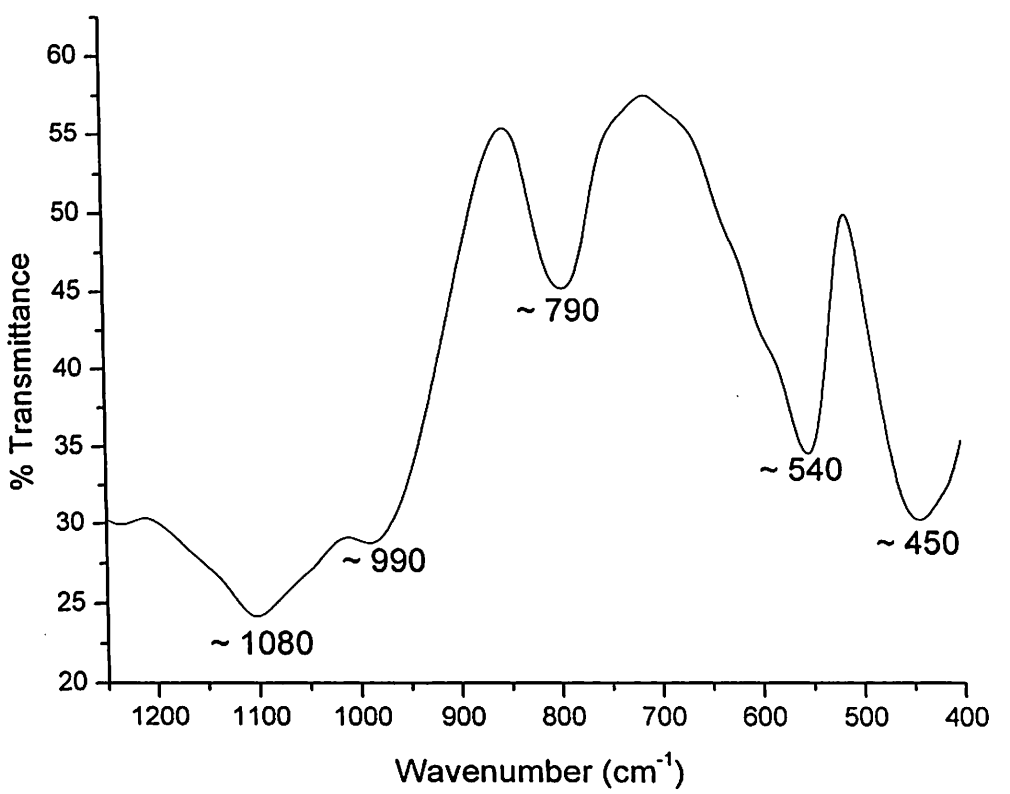

Fig.3.26 FT-IR spectra of S100Ru3

The TGA curves of Ru-MFI zeolites samples are shown in **Figures 3.27** to **3.29**. The initial mass loss up to 423 K is attributed to physically adsorbed water in the porous materials [14]. Beyond 423 K mass loss increased in the temperature range 423-893 K while it decreased in the temperatures beyond 893 K. The mass loss during second and third phase have been explained already in the previous discussion in case of In-MFI. The first two types are TPA^+ cations ion-paired to crystal surface defects and TPA^+ cations occluded in the zeolite channels. These two types are least strongly bound and therefore, more easily lost at a comparatively lower temperature range (423-773 K). The TPA^+ cations that neutralize the framework negative metal centers (MO_4^-) coordinated into the silica framework are the third types of TPA^+ cations which are more strongly bound counter ion species and thus lost at high temperature above 893 K. In the present work it is observed that the mass loss is more or less constant in the three temperature ranges even if the level of Ru content increases (simultaneously Al content decreases) in the MFI structure. This can be considered as proof of incorporation of ruthenium into the framework of MFI structure. The percentage weight losses for various temperature ranges for different samples are presented in **Table 3.11**.

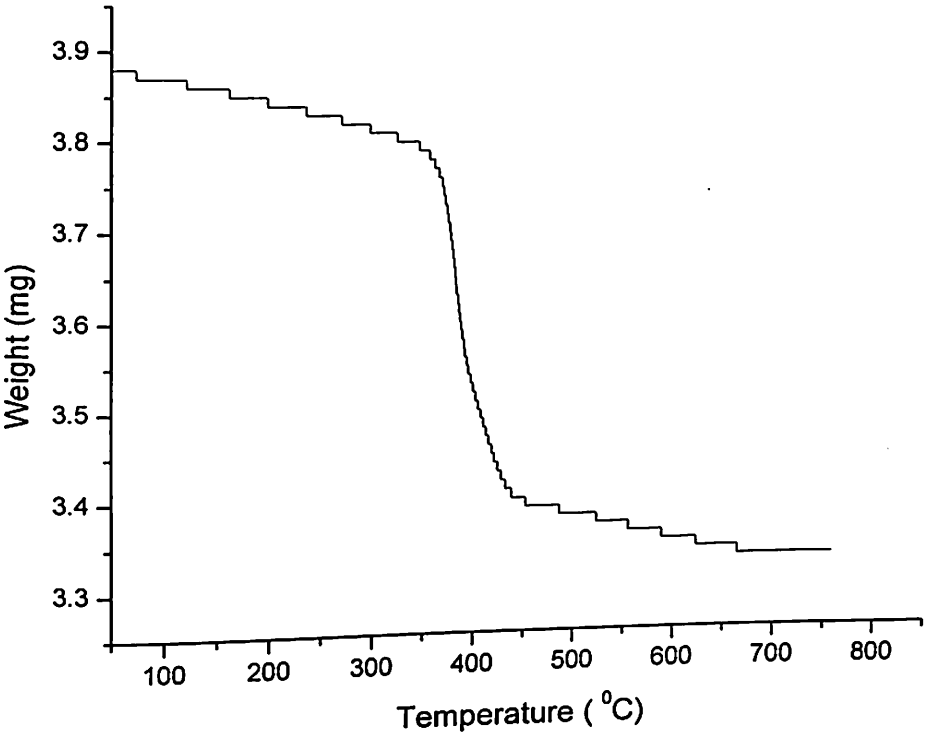

Fig.3.27 TGA curve of S100Ru1

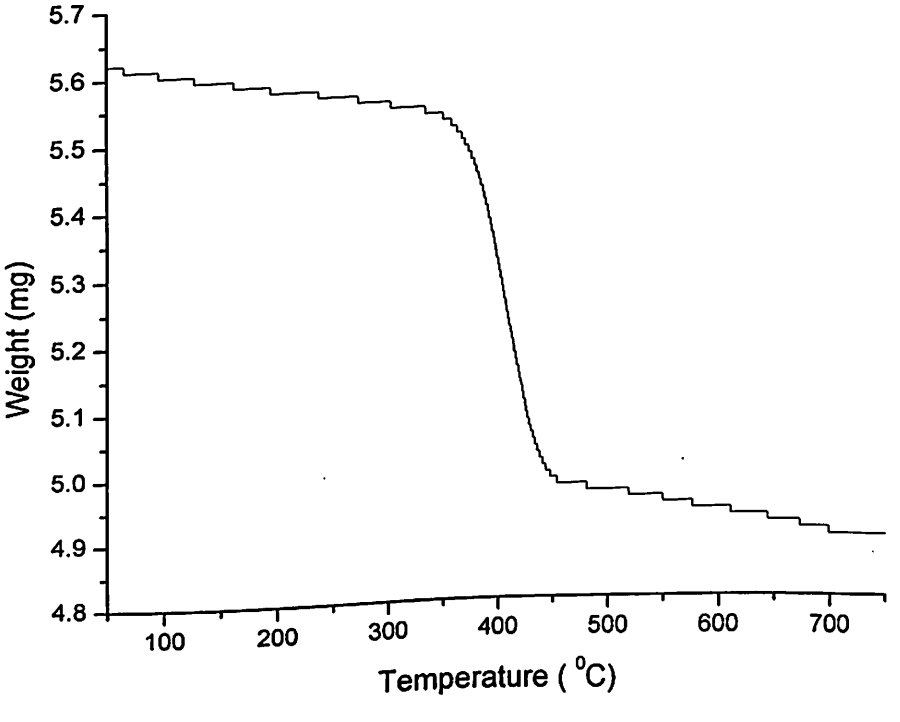

Fig. 3.28 TGA curve of S100Ru2

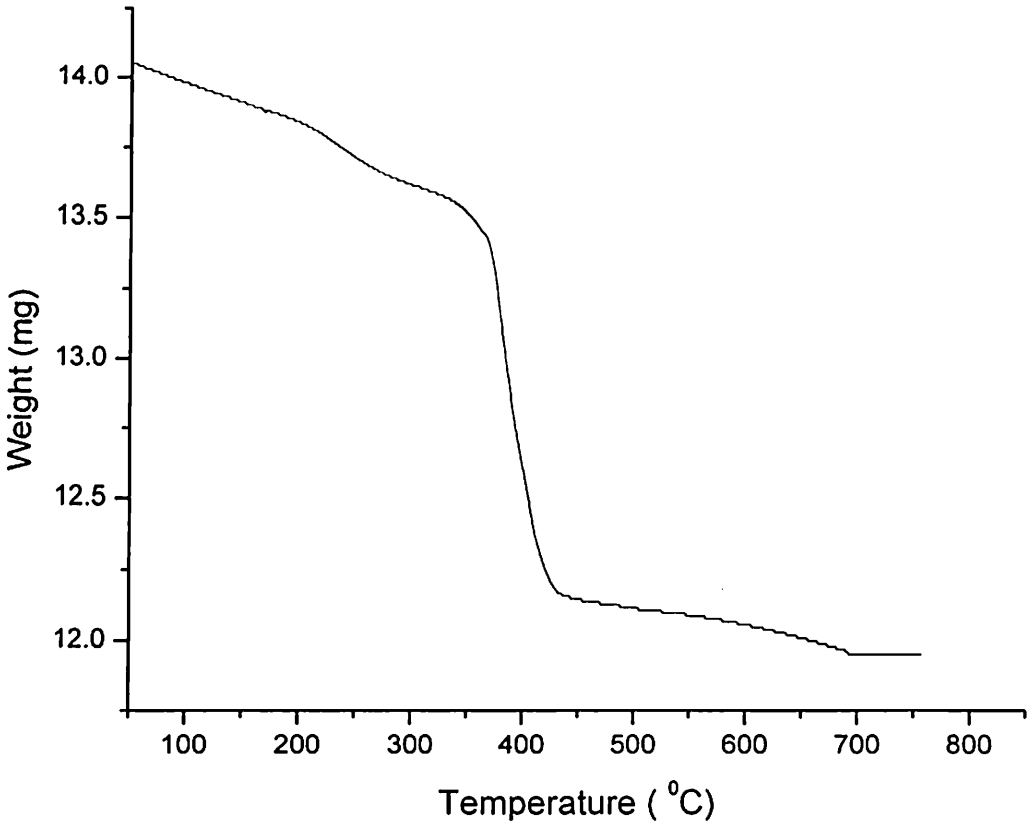

Fig.3.29 TGA curve of S100Ru3

Table 3.11 Percentage of weight loss of the Ru-MFI samples observed during TG Analysis

Sample	Ru^{3+} mol in the gel	Temperature range (K)	% Weight loss	Total % Weight loss as synthesised sample
S100Ru1	0.50	313-423	1.06	15.19
		423-893	12.67	
		893-1023	1.46	
S100Ru2	0.33	313-423	1.32	14.55
		423-893	11.69	
		893-1023	1.54	
S100Ru3	0.25	313-423	1.37	14.47
		423-893	11.54	
		893-1023	1.56	

The UV-Vis-DR spectra of the Ru-MFI samples are shown in **Figures 3.30** to **3.32.** The UV-Vis-DR spectra of the Ru-MFI samples indicate the existence of a band at around 212 nm. The band at around 212 nm is assigned for heteroatom with tetrahedral coordination [16]. This means that ruthenium metal has been incorporated into the framework of MFI structure although some species may be present as extra framework. The peak around 250 nm is an indication of Ru in the extra framework.

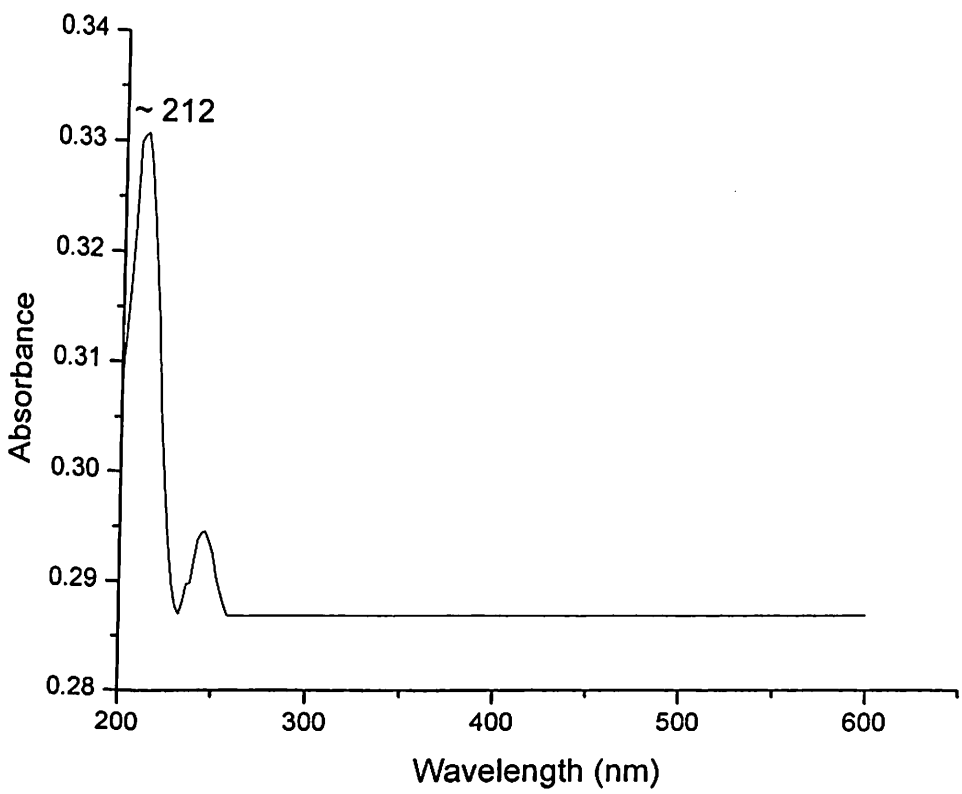

Fig.3.30 UV-Vis (DR) spectra of S100Ru1

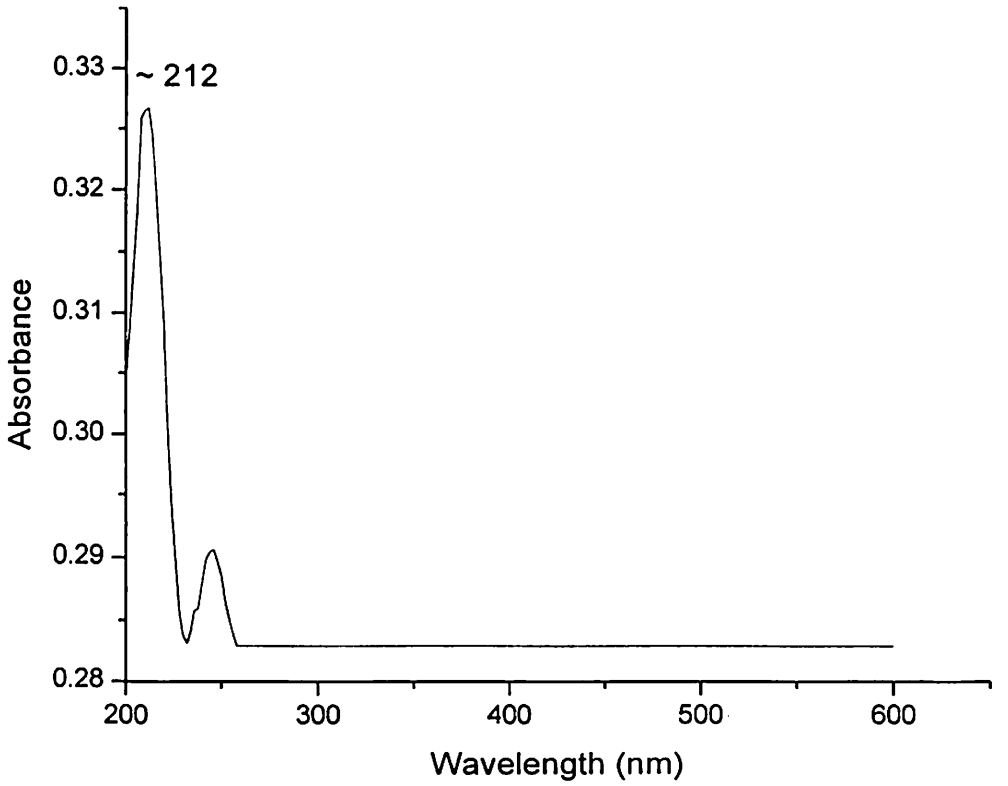

Fig.3.31 UV-Vis (DR) spectra of S100Ru2

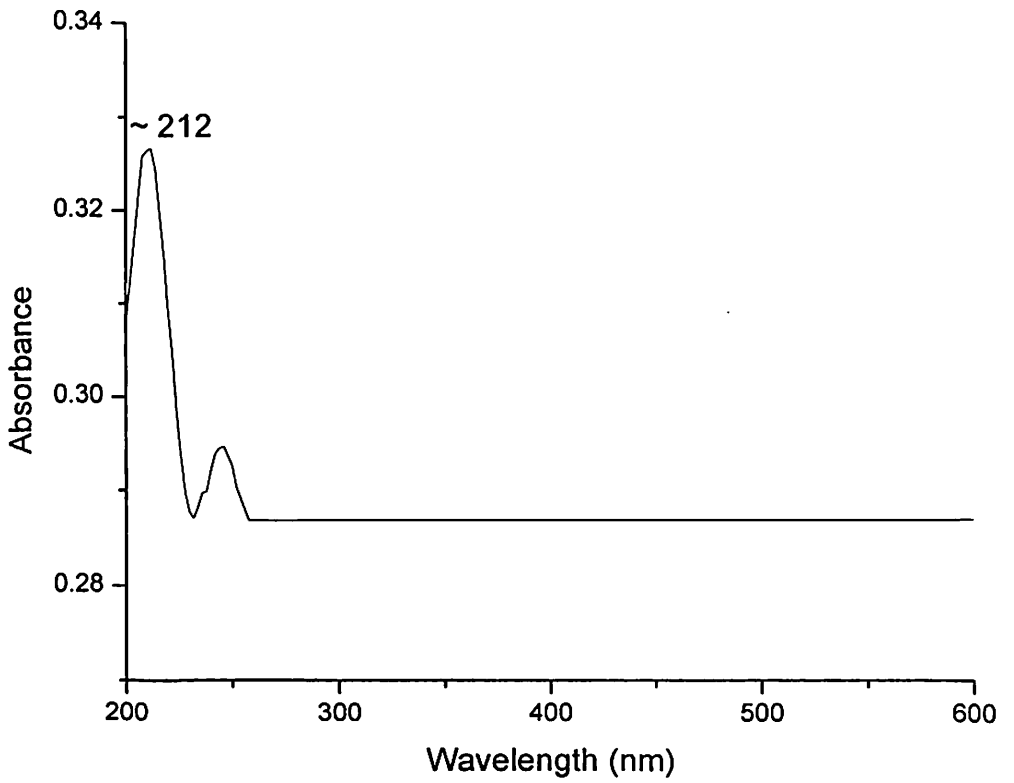

Fig.3.32 UV-Vis (DR) spectra of S100Ru3

Nitrogen adsorption isotherms of calcined Ru-MFI samples are depicted in **Figures 3.33** to **3.35**. The N_2 adsorption isotherms of the MFI samples basically belong to the IUPAC type 1 classification which is indicative of microporosity. The N_2 adsorption isotherms of the ruthenium incorporated zeolite samples have type H-1 hysteresis loops with almost similar adsorption desorption branches at p/p_0 = 0.12 to 0.21 to those for In-MFI samples. The analysis also showed that the specific surface area ranged from ~359 to ~364 m^2g^{-1} and the pore volume of the synthesized samples ranged from 0.179 to 0.188 cm^3g^{-1} as the content of the ruthenium in the gel increased from 0.25 to 0.50 M for the Ru-MFI samples. This means that with the increase in the level of substitution of ruthenium, the surface area as well as the pore volume increased. Specific surface area, pore size and pore volume of synthesized Ru-MFI Samples are shown in **Table 3.12**. The pore size is found to be both in microporous and mesoporous range.

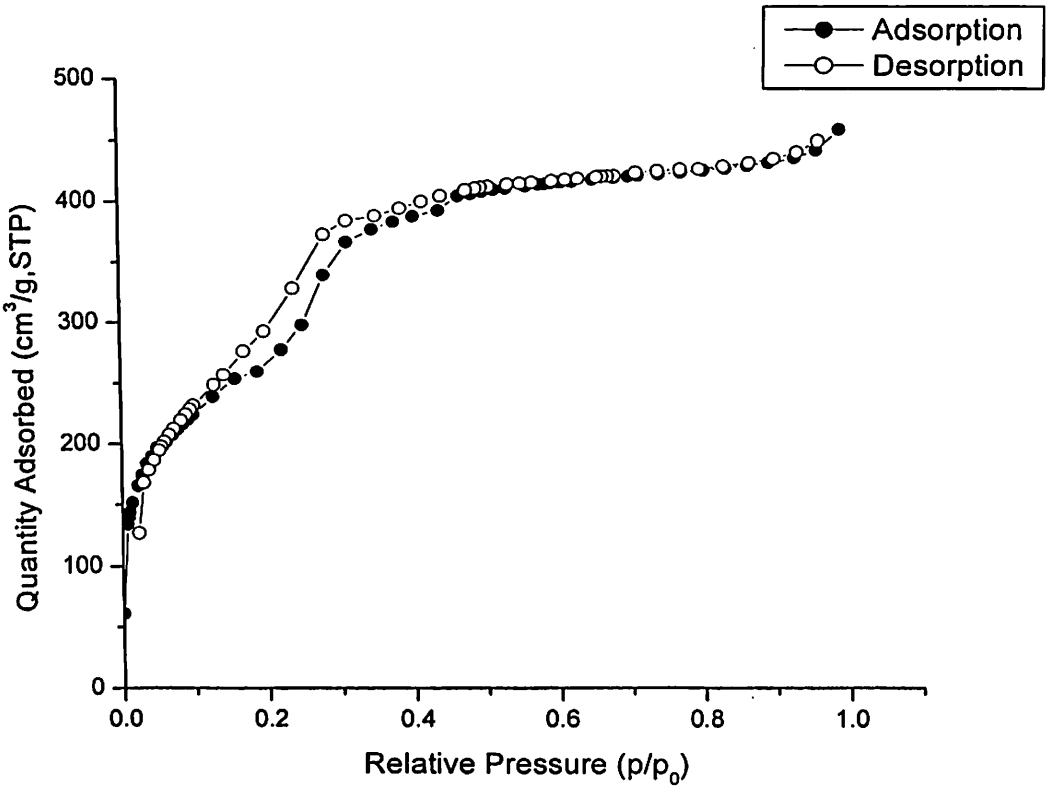

Fig.3.33 Nitrogen adsorption isotherm of calcined S100Ru1

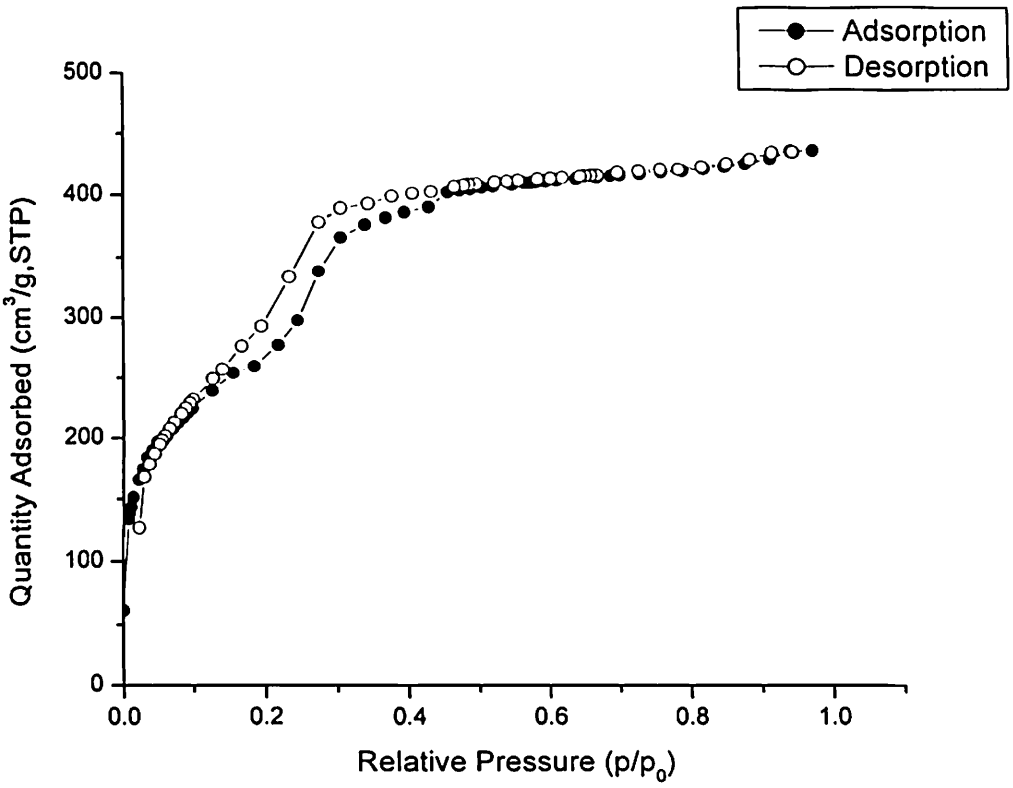

Fig.3.34 Nitrogen adsorption isotherm of calcined S100Ru2

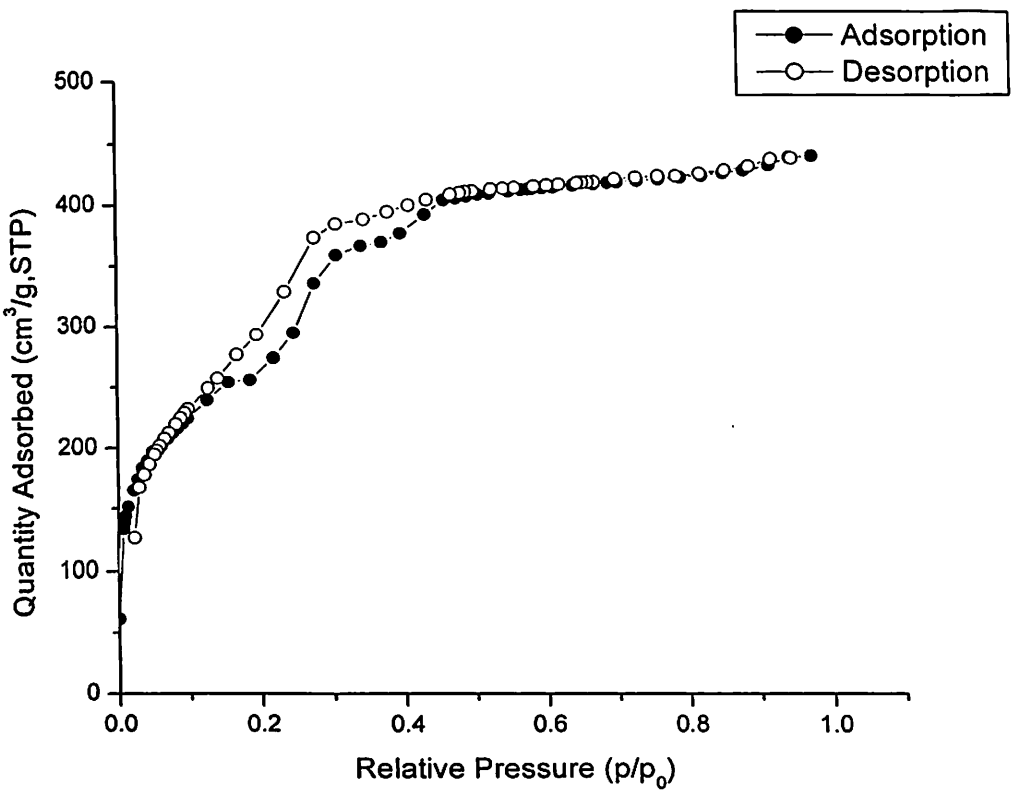

Fig.3.35 Nitrogen adsorption isotherm of calcined S100Ru3

Table 3.12 Specific surface area, pore size and pore volume of synthesized Ru-MFI samples

Sample	Ru^{3+} mol in gel	Surface area (BET)(m^2g^{-1})	Pore volume (cm^3g^{-1})	Mesopore size (nm)	Micropore size (nm)
S100Ru1	0.50	364.38	0.188	2.3	0.51
S100Ru2	0.33	360.72	0.184	2.1	0.52
S100Ru3	0.25	359.34	0.179	2.2	0.53
S100	-	355.34	0.175	2.1	0.51

The size and shape of the crystalline MFI particles were investigated by SEM analysis. SEM micrographs of synthesized Ru-MFI samples are shown in **Figures 3.36** to **3.38**. From the micrographs of ruthenium incorporated samples it can be seen that quite uniform rectangular and twinned rectangular shaped MFI particles were formed and the size of the particles was found to be nearly 27 μm. Ruthenium substituted zeolite samples synthesized using different metal concentration in the gel did not show any distinct difference in morphological features among themselves. However, their shape and size are markedly different from undoped MFI [**Figure 2.7**]. Again, lower Ru containing samples showed greater agglomeration of the particles which may be due to residual silica remaining during crystallization process. Crystal growth (crystallinity and crystallite size) increases with increasing metal concentration in the gel. Otherwise, no major change in MFI phases due to variation in Ru concentration was observed.

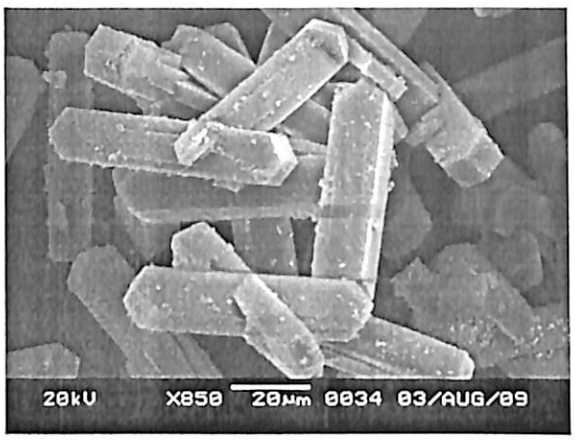

Fig.3.36 SEM Picture of S100Ru1

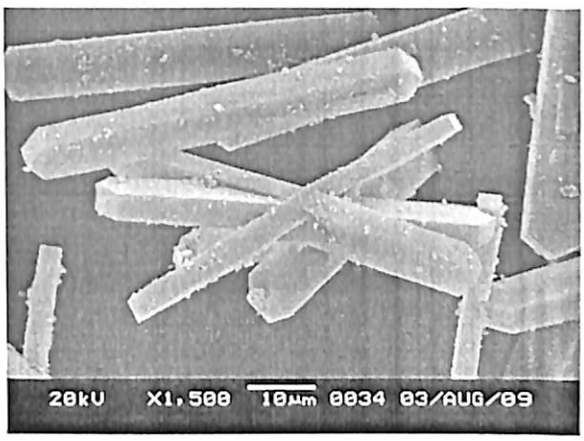

Fig.3.37 SEM Picture of S100Ru2

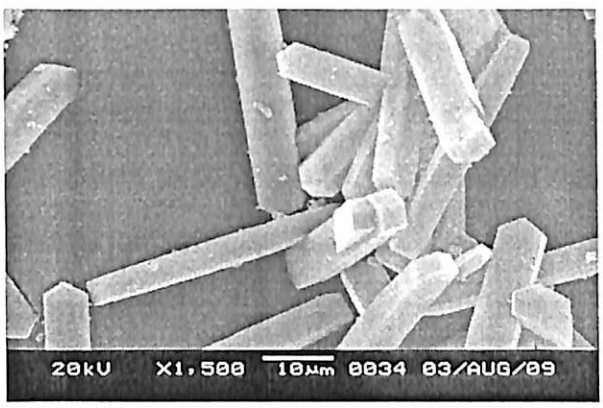

Fig.3.38 SEM Picture of S100Ru3

3.4 Conclusion

In and Ru incorporated MFI samples have been successfully synthesized using fluoride gel as mineralizer in slightly acidic or neutral media. The synthesized samples are characterized by XRD, FT-IR, TGA, UV-Vis (DRS), N_2 adsorption-desorption isotherm and SEM. XRD and FTIR spectra of the samples confirm the formation of MFI zeolite phase, while thermogravimetric analysis as well as the DR spectra support the successful incorporation of In and Ru in MFI samples. All the samples of In-MFI under

the present investigation are found to exhibit high crystallinity (~ 92%). The crystallite sizes of the samples are found in the range from about 49 to 55 nm. In case of Ru-MFI samples the crystallinity of the samples are found to be ~ 91% and that of the crystallite sizes of the samples are found in the range from about 53 to 57 nm. The unit cell volumes are found to increase with the increasing level of metal substitution.

From thermogravimetric analysis it is observed that, the mass loss increases in the temperature range above 423-893 K and comparatively decreases in the temperature range 893-1023 K as the level of metal content (In, Ru) increased in the synthesized samples.

The nitrogen adsorption isotherm analysis showed that the specific surface area of the synthesized samples increases from ~357 to ~361 m^2g^{-1} and pore volume increases from 0.177 to 0.182 cm^3g^{-1} as the content of the In in the gel increases from 0.25 to 0.50 M for the MFI samples. In case of Ru incorporated samples the specific surface area of the synthesized samples are found to increase from ~359 to ~364 m^2g^{-1} and that of the pore volume are found to increase from 0.179 to 0.188 cm^3g^{-1} as the content of Ru in the gel increases from 0.25 to 0.50M.

Indium and ruthenium substituted zeolite samples synthesized using different metal concentrations in the gel do not show any distinct difference in morphological features among themselves. However, their shape and size are markedly different from undoped MFI. Again, lower In and Ru containing samples showed greater agglomeration of the particles which may be due to residual silica remaining during crystallization process.

3.5 References

[1] C. T. Chu and C. D. Chang, *J. Phys. Chem.*, 89 (1985) 1569; J. Dwyer and P. J. O'Malley, *Stud. Surf. Sci. Catal.*, 35 (1987) 219; R. B. Borade, *Zeolites*, 7 (1987) 398.

[2] C. S. John, D. M. Clark and I. E. Maxwell, *Perspective in Catalysis*, Ed. J. M. Thomas and K. I. Zamaroev, Blackwell Science, Oxford (1991), 387; W. F. Holderich, M. Hesse and F. Naumann, *Angew. Chem., Int. Ed. Engl.*, 27 (1988),226; B. Delmon, *Catal. Lett.*, 22 (1993) 1.

[3] B. Sulikowski, *Heterog. Chem. Rev.* 3 (1996) 203.

[4] R.M. Barrer, *Zeolites, Clay Minerals as Sorbents and Molecular Sieves,* Academic Press, London, (1978) 339.

[5] H.G. Karge, H.K. Beyer, *Stud. Surf. Sci. Catal.* 69 (1991) 43.

[6] R.M. Miha'lyi, H.K. Beyer, M. Keindl, *Stud. Surf. Sci. Catal.* 135 (2001) CD Edition 10-P-06.

[7] J. Hala'sz et al., *J. Mol. Struc., 651* (2003) 315.

[8] M. Breysse, M. Cattenot, V. Kougionas, J. C. Lavalley, F. Mauge, J. L. Portefaix and J. L. Zotin, *J. Catal.*, 168(2) (1997) 143; S. K. Das and P. K. Dutta, *Micropor.Mesopor.Mater.*, 22(1-3) (1998) 475; P. K. Dutta, *J. Incl. Phenom. Mol. Recogit. Chem.*, 21(1-4) (1995) 215.

[9] M.M.J. Treacy, J.B. Higgins (Eds.) *Collection of Simulated XRD Powder Patterns for Zeolites*, Elsevier (2001) 234.

[10] W. Zhan, G. Lu, G.Yanglong, G. Yun, W.Yanqin, W. Yunsong, Z. Zhigang, Liu Xiaohui, *J. Rare Earths* 26, 4 (2008) 515.

[11] R. Szostak, Molecular Sieve, 2nd Edn. (Blackie-Academic & Professional , London, (1998), 306, 310, 311.

[12] C.I. Round, C.D. Williams, K. Latham, C.V.A. Duke, *Chem. Mater.* 13 (2001) 468.

[13] B. Rakshe, V. Ramaswamy, S.G Hegde, R. Vetrivel, A.V. Ramaswamy, *Catal. Lett.* 45 (1997) 41.

[14] J.L. Guth, H. Kessler, J.M. Higel, J.M. Lamblin, J. Patarin, A Seive, J.M. Chezeau, R. Wey, zeolite synthesis, in : ACS Symp.Ser. 398, Washington DC, (1989) 176.

[15] J.L. Guth, L. Delmotte, M. Soulard, N. Brunard, J.F. Joly, D. Espinat, Zeolites 12 (1992) 929.

[16] L. B. Newalkar, O. Johnson, S.R. Komarneni, *J. Phys. Chem.* B 105 (2001) 8356.

[17] J. Bonardet, J. Fraissard, K. Onger, D. Kumar, M. Ferrero, J. Ragle, W. C.Conner, *Stud. Surf. Sci. Catal* 87(1994) 319.

CHAPTER-4

Catalytic Activity of the Synthesized Samples

Chapter Summary

This chapter starts with a concise note on role of heterogeneous catalysts in organic reactions. A detailed study of hydroxylation of phenol by hydrogen peroxide with parent and modified MFI zeolite is presented in this chapter. The hydroxylation of phenol by hydrogen peroxide, studied with respect to reaction time, amount of catalyst, nature of catalyst, temperature, solvent and different proportions of metal in the catalyst is also presented in this chapter.

4. Introduction

4.1 Role of heterogeneous catalyst in organic reactions

The organic reactions using homogeneous catalysts, such as organic bases like pyridine in triethylamine or pyridine with 4-(dimethylamine) pyridine [1], traditional oxidants like dichromate, chromate, permanganate, osmium tetroxide, lead tetraacetate etc. [2] encounter several disadvantages like increase in overall process cost, generation of waste products, requirement of greater than stoichiometric amount , difficulty in recovering the catalyst for reuse, difficulty in separation of the product etc. Obviously, the principles of green chemistry are not followed here.

In order to follow the general principles of green chemistry, it is utmost important to develop catalysts that are inexpensive, eco friendly, reusable etc. In the recent years solid acid catalysts like clay, zeolite etc. play an important role in chemical industries. Although the catalytic activity of porous materials is governed by different factors, but their role as heterogeneous catalysts has been

subject to intensive research in the recent past [3]. The reactions catalyzed by porous heterogeneous catalysts are accomplished by the following processes:

- Transport of the reactant to the surface followed by diffusion of the reactant to an active site inside the pore.
- Adsorption of the reactant to an active site.
- Chemical reaction of the adsorbed reactant to form adsorbed product(s).
- Desorption of the adsorbed product(s).
- Diffusion of the adsorbed product(s) from interior active site to the outer surface of the catalyst.
- Transfer of the product(s) away from the porous surface.

4.2 Hydroxylation of phenol

Oxidation of phenol by hydrogen peroxide should produce catechol (CL) and hydroquinone (HQ) as shown in **Scheme 4.1**.

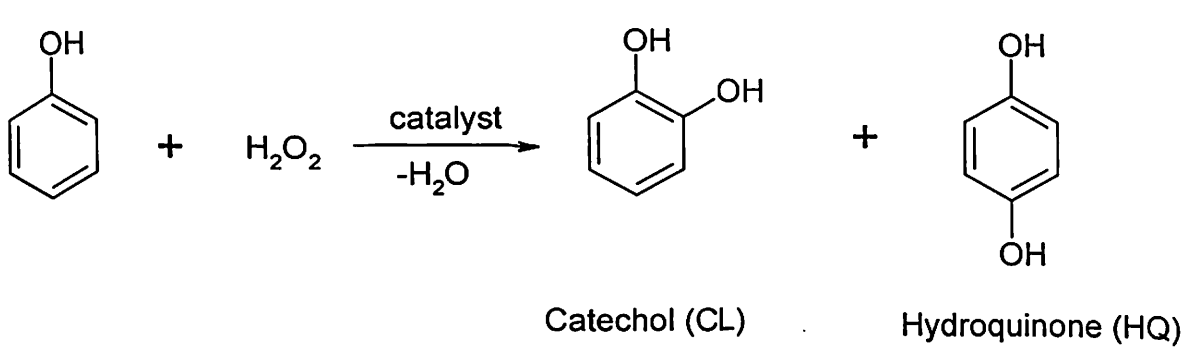

Scheme 4.1 Hydroxylation of phenol into diphenols.

The reaction is very important process because CL and HQ are widely used as starting materials for preparation of medicine, perfume and many fine

chemicals [4]. Phenol hydroxylation has been studied over various catalysts, which include both homogeneous and heterogeneous catalysts. Though metal ions in homogeneous phase are active for diphenols production, the reaction rate and selectivity to diphenols are not appreciable [5, 6]. Other than simple metal ions, metal complexes, have also been used. Though these metal complexes exhibit better catalytic activity and selectivity than metal ions, these complexes are not desirable for industrial applications due to shortcomings of handling and recovery of these homogeneous catalysts. Homogeneous catalysts have also been immobilized in the cavities of well-defined microporous zeolites and used as catalysts for phenol hydroxylation. However, the results are disappointing due to the narrow pores of the host species. Zeolites containing transition metal ions in their framework exhibit unique redox properties in hydroxylation of organic substrates with peroxides as hydroxylating agents. Some of the hydroxylation of phenol reaction performed earlier on other catalysts is shown in **Table 4.1**.

Table 4.1 Hydroxylation of phenol reaction performed on other catalysts earlier

Catalyst	Phenol:H_2O_2	Solvent	Conv. (%)	Selectivity		Temp (K)	Ref.
				CL (%)	HQ (%)		
H-MFI (40)*	10:1(60%)	-	14.6	10.4	4.22	373	[4]
H-MOR (18)*	10:1(60%)	-	0.6	0.00	0.61	373	[4]
H-USY (18)*	10:1(60%)	-	15.9	10.0	5.94	373	[4]
H-BEA (150)*	10:1(60%)	-	31.1	27.9	3.25	373	[4]
H-BEA	10:1(60%)	Diethyl ketone	85.0	51.4	33.6	373	[7]
Mg/H-BEA	10:1(60%)	Diethyl ketone	93.3	54.0	39.3	373	[7]
Ca/H-BEA	10:1(60%)	Diethyl ketone	96.1	55.6	40.5	373	[7]
Sr/H-BEA	10:1(60%)	Diethyl ketone	94.0	53.6	40.4	373	[7]
Ba/H-BEA	10:1(60%)	Diethyl ketone	94.0	54.0	40.0	373	[7]
Cu-MFI	3:1	H_2O	23.5	67	33	353	[8]
Fe-ZSM-5	3:1	H_2O	32.9	60.5	39.5	353	[8]

*The numbers given in the parenthesis indicates the SiO_2/Al_2O_3.

The catalytic activity of H-MFI and M-MFI [M = Zr, In and Ru] for phenol hydroxylation with 30 % H_2O_2 has been investigated in the present study. Phenol hydroxylation has been carried out primarily using acetonitrile as solvent. The reaction has also been carried out in different temperatures taking water as solvent. It has been observed that all the catalysts are active for phenol

hydroxylation and in all the cases, a mixture of catechol and hydroquinone are formed. The formation of catechol and hydroquinone could be more likely due to electrophilic substitution of (- OH) on the benzene ring of phenol at *ortho* and *para* positions.

Phenol hydroxylation was carried out in liquid phase in a three-necked round bottom flask equipped with reflux condenser. The reaction was performed in the temperature range of 333 to 353 K. Prior to use in the reaction, all the catalysts were activated at 393 K for 4 h. The temperature of the reaction was maintained by a thermostated oil bath. After each experiment the catalyst was separated by filtration and then dried at 383 K for 12 h. The dried catalysts were then calcined in air at 753 K for 6 h and reused. It was observed that the performance of the catalyst was not significantly affected even after two runs. The reaction products were identified by GC-MS (Perkin Elmer, Clarus - 500). Two major products (catechol and hydroquinone) were obtained with few minor products which were not identified.

4.3 Hydroxylation of phenol with synthesized catalysts

4.3.1 Effect of reaction time on phenol hydroxylation

Hydroxylation of phenol reaction was carried out over different catalysts at temperature 353 K with mole ratio of the reactants (Phenol: H_2O_2) 1:1 and with catalyst amount 5 (W/W) % with respect to the total substrate both under organic solvent free condition and acetonitrile as solvent. In order to study the effect of reaction time, the products were withdrawn at 2, 4, 6 and 8 h intervals and were analyzed by GC-MS. The results of phenol hydroxylation over metal unloaded and Zr, In and Ru loaded MFI samples are presented in **Tables 4.2** to **4.6** and corresponding plots are shown in **Figures 4.1** to **4.5**.

Conversion increased with time on stream for all the catalysts. It appears from the data that the reaction slowed down after 6 h. However, ratios of

selectivity of catechol to that of hydroquinone increases marginally with TOS indicating favourable formation of *o*-isomer over *para* one. The results of phenol hydroxylation over the same catalysts under similar reaction conditions using additional water as solvent are reported in the **Tables 4.7** to **4.11** and presented in **Figures 4.6** to **4.10**, while the results of the same reaction under same conditions using acetonitrile as solvent with the catalysts are shown in **Tables 4.12** to **4.16** and **Figures 4.11** to **4.15**. It is clear from the results that after about 6 h the reactions slowed down in all cases. Germain et al [9] found a progressive growth in the conversion of phenol on an induction time. Marginal increase in CL/HQ ratio was observed suggesting a possibility of inter conversion and/or consecutive reactions in case of acetonitrile and additional water used as solvents in the present study.

4.3.1.1 Effect of reaction time on phenol hydroxylation with 30 % H_2O_2

Table 4.2 Effect of reaction time on phenol hydroxylation on S100

Reaction conditions

Catalyst: H-MFI zeolite (S100),
Temperature: 353 K
Mole ratio of the reactants = phenol: H_2O_2 (30%) = 1: 1
Catalyst amount: 5 (W/W) % with respect to total substrate

Reaction Time (h)	Conversion of phenol (%)	Product selectivity (%)		Ratio (CL/HQ)
		Catechol	Hydroquinone	
2	18.6	74.8	22.8	3.28
4	24.8	76.3	22.1	3.45
6	32.6	76.8	21.7	3.54
8	34.4	76.4	21.6	3.54

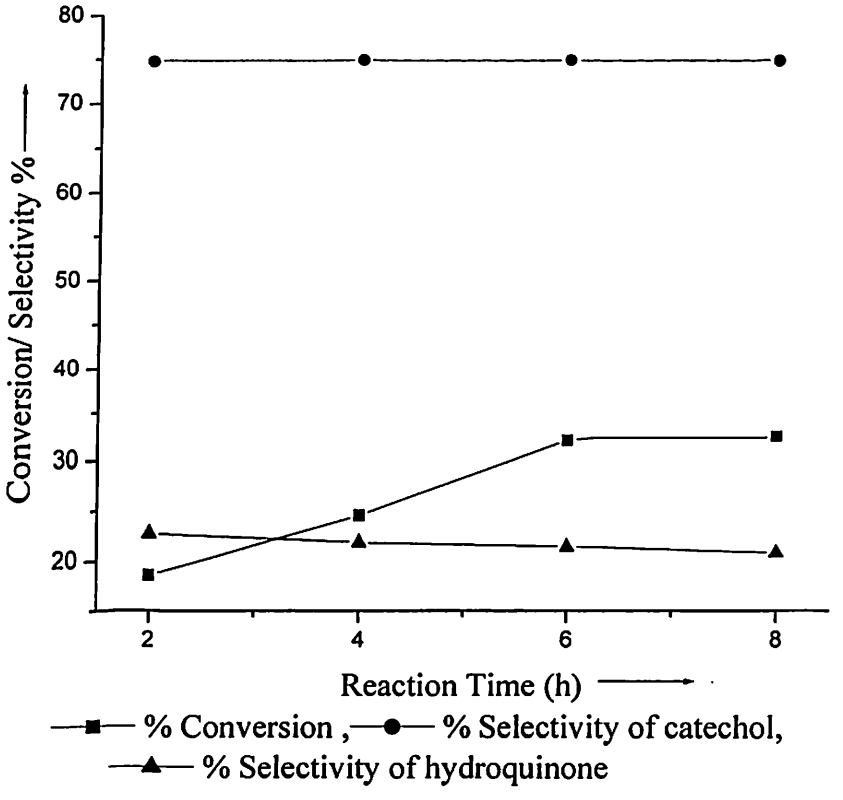

Fig.4.1 Effect of reaction time on hydroxylation of phenol on S100

Table 4.3 Effect of reaction time on phenol hydroxylation on S200

Reaction conditions

Catalyst: MFI zeolite (S200),
Temperature: 353 K
Mole ratio of the reactants = phenol: H_2O_2 (30%) = 1: 1
Catalyst amount: 5 (W/W) % with respect to total substrate

Reaction Time (h)	Conversion of phenol (%)	Product selectivity (%)		Ratio (CL/HQ)
		Catechol	Hydroquinone	
2	19.6	75.3	23.2	3.25
4	25.4	75.4	22.4	3.37
6	33.8	76.8	21.6	3.56
8	35.4	75.4	21.1	3.57

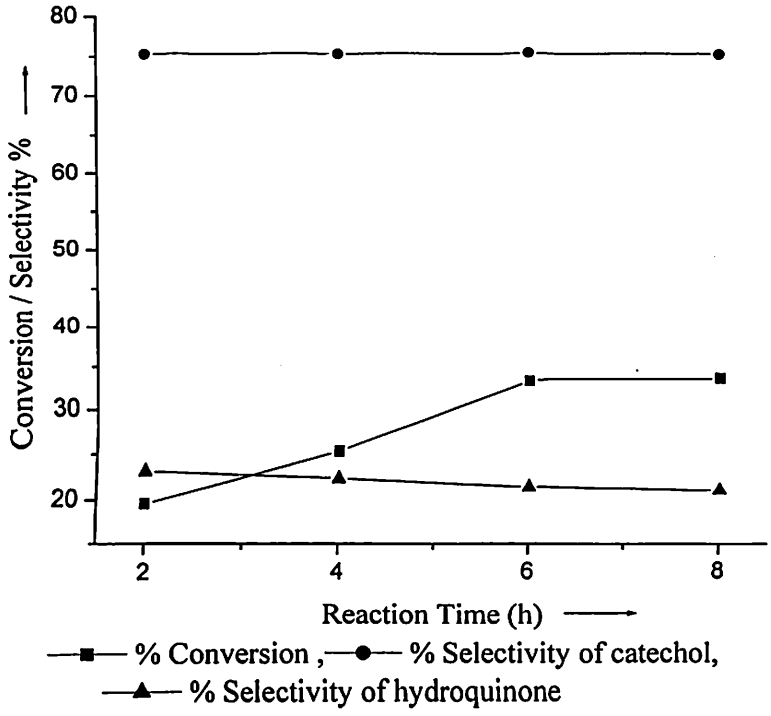

Fig.4.2 Effect of reaction time on hydroxylation of phenol on S200

Table 4.4 Effect of reaction time on phenol hydroxylation on S100Zr3

Reaction conditions

Catalyst: MFI zeolite (S100Zr3),
Temperature: 353 K,
Mole ratio of the reactants = phenol: H_2O_2 (30%) = 1: 1
Catalyst amount: 5 (W/W) % with respect to total substrate

Reaction Time (h)	Conversion of phenol (%)	Product selectivity (%)		Ratio (CL/HQ)
		Catechol	Hydroquinone	
2	28.6	78.6	19.8	3.97
4	34.8	78.2	18.9	4.13
6	40.4	78.3	18.9	4.14
8	44.2	79.7	18.7	4.26

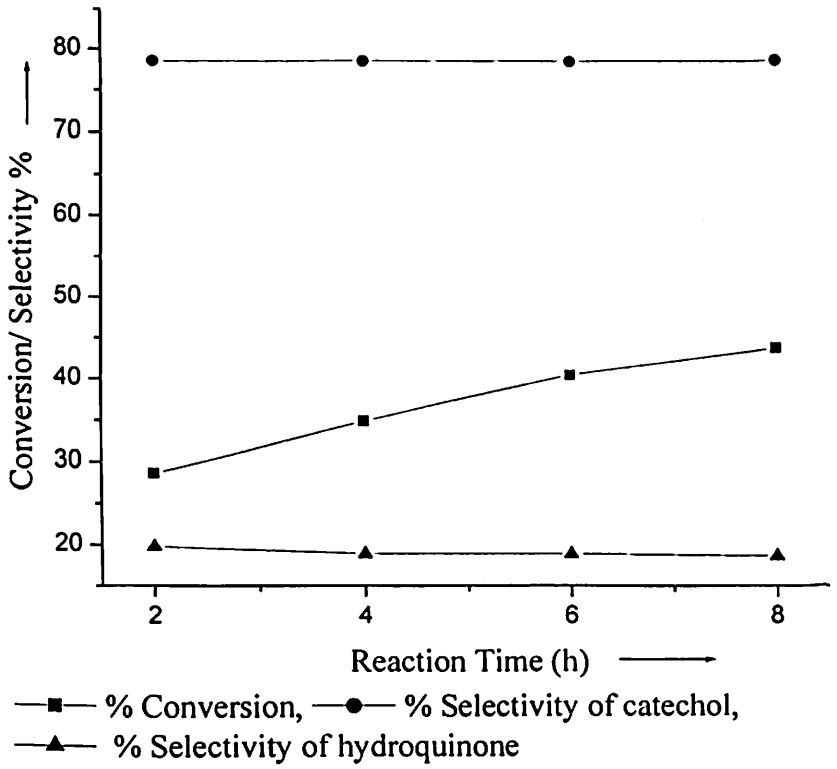

Fig. 4.3 Effect of reaction time on hydroxylation of phenol on S100Zr3

Table 4.5 Effect of reaction time on phenol hydroxylation on S100In3

Reaction conditions

Catalyst: MFI zeolite (S100In3),
Temperature: 353 K
Mole ratio of the reactants = phenol: H_2O_2 (30%) = 1: 1
Catalyst amount: 5 (W/W) % with respect to total substrate

Reaction Time (h)	Conversion of phenol (%)	Product selectivity (%)		Ratio (CL/HQ)
		Catechol	Hydroquinone	
2	24.4	75.1	23.3	3.22
4	31.3	75.5	22.5	3.36
6	38.2	75.8	22.3	3.40
8	40.7	76.7	21.8	3.52

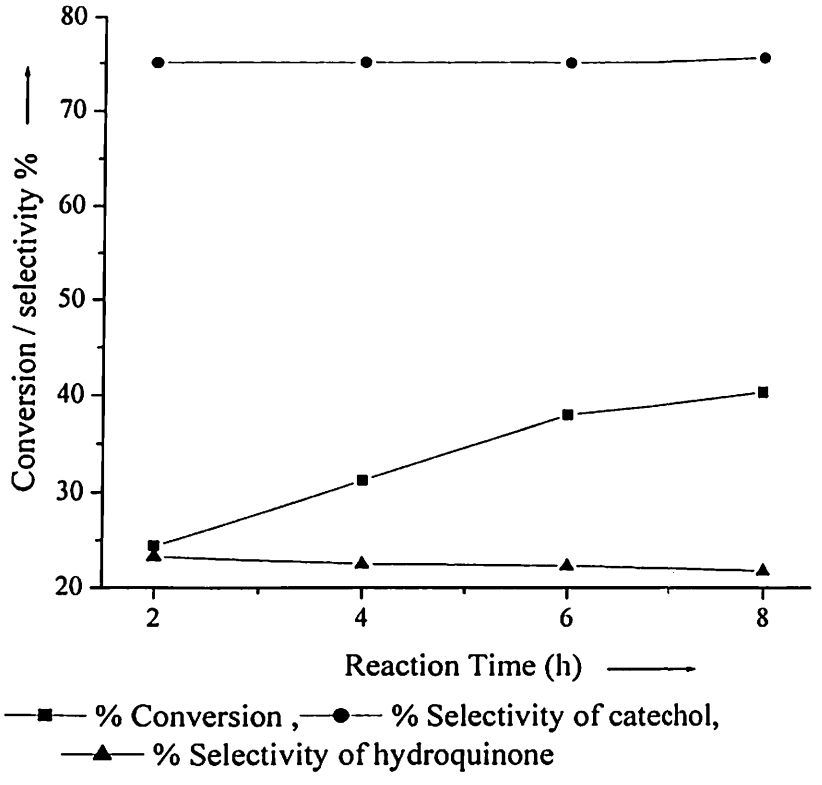

Fig.4.4 Effect of reaction time on hydroxylation of phenol on S100In3

Table 4.6 Effect of reaction time on phenol hydroxylation on S100Ru3

Reaction conditions

Catalyst: MFI zeolite (S100Ru3),
Temperature: 353 K
Mole ratio of the reactants = phenol: H_2O_2 (30%) = 1: 1
Catalyst amount: 5 (W/W) % with respect to total substrate

Reaction Time (h)	Conversion of phenol (%)	Product selectivity (%)		Ratio (CL/HQ)
		Catechol	Hydroquinone	
2	25.6	71.7	26.5	2.71
4	32.5	72.3	26.4	2.74
6	39.8	71.1	25.8	2.75
8	42.4	70.8	25.7	2.75

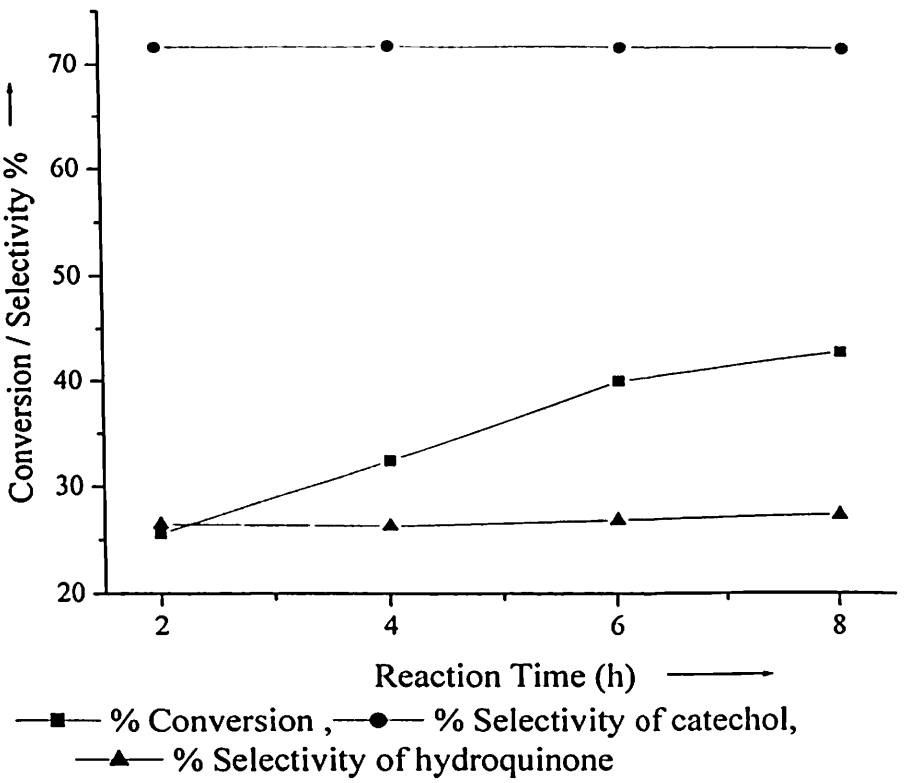

Fig.4.5 Effect of reaction time on hydroxylation of phenol on S100Ru3

4.3.1.2 Effect of reaction time on phenol hydroxylation with 30 % H_2O_2 and additional water

Table 4.7 Effect of reaction time on phenol hydroxylation in additional water on S100

Reaction conditions

Catalyst: H- MFI zeolite (S100), Temperature: 353 K,
Mole ratio of the reactants = phenol: H_2O_2 (30%): solvent = 1: 1:10,
Catalyst amount: 5 (W/W) % with respect to total substrate

Reaction Time (h)	Conversion of phenol (%)	Product selectivity (%)		Ratio (CL/HQ)
		Catechol	Hydroquinone	
2	25.8	81.3	16.8	4.83
4	33.6	82.1	16.7	4.92
6	41.3	81.1	16.2	5.01
8	42.4	81.4	15.9	5.12

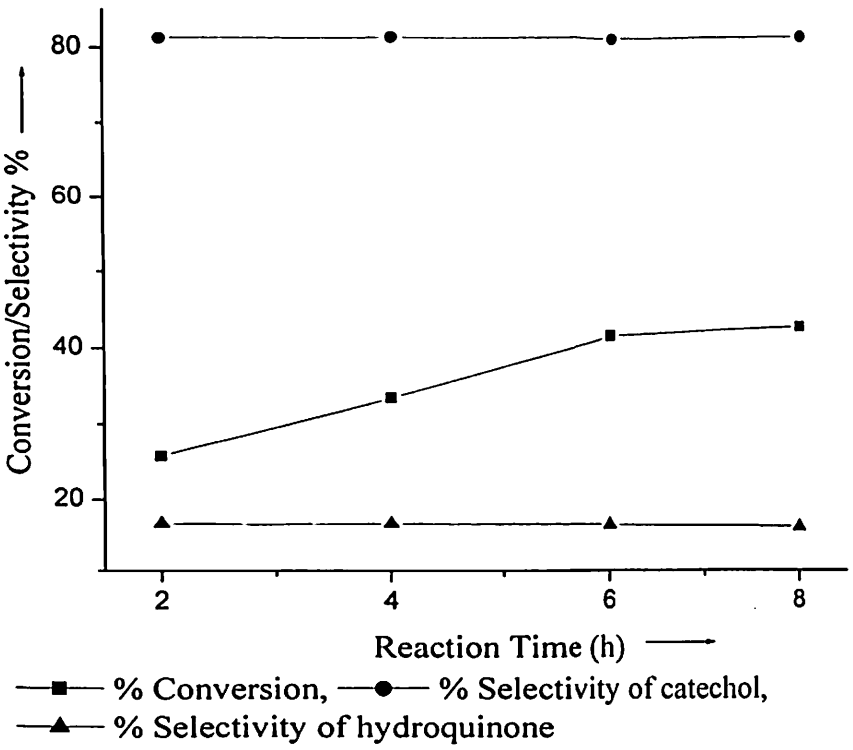

Fig. 4.6 Effect of reaction time on hydroxylation of phenol in water on S100

Table 4.8 Effect of reaction time on phenol hydroxylation in additional water on S200

Reaction Conditions

Catalyst: H- MFI zeolite (S200)
Temperature: 353 K
Mole ratio of the reactants = phenol: H_2O_2 (30%): solvent = 1: 1:10
Catalyst amount: 5 (W/W) % with respect to total substrate

Reaction Time (h)	Conversion of phenol (%)	Product selectivity (%)		Ratio (CL/HQ)
		Catechol	Hydroquinone	
2	26.5	80.2	16.9	4.74
4	32.2	79.9	16.8	4.76
6	46.7	80.8	16.9	4.78
8	48.5	81.7	15.9	5.14

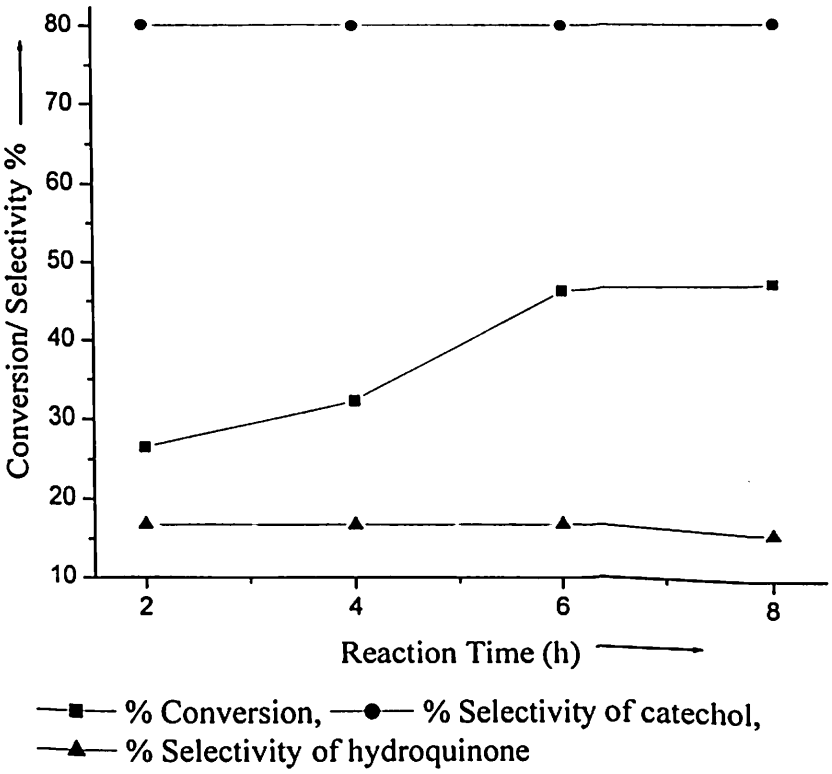

Fig. 4.7 Effect of reaction time on hydroxylation of phenol in water on S200

Table 4.9 Effect of reaction time on phenol hydroxylation in additional water on S100Zr3

Reaction conditions

Catalyst: MFI zeolite (S100Zr3)
Temperature: 353 K
Mole ratio of the reactants = phenol: H_2O_2 (30%): solvent = 1: 1:10
Catalyst amount: 5 (W/W) % with respect to total substrate

Reaction Time (h)	Conversion of Phenol (%)	Product selectivity (%)		Ratio (CL/HQ)
		Catechol	Hydroquinone	
2	26.8	83.9	13.2	6.36
4	39.8	85.7	13.0	6.59
6	60.2	85.3	12.8	6.66
8	62.4	85.4	12.3	6.94

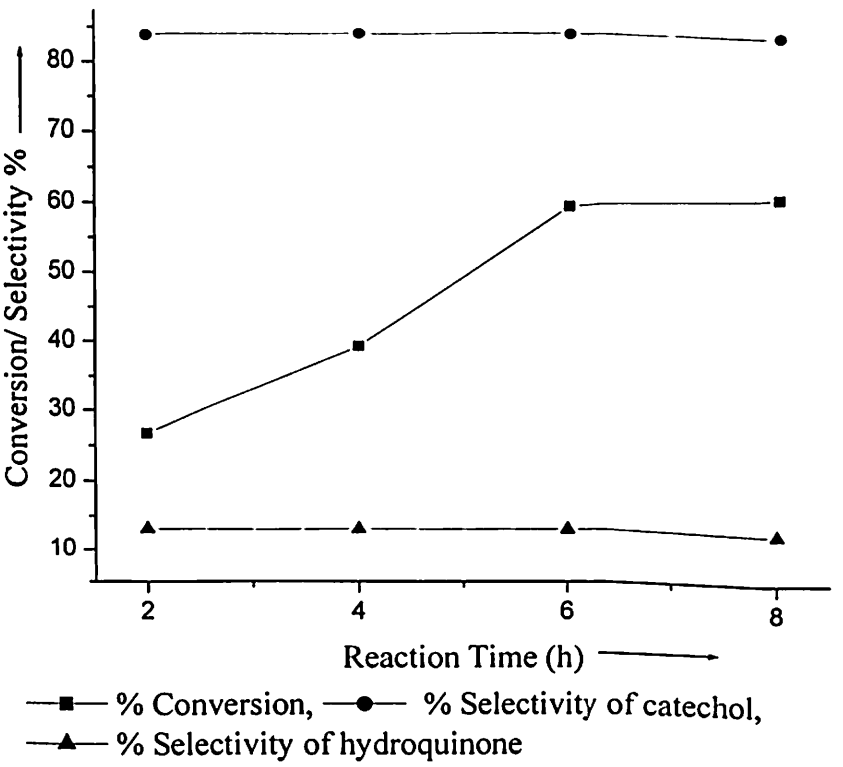

Fig. 4.8 Effect of reaction time on hydroxylation of phenol in water on S100Zr3

Table 4.10 Effect of reaction time on phenol hydroxylation in additional water on S100In3

Reaction conditions

Catalyst: MFI zeolite (S100In3)
Temperature: 353 K
Mole ratio of the reactants = phenol: H_2O_2 (30%): solvent = 1: 1:10
Catalyst amount: 5 (W/W) % with respect to total substrate

Reaction Time (h)	Conversion of phenol (%)	Product selectivity (%)		Ratio (CL/HQ)
		Catechol	Hydroquinone	
2	25.2	76.8	21.7	3.54
4	36.3	76.1	20.9	3.64
6	52.3	77.4	21.2	3.65
8	55.6	77.6	20.1	3.86

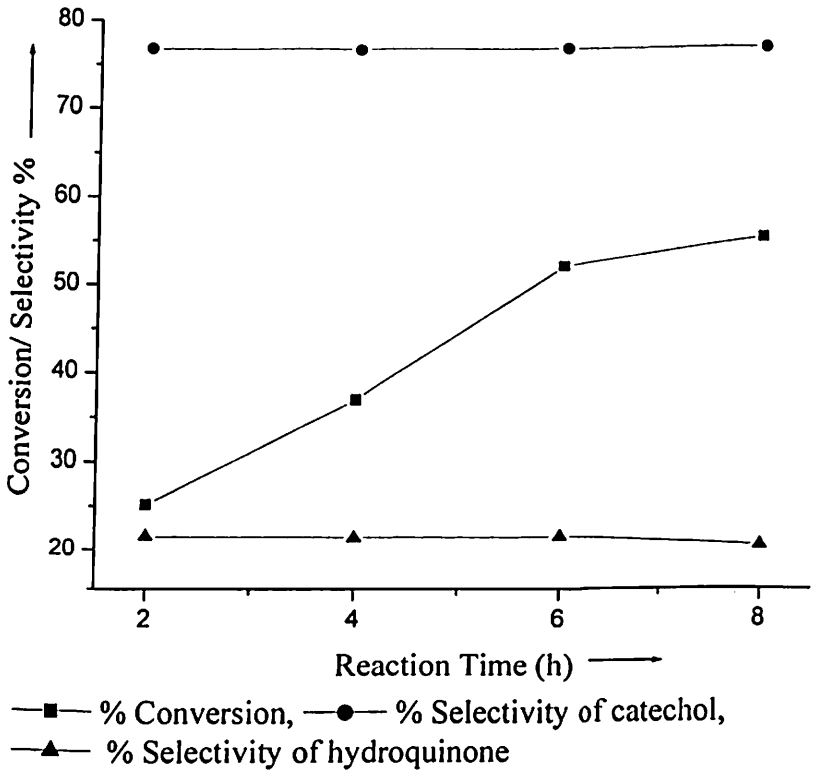

Fig. 4.9 Effect of reaction time on hydroxylation of phenol in water on S100In3

Table 4.11 Effect of reaction time on phenol hydroxylation in additional water on S100Ru3

Reaction conditions

Catalyst: MFI zeolite (S100Ru3)
Temperature: 353 K
Mole ratio of the reactants = phenol: H_2O_2 (30%): solvent = 1: 1:10
Catalyst amount: 5 (W/W) % with respect to total substrate

Reaction Time (h)	Conversion of phenol (%)	Product selectivity (%)		Ratio (CL/HQ)
		Catechol	Hydroquinone	
2	26.1	73.4	23.5	3.12
4	36.9	73.9	23.1	3.20
6	57.7	75.7	22.8	3.32
8	59.3	75.6	22.2	3.41

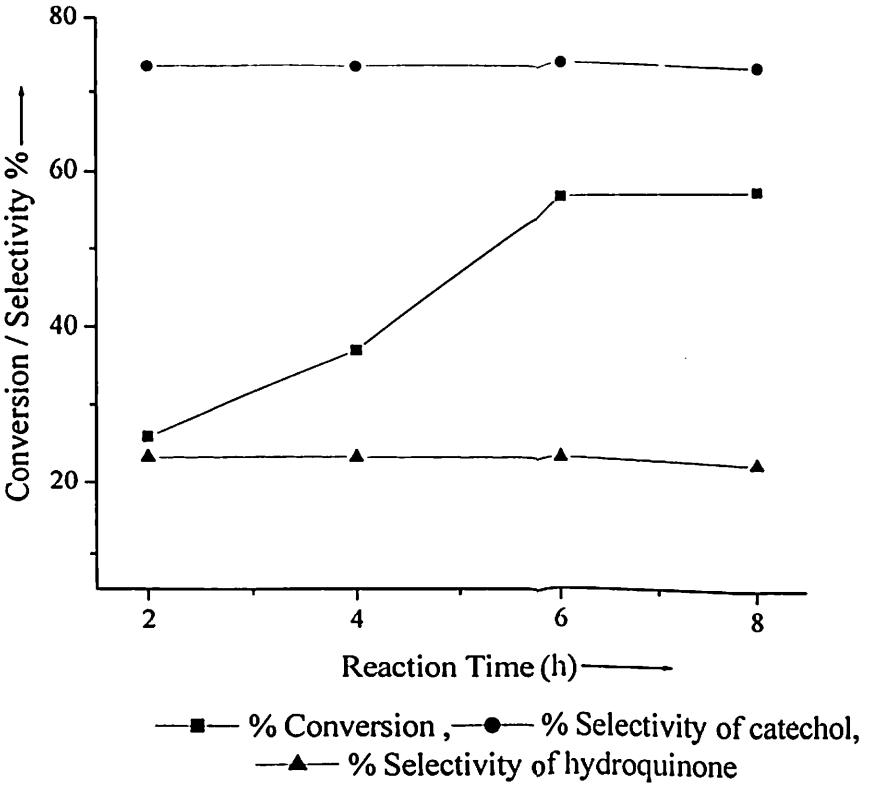

Fig.4.10 Effect of reaction time on hydroxylation of phenol in water on S100Ru3

4.3.1.3 Effect of reaction time on phenol hydroxylation with 30 % H_2O_2 in acetonitrile

Table 4.12 Effect of reaction time on phenol hydroxylation in CH_3CN on S100

Reaction conditions
Catalyst: H-MFI zeolite (S100), Temperature: 353 K
Mole ratio of the reactants = phenol: H_2O_2 (30%): solvent = 1: 1:10
Catalyst amount: 5 (W/W) % with respect to total substrate

Reaction Time (h)	Conversion of phenol (%)	Product selectivity (%)		Ratio (CL/HQ)
		Catechol	Hydroquinone	
2	23.7	81.2	16.9	4.81
4	30.6	80.1	16.4	4.88
6	39.4	80.8	15.9	5.08
8	40.6	81.3	15.7	5.18

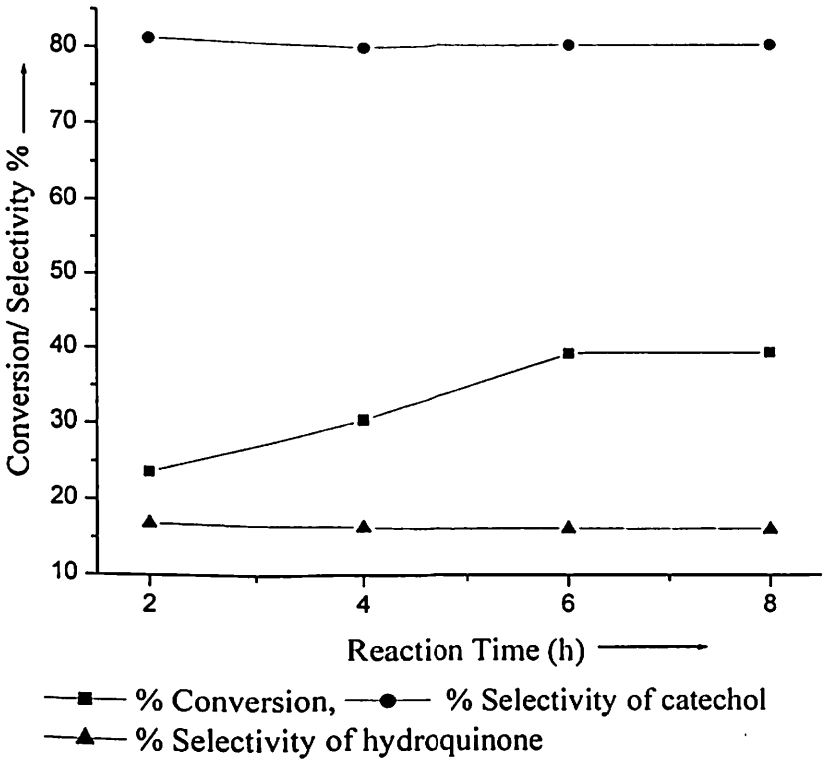

Fig. 4.11 Effect of reaction time on hydroxylation of phenol in CH_3CN on S100

Table 4.13 Effect of reaction time on phenol hydroxylation in CH_3CN on S200

Reaction conditions

Catalyst: H-MFI zeolite (S200), Temperature: 353 K
Mole ratio of the reactants = phenol: H_2O_2 (30%): solvent = 1: 1:10
Catalyst amount: 5 (W/W) % with respect to total substrate

Reaction Time (h)	Conversion of phenol (%)	Product selectivity (%)		Ratio (CL/HQ)
		Catechol	Hydroquinone	
2	23.9	80.1	15.9	5.04
4	31.2	81.4	16.1	5.06
6	43.6	81.7	15.6	5.24
8	46.7	83.2	15.2	5.47

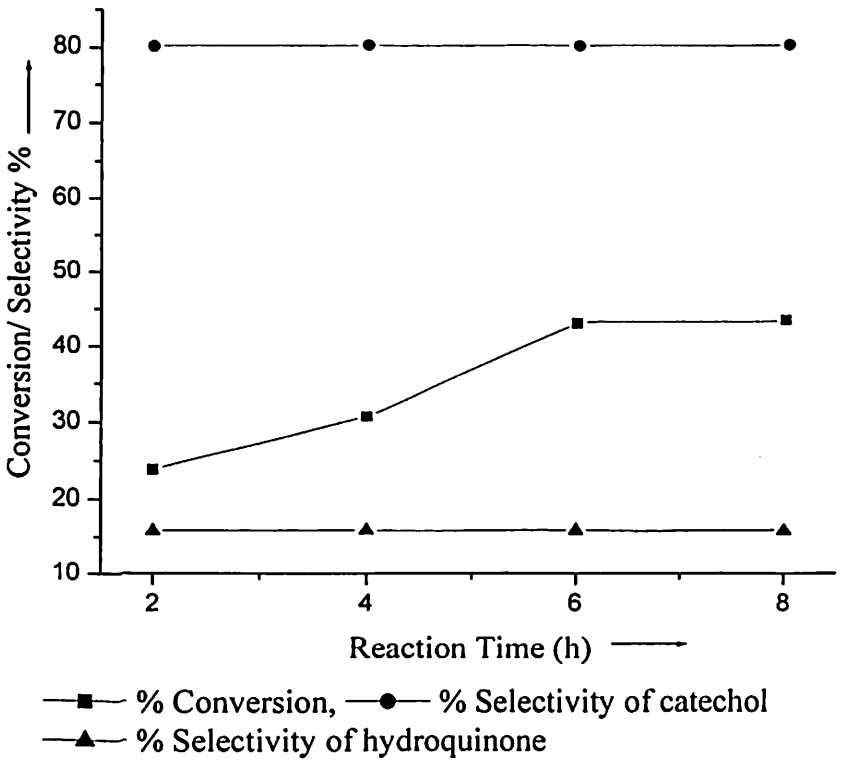

Fig. 4.12 Effect of reaction time on hydroxylation of phenol in CH_3CN on S200

Table 4.14 Effect of reaction time on phenol hydroxylation in CH_3CN on S100Zr3

Reaction conditions

Catalyst: MFI zeolite (S100Zr3), Temperature: 353 K
Mole ratio of the reactants = phenol: H_2O_2 (30%): solvent = 1: 1:10
Catalyst amount: 5 (W/W) % with respect to total substrate

Reaction Time (h)	Conversion of phenol (%)	Product selectivity (%)		Ratio (CL/HQ)
		Catechol	Hydroquinone	
2	25.4	84.6	13.9	6.07
4	35.6	85.5	12.6	6.79
6	57.5	85.7	12.4	6.91
8	60.2	86.0	12.3	6.99

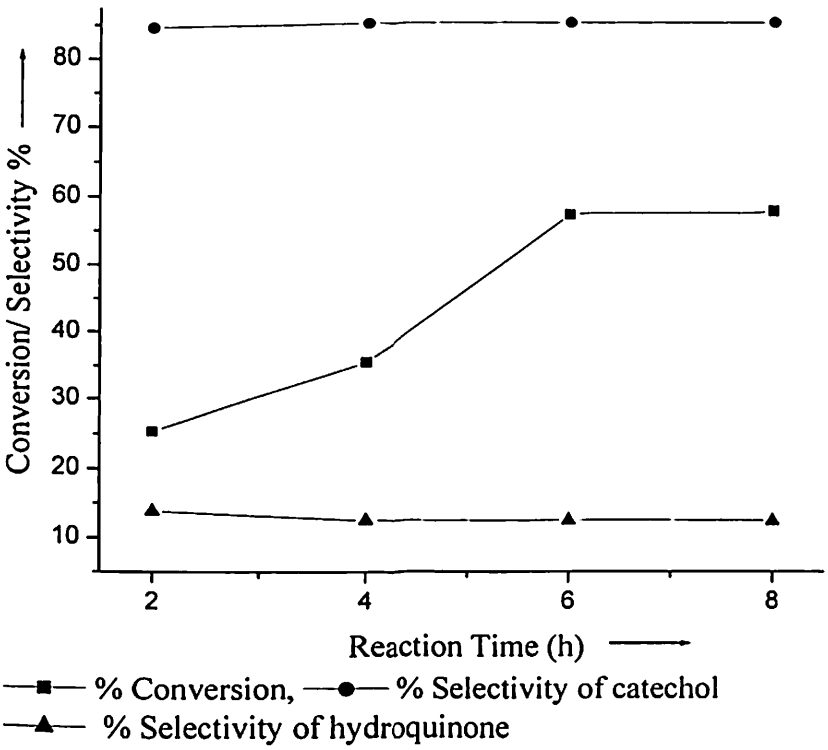

Fig. 4.13 Effect of reaction time on hydroxylation of phenol in CH_3CN on S100Zr3

Table 4.15 Effect of reaction time on phenol hydroxylation in CH_3CN on S100In3

Reaction conditions

Catalyst: MFI zeolite (S100In3), Temperature: 353 K
Mole ratio of the reactants = phenol: H_2O_2 (30%): solvent = 1: 1:10
Catalyst amount: 5 (W/W) % with respect to total substrate

Reaction Time (h)	Conversion of phenol (%)	Product selectivity (%)		Ratio (CL/HQ)
		Catechol	Hydroquinone	
2	24.2	79.1	19.2	4.12
4	34.6	79.6	18.3	4.35
6	49.3	80.4	17.9	4.49
8	51.2	80.8	18.0	4.49

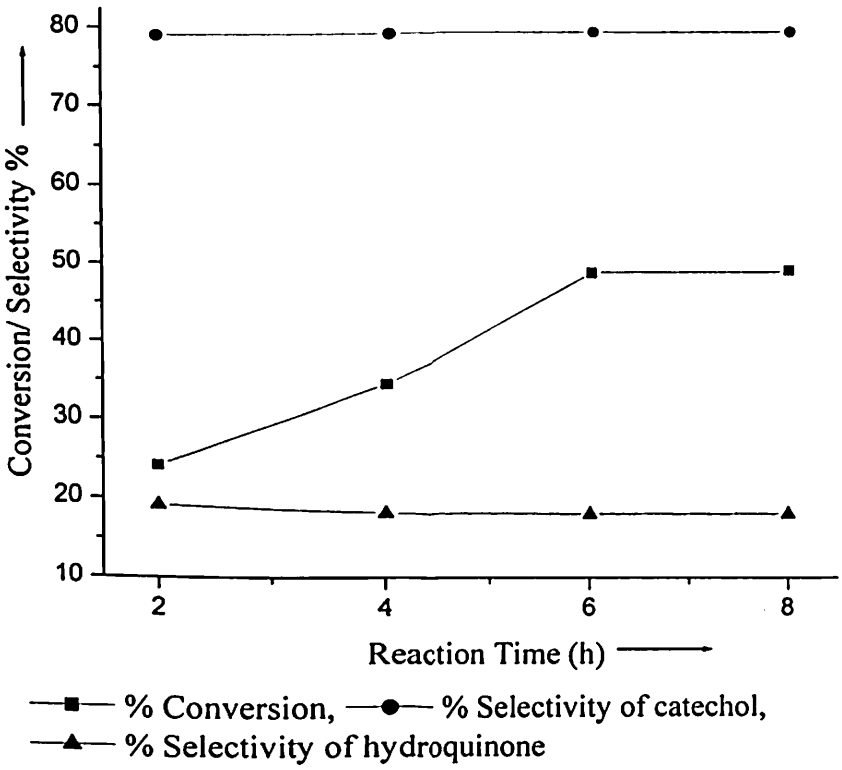

Fig. 4.14 Effect of reaction time on hydroxylation of phenol in CH_3CN on S100In3

Table 4.16 Effect of reaction time on phenol hydroxylation in CH_3CN on S100Ru3

Reaction conditions

Catalyst: MFI zeolite (S100Ru3), Temperature: 353 K
Mole ratio of the reactants = phenol: H_2O_2 (30%): solvent = 1: 1:10
Catalyst amount: 5 (W/W) % with respect to total substrate

Reaction Time (h)	Conversion of phenol (%)	Product selectivity (%)		Ratio (CL/HQ)
		Catechol	Hydroquinone	
2	24.9	75.9	23.7	3.20
4	34.6	75.8	23.6	3.21
6	51.8	77.2	22.3	3.46
8	54.4	78.1	21.4	3.65

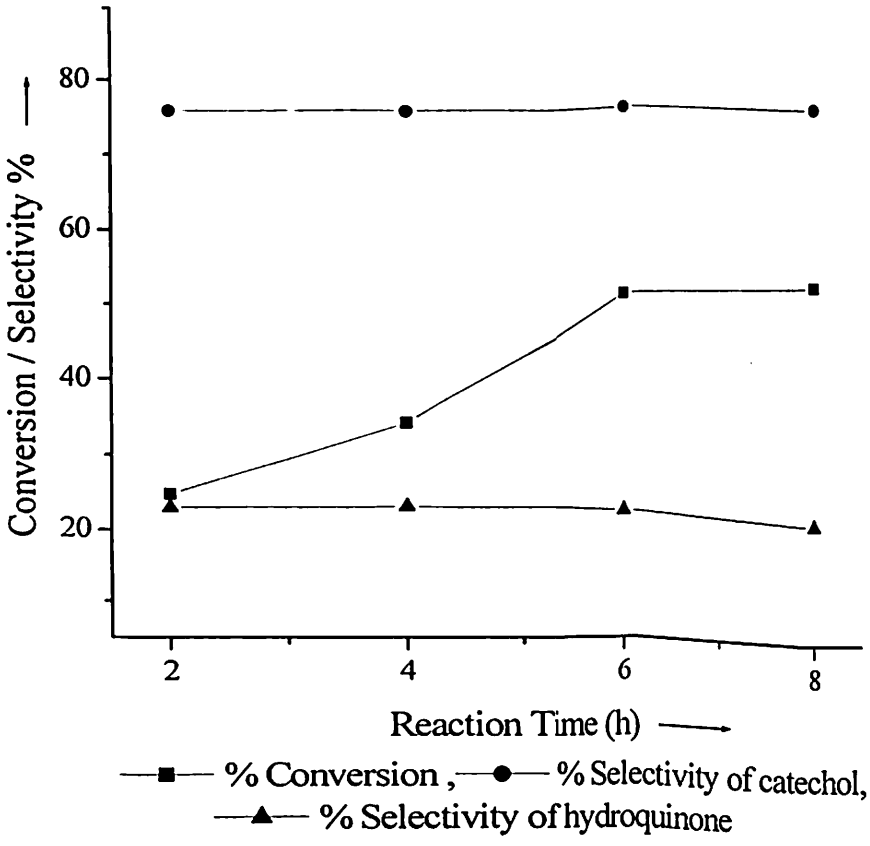

Fig.4.15 Effect of reaction time on hydroxylation of phenol in CH_3CN on S100Ru3

4.3.2 Effect of temperature on phenol hydroxylation in additional H_2O

Hydroxylation of phenol reaction was carried out over different catalysts at the temperature range of 333K to 353 K with mole ratio of the reactants (phenol: H_2O_2) 1:1 and with catalyst amount 5 (W/W) % with respect to the total substrate in additional water. In order to study the effect of temperature in this reaction, the products were withdrawn after 8 h interval and were analyzed by GC-MS. Maximum conversion was found with the Zr incorporated MFI sample at 353 K temperature. The results are shown in **Table 4.17** to **4.21** and are plotted in **Figures 4.16** to **4.20**. The conversion increased markedly from 25.6 to 36.2 for

S100, from 29.8 to 41.9 for S200, from 32.2 to 55.4 for S100Zr3, from 30.1 to 48.7 for S100In3, from 30.4 to 49.5 for S100Ru3 for increase of temperature upto 343 K from 333 K. However, when temperature was further increased upto 353 K, the rate was slowed down to some extent. This could be ascribed to the competitive thermal decomposition of H_2O_2 at higher temperature without being involved in desired reaction. This was also observed by Dubey et. al [10] while studying hydroxylation of phenol over ternary hydrotalcites containing Cu, Ni and Al.

Table 4.17 Effect of temperature on phenol hydroxylation in additional H_2O on S100

Reaction conditions

Catalyst: H-MFI zeolite (S100), Time: 8 h,
Mole ratio of the reactants = phenol: H_2O_2 (30%): solvent = 1: 1:10,
Catalyst amount: 5 (W/W) % with respect to total substrate

Temperature (K)	Conversion of phenol (%)	Product selectivity (%)		Ratio (CL/HQ)
		Catechol	Hydroquinone	
333	25.6	80.8	16.3	4.96
343	36.2	80.2	16.7	4.80
353	42.4	81.4	15.9	5.12

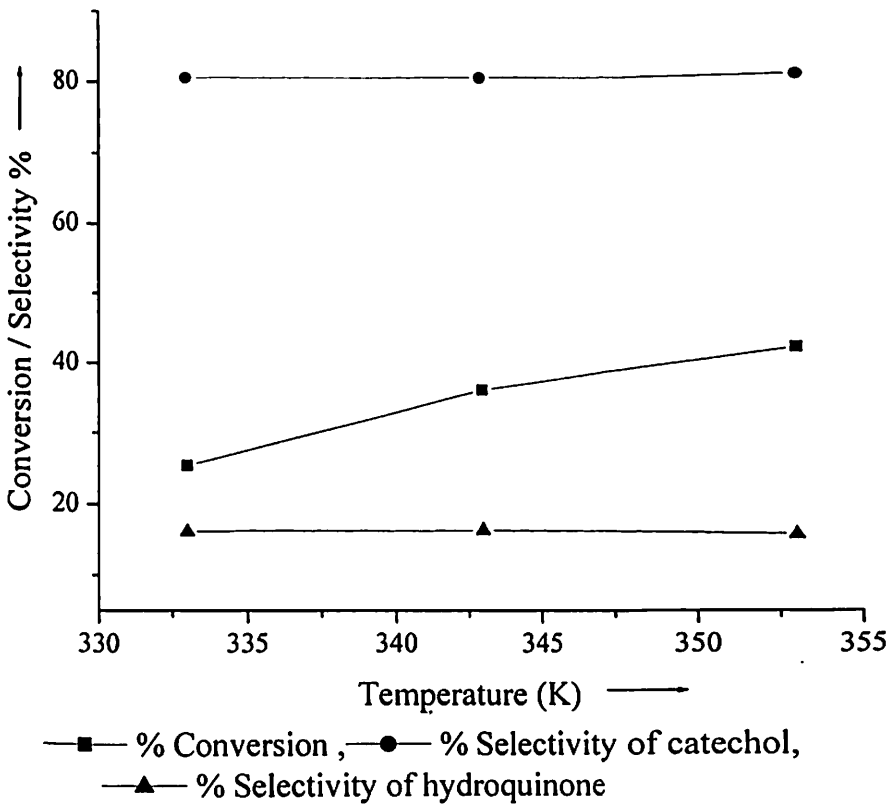

Fig.4.16 Effect of temperature on hydroxylation of phenol on S100

Table 4.18 Effect of temperature on phenol hydroxylation in additional H_2O on S200

Reaction conditions

Catalyst: H- MFI zeolite (S200), Time: 8 h
Mole ratio of the reactants = phenol: H_2O_2 (30%): solvent = 1: 1:10
Catalyst amount: 5 (W/W) % with respect to total substrate

Temperature (K)	Conversion of phenol (%)	Product selectivity (%)		Ratio (CL/HQ)
		Catechol	Hydroquinone	
333	29.8	80.9	16.5	4.90
343	41.9	80.1	16.9	4.74
353	48.5	81.7	15.9	5.14

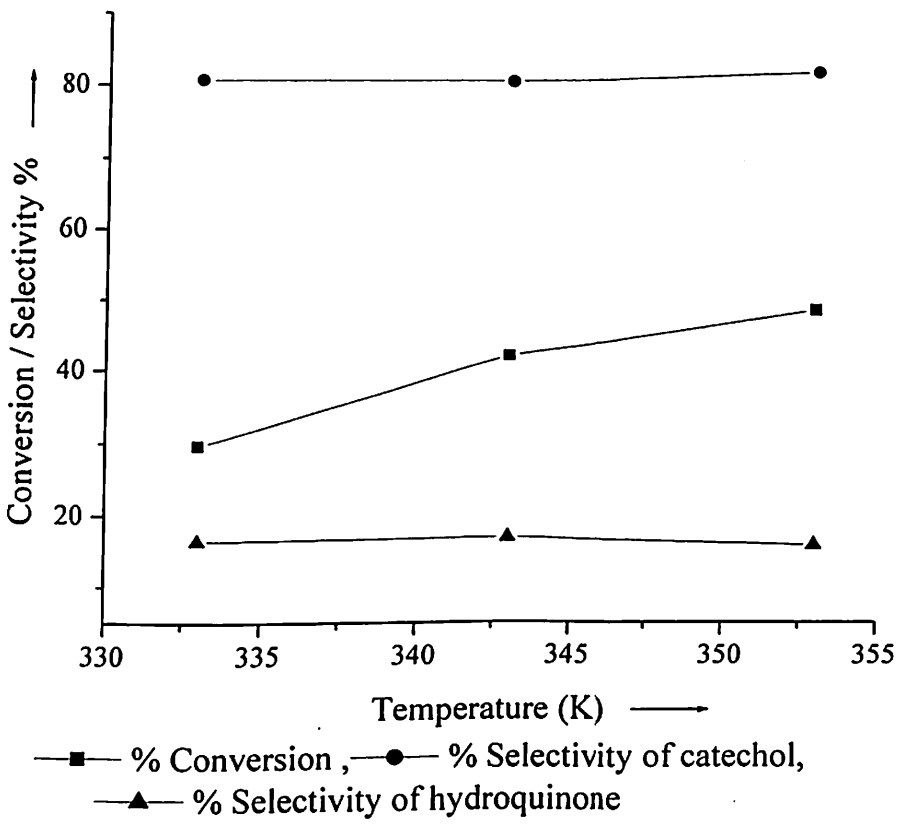

Fig.4.17 Effect of temperature on hydroxylation of phenol on S200

Table 4.19 Effect of temperature on phenol hydroxylation in additional H_2O on S100Zr3

Reaction conditions

Catalyst: MFI zeolite (S100Zr3), Time: 8 h
Mole ratio of the reactants = phenol: H_2O_2 (30%): solvent = 1: 1:10
Catalyst amount: 5 (W/W) % with respect to total substrate

Temperature (K)	Conversion of phenol (%)	Product selectivity (%)		Ratio (CL/HQ)
		Catechol	Hydroquinone	
333	32.2	83.7	14.0	5.98
343	55.4	83.2	14.6	5.70
353	62.4	84.4	13.3	6.35

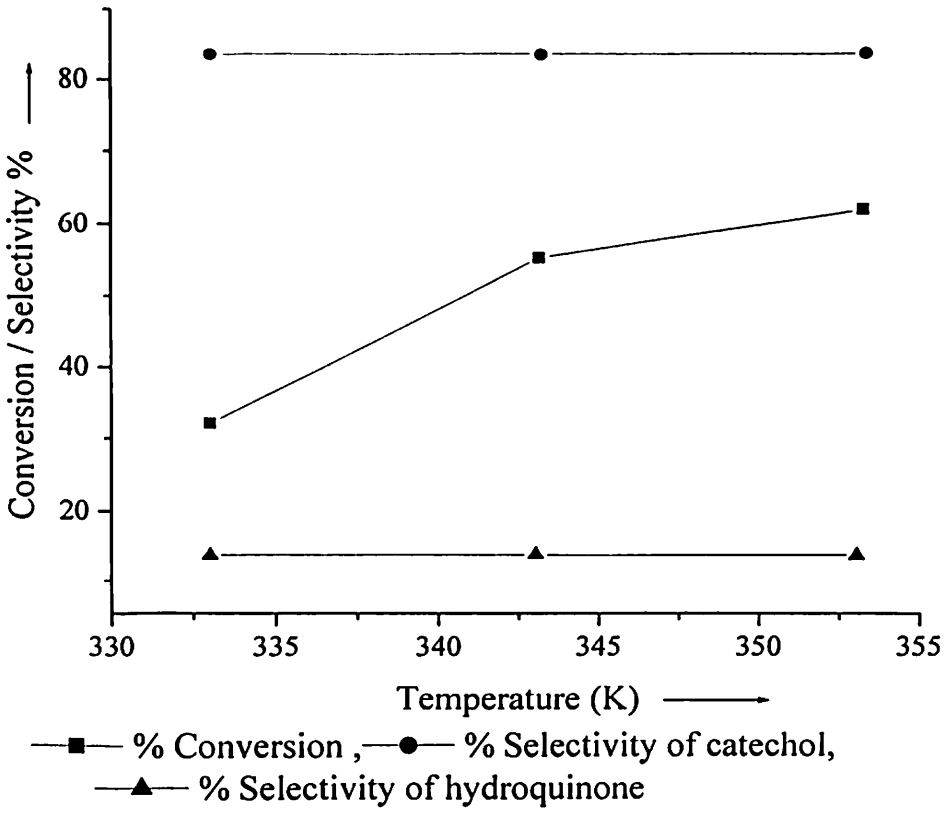

Fig.4.18 Effect of temperature on hydroxylation of phenol on S100Zr3

Table 4.20 Effect of temperature on phenol hydroxylation in additional H_2O on S100In3

Reaction conditions

Catalyst: MFI zeolite (S100In3), Time: 8 h
Mole ratio of the reactants = phenol: H_2O_2 (30%): solvent = 1: 1:10
Catalyst amount: 5 (W/W) % with respect to total substrate

Temperature (K)	Conversion of phenol (%)	Product selectivity (%)		Ratio (CL/HQ)
		Catechol	Hydroquinone	
333	30.1	77.1	20.8	3.71
343	48.7	76.4	20.5	3.73
353	55.6	77.6	20.1	3.86

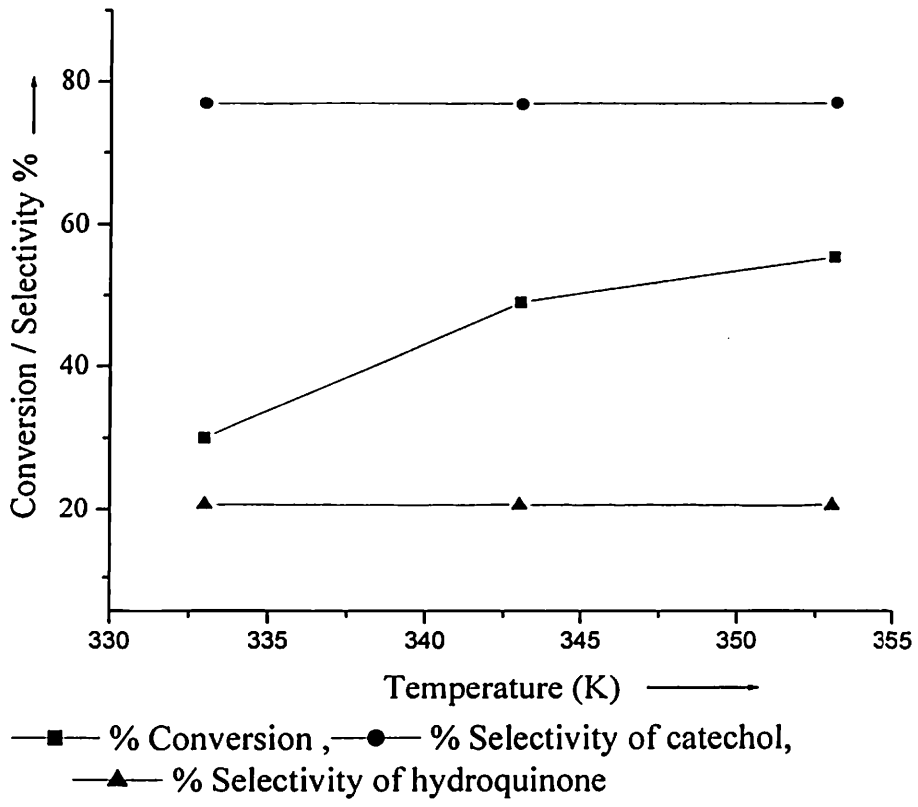

Fig.4.19 Effect of temperature on hydroxylation of phenol on S100In3

Table 4.21 Effect of temperature on phenol hydroxylation in additional H_2O on S100Ru3

Reaction conditions

Catalyst: MFI zeolite (S100Ru3), Time: 8 h
Mole ratio of the reactants = phenol: H_2O_2 (30%): solvent = 1: 1:10
Catalyst amount: 5 (W/W) % with respect to total substrate

Temperature (K)	Conversion of phenol (%)	Product selectivity (%)		Ratio (CL/HQ)
		Catechol	Hydroquinone	
333	30.4	76.4	21.3	3.59
343	49.5	74.7	23.6	3.16
353	59.3	75.6	22.2	3.41

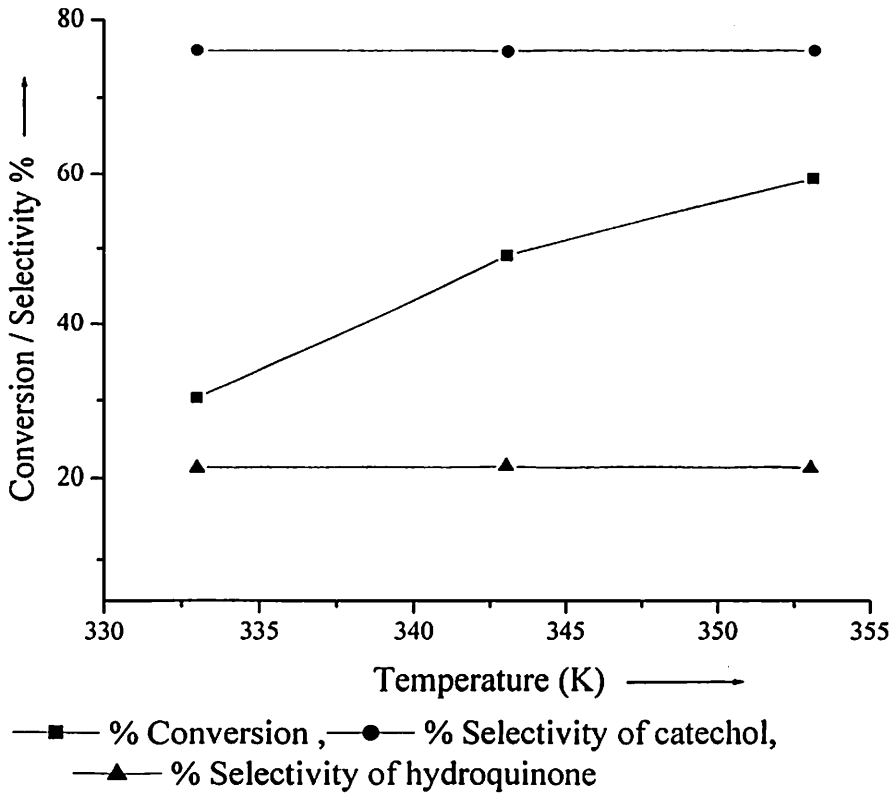

Fig.4.20 Effect of temperature on hydroxylation of phenol on S100Ru3

4.3.3 Effect of amount of catalyst on phenol hydroxylation

In order to study the effect of amount of catalyst on hydroxylation of phenol the reaction was carried out over different catalysts at temperature 353 K with mole ratio of the reactants (phenol: H_2O_2) 1:1 and with catalyst amount 5, 7 and 10 (W/W) % with respect to the total substrate in additional water. The products were withdrawn at 8 h interval and were analyzed by GC-MS. The results are shown in **Table 4.22** to **4.26** and depicted in **Figures 4.21** to **4.25**. Maximum conversion was found with the Zr incorporated MFI sample with catalyst amount 10 (W/W) %, but the increase in the % of conversion is not significantly high in comparison to the change in the amount of catalyst.

Table 4.22 Effect of amount of catalyst on phenol hydroxylation on S100

Reaction conditions

Catalyst: H- MFI zeolite (S100), Temperature: 353 K, Time: 8 h
Mole ratio of the reactants = phenol: H_2O_2 (30%): solvent = 1: 1:10

Amount of Catalyst (W/W) % w.r.t. total substrate	Conversion of phenol (%)	Product selectivity (%)		Ratio (CL/HQ)
		Catechol	Hydroquinone	
5	42.4	81.4	15.9	5.12
7	43.2	80.7	16.7	4.83
10	44.6	81.1	16.2	5.01

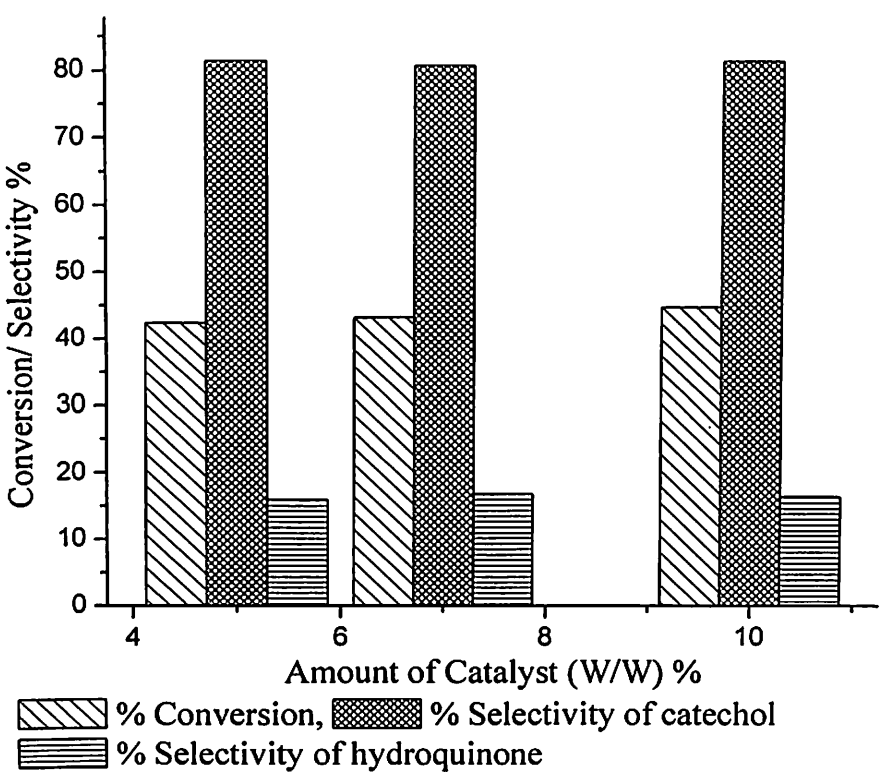

Fig.4.21 Effect of amount of catalyst on hydroxylation of phenol on S100

Table 4.23 Effect of amount of catalyst on phenol hydroxylation on S200

Reaction conditions

Catalyst: H-MFI zeolite (S200), Time: 8 h, Temperature: 353 K
Mole ratio of the reactants = phenol: H_2O_2 (30%): solvent = 1: 1:10

Amount of Catalyst (W/W) % w.r.t. total substrate	Conversion of phenol (%)	Product selectivity (%)		Ratio (CL/HQ)
		Catechol	Hydroquinone	
5	48.5	81.7	15.9	5.14
7	49.9	80.6	16.9	4.77
10	50.5	81.9	15.8	5.18

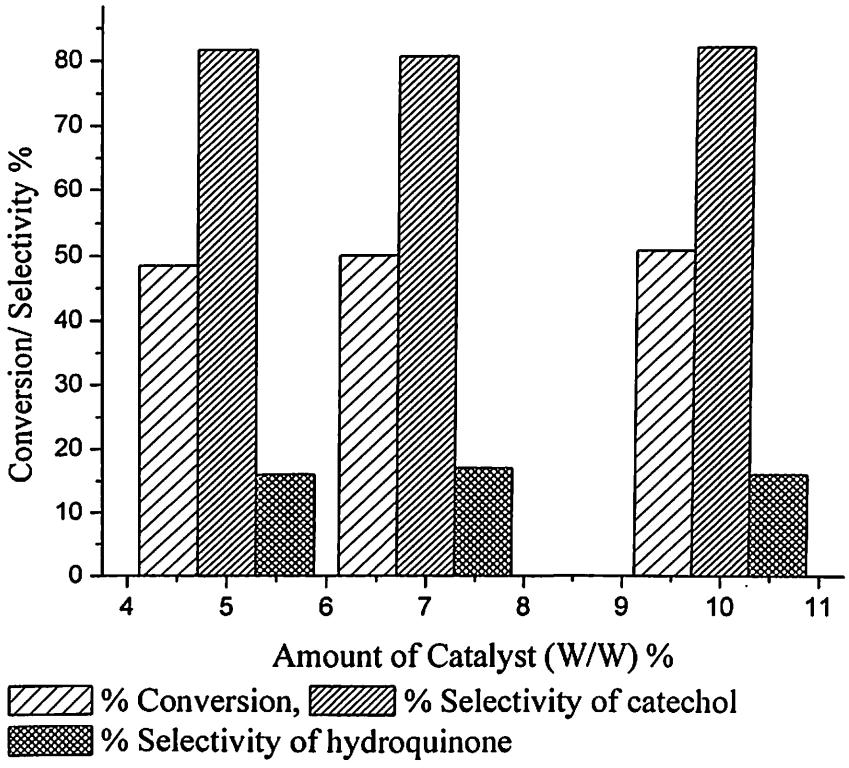

Fig. 4.22 Effect of amount of catalyst on hydroxylation of phenol on S200

Table 4.24 Effect of amount of catalyst on phenol hydroxylation on S100Zr3

Reaction conditions

Catalyst: MFI zeolite (S100Zr3), Time: 8 h, Temperature: 353 K
Mole ratio of the reactants = phenol: H_2O_2 (30%): solvent = 1: 1:10

Amount of Catalyst (W/W) % w.r.t. total substrate	Conversion of phenol (%)	Product selectivity (%)		Ratio (CL/HQ)
		Catechol	Hydroquinone	
5	62.4	84.4	13.3	6.35
7	63.7	83.1	14.7	5.65
10	64.4	84.7	13.8	6.14

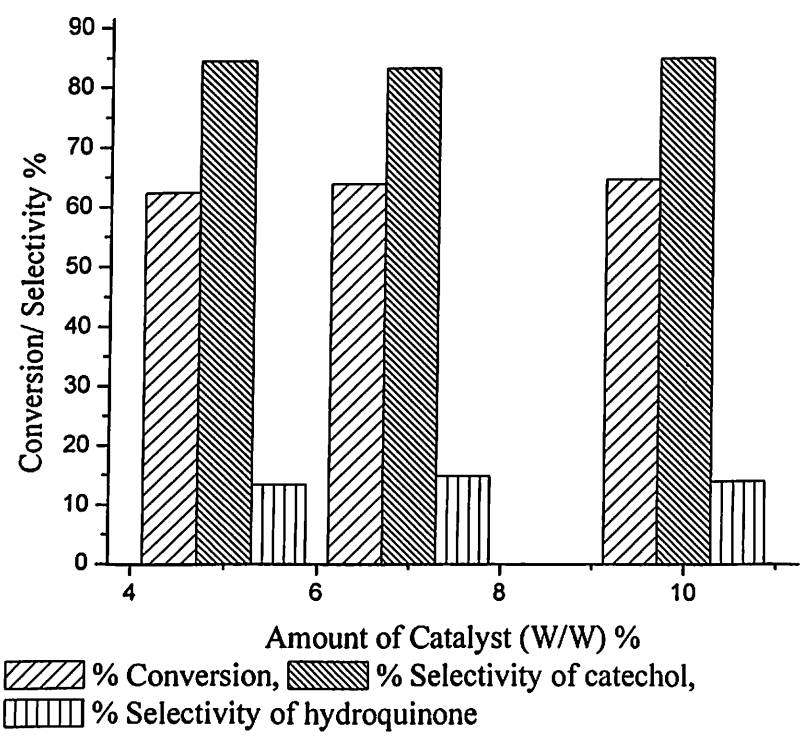

Fig.4.23 Effect of amount of catalyst on hydoxylation of phenol on S100Zr3

Table 4.25 Effect of amount of catalyst on phenol hydroxylation on S100In3

Reaction conditions

Catalyst: MFI zeolite (S100In3), Temperature: 353 K, Time: 8 h,
Mole ratio of the reactants = phenol: H_2O_2 (30%): solvent = 1: 1:10

Amount of Catalyst (W/W) % w.r.t. total substrate	Conversion of phenol (%)	Product selectivity (%)		Ratio (CL/HQ)
		Catechol	Hydroquinone	
5	55.6	77.6	20.1	3.86
7	56.7	76.1	22.5	3.38
10	57.7	77.9	20.6	3.78

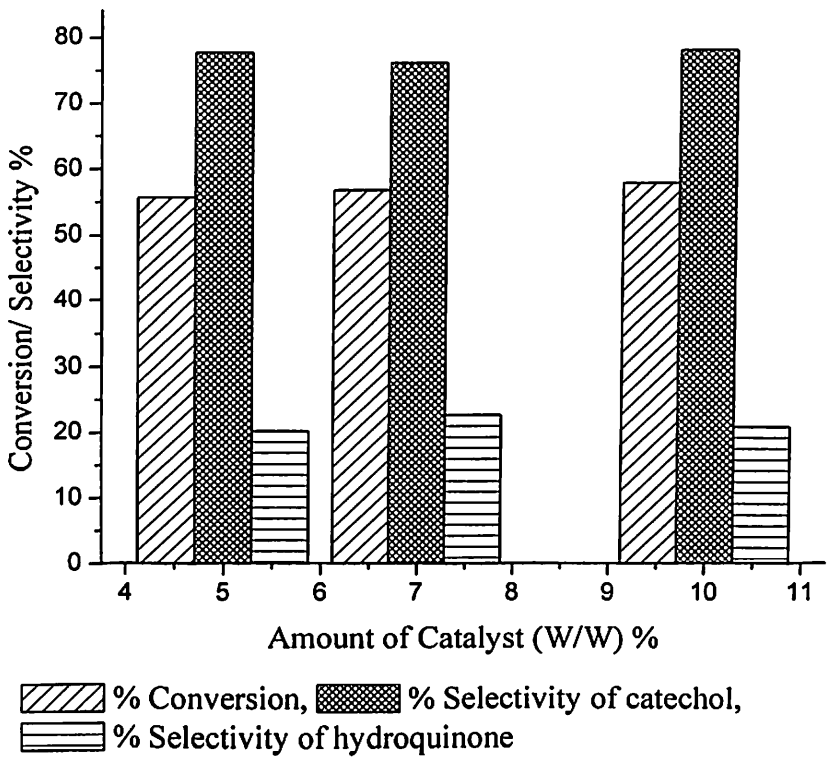

Fig. 4.24 Effect of amount of catalyst on hydroxylation of phenol on S100In3

Table 4.26 Effect of amount of catalyst on phenol hydroxylation on S100Ru3

Reaction conditions

Catalyst: MFI zeolite (S100Ru3), Time: 8 h, Temperature: 353 K,
Mole ratio of the reactants = phenol: H_2O_2 (30%): solvent = 1: 1:10

Amount of Catalyst (W/W) % w.r.t. total substrate	Conversion of phenol (%)	Product selectivity (%)		Ratio (CL/HQ)
		Catechol	Hydroquinone	
5	59.3	75.6	22.2	3.40
7	60.5	74.3	23.7	3.14
10	61.2	75.8	22.9	3.31

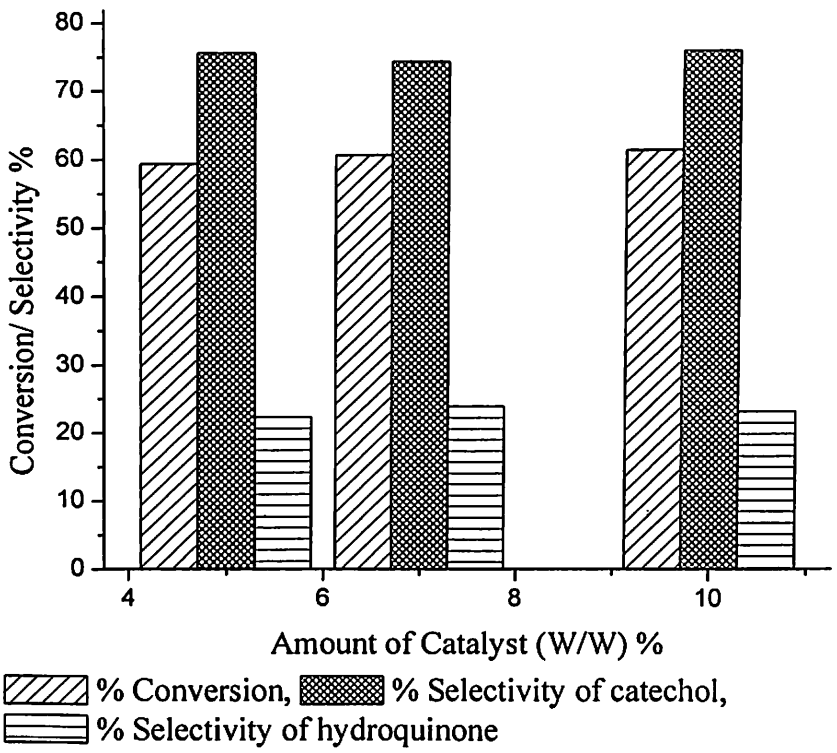

Fig. 4.25 Effect of amount of catalyst on hydroxylation of phenol on S100Ru3

4.3.4 Comparison of the hydroxylation of phenol using MFI zeolite with different metal contents

Hydroxylation of phenol was carried out over different Zr-MFI catalysts containing different contents of Zr in the zeolite at temperature 353 K with mole ratio of the reactants (phenol: H_2O_2) 1:1 and with catalyst amount 5 (W/W) % with respect to the total substrate. The products were withdrawn after 8 h interval and were analyzed by GC-MS. The results are shown in **Table 4.27** and depicted in **Figure 4.26**. Maximum conversion was found with the catalyst S100Zr3 i.e. the catalyst containing highest amount of Zr in the MFI sample [**Table 2.2, Page 59, Chapter 2**]. The conversion was found to increase with the increase in the Zr loading in the samples. A distinctive effect on the product selectivity was observed with the variation in Zr loading. High selectivity to catechol formation was observed at low Zr loading. As such the ratio of CL/HQ was found to decrease gradually with increase in Zr content in zeolite. Jun Wang et al. observed similar result while studying the hydroxylation of phenol on Cu exchanged zeolite [11].

Similarly, the reaction was carried out over different In-MFI catalysts containing different contents of In in the structure at the same temperature as above with mole ratio of the reactants (phenol: H_2O_2) 1:1 and with catalyst amount 5 (W/W) % with respect to the total substrate. The products were withdrawn after 8 h interval and were analyzed by GC-MS. Here also, maximum conversion was found with the catalyst S100In1 i.e. the catalyst containing highest amount of In in the MFI sample [**Table 3.1, Page 93, Chapter 3**]. The conversion was found to increase with the increase in the In loading in the samples. A profound influence in the product selectivity was observed with the variation in In loading. Low indium content in the zeolite structure favoured catechol formation as evident from the decrease of CL/HQ ratio with gradual

increase in indium content. The results are shown in **Table 4.28** and depicted in **Figure 4.27.**

Similar experiment was carried out over different Ru-MFI catalysts containing different contents of Ru in the zeolite at temperature 353 K with same mole ratio of the reactants as above and with catalyst amount 5 (W/W) % with respect to the total substrate. 8 h product analysis by GC-MS gave maximum conversion with the catalyst S100Ru1 i.e. the catalyst containing highest amount of Ru in the MFI sample **[Table 3.2, Page 94, Chapter 3]**. The conversion was found to increase with the increase in the Ru loading in the samples. The product selectivity was also found to be influenced with the variation in Ru loading. High selectivity to catechol formation was observed at low Ru loading. The ratio of CL/HQ was found to decrease gradually with increase in Ru content in zeolite. The results are shown in **Table 4.29** and depicted in **Figure 4.28.**

The phenol hydroxylation reaction does not take place in absence of a catalyst [12]. It was reported that even the reaction proceeded very slowly in presence of silicalite-2, amorphous SiO_2 or TiO_2. In the present investigation, introduction of metals like zirconium, ruthenium and indium to MFI structure was found to increase the conversion of phenol and conversion increased with increase of metal content in the MFI zeolite. Dubey et al. [10] studied the hydroxylation of phenol reaction over ternary hydrotalcites containing copper, nickel and aluminium. The authors also found that conversion increased with increase of copper content in the material.

Table 4.27 Comparison of the hydroxylation of phenol using different content of Zr in the catalyst

Reaction conditions

Temperature: 353 K, Time: 8 h,
Mole ratio of the reactants = phenol: H_2O_2 (30%): solvent = 1: 1:10
Catalyst amount: 5 (W/W) % with respect to total substrate

Catalyst	Conversion of phenol (%)	Product selectivity (%)		Ratio (CL/HQ)
		Catechol	Hydroquinone	
S100Zr3	62.4	83.8	14.4	5.82
S100Zr6	61.6	84.1	14.2	5.92
S100Zr9	61.0	84.4	13.8	6.12
S200Zr6	60.6	84.8	13.3	6.37

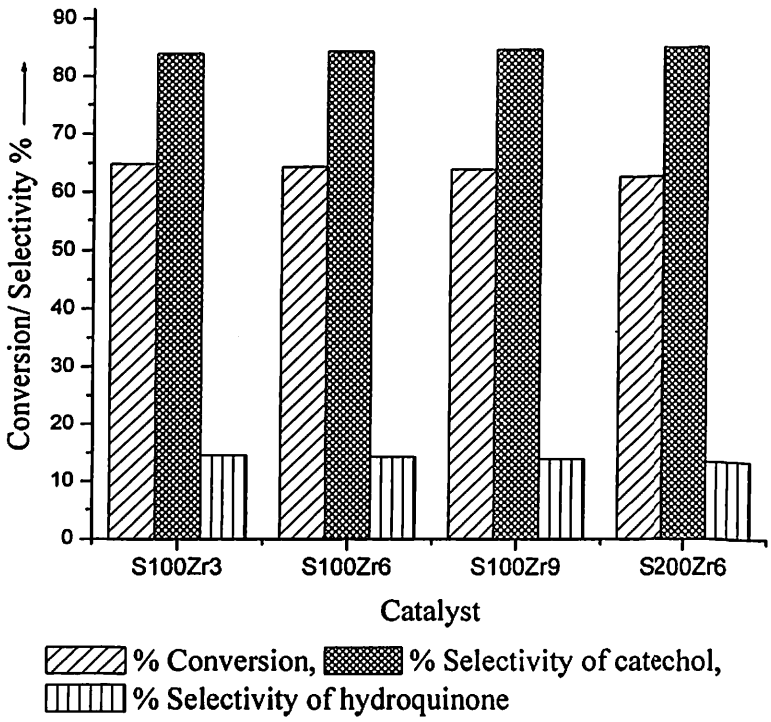

Fig. 4.26 Comparison of catalytic activity of catalysts containing different content of Zr on hydroxylation of phenol

Table 4.28 Comparison of the hydroxylation of phenol using different content of In in the catalyst

Reaction conditions

Temperature: 353 K, Time: 8 h,
Mole ratio of the reactants = phenol: H_2O_2 (30%): solvent = 1: 1:10
Catalyst amount: 5 (W/W) % with respect to total substrate

Catalyst	Conversion of phenol (%)	Product selectivity (%)		Ratio (CL/HQ)
		Catechol	Hydroquinone	
S100In1	56.6	76.8	20.7	3.71
S100In2	56.1	77.1	20.5	3.76
S100In3	55.6	77.6	20.1	3.86

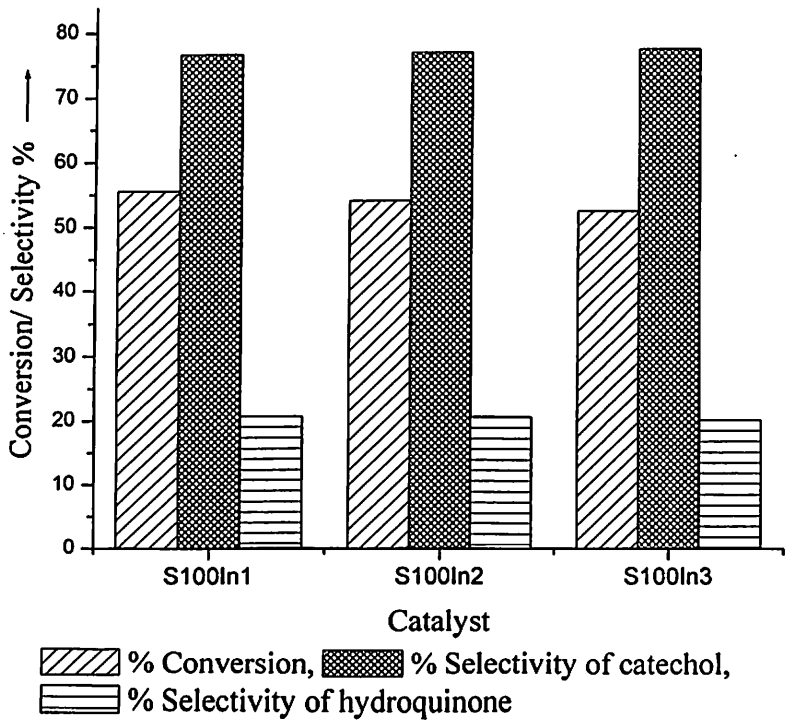

Fig. 4.27 Comparison of catalytic activity of the catalysts containing different content of In on hydroxylation of phenol

Table 4.29 Comparison of the hydroxylation of phenol using different content of Ru in the catalyst

Reaction conditions

Temperature: 353 K, Time: 8 h,
Catalyst amount: 5 (W/W) % with respect to total substrate
Mole ratio of the reactants = phenol: H_2O_2 (30%): solvent = 1: 1:10

Catalyst	Conversion of phenol (%)	Product selectivity (%)		Ratio (CL/HQ)
		Catechol	Hydroquinone	
S100Ru1	60.2	75.1	22.8	3.29
S100Ru2	59.6	75.6	22.7	3.33
S100Ru3	59.3	76.1	22.2	3.42

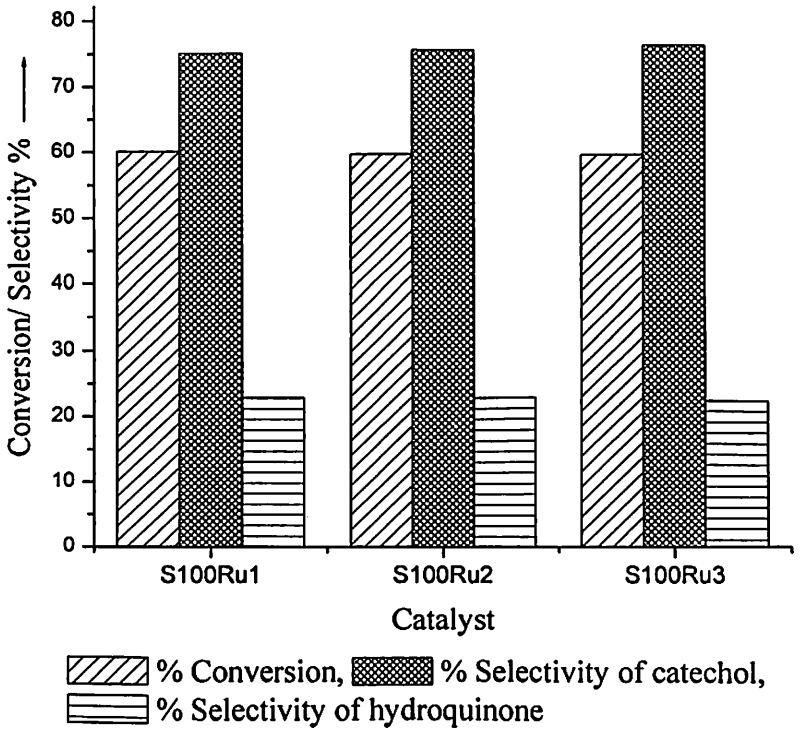

Fig. 4.28 Comparison of catalytic activity of the catalysts containing different content of Ru on hydroxylation of phenol

4.3.5 Comparison of phenol hydroxylation in different media using different catalysts

The phenol hydroxylation was investigated in three different reaction media i.e. with 30% H_2O_2, 30% H_2O_2 + additional water and 30% H_2O_2 + acetonitrile at 353 K taking 5 (W/W) % catalyst with respect to substrate. The products were analyzed after different periods of time. The results are presented in **Tables 4.30** to **4.32** and depicted in **Figures 4.29** to **4.31.**

Table 4.30 Comparison of phenol hydroxylation (without additional water and organic solvent) using different catalyst

Reaction conditions

Temperature: 353 K, Mole ratio of the reactants = phenol: H_2O_2 (30%) = 1: 1
Catalyst amount: 5 (W/W) % with respect to total substrate, Time: 8 h

Catalyst	Conversion of phenol (%)	Product selectivity (%)		Ratio (CL/HQ)
		Catechol	Hydroquinone	
S100	34.4	76.4	21.6	3.54
S200	35.4	75.4	21.1	3.57
S100Zr3	44.2	79.7	18.7	4.26
S100In3	40.7	76.7	21.8	3.52
S100Ru3	42.4	70.8	25.7	2.76

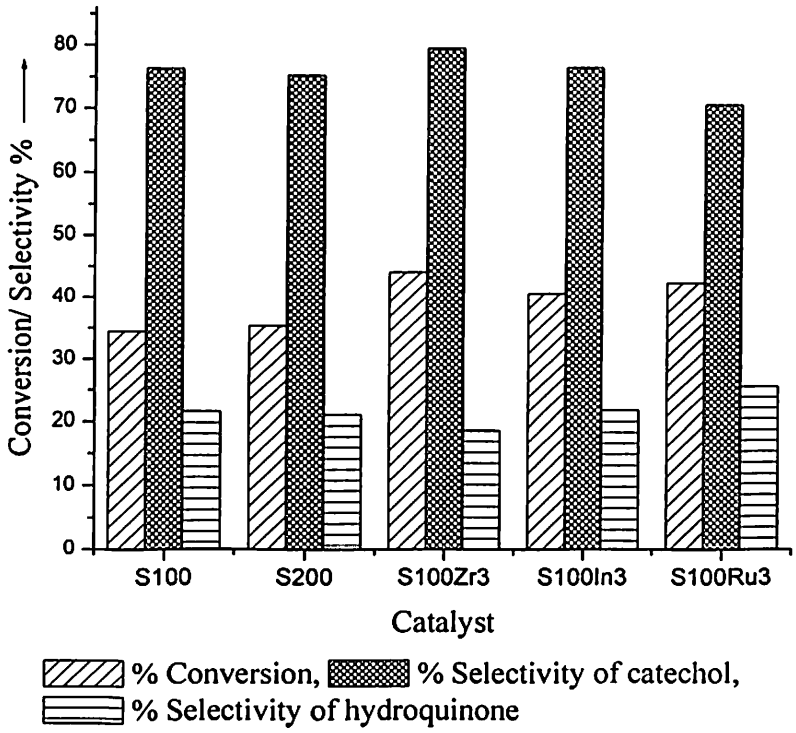

Fig.4.29 Comparison of hydroxylation of phenol (without additional water and organic solvent) using different catalyst

Table 4.31 Comparison of phenol hydroxylation in additional water using different catalysts

Reaction conditions

Temperature: 353 K
Mole ratio of the reactants = phenol: H_2O_2 (30%) = 1: 1:10
Catalyst Amount: 5 (W/W) % with respect to total substrate, Time: 8h

Catalyst	Conversion of phenol (%)	Product selectivity (%)		Ratio (CL/HQ)
		Catechol	Hydroquinone	
S100	42.4	81.4	15.9	5.12
S200	48.5	81.7	15.9	5.14
S100Zr3	62.4	85.4	12.3	6.94
S100In3	55.6	77.6	20.1	3.86
S100Ru3	59.3	75.6	22.2	3.41

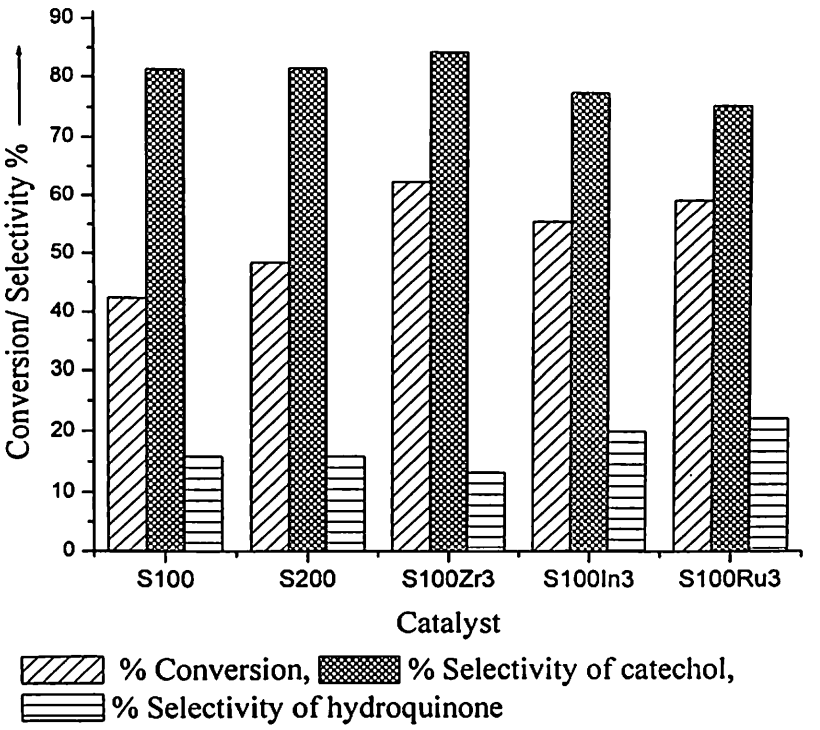

Fig. 4.30 Comparison of hydroxylation of phenol(with additional water) using different catalyst

Table 4.32 Comparison of phenol hydroxylation in acetonitrile using different catalyst

Reaction conditions

Temperature: 353 K
Mole ratio of the reactants = phenol: H_2O_2 (30%): solvent = 1: 1:10
Catalyst Amount: 5 (W/W) % with respect to total substrate, Time: 8h

Catalyst	Conversion of phenol (%)	Product selectivity (%)		Ratio (CL/HQ)
		Catechol	Hydroquinone	
S100	40.6	81.3	15.7	5.18
S200	46.7	83.2	15.2	5.47
S100Zr3	60.2	86.0	12.3	6.99
S100In3	51.2	80.8	18.0	4.49
S100Ru3	54.4	78.1	21.4	3.65

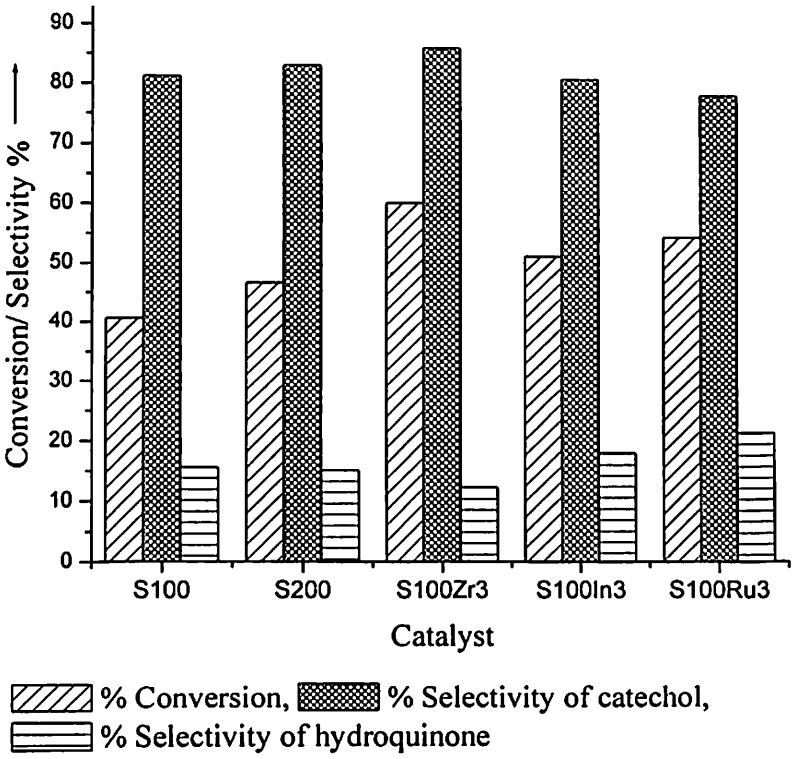

Fig.4.31 Comparison of hydroxylation of phenol in CH_3CN on different catalyst

Table 4.33 and **Figure 4.32** summarize the effect of different solvent media on the hydroxylation reaction (8h products). Previous reports have indicated that solvent effect to be a critical deciding factor in phenol hydroxylation process [13-16]. In the present studies, conversion of phenol was found to be better when 30% H_2O_2 was used with additional water as solvent in all cases. The influence of solvent can be interpreted on the basis of its polarity. Phenol conversion increases with solvent polarity. This may be due to the fact that phenol and H_2O_2 can reach the active sites more easily in water medium than in organic solvents. We believe that the proximity of the hydroxylating agent and the

substrate molecule on or near the active catalyst site is essential for driving the reaction. In water, both phenol and H_2O_2 dissolve simultaneously and approach the active center, thereby generating hydroxy radicals, thought to be the active species involved in the hydroxylation reaction. Moreover, such an electrophile is easily produced and stabilized in water than in organic solvents. Possibly, the lack of a hydroxylated nature for the other organic solvents may be responsible for the non-occurrence of this reaction in some cases [17].

It is observed that under all reaction conditions catechol selectivity was higher than the hydroquinone selectivity. This is more evident when additional water or acetonitrile were used as solvent. According to Perego et al. [18] the ratio (CL/HQ) depends on the solvent used. However, various effects may come into play like shape selectivity of the catalysts, diffusivity of *o*- and *p*-product, cross sectional area of the substrate etc. Considering these factors hydroxylation should take place at less hindered *p*-position. However, according to Tuel and Ben Taarit hypothesis [19] catechol should be major product as this can form at the external surface of metal loaded catalyst. Protic solvents have been seen to favour the formation of HQ whereas aprotic solvents have been seen to favour the formation of CL. Aprotic solvents like acetone and acetonitrile cannot form stable complexes with incorporated metal sites thus limiting the formation of peroxo intermediates at the active sites in the pores, so that CL formation at the external surface sites dominates. In the present investigation also the ratio of CL/HQ is found to be higher for acetonitrile than in water.

Table 4.33 Comparison of conversion of phenol in different media.

Reaction conditions

Temperature: 353 K, Mole ratio of the reactants = phenol: H_2O_2 (30%) = 1: 1
Catalyst Amount: 5 (W/W) % with respect to total substrate, Time: 8h

Catalyst	Conversion of Phenol (%)			Ratio (CL/HQ)		
	With 30% H_2O_2 (I)	With 30% H_2O_2 + additional Water (II)	With 30% H_2O_2 + Acetonitrile (III)	(I)	(II)	(III)
S100	34.4	42.4	40.6	3.54	5.12	5.18
S200	35.4	48.5	46.7	3.57	5.14	5.47
S100Zr3	44.2	62.4	60.2	4.26	6.94	6.99
S100In3	40.7	55.6	51.2	3.52	3.86	4.49
S100Ru3	42.4	59.3	54.4	2.75	3.41	3.65

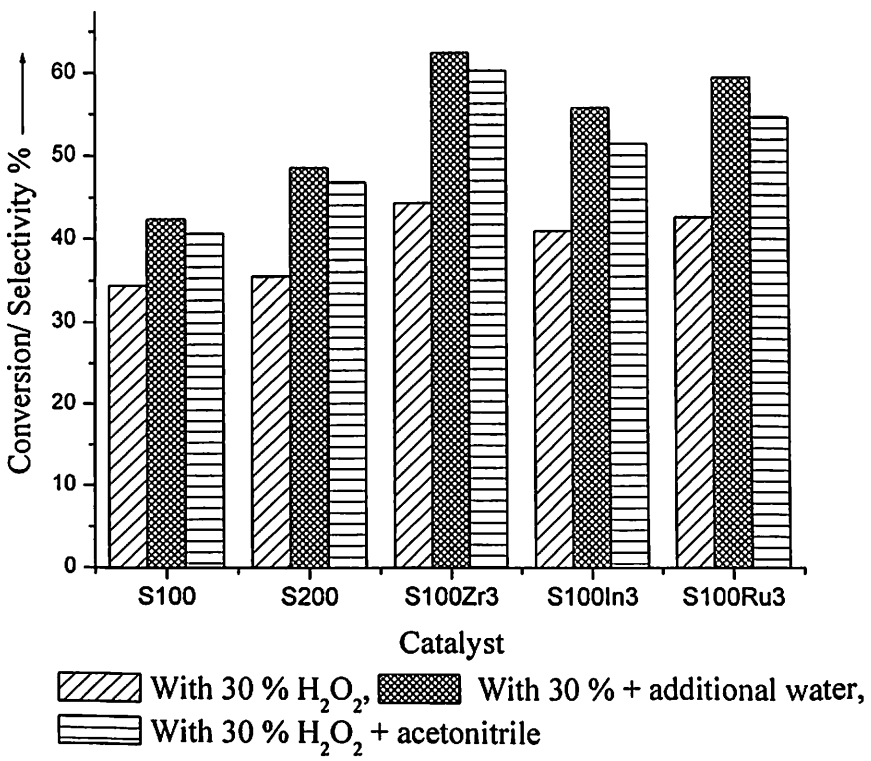

Fig. 4.32 Comparison of hydroxylation of phenol in different solvent condition

4.3.6 Mechanism of phenol hydroxylation

The hydroxylation of phenol reaction was found to take place with both metal loaded and unloaded MFI and the reaction occurs exclusively at the *o*- and *p*-positions which suggests that the reaction might be an electrophilic substitution, probably involving $(OH)^+$ species. Yields and kinetics of hydroxylation of phenol are dependent on the polarity, crystal size, concentration of metal in the MFI structure, temperature etc. Conversion was found to be higher in case of Zr, Ru and In introduced metal zeolite than those achieved by acidic catalysts. This was also observed in phenol hydroxylation with H_2O_2 by Romano et al. [20]. So, the following mechanism has been proposed for H-MFI (**Figure 4.33**).

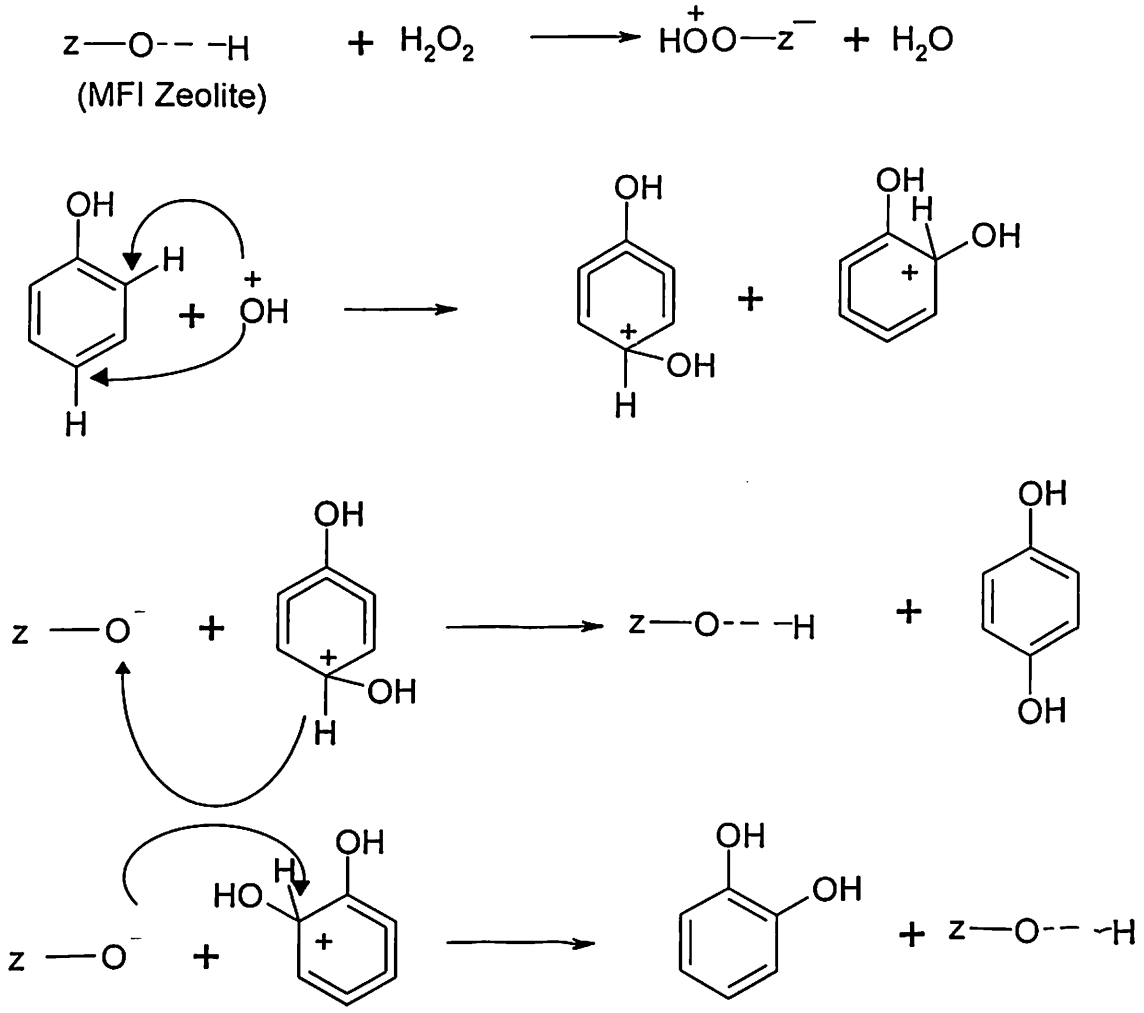

Fig.4.33 Mechanism of phenol hydroxylation on H-MFI

The active site in the metal substituted MFI is thought to be the metal peroxo species formed by the reaction of H_2O_2 with metal incorporated in the silica environment [21]. The absence of resorcinol in the product of the reaction indicates that the heterolytic electrophilic aromatic substitution mechanism is favoured in the phenol hydroxylation reaction by H_2O_2. Based on our results and previous findings [22], the following mechanism is proposed for the reaction with metal loaded MFI catalyst (**Figure 4.34**).

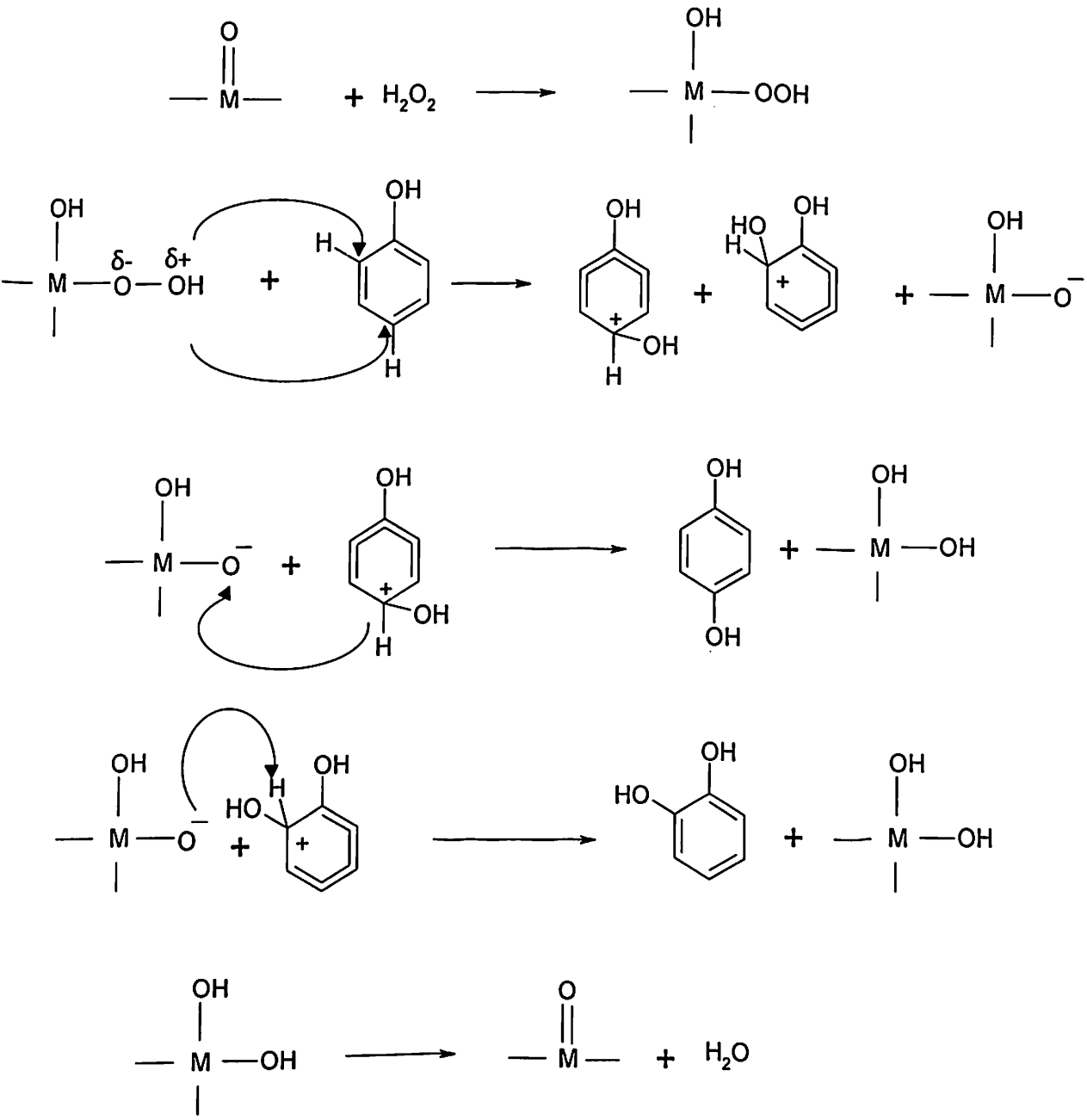

Fig.4.34 Mechanism of phenol hydroxylation on M-MFI

4.4 Conclusion

Hydroxylation of phenol was successfully carried out at the temperature range 333-353 K with 30 % H_2O_2, 30 % H_2O_2 + additional water and 30 % H_2O_2 + acetonitrile with phenol to hydrogen peroxide mole ratio of 1:1 using parent and modified MFI Zeolite. Under the present reaction conditions, catechol was the predominant product. When the progress of the reaction was monitored with time during the hydroxylation of phenol, it was observed that in all cases conversion was found to increase with increase of reaction time. In case of parent MFI samples, it is observed that conversion increases with increase in the silicon to aluminium ratio while in case of Zr, In and Ru doped MFI samples, it is observed that conversion increases with increase in the amount of metals in the samples. However, the CL/HQ ratios were found to decrease with increase in the level of metal content. The conversion was found to increase with increase of temperature upto 343 K from 333 K. However, when temperature was further increased upto 353 K, the increase rate was lowered to some extent. This could be ascribed to the competitive thermal decomposition of H_2O_2 at higher temperature without being involved in desired reaction. Conversion of phenol was found to be better when 30% H_2O_2 was used with additional water as solvent in all cases. The influence of solvent can be interpreted on the basis of its polarity. Phenol conversion increases with solvent polarity. The conversion was found to increase with the increase in the amount of catalysts in all cases.

For hydroxylation of phenol the order of activity for conversion in case of metal incorporated MFI samples was found to be In-MFI < Ru-MFI < Zr-MFI.

4.5 References

[1] R.I.Zhdanov, S.M. Zhenodarova, *Synthesis* 4 (1975) 222.

[2] A. Corma, H. Garcia, *Chem. Rev.* 102 (2002) 3837.

[3] J.M.Smith, *Chemical Engineering Kinetics,* Mc Graw-Hill, New York, NY, 2nd Ed., 274 (1974).

[4] T. Atoguchi, T. Kanougi, T. Yamamoto, S. Yao, *J Mol. Catal. A: Chem.* 220 (2004) 183.

[5] Sheldon, R.A. (1996) Selective catalytic synthesis of fine chemicals: opportunities and trends. *J Mol. Catal. A: Chem.,* 107, 75.

[6] Sheldon, R.*A.*, I.W.C.E. Arends and H.E.B. Lempers Liquid phase oxidation at metal ions and complexes in constrained environments, *Catal. Today*, 41 (1998) 387.

[7] T. Atoguchi, T. Kanougi, *J Mol. Catal. A: Chem.,* 222 (2004) 253.

[8] A.L. Villa et al., *J Mol. Catal. A: Chem.,* 228 (2005) 233–240.

[9] A. Germain, M. Allian, F. Figueras, *Catal. Today* 32 (1996),145.

[10] A. Dubey et al., *J Mol. Catal. A: Chem.,* 181 (2002)151.

[11] Jun Wang et al, *Energy and Fuels*, 18 (2004),473.

[12] J. Sudhakar Reddy, S. Sivasanker and P. Ratnasamy, *J Mol. Catal. A: Chem., 71* (1992) 376.

[13] S.Lin, Y.Zhen, S-M.Wang, Y-M.Dai. *J Mol. Catal. A: Chem.,* 156 (2000) 113.

[14] R.Yu, F-S. Xiao, D.Wang, J.Sun. Y.Liu, G.Pang. S.Feng, S.Qiu, R.Xu. C.Fang. *Catal.Today,* 51 (1999) 39.

[15] R.Yu, F-S. Xiao, D.Wang, Y.Liu. G.Pang, S.Feng. S.Qiu, R.Xu, *Catal. Lett.* 49 (1997) 49.

[16] Ch.Subrahrnanyam, B.Louis, B.Viswanathan. A.Renken, T.K.Varadarajan, *Eurasian Chem. Tech. Journal.* 3 (2001) 59.

[17] A. Dubey et al., *J Mol. Catal. A: Chem.,* 181 (2002)155.

[18] C. Perego et al. / *Appl. Catal. A: General* 221 (2001) 66.

[19] A. Tuel, Y. Ben Taarit, *Appl. Catal. A* 102 (1993) 69.

[20] U. Romano, A. Esposito, F. Maspero, C. Neri, M.G. Clerici, *Chim. Ind.* 72 (1990) 610.

[21] Clerici, M.G.,*Appl. Cat.*68 (1991) 249.

[22] J. Sudhakar Reddy, S. Sivasanker and P. Ratnasamy, *J Mol. Catal.., 71* (1992) 380.

List of Publications and Papers Presented in the Seminars/ workshops

Publications:

1. Synthesis and characterization of isomorphously zirconium substituted Mobil Five (MFI) zeolite, **Kishor Kr. Shah**, Jitu Saikia, Durlov Saikia, Anup K. Talukdar, *Materials Chemistry and Physics*(Elsevier), 134 (2012) 43– 49.

Papers Presented:

1. Zeolite as Green Catalyst, **Kishor Kr. Shah** and Anup K. Talukdar, UGC Sponsored National Seminar on *"Green Chemistry for Sustainable Future of Humanity"* organized by ADP College, Nagaon, 19 & 20, October, 2008.

2. Synthesis of Isomorphously substituted Zr-MFI from fluoride containing gel, **Kishor Kr. Shah,** Dhanju Mani Pathak and Anup K. Talukdar ,*14th National Workshop on Catalysis*, organized by Dept. of Chemical Sciences, Tezpur University,21-23, December, 2009.

3. Synthesis of T-Atom substituted MFI zeolite, **Kishor Kr. Shah,** Jitu Saikia and Anup K. Talukdar, *Recent Advances in Synthesis and Catalysis,* organized Dept. of Chemistry, Dibrugarh University, 10-12, February, 2011.

4. Synthesis and Characterization of Indium Substituted nanocrystalline Mobil Five(MFI) Zeolite, **Kishor Kr. Shah,** D.Saikia, J.Saikia and Anup K. Talukdar, *Recent Aspects of Chemistry Education and Research,* organized by Department of Chemical Science ,Gauhati University, 24-25, February, 2012